EXPERIMENTAL STUDY ON THE BEHAVIOUR OF AN I-BEAM TO SHS-COLUMN BY T-STUB BOLTED CONNECTION

by

Kağan Yemez

B.S., Civil Engineering, Boğaziçi University, 1997

M.S., Civil Engineering, Boğaziçi University, 2000

Submitted to the Institute for Graduate Studies in
Science and Engineering in partial fulfillment of
the requirements to the degree of
Doctor of Philosophy

Graduate Program in Civil Engineering

Boğaziçi University

2007

EXPERIMENTAL STUDY ON THE BEHAVIOUR OF AN I-BEAM TO SHS-COLUMN BY T-STUB BOLTED CONNECTION

APPROVED BY:

Prof. Gülay Altay (Thesis Supervisor)	……
Assoc. Prof. Emre Otay	……
Prof. Turan Özturan	……
Assoc. Prof. Cem Yalçın	……
Prof. Nesrin Yardımcı	……

DATE OF APPROVAL: 19.01.2007

"To succeed, we must first believe that we can"

Michael Korda

To my lovely wife,

Hanzade

ACKNOWLEDGEMENTS

The research presented in this thesis was conducted at the Civil Engineering Department of Boğaziçi University with limited financial support. The required materials and instruments, necessary fabrication were provided by the supports of the companies in steel construction sector in Turkey; firstly steel hollow section profiles and instruments by Borusan, then steel beams by Arcelor and Rozak, bolts and studs by AS Cıvata, fabrication of the specimens by Tabosan and the fabrication of the rigid-link used in the test set-up by Çeçen İnşaat. The supports are highly appreciated.

I would like to express my sincere gratitude to my thesis advisor, Prof. Gülay Altay for her guidance and valuable suggestions that she provided throughout the preparation of this thesis.

I would like to thank to my jury Prof. Turan Özturan, Prof. Nesrin Yardımcı, Assoc. Prof. Emre Otay and Assoc. Prof. Cem Yalçın for their time they have devoted for reading and commenting on my thesis.

Heartfelt thanks to the staff of the Structures, Materials and Mechanics Laboratories with special thanks to Osman for their contributions. Without their help this thesis would have never been completed.

I am specially grateful to "*ma femme*" Hanzade for her great support, especially her kind help on writing the thesis. For their endless love and support; I thank to my Mom, Dad, Grand Dady, brother and his wife deep from my heart. While preparing my thesis, I got married. Also special thanks to my new family.

Great thanks to Arcelor International-Istanbul Office for allowing me time while following up and carrying on my experimental study.

I would like to express my special thanks to Didem for her help during literature survey; to Müge&Bülent and Melek&Cenk for their moral support.

ABSTRACT

EXPERIMENTAL STUDY ON THE BEHAVIOUR OF AN I-BEAM TO SHS-COLUMN BY T-STUB BOLTED CONNECTION

In 80's and 90's hollow sections (HS) were mainly used in compression and tension elements of truss systems. Nowadays, architects are more and more using hollow sections in building applications where limited amount of research is available especially considering the economics of prefabrication to produce connections with acceptable ductility performance. In most of the examined joint types, the connection elements were welded on the tubular sections. This research is focused on the behaviour of I-beam to HS-column t-stub bolted connections under monotonic and cyclic loading conditions. In view of easy and economic bolted field application and transportation without damage by leaving the column exterior without projections, in proposed joint type t-stubs are bolted by using long partially threaded studs through HS column. Four full scale beam-column specimens have been tested in two groups. As a difference the rear face of the HS column at the connection area has been reinforced by backing plate in the second group of specimens. Considering the cyclic performances, both joints maintain high plastic rotations in adequate resistance levels with acceptable energy dissipation capacities; consequently are suitable for use as semi-rigid partial strength joints in simply designed braced steel frames in seismic areas or in unbraced steel frames in less seismic areas. Additional research on the connection components has also been performed to observe the component behaviour of the column face in bending. Applicability of the component method described in Eurocode 3 part 1-8 with proposed design approach is checked by comparing with the test results both in resistance and stiffness point of view.

ÖZET

I-KİRİŞİN KUTU KOLONA T-ELEMANI İLE BULONLU BİRLEŞİMİNİN DAVRANIŞI ÜZERİNE DENEYSEL ÇALIŞMA

Seksenli doksanlı yıllarda kutu kesitler genellikle makasların basınç ve çekme elemanlarında kullanılıyordu. Günümüzde mimarlar kutu kesitleri bina uygulamalarında daha sıklıkla kullanıyorlar. Bu alanda kabul edilebilir süneklikte üretilen birleşimleri prefabrikasyon ekonomisi ile değerlendiren kısıtlı miktarda araştırma bulunmaktadır. İncelenen çoğu birleşim tipinde bağlantı elemanları boru profillere kaynaklıydı. Bu araştırma I-kirişin kutu kesit kolona t-bağlantı elemanı ile bulonlu birleşimini tek yönde ve çift yönde tekrarlı yükleme koşulları altında davranışına odaklanmıştır. Önerilen birleşim detayında şantiye ortamında kolay ve ekonomik uygulama ve hasarsız nakledebilmek için kolon dışına uzanan bağlantı elemanları olmaması koşulları değerlendirilerek t-bağlantı elemanları uzun kısmen yivli saplamalar ile kutu profilin içinden geçerek arka yüzeyine bulonlanmaktadır. Dört tam ölçekli kolon-kiriş birleşim numumeleri iki grup halinde test edilmiştir. Farklı olarak ikinci grupta kutu kolonun birleşim bölgesinde arka yüzeyi destek plakası ile takviye edilmiştir. Tersinir tekrarlı yükleme performansları değerlendirilirse her iki birleşim de yeterli dayanım seviyesinde yüksek plastik dönme ve kabul edilebilir enerji yutma kapasitesitesi sağlamıştır. Dolayısıyla bu birleşimler yarı-rijit kısmen güçlü birleşimler olarak depremselliği düşük olan bölgelerde moment aktaran çelik çerçevelerde veya yüksek depremsel bölgelerde çaprazlı çerçeveler ile tasviyeli çelik çerçevelerde kullanılabilir. Kolon yüzeyinin eğilmesi bileşeninin davranışını incelemek için de ek deneysel araştırma yapılmıştır. Eurocode 3 bölüm 1-8'de anlatılan bileşen metodunun önerilen tasarım yaklaşımı ile birlikte uygulanabilirliği test sonuçları ile hem dayanım hem de eğilmezlik açısından karşılaştırılmıştır.

TABLE OF CONTENTS

LIST OF FIGURES

LIST OF TABLES

LIST OF SYMBOLS / ABREVIATIONS

A	Area of the related cross-section
A_i	Area of the half cycles
A_s	Resistance area of a bolt
A_{vc}	Shear area of the related cross-section
b_0	Distance between bolt holes close to opposite sidewalls
b_c	Width of a square hollow section
B_p	Punching shear resistance
c_0	Distance between bolt rows
d	Beam depth
d_c	Clear depth of a square hollow section sidewall
d_w	Nominal diameter of a bolt head
$\overline{E}$	Non-dimensional dissipated energy
E	Modulus of elasticity
e_1	Distance from bolt hole to the free end of the related material in the direction of load transfer
e_2	Distance from bolt hole to the free end of the related material in the transverse direction of load transfer
e_i	Extreme displacement
e_y	Yield displacement
F	Resistance force
F_i	Value of force corresponding to extreme displacement
F_p	Force applied at the end of the cantilever beam leading to the yielding of the beam
F_{Rd}	Resistance of the related component
f_u	Ultimate strength of the related material
F_u	Ultimate load
F_v	Shear resistance of a bolt
f_y	Yield strength of the related material
F_y	Yield load

h_c	Depth of a square hollow section
i	Radius of gyration of the related cross-section
I	Moment of inertia of the related cross-section
k	Stiffness coefficient
$\overline{K}$	Non-dimensional stiffness of a joint
k_c, k_f, k_s, k_t	Initial stiffness of corner rotation, face in bending, sidewall and total
L	Width of a yield area of a square hollow section
l_b	Effective buckling length
L_b	Beam length
l_{eff}	Effective length
L_{stiff}	Equivalent yield length for stiffness determination of square hollow section
$\overline{m}$	Non-dimensional moment
M_e	Elastic moment resistance
M_{pl}, m_p, M_{pb}	Plastic moment of the related cross-section
M_{Rd}	Plastic moment resistance
M_u	Ultimate moment resistance
N_b	Buckling resistance capacity of a compression member
p	Distance between bolt rows of an equivalent t-stub
r	Corner radius
S_j	Rotational stiffness
t	Thickness of the related material
t_c	Thickness of the hollow section
t_w	Thickness of the hollow section
V_{wp}	Resistance of a column in shear component
W_{pl}	Plastic section modulus of the related cross-section
z	Lever arm
α	Slope of the tangent of a curve at the related location
γ	Shear rotation of a column web
γ_M	Partial safety factor

δ	Displacement
ε	Strain
ε_i	Resistance ratio
η	Dissipated energy ratio
θ	Rotation of the connection
θ_c	Rotation of the column
θ_f	Flexural rotation of the column
κ	Reduction factor used in buckling resistance capacity of a tube
λ	Slenderness ratio
μ_o	Partial ductility
μ_i	Full ductility
v_p	Beam end displacement evaluated for ideally rigid condition
ξ	Rigidity ratio
ρ	Calibration factor
φ	Joint relative rotation
$\overline{\varphi}$	Non-dimensional joint rotation
ψ	Full ductility ratio

AISC	American Institute of Steel Construction
CFT	Concrete filled tubular
CFST	Concrete filled steel tubular
CIDECT	Comité International pour le Développement et l'Etude de la Construction Tubulaire (International committee for the research and development of the construction with hollow steel sections)
EC	Eurocode 3 part 1-8
FEMA	Federal Emergency Management Agency
HS	Hollow section
KY	Model proposed in this study
RHS	Rectangular hollow section
SHS	Square hollow section

1. INTRODUCTION

1.1. Literature Review

The increase in the use of hollow sections (HS) in the mainstream structures, coupled with the economics of prefabrication, has highlighted the need for research that produce economical connections with acceptable ductility performance.

Since hollow sections were mostly used in compression and tension elements of truss systems, most of the research activities in 80's and 90's were focused on welded or bolted tubular connections under axial loading conditions. Seeing as the tubular columns were gaining popularity in the building construction industry, recent research activities were concentrated on the flexural behavior of tubular moment connections. However there is still limited amount of research on this area.

The moment end plate connection joining I-section members has been extensively studied by Grundy et al. in 1980 [1] and considerable documentation on its behavior exists in the literature. Furthermore the research on tubular end plate connections by Packer et al. in 1989 [2] that has been conducted has concentrated primarily on pure tensile loading or combined compression and bending as in column-to-column bolted flange splice connection, rather than pure flexural loading.

Compared to conventional steel or reinforced concrete columns, concrete filled tubular (CFT) columns possess many advantages such as steel tube providing confinement and formwork for the concrete core; stability, stiffness and fire resistance of the steel tube is improved and lower construction costs [3]. On the other hand, depending on the sizes, some fabricators point out the difficulties while filling the tubular sections with concrete. Schneider and Alostaz [4] investigated seismic performance of various connection details. Six connections have been studied and characterized as two types of connection details, through column and through beam in 1998. Through column connections utilized diaphragms or other stiffeners to connect steel beams to CFT columns. On the other hand,

beams passing through panel zone are referred as through beam connections. Test results showed that extending the girder connection stub through the entire CFT column was sufficient to develop the full plastic bending strength of the connected girder and exhibited favorable inelastic cyclic performance. However, these connections may have difficulty in field construction due to its complex nature in the panel zone. Continuing flange plates can be used in moment resisting frames if the connection is improved by preventing the slip of the connection stub flange plates.

Typical connection details for simple framing between tubular columns and open section beams usually employ a fitting welded to the column which supports the beam and allows clearance for site bolting. Figure 1.1 indicates examples of some of the more common types of simple joints which include the seating angle, web cleats, top and bottom angles or the fin plate (tab plate). A detailed survey of the use of these connections has been conducted in the literature. The tab plate or fin plate is probably the most frequently used of all because of its simplicity and the ease with which the beam and column can be bolted together. However, all of these conventional methods suffer from the disadvantage of requiring fittings to the column which can prove costly to fabricate and make the section more difficult to transport without damage. The ideal system is one which allows site bolting, leaves the column exterior without projections, is similar to traditional beam to open column joints and uses ordinary bolts. To achieve these objectives, the face of the tubular column must be drilled or incorporate the thread to allow the bolt connection.

France et al. conducted series of tests to investigate the moment capacity and rotational stiffness of simple and moment connections bolted to tubular columns using flowdrill connectors in 1999 [5 - 7]. The influence of filling the tubes with concrete is also investigated. Reversed cyclic tests showed the connections to behave in a manner suitable for use as either pinned or partial strength connections for simply designed braced steel frames. The coexistence of axial stress of up to about 50% of yield for grade 275 material has little influence on the moment–rotation characteristic up to about 20 milliradians, which more than covers the range applicable to most braced construction, but subsequent post-yield stiffness in the range 20–60 milliradians is reduced significantly. This is more important for unbraced frames where stiffer and stronger joints - heavy flush endplates or extended endplates - would be more appropriate. All joints performed satisfactorily over

the important ranges of rotation, i.e. 20 milliradians for non-sway frames and 40 milliradians for sway frames. The initial and unloading stiffnesses of all connections were found to be appreciable; the former is important in the context of beam deflection control whilst the latter is particularly significant in column stability. Concrete filling tubular steel column sections significantly increases axial load capacity and also improves resistance to fire. The dramatic increase in strength and stiffness of concrete-filled flowdrill joints when compared directly to their unfilled equivalent is clearly demonstrated. The tests have shown that the resistance of the column in the compression zone is substantially increased. By filling with concrete inside, less deformation has been observed inwards to column. Increased moment capacity is at the expense of ductility of the joint, which is significantly less for concrete-filled tubes. Failure of the joints is by bolt pull-out, although this only occurs after the column face has undergone gross deformation. On the other hand, the disadvantages of these blind connections are the flexibility of the SHS face may limit the moment capacity of the connection when thin walls and narrow bolt gauges are employed. For that reason, some fabricators do not like to work in those close tolerance levels.

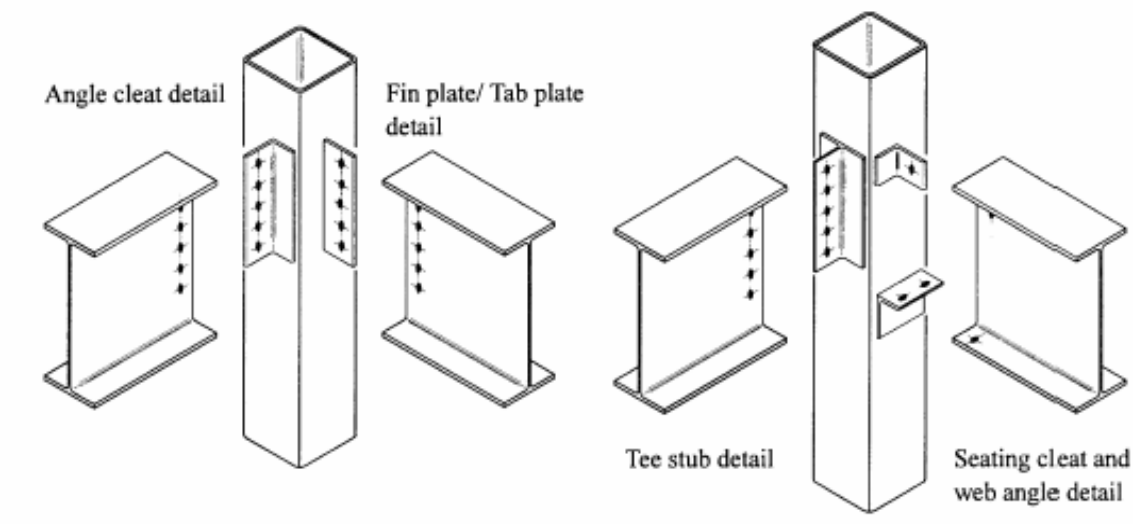

Figure 1.1. Typical connection details for simple I-beam to HS-column connections

Beutel et al.(2002)[8] conducted an experimental investigation into the behaviour of composite column-to-beam connections using ten large-scale connections, four under monotonic loading and six under cyclic loading. All connections consisted of a concrete-filled steel tube (CFST) column (circular), a compact universal beam section and a shop

fabricated connection stub by using flange connection plates, and web cleat plates) and reinforcing bars welded to the top and bottom flanges (specimen SC24t), embedded into the concrete core (specimen SC24c). Tests showed that when the connection's strength was such that a full hinge formed in the framing beam, as was the case with specimens SC24c and SC24t (given in Figure 1.2), the specimen's overall seismic performance improved, and resulted in plastic hinge rotations of the order of 3.5%. These specimens suffered a very minor tube wall tear at the corner of the beam flange to column connection, which did not however propagate entirely through the wall. Based on the behaviour of the models tested, it is possible to design a joint with a component strength hierarchy that will rely on the ductility of the beam only.

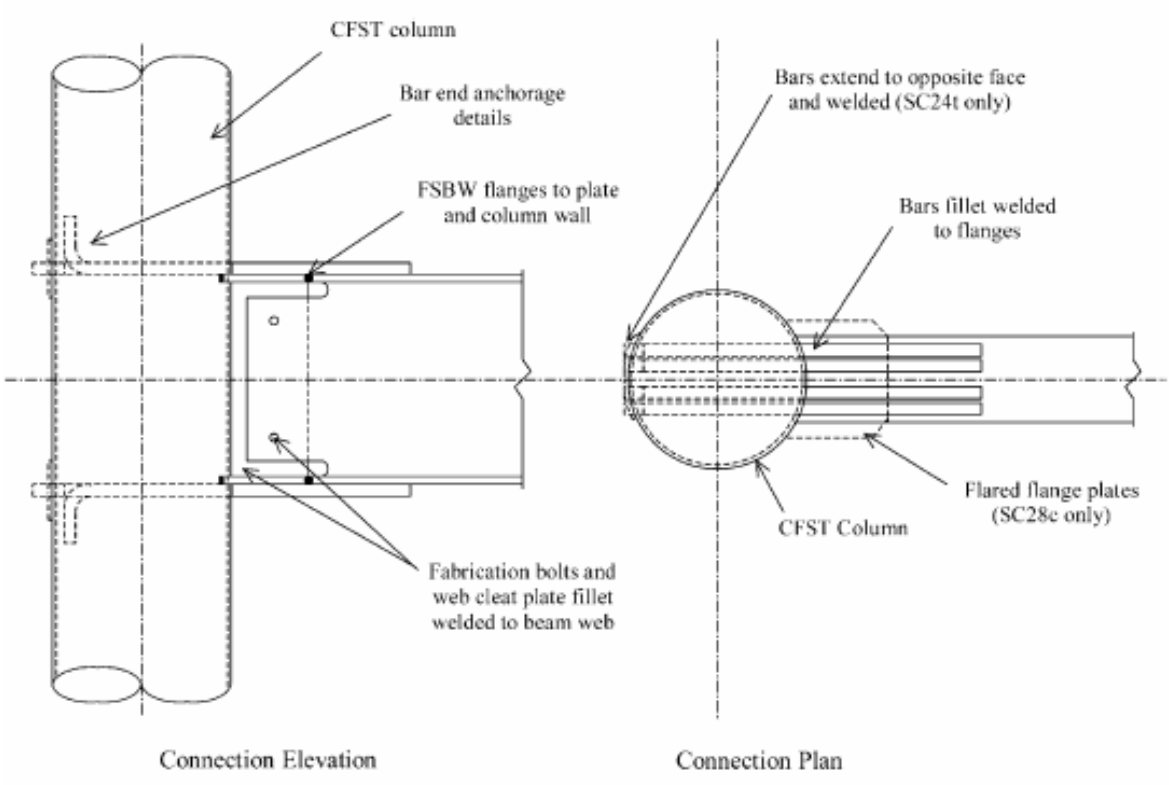

Figure 1.2. Typical moment connection detail for I-beam to HS-column connections [8]

In most of the examined connection types, the connection elements were welded on the tubular sections. Connection types that are bolted to the beam and the column with connection elements were rarely used.

In the research of Shih-Wei Peng [9] together with J. Ricles [10], the effect of different connection details were examined on cyclic performance. Various connection details were investigated, including: interior diaphragms, exterior extended structural tees, and split tees. The performance of the connection details is evaluated by a comparison of the specimen cyclic strength, stiffness, ductility, and energy dissipation capacity. The AISC Seismic Provisions (1997) requires an inelastic story drift capacity for connections of 0.03 rad prior to degrading to 80% of the nominal capacity, while the new FEMA design recommendations for steel frames (FEMA 2000) require a total story drift capacity of 0.04 rad prior to degrading to the nominal capacity. The latter of 0.04 rad is comparable to about 0.03 rad of inelastic drift. Based on a comparison of specimen response with the AISC Seismic Provisions and FEMA recommendations, split-tee connection details appear to be suitable for seismic resistant design. Reinforcing the bolt holes by washer plates in the beam flanges of the bolted split-tee connections prevented hole elongation and fracture, reduced the slip and pinching in the hysteretic response. The development of a diagonal compression strut by shear studs in the concrete of the panel zone enhanced the shear resistance of the joint with split-tee connection details. The split-tee connection detail allows a better mobilization of this concrete strut. In these connections the presence of beam shear tabs was found to have only a minor effect on overall behavior.

Joints between I-beams and rectangular hollow sections present a distinct behavior that differentiates them from major axis joints between I-sections. In fact, the absence of a central stiffening web means that the loaded chord of the column must resist the tensile and compressive forces arising from the beam flanges in bending, similar to a plate supported on its vertical sides. This typical behavior may in fact also be found in weak-axis joints [11].

Characterization of the behavior of the joint between a SHS and an I-beam requires the identification of its strength, stiffness, and ductility. As far as the strength of the chord face is concerned, Gomes et al. [12] proposed solutions after experimental and numerical studies, in the context of weak-axis joints for single bolt rows in tension [13], and the adaptation of these models to SHS joints by Vandegans [14] provided some guidance to the evaluation of strength of SHS joints.

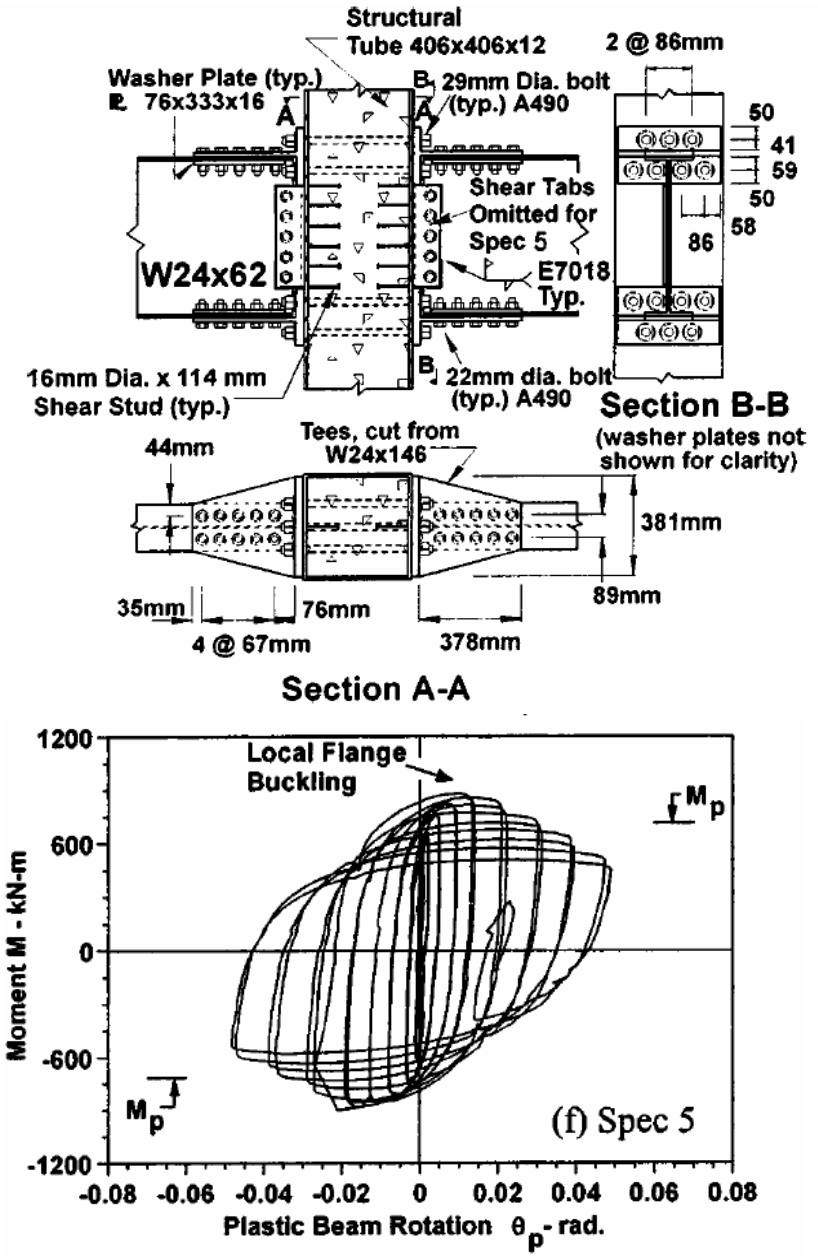

Figure 1.3. Cyclic response of the connection detail[10]

The load transfer from the beam to the column by the connecting elements shown, as an example, as flange cleats in Figure 1.4 could, in the general case, lead to a mechanism involving the upper cleat (tension zone) and the bottom cleat (compression zone). In the present situation of concrete-filled columns, the infilling concrete supports the compression zone, leading to the out-of-plane deformation of the column face. The yielding mechanism involves the tension zone alone, and the deformation of the compression zone may be neglected [14].

In terms of stiffness, an analytical model for concrete-filled RHS composite joints is proposed which was also developed in the context of weak-axis joints by Neves and Gomes in 1996 [11] and later on discussed with an analytical model based on an equivalent strip of the loaded face by Silva et al. in 2003 [15]. Finally, besides some observation of experimental evidence of some ductility, fairly limited guidance exists in this area. It is also pointed out that extension to the more complex problem of unfilled RHS/I-beam joints loaded in bending still presents a few shortcomings to be solved: position of center of compression for the various connection types and, consequently, the appropriate lever arm; and influence of the deformation of the side chords.

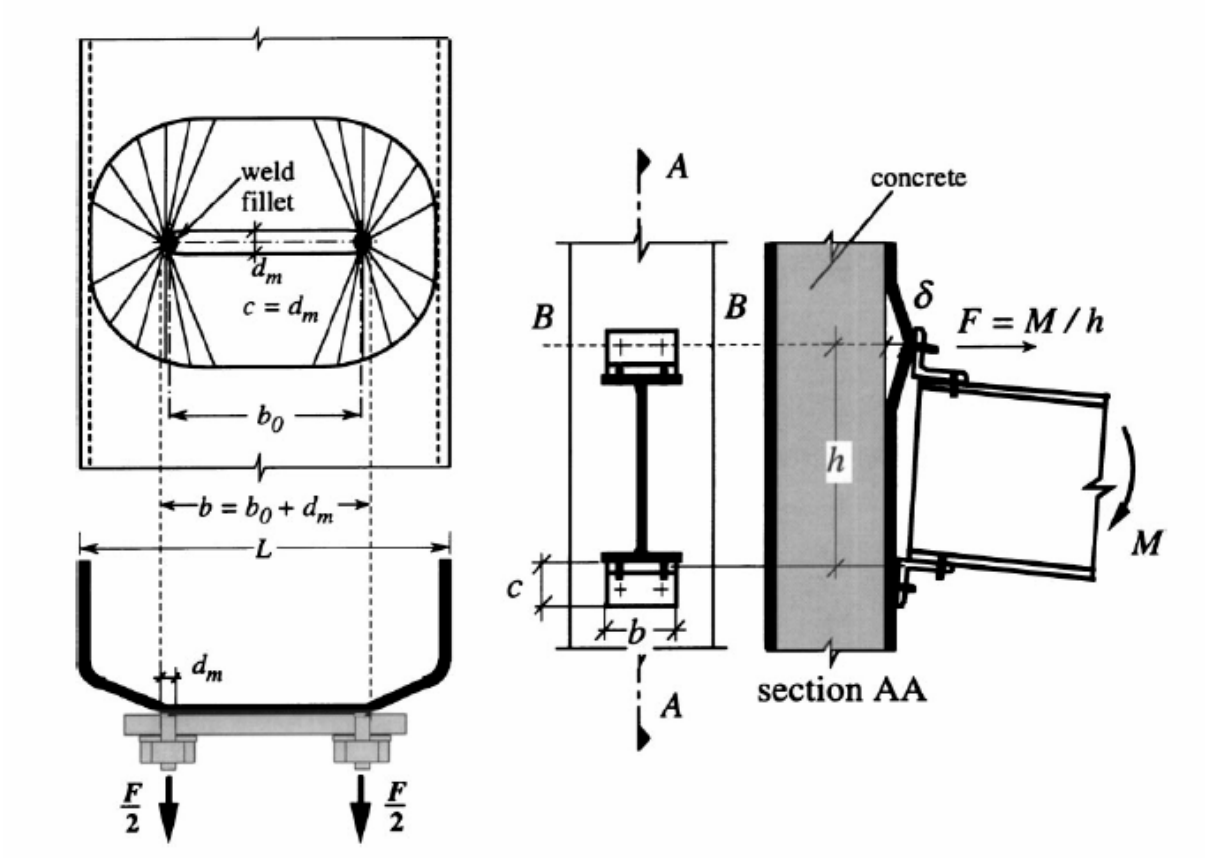

Figure 1.4. Yielding mechanism [15]

In most of the examined connection types in CIDECT (Comité International pour le Développement et l'Etude de la Construction Tubulaire) researches, the connection elements were welded on the tubular sections where recent studies (CIDECT Research Project 5BM [16]) were much focused on bolted connections in relation with semi-rigid

connection research . Latest research [17] gathered all the information available to the designer and helpful for the design of a wide range of structural steel joints connecting hollow and/or open sections. Simple design aids (called design sheets) more appropriate to daily practice have been prepared for some selected joint configurations. These ones have been complemented by worked examples. Most of these researches are analytical and based on the experimental studies under static loading conditions. Further complementary studies need to be done, also under cyclic conditions.

2. EXPERIMENTAL STUDY

2.1. Introduction

Considering the easy bolted field application and leaving the column exterior without projections, similar to traditional beam to open column joints, T-stub connections bolted by only using longer ordinary bolts through HS columns is proposed (see Figure 2.1). Instead of top and seat angle connection, more stiff and strong top and seat t-stub connection is proposed in order to achieve more rigid moment resisting connection. Taking into account the 3D building system, if there exists web cleats in the moment connection, the presence of at least a shear connection need to be bolted though the tubular section in the transverse direction will cause difficulty in application. Therefore there is no web connection on the proposed connection type.

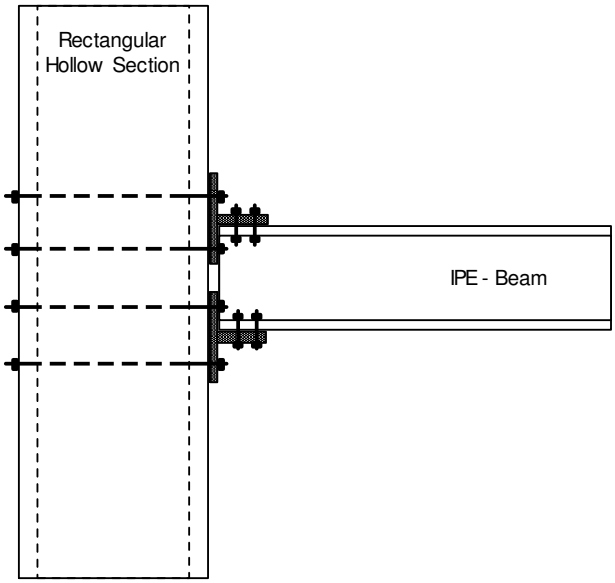

Figure 2.1. I-beam to HS-column connection with T-stub section

Although the application of through bolt connections to tubular sections is similar to the through welded plate connections, the difference arises from the cyclic behavior. Rear and front faces of the tubular section is welded in through welded plate connections and

during axial load cycles both column faces act together. Whereas in through bolt connections since there is no bolt to clamp inside the tube, the rear and front faces can not be considered to be acting together against axial loads cycles but both of the faces only tend to deform inside.

The test parameters and the element sizes are chosen to have energy dissipation, deformation patterns and failure modes at the t-stub and at the face of the tubular column. Since the thickness of the t-stub is relatively less than the flange thickness of the beam, no plastic deformation or plastic hinge formation at the beam is expected. That's to say the connecting element will always fail earlier. Therefore the only contribution on the hysteresis behaviour of the connection mainly comes from the column and connecting elements considering the element sizes.

As shown in Figure 2.2, two major deformation patterns concerning the t-stub can be distinguished. Deformation pattern 1 corresponds to the specimens having a low t-stub strength compared with the bolt strength, and the plastic zones in these specimens are formed in the column face. Deformation pattern 2 occurs in the specimens having a relatively strong t-stub, and the plastic deformations are shared by the t-stub fillet and bolts [18, 19].

The prying action of the t-stubs is expected to decrease when relatively thicker t-stub is selected compared with the column face thickness. Concerning the tubular column faces, since the rear and front faces is not acting together against axial loads cycles along the bolts, there will be prying actions towards inside at both of the faces as given in Figure 2.3. Considering the strong column- weak beam or weak connection concept, steel plate stiffeners (backing plates) might be necessary at the rear faces of the columns in order to reduce the local plastic deformations and consequently decrease this prying action. Other than rear face deformations of hollow sections, typical failure modes [20] are given in Figure 2.4.

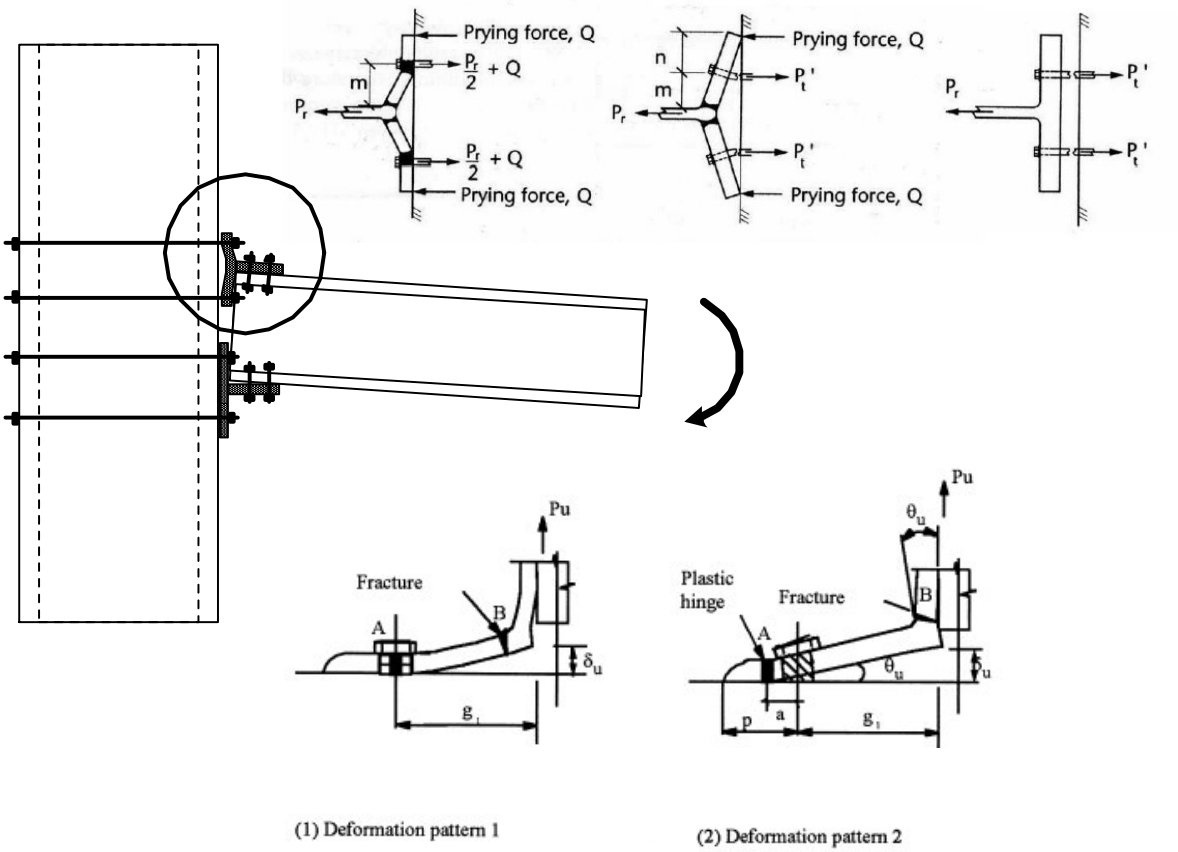

Figure 2.2. Deformation patterns of t-stub connection element [19]

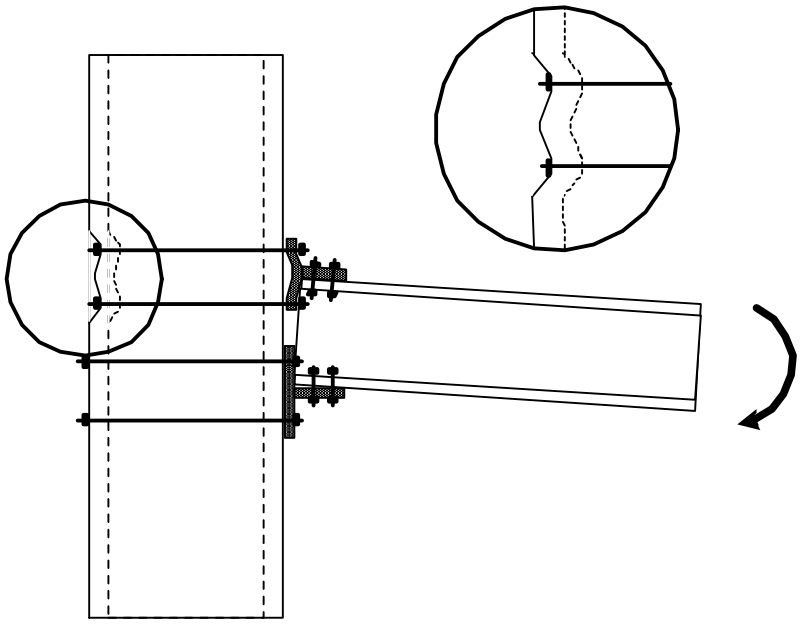

Figure 2.3. Deformation pattern of HS-column face

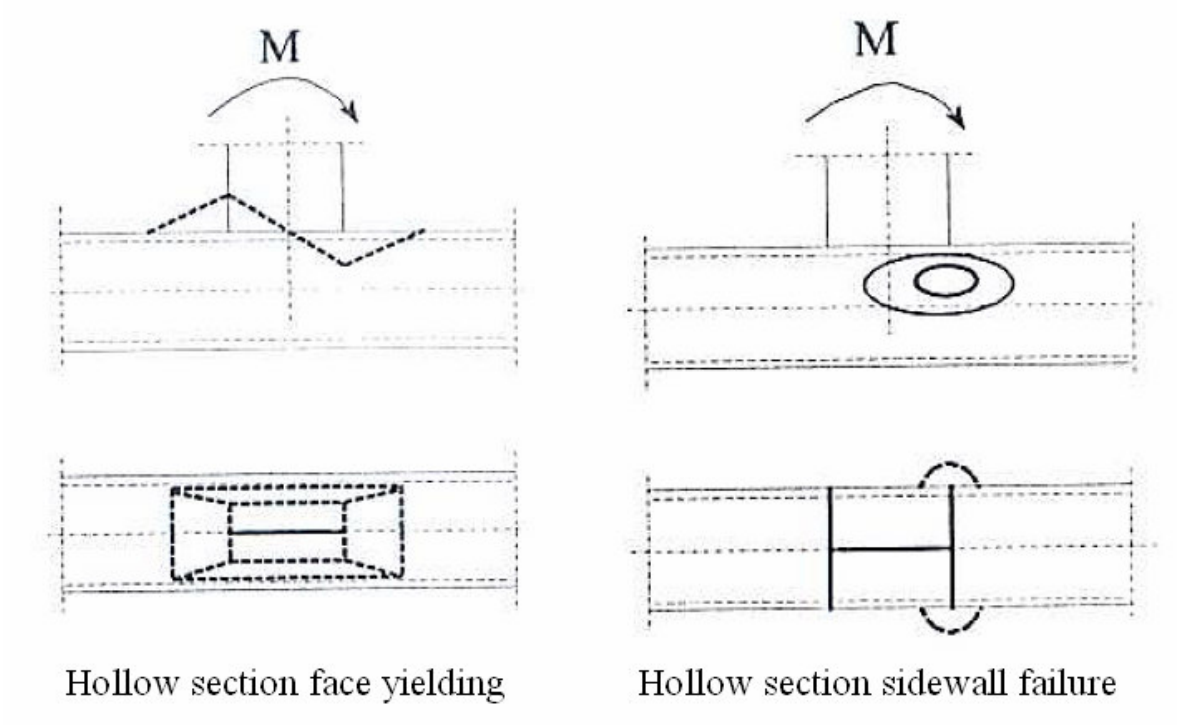

Figure 2.4. Failure modes of HS-column face [20]

In order to find out the resistance of the semi-rigid connections, previously Eurocode 3 part 1-1 Annex J [21], now Eurocode 3 part 1-8 [22] offers component method for mainly H and I sections. Table 2.1 summarizes the basic joint components in such connections and related available references. The reference column abbreviations EC and CIDECT refers respectively to Eurocode 3 Part 1-8 [22] and CIDECT Report 5BP-4/05[17]. The column components related to the flange face bending of HS are completely different than H and I-sections because flange face of HS is supported at both sides whereas in H and I sections the flange is supported in the middle by the web. Other column components might be adapted by small modifications for HS. Therefore for HS sections there is a need of research to identify HS column face in bending and HS face reinforcement by backing plate components.

The proposed connection was examined in two phases. In the first phase component tests were carried out to observe the behaviour of the hollow section face in bending by focusing on the stiffness and strength properties. In order to measure the performance of the proposed connection, sub-assemblage tests were carried out in the second phase under monotonic and cyclic loading conditions.

Table 2.1. Joint components of I-beam to HS-column connection with t-stub

Component	Component Number or Related Chapter in the Reference		Notes
	EC	CIDECT	
SHS column web panel in shear	1	A1	shall be adapted
SHS column sidewall (web) in transverse compression	Chapter 7.5	A34-A35	no sufficient information available for stiffness
SHS in transverse compression - face failure in bending	-	A32	Not covered by EC, CIDECT proposal is limited
Backing plate in bending	4	-	Stiffness not covered
T-stub in bending	6	A6	EC covers
Beam flange in compression	7	A7	EC covers
Bolts (partially threaded studs) in tension	10	A10	EC covers
Bolts in shear	11	A11	EC covers
Plate in bearing (plate in general, beam flange or web, column flange or face, end-plate, cleat or base plate)	12	A12	EC covers

2.2. Material Properties of the Test Specimens

Connection configuration and geometry have been preferred in order to represent the common practice which is especially applied in Europe and in the USA. In particular, the t-stub and SHS sizes have been chosen in order first to obtain a semi-rigid partial strength connection, where t-stub is the weakest component, and secondly to observe the effect of the column face flexibility to the connection performance.

Tee joint test specimens consisted of IPE 270 beam section joined to 200x10 mm square hollow section by means of bolted t-stub connecting elements which was fabricated out of split HEB 200 profile. Each top and bottom t-stubs were connected by five long partially threaded M 16 studs in two rows through the column and by six M16x45 bolts to the beam flanges. The thread lengths of the bolts were chosen such that the shear plane

passes through the unthreaded portion of the bolts. Dimensions of the bolts are given in Figure 2.5. The thickness of the backing plates was 15 mm. Properties of the materials are given in Table 2.2.

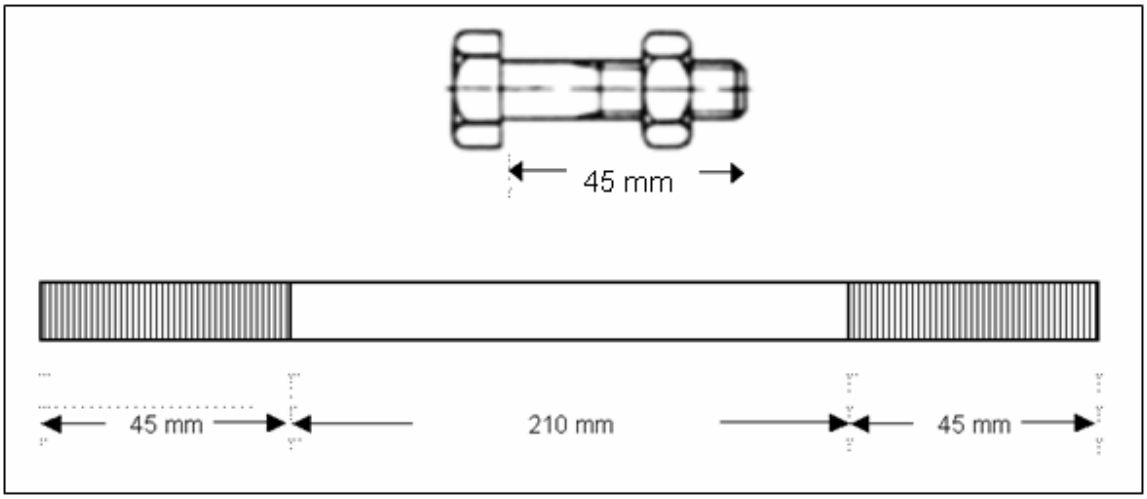

Figure 2.5. Dimensions of hexagon bolt and partially threaded stud

In order to figure out the stress-strain relationships, samples have been taken and coupon tests have been performed according to EN 10002-1: 2001 [23] for each section type, connecting elements in Materials Laboratory in the Civil Engineering Department of Boğaziçi University. Some photos taken during the coupon tests are given in Appendix C. The results of the coupon tests are given in Table 2.3 and Figure 2.6. Since there is no clear yield point for cold formed welded structural hollow sections, threaded studs and electric – welded steel tubes, 0.2% proof stress is normally quoted for yield strength.

Table 2.2. Material properties of the test specimens

Material	**Size**	**Grade**	**Phase I**	**Phase II**
Cold formed welded structural hollow section according to EN 10219-2:1997	SHS 200x200x10 mm	S235JRH according to EN 10219-1:1997	x	x
Hot Rolled Products of Structural Steel	IPE 270	S275JR according to EN 10025-2:2004		x
	HEB 200			x
	Plate 15 mm	S235JR according to EN 10025-2:2004		x
Hexagon Bolts with large widths accross flats for steel structures according to DIN 6914	M16 x 45 mm	8.8	x	x
Hexagon Nuts with large widths accross flats for steel structures according to DIN 6915	Hexagon Nuts			x
Plain washers for steel construction hardened and tempered according to DIN 6916	Plain Washers			x
Partially threaded studs	M16 x 300 x front 45, end 45 mm	8.8		x
Electric – welded steel tubes according to DIN 2394	Tube ϕ21.3 x 2 mm	S235JR according to EN 10025-2:2004	x	

Table 2.3. Mechanical properties of the materials

Sample from	**Yield Strength (N/mm2)**	**Tensile Strength (N/mm2)**	**% elongation**
SHS 200x200x10	253	409	25
IPE 270	294	435	21
HEB 200	302	443	31
Plate 15 mm	266	416	33
Partially threaded M16 stud	640	880	11
Tube ϕ21.3 x 2 mm	235	320	20

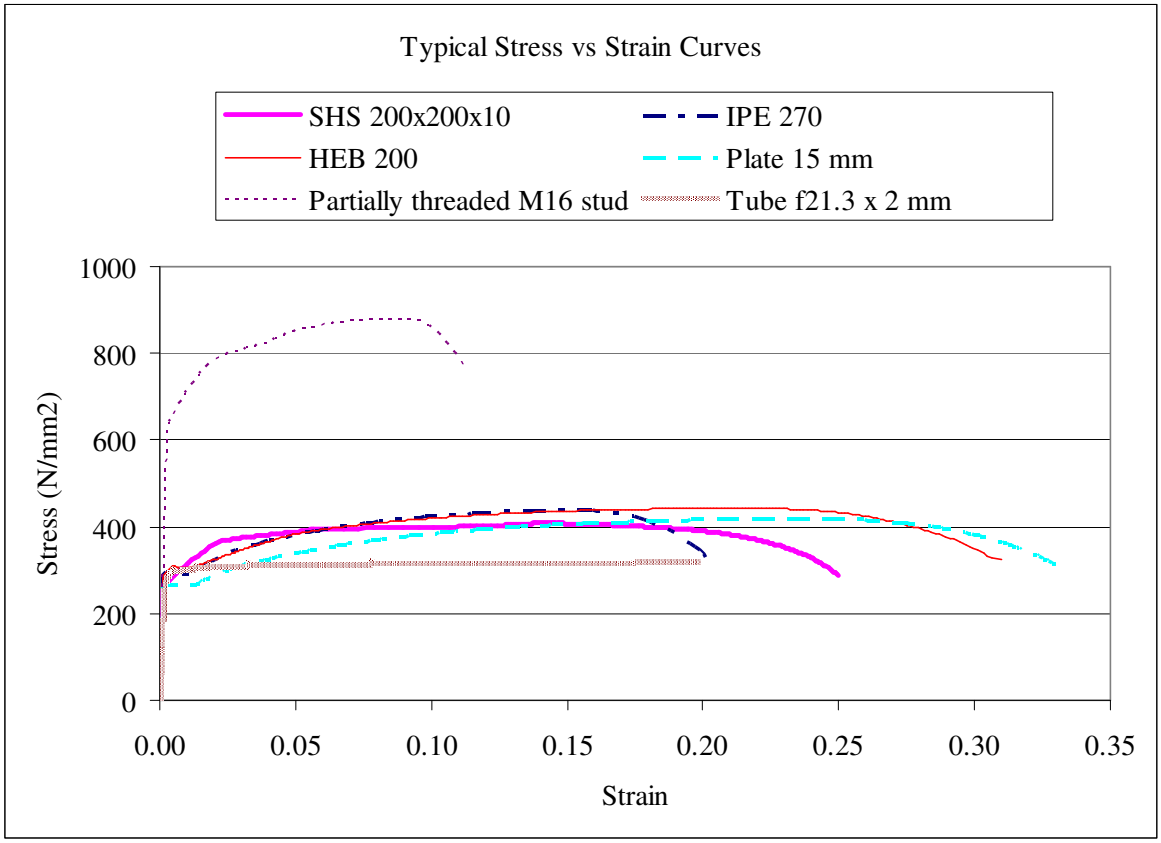

Figure 2.6. Typical stress vs strain curves of the materials

2.3. Phase I – Component Tests

2.3.1. Test Setup and Instrumentation

All tests have been performed at Structures Laboratory in the Civil Engineering Department of Boğaziçi University.

The SHS face have been pushed inside by using plates in different dimensions (P-type of specimens) or six bolts (B-type of specimens) in different spacing configurations. A gradually increased load which is controlled by 1000 kN hydraulic press has been applied upto failure. Photographic views of the test setup are presented in Appendix C. As shown in Figure 2.7 to Figure 2.9, several LVDT and dial gauges have been used to measure the necessary displacements to evaluate the load vs SHS face and sidewall displacements as well as the corner rotation behaviours. 10 mm uniaxial strain gages have been mounted on the test specimens as shown in Figure 2.10. In order to monitor axial and bending strains at the corners of the SHS, strain gages have been placed at both inner and outer faces of these locations. All data were collected with a 50 Hz data acquisition box. The evaluation of the displacements is described in Appendix A.

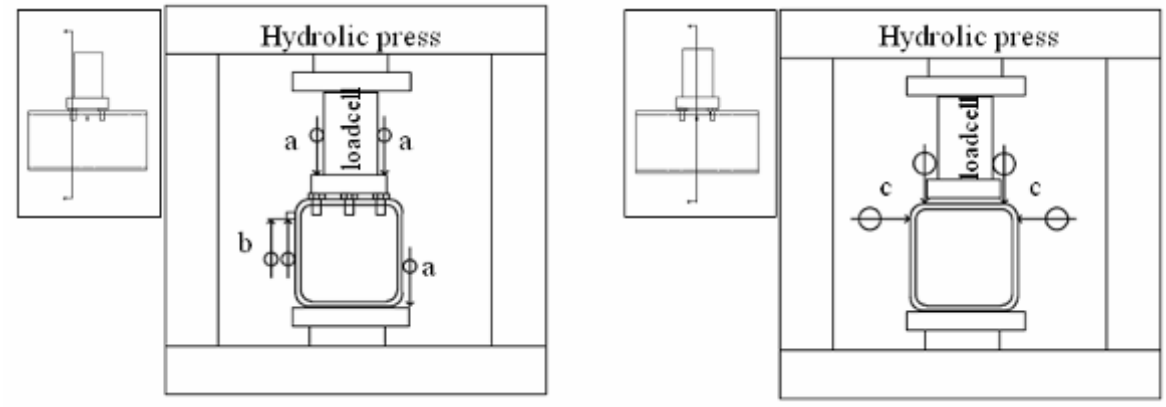

Figure 2.7. LVDT and dial gage locations of B-type of specimens

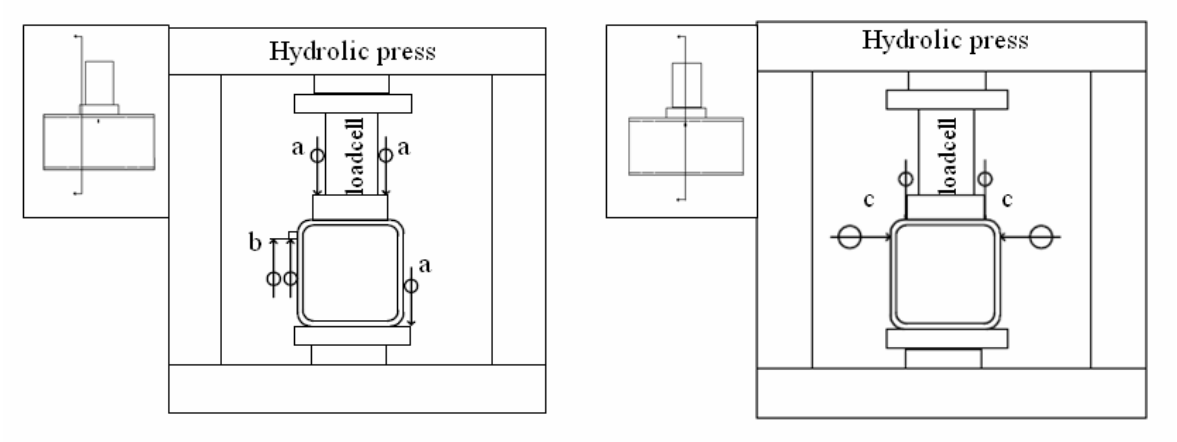

Figure 2.8. LVDT and dial gage locations of P1-type of specimens

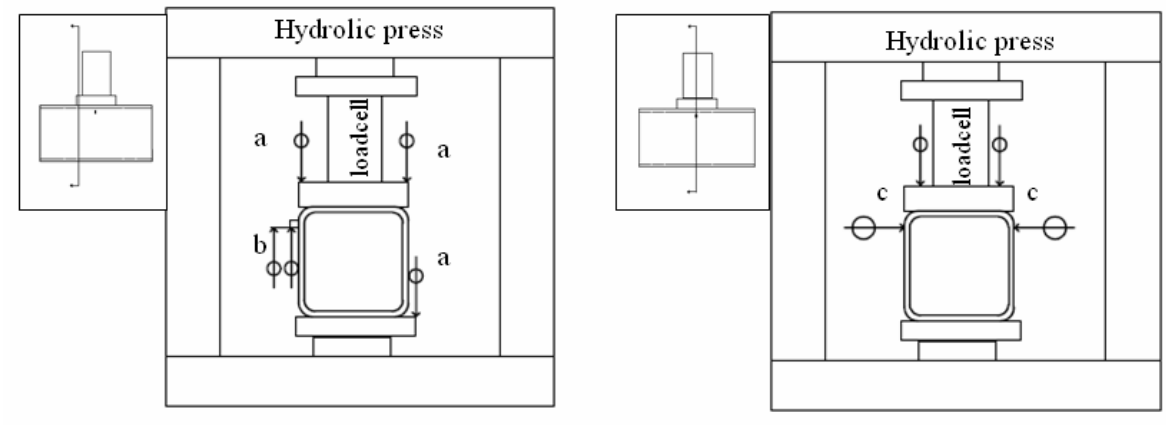

Figure 2.9. LVDT and dial gage locations of P2-type of specimens

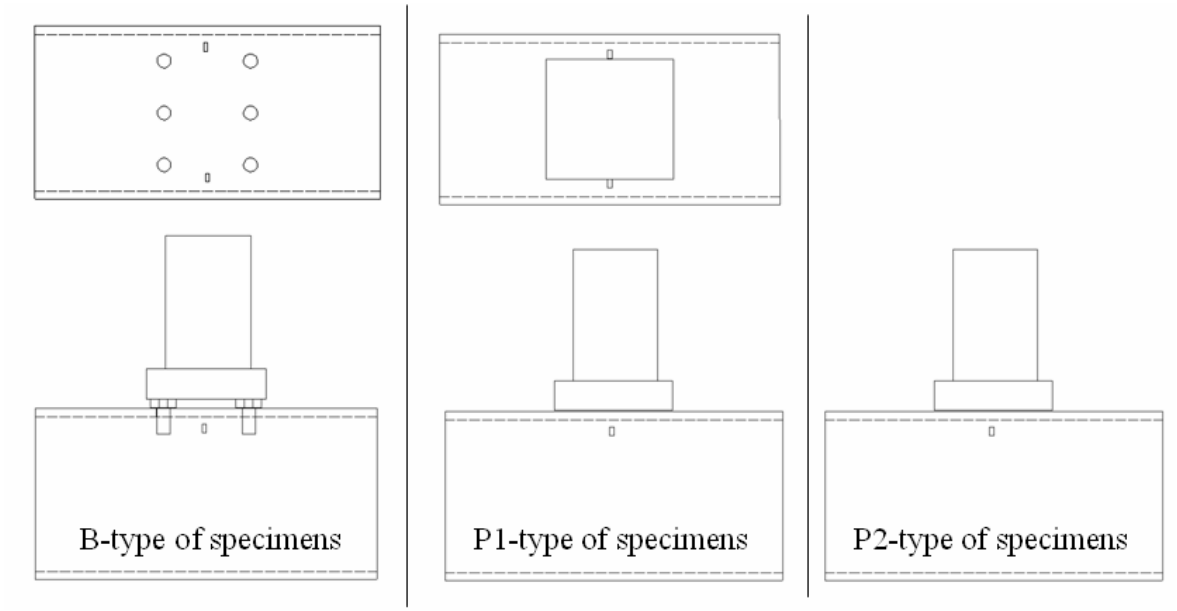

Figure 2.10. Strain gage locations of B and P type of specimens.

2.3.2. Test Procedure

As far as the loading history is concerned, Complete Testing Procedure provided by ECCS Recommendations [24] has been applied in order to follow the specimen up to complete failure with increasing amplitude deformations.

Classical monotonic load increase test has been applied by hydraulic press. In particular, initial stiffness, yielding push thru load capacity and ultimate push thru load capacity have been evaluated.

2.3.3. Test Parameters

In order to observe the behaviour of SHS face in bending, six bolts has been pushed inside the columns face. The configuration of the bolt locations have been chosen both to be incompatible with the sub-assemblage test (phase II) configuration and taking into account the other bolting possibilities. Referring to Figure 2.11, the bolt configurations are

defined as “a x b1/b2/b3/b4” in Table 2.4. HS face reinforcement by backing plates has also been studied by plate push thru the SHS face tests. B and P type of specimens have been prepared in two sets.

There is also another reinforcing way of SHS face which is by connecting the holes with tube. In this case ϕ21.3x2 mm tube has been used considering the M16 bolt size. Additional compression test has been performed on single ϕ21.3 mm tube to obtain the stiffness and capacity levels. The configurations of all specimens are given in Table 2.4.

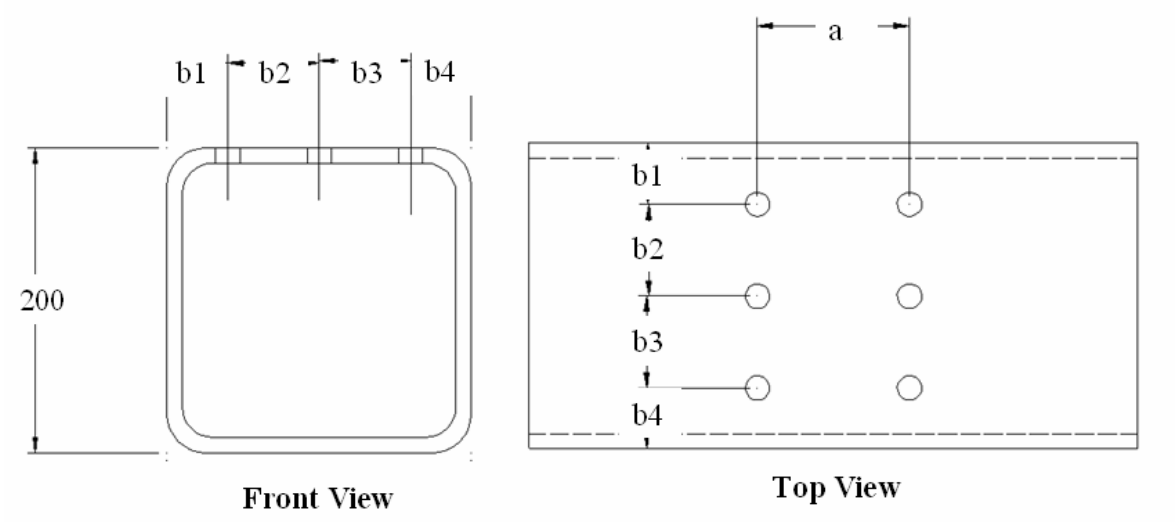

Figure 2.11. Phase I - bolt locations

Table 2.4. Specimen configurations of phase I – component tests

Experiment	Definition	Material
Phase I - B1	125 mm x 50/50/50/50	SHS 200x200x10 mm
		Bolts M16
Phase I - B2	125 mm x 40/60/60/40	SHS 200x200x10 mm
		Bolts M16
Phase I - B3	135 mm x 50/50/50/50	SHS 200x200x10 mm
		Bolts M16
Phase I - B4	135 mm x 40/60/60/40	SHS 200x200x10 mm
		Bolts M16
Phase I – B5	100 mm x 40/60/60/40	SHS 200x200x10 mm
		Bolts M16, M20
Phase I - P1	plate push thru	SHS 200x200x10 mm
		Plate 20x200x140 mm
		Plate 30x200x140 mm
Phase I - P2	plate push thru	SHS 200x200x10 mm
		Plate 20x200x200 mm
		Plate 30x140x200 mm
Phase I - Tube	Compression of tube	Tube ϕ 21.3x2 mm

2.4. Phase II – Subassemblage Test

2.4.1. Test Setup and Instrumentation

All tests have been performed at Structures Laboratory in the Civil Engineering Department of Boğaziçi University.

Test specimens are subassemblages as shown Figure 2.12. Tee-joints are representative of outer joints in a real framework. The height of the column is chosen so that it represents roughly the depth of one storey. The beam is connected at mid-height of

the column so that the ends of the latter may be considered as points of contra flexure in the columns of a sway frame subject to horizontal loads. In semirigid connections high rotation levels are expected. Therefore the length of the beam is chosen based on the expected deformability of the connection. Bending in the beam is produced by displacement controlled point load applied at the end of the cantilever. Bending in the column as a result of the loading of the beam will be produced by the horizontal pin support reactions at the ends of the column. Since the objective of the study is to focus on the connection behaviour, axial load simulating the gravity loads of the upper floors is not applied on the column element. The beam is prevented to move in transverse direction by lateral supports. Photographic views of the test setup are presented in Appendix C.

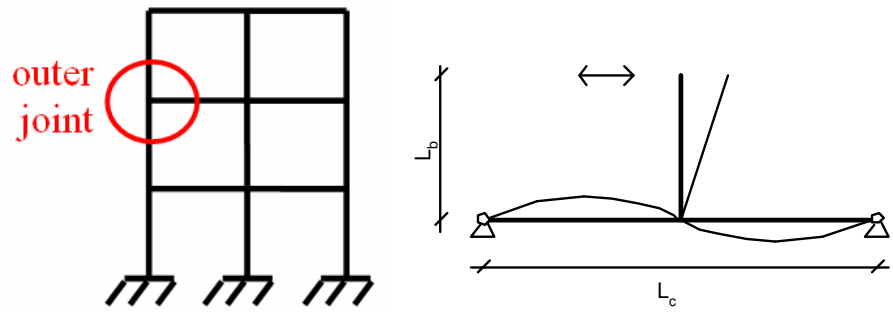

Figure 2.12. The sub-assembly

The length of the beam (L_b) is decided to be 910 mm. Considering the stroke capacity (d) of 100 mm in one direction under cyclic loading (see Figure 2.13), by simple geometric calculation, the maximum prying displacement of 29 mm ($dx270/L_b$) or roughly about 0.1 rad rotation which is sufficient to achieve the plastic rotation.

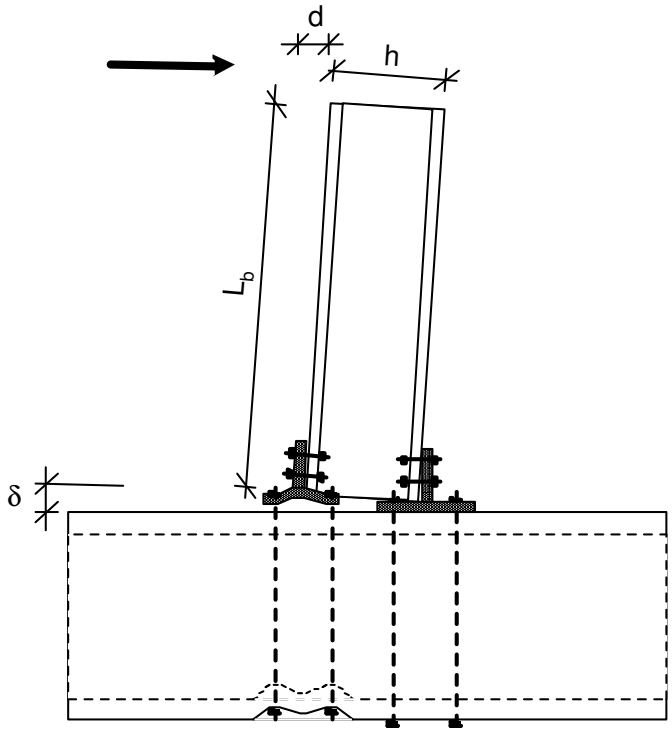

Figure 2.13. Connection sub-assembly

A closed loop double acting actuator with a load capacity of 250 kN and 200 mm stroke capacity has been used in testing. The available 2000 kN capacity reaction wall and out-of-plane frames are parts of the test setup. Top view of the test setup and the directions are presented in Figure 2.14.

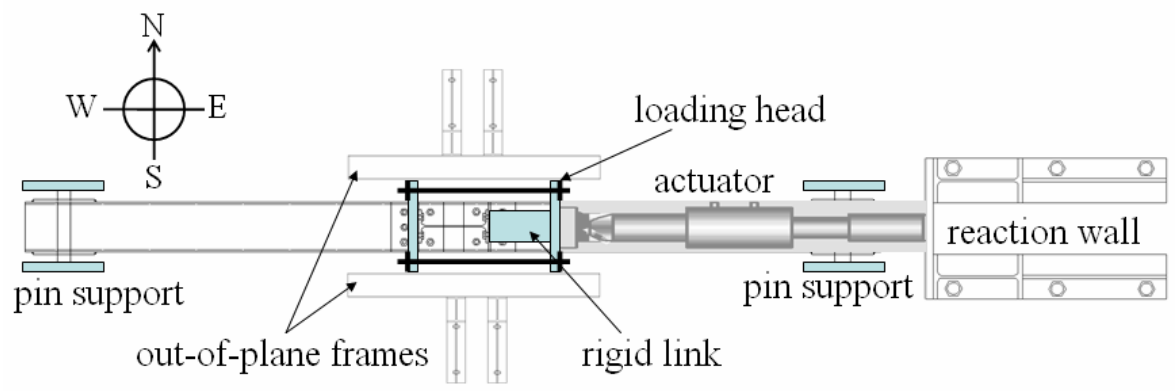

Figure 2.14. Top view of the test setup

The tests are instrumented so that the measurements allow for determining the amplitude of all the components of the joint deformability at any level of the loading. It is useful to perform measurements of horizontal and vertical displacements as well as of rotations in appropriate sections. For this purpose, several LVDT and dial gauges has been mounted on the test specimens as given in Figure 2.15 in order to measure;

- horizontal displacements at the loading level on the beam;
- vertical and/or horizontal displacements at the pin support locations on the column (in order to measure the support settlements);
- beam, column and joint rotations;
- rotation due to the slip at the junction of t-stub-beam flange;
- rotation due to the slip at the junction of t-stub-column face;
- rotation due to deformation of the column face (including rotation associated to the load introduction deformability of column sidewall);
- rotation due to deformation of the t-stub;

10 mm uniaxial strain gages have been installed at beam flange close to the connection and at each partially threaded stud which would be under tension during monotonic testing as given in Figure 2.17. In order to monitor the strains on the t-stub, 10 mm uniaxial strain gages have been installed at each bolt lines of the bolts connecting t-stub to the beam flange and in between the bolts connecting t-stub to the column flange. 10 mm triaxial strain gages have been installed in order to monitor the shear strains in the panel zone. All data were collected with a 50 Hz data acquisition box. The evaluation of the displacements and strains is described in Appendix B. Photographic views of the instrumentation are also presented in Appendix C.

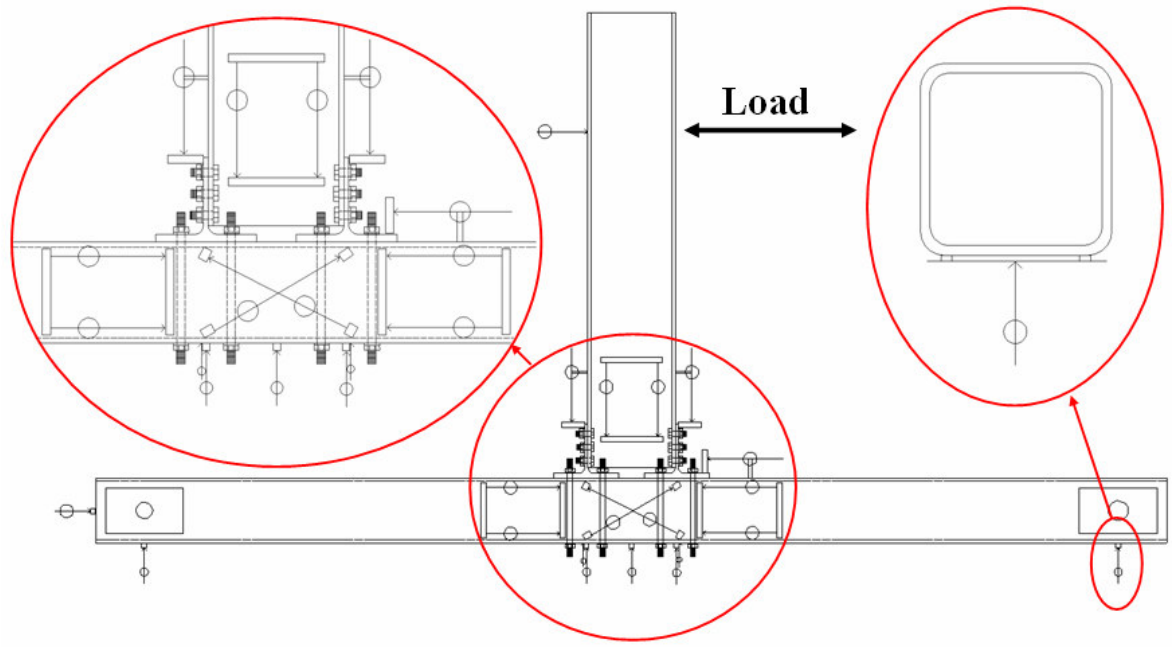

Figure 2.15. LVDT and dial gage locations of T-type of specimens

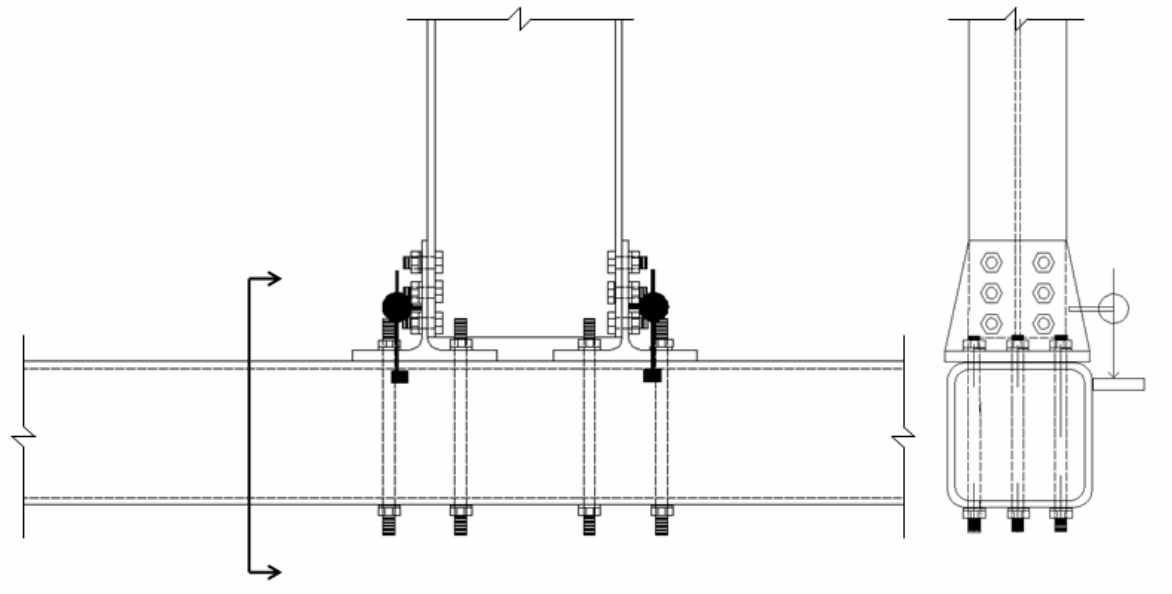

Figure 2.16. Dial gage locations on t-stub

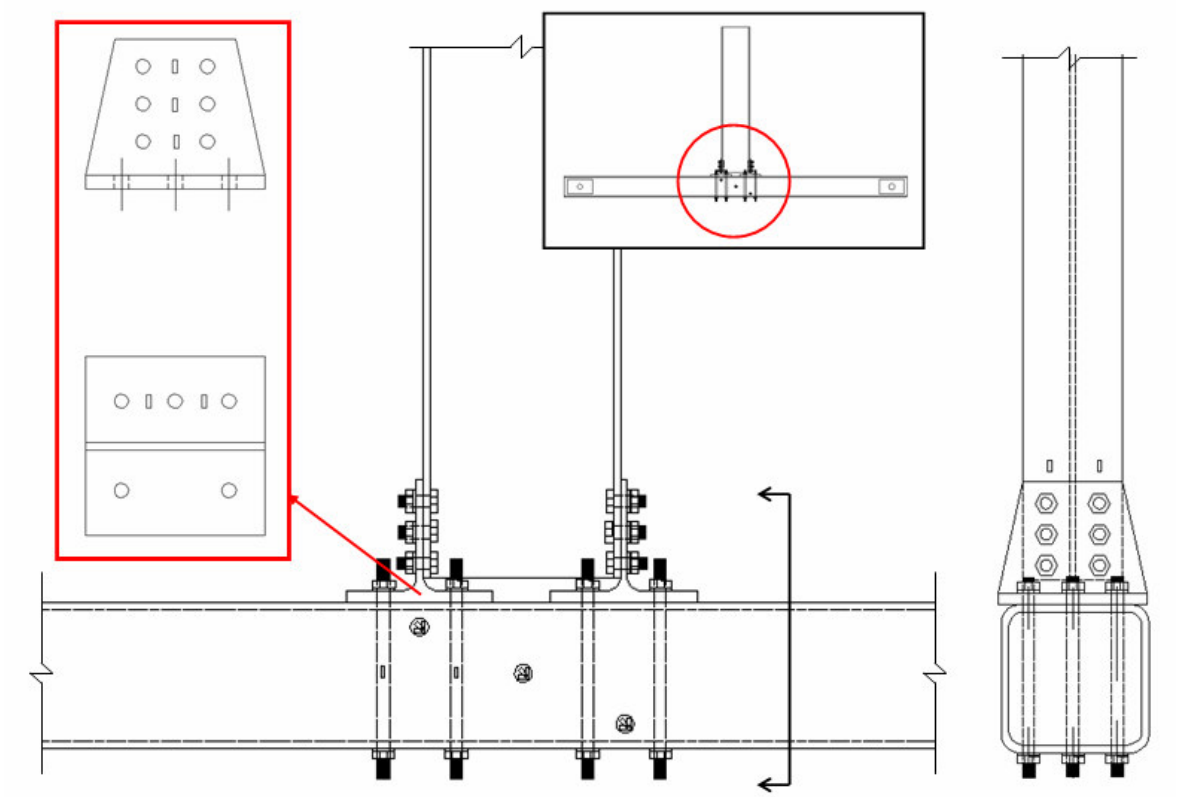

Figure 2.17. Strain gage locations of T-type of specimens

2.4.2. Test Procedure

As far as the loading history is concerned, complete testing procedure provided by ECCS Recommendations [24] has been applied. Since the focus of the study is more on deformability performance of the connection components, the column is not axially loaded in order to simulate the weight of the upper stories.

According to the complete testing procedure, first classical monotonic displacement increase test has to be performed. Such tests allow the actual features of the joints to be more easily and correctly assessed. In particular, initial stiffness, yield load (F_y) and displacement (e_y) can be deduced as shown in Figure 2.18. Besides, failure modes can be compared with the ones concerned with cyclic actions. Since the specimens are symmetrical, there is no need to perform the monotonic test in the other direction.

Subsequently reversed cyclic test with increase of displacement has to be executed with the following cyclic sequence:

- One fully reversed cycle in elastic range for each interval with a semi-amplitude equal to: $e_y/4$, $2e_y/4$, $3e_y/4$, and e_y, where e_y is the elastic yield displacement.
- Then three fully reversed cycles in the $(2+2n)e_y$, where n = 0,1,2,… up to complete specimen failure

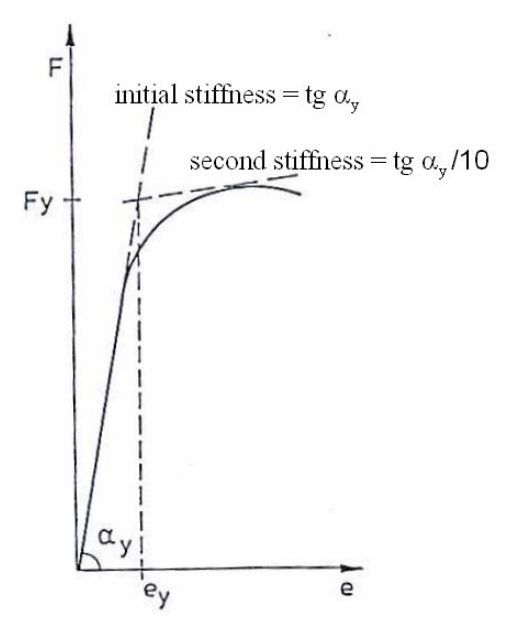

Figure 2.18. Evaluation of stiffness initial stiffness, yield load and displacement [24]

2.4.3. Test Parameters

As shown in Figure 2.19, tests have been performed in two steps. Each specimen has been tested in a monotonic way and reversed cyclic way. The reinforcing effect of backing plate to the rear face of the SHS has been observed. When the column face is weak, the prying action of the column face will give flexibility to the connection. By introducing the backing plate stiffener, the column face becomes stiffer than the t-stub and yielding in the t-stub governs. Since the main interest of the study is to observe the performance of I-beams connected to hollow column sections, the parameters are chosen in relation with the column and connecting elements. However, there is also sensitive relation between

t-stub and the beam. Possible yielding of the beam flanges and possible bearing failure at t-stub and beam interface have to be controlled.

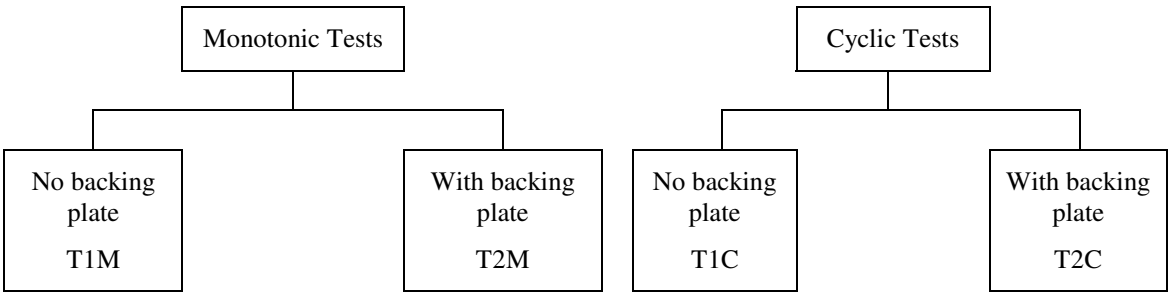

Figure 2.19. Parameters of phase II – sub-assemblage tests

Pre-tensioning of the partially threaded studs is not necessarily needed since as soon as column flange is deforming, the studs lose their pre-tension.

Drawings of the specimens are given in Figure 2.20 to Figure 2.23.

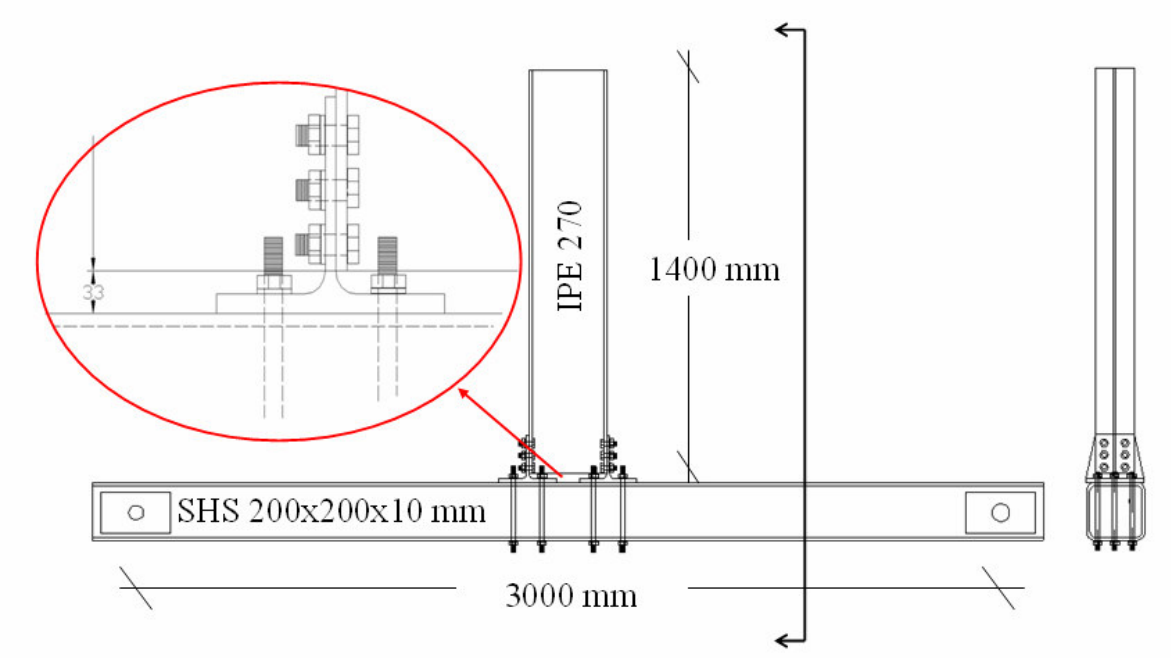

Figure 2.20. Specimen phase II – T1

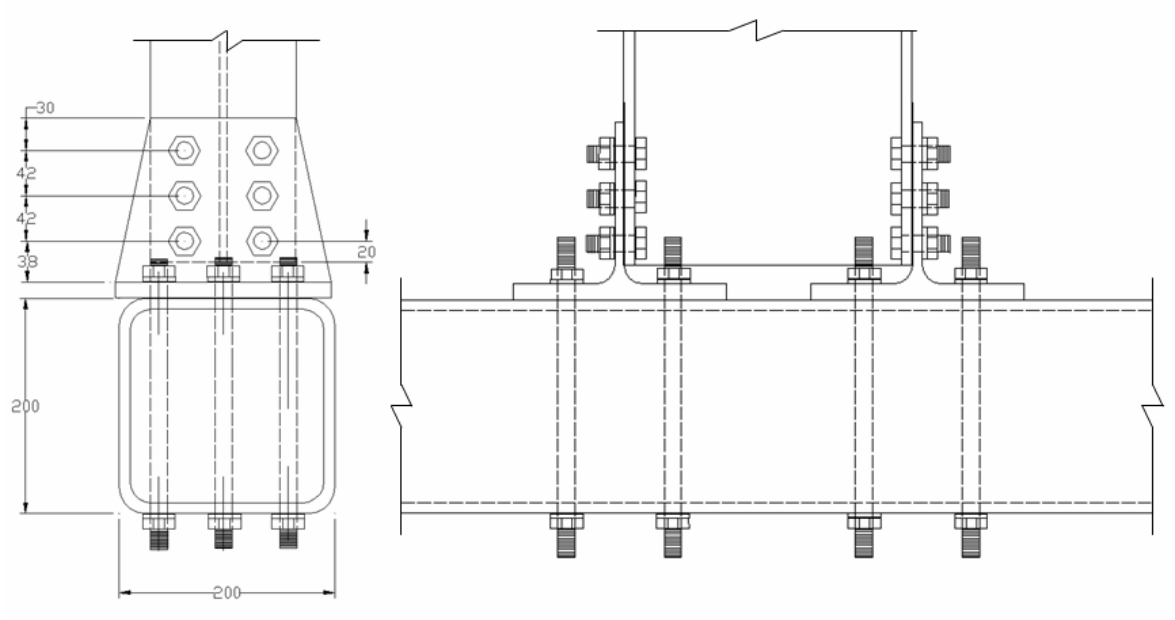

Figure 2.21. Connection detail drawings of specimen phase II – T1

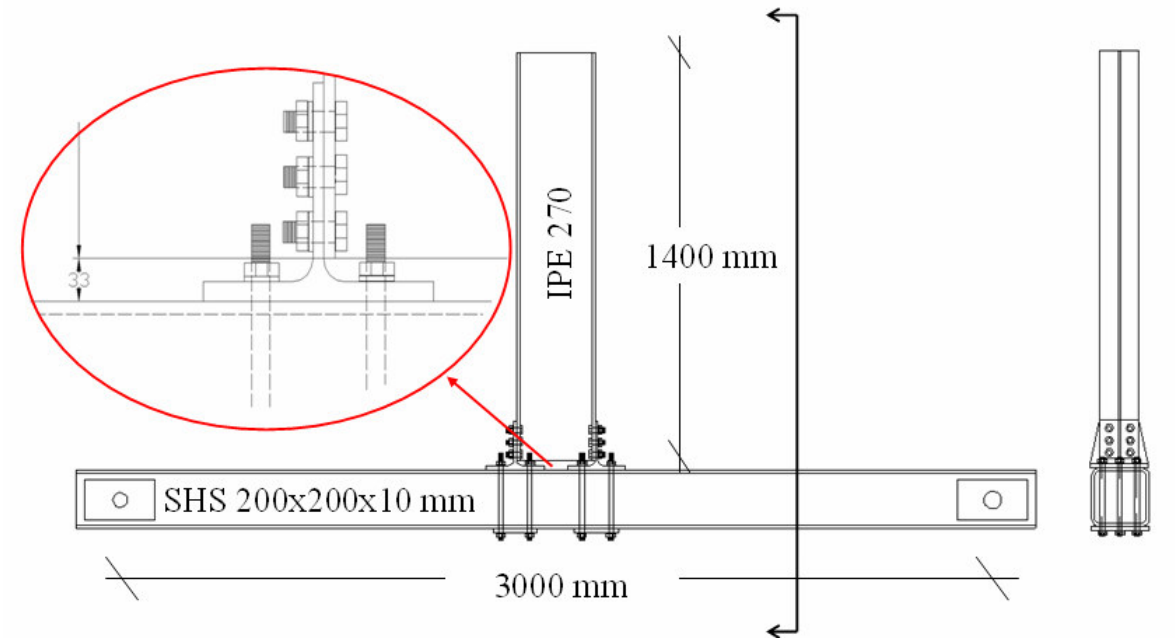

Figure 2.22. Specimen phase II – T2

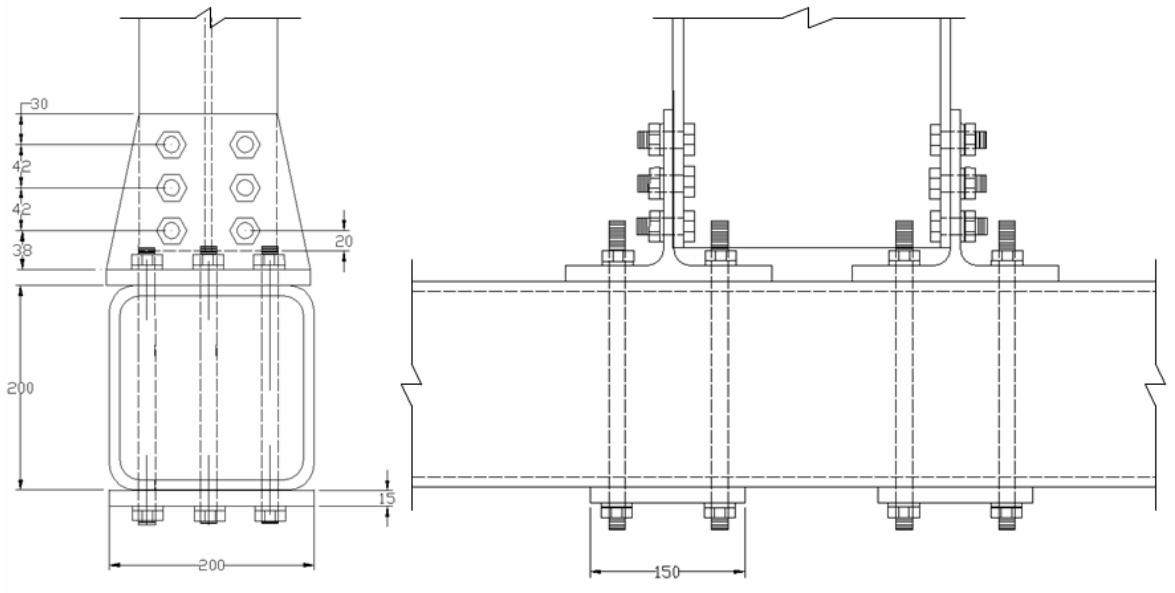

Figure 2.23. Connection detail drawings of specimen phase II – T2

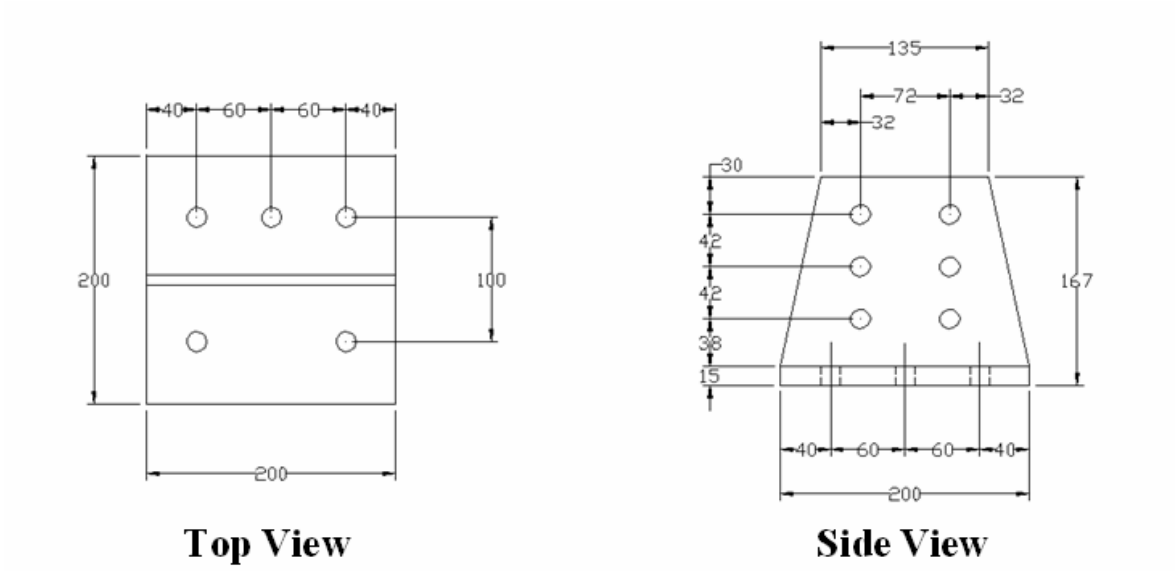

Figure 2.24. T-stub detail drawings of specimens phase II – T1 and T2

The specimens have been produced in fabrication-shop of one of the experienced steelwork contractors in Turkey. Bolt hole diameters have been drilled in 17 mm for M16 bolts and studs. Only at the rear face of specimens T1M and T2M, bolt holes have been drilled in 18 mm diameter in order to allow strain gage cables pass through. After putting in the cables, 18 mm hole have been narrowed by wrapping round the stud with 0.5 mm thin curved steel sheet. Some photos taken during fabrication stage are given in Appendix C.

3. TEST RESULTS

3.1. Phase I – Component Tests

The pilot tests have been done on specimens B1 and P2. Because of the setup the load on the pilot specimen B1 was applied eccentrically. Therefore the test data received from this pilot test was not suitable to use in the study. Pilot test of specimen P2 was gone better but still necessary adjustments were needed on the setup. Hopefully the test data of pilot specimen P2 could be used at least partially. After pilot tests, necessary adjustments on the instrumentation have also been done. During the tests the rigid plates which equally distribute the load over the bolt heads have been slightly deformed as expected. Necessary adjustments have been made during evaluation of the test data by using the related displacement readings.

While evaluating the test data maximum loads have been recorded and yield load have been calculated by the method defined in Section 2.4.2. Axial and bending strains at the top corners of the specimens have been calculated by using the strain values recorded at outer and inner faces as follows:

$$\varepsilon_{axial} = \frac{\varepsilon_{outer} + \varepsilon_{inner}}{2},\ \varepsilon_{bending} = \frac{\varepsilon_{outer} - \varepsilon_{inner}}{2} \tag{3.1}$$

The deformability of the specimen is associated not only with the deformation of the hollow section face but also with the sidewall deformation and the corner rotation. Relative horizontal and vertical displacements of the corners are much smaller compared to the face deformation. By assuming that the corners do not displace or neglecting the corner displacements, the components of deformation can be summarized as shown in Figure 3.1. Therefore, the test data has been evaluated to figure out the influence of these components to the initial stiffness of the specimen. The terms k_s, k_f and k_c refer respectively to initial stiffness of sidewall, face in bending and corner rotation. Similarly δ terms are their

displacements. During the tests although the sidewall displacement records were limited by the dial gage capacities, the records were sufficient for obtaining initial stiffness values.

Photographic views of the specimens before, during and after experiments are presented in Appendix C.

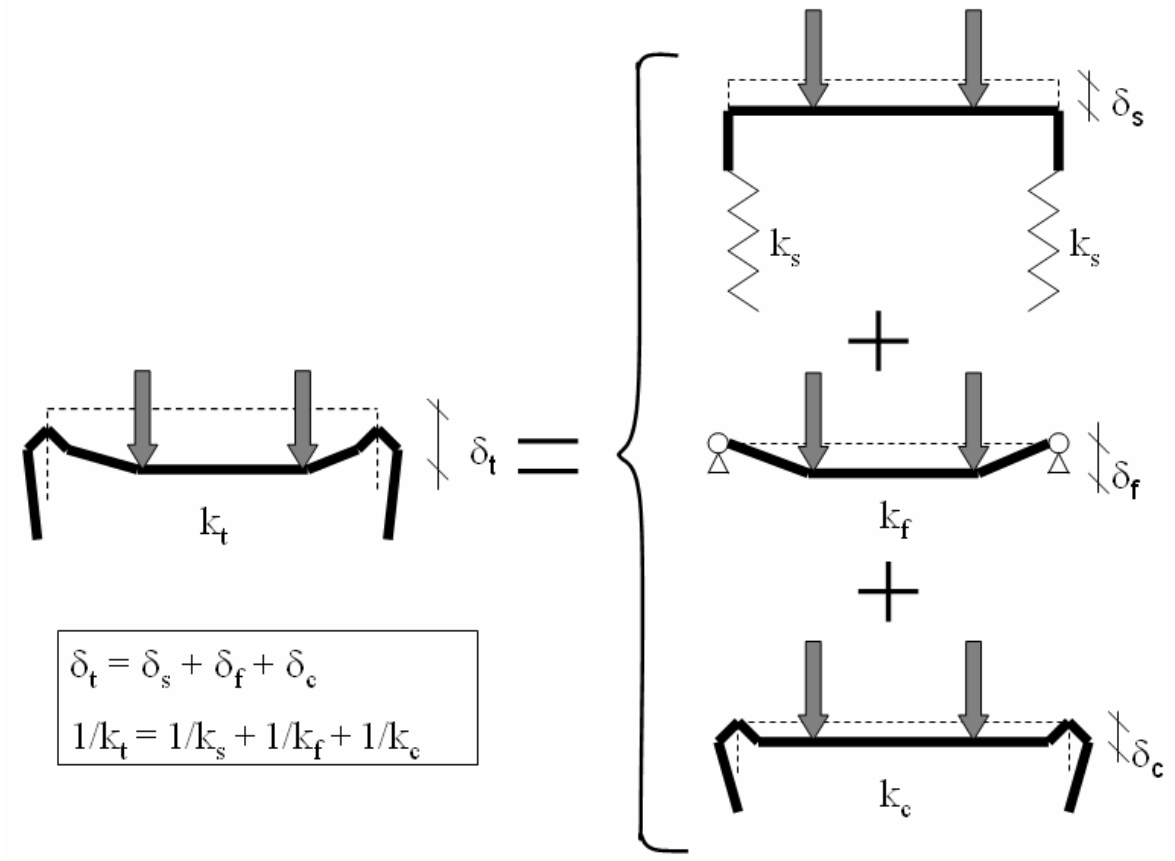

Figure 3.1. Components of the specimen deformation

3.1.1. Test Specimen B1

The specimen has been successfully tested until rigid plate touched the face of the hollow section. The failure mechanism was bending of the SHS top face inside and sidewalls outside.

The load vs displacement behaviour of the specimen B1 is given Figure 3.2. The ultimate load capacity has been recorded in the level of 376 kN and the yield load and the initial stiffness have been calculated as 309 kN and 87 kN/mm, respectively. Components of the specimen deformation and the initial stiffness values of the components are given in Figure 3.3.

Axial and bending strains at the top corners of the specimen are drawn in Figure 3.4 and Figure 3.5. Bending strains improved more rapidly than axial strains. Considering the strain values, first bending strains at the top corner of the sidewall reached 0.002 strains at the load levels of 200 kN. This is followed by bending strains at the top face corner of the specimen which reached yield level at the load levels of 340 kN. While axial strains at the top face corner of the specimen remained lower than 0.002, at the top corner of the sidewall, axial strains reached yield levels just at ultimate load levels.

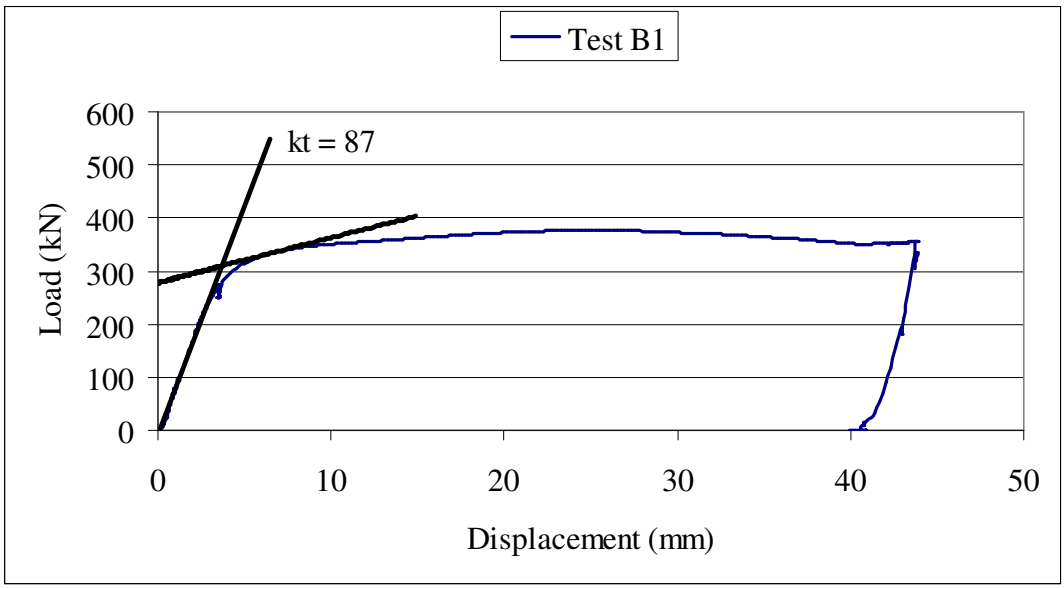

Figure 3.2. Load vs Displacement curve of the specimen B1

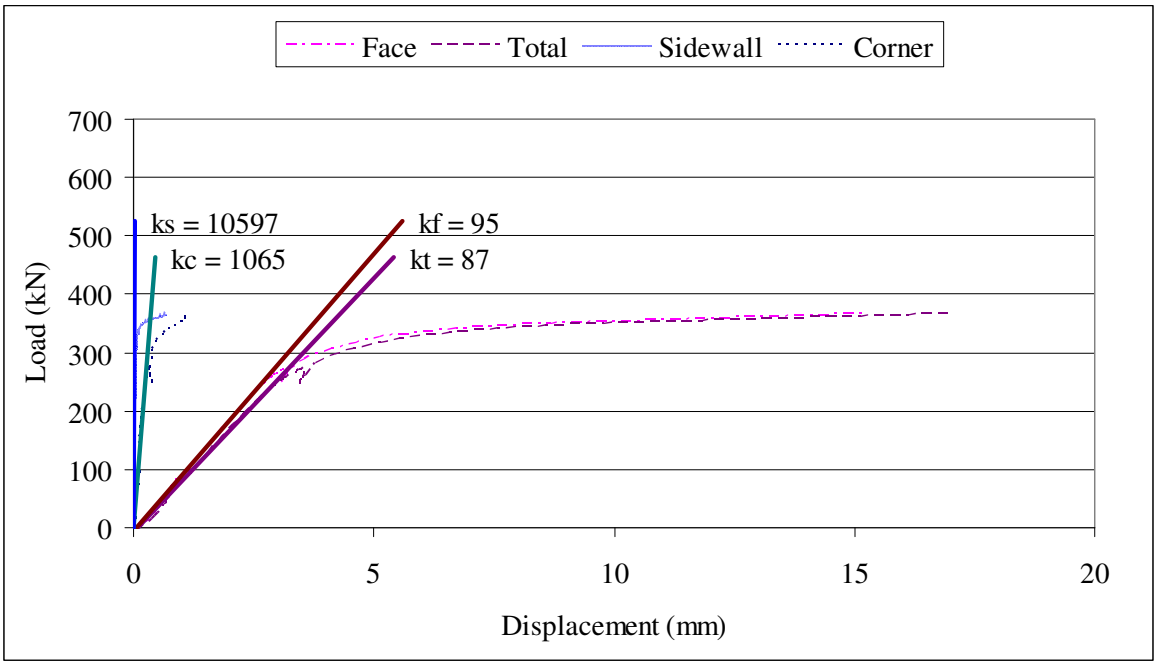

Figure 3.3. Components of deformation of the specimen B1

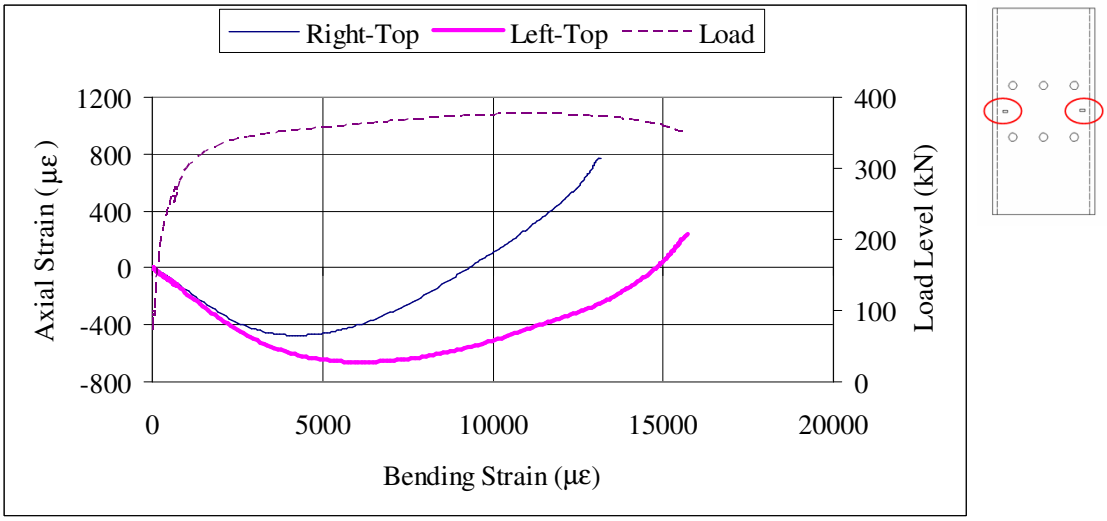

Figure 3.4. Axial and bending strains top face of the specimen B1

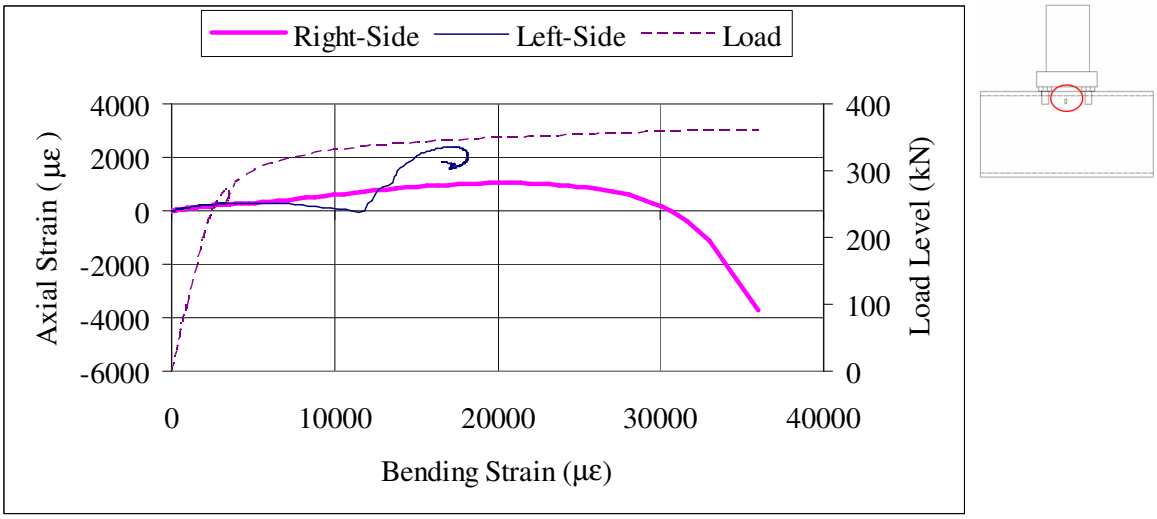

Figure 3.5. Axial and bending strains sidewall of the specimen B1

3.1.2. Test Specimen B2

Two specimens have been successfully tested until rigid plate touched the face of the hollow section for the first test and until the limits of the dial gages for the second one. Strain gages were used only in the first test. Failure mechanisms were bending of the SHS top face inside and sidewalls outside for both of the specimens.

The load vs displacement behaviours of the specimens are given Figure 3.6 and 3.7. The ultimate load capacities for test one and test two have been recorded in the levels of 432 and 444 kN respectively and the yield loads have been calculated as 377 and 393 kN and the initial stiffness 124 and 106 kN/mm, respectively. Components of the specimen deformation and the initial stiffness values of the components are given in Figures 3.8 and 3.9.

Axial and bending strains at the top corners of the specimen are drawn in Figures 3.10 and 3.11. Bending strains improved more rapidly than axial strains. Considering the strain values, first bending strains at the top corner of the sidewall reached 0.002 strains at the load levels of 290 kN. This is followed by bending strains at the top face corner of the specimen which reached yield level at the load levels of 370 kN. While

axial strains at the top corner of the left sidewall remained lower than 0.002, other axial strains reached yield levels just at ultimate load levels.

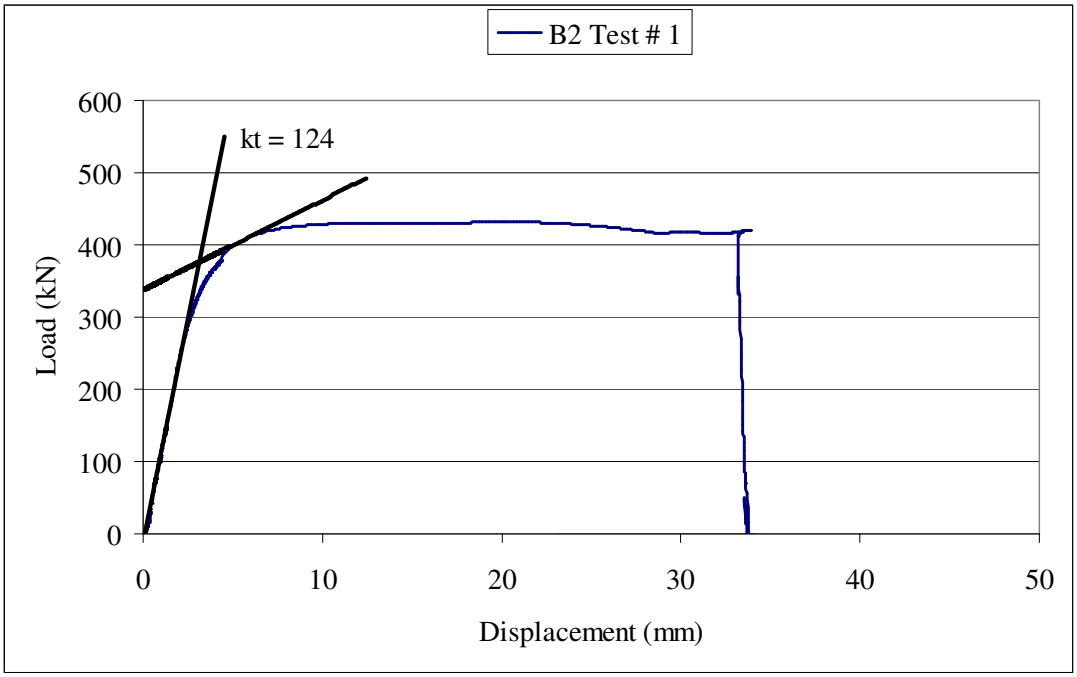

Figure 3.6. Load vs displacement curve of the specimen B2 – test 1

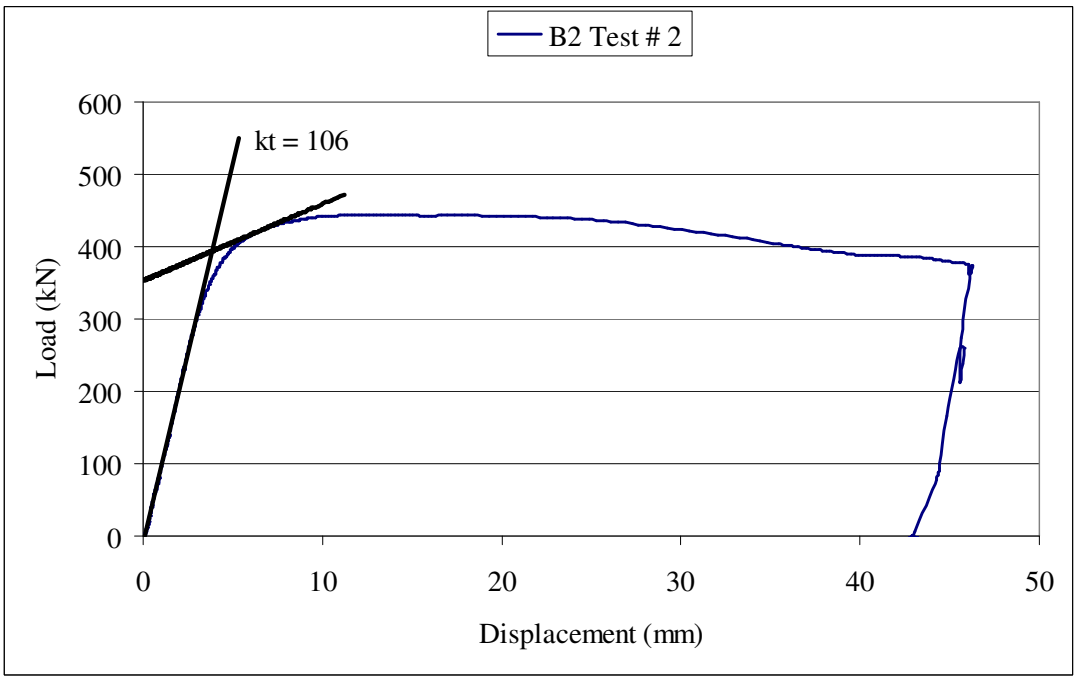

Figure 3.7. Load vs displacement curve of the specimen B2 – test 2

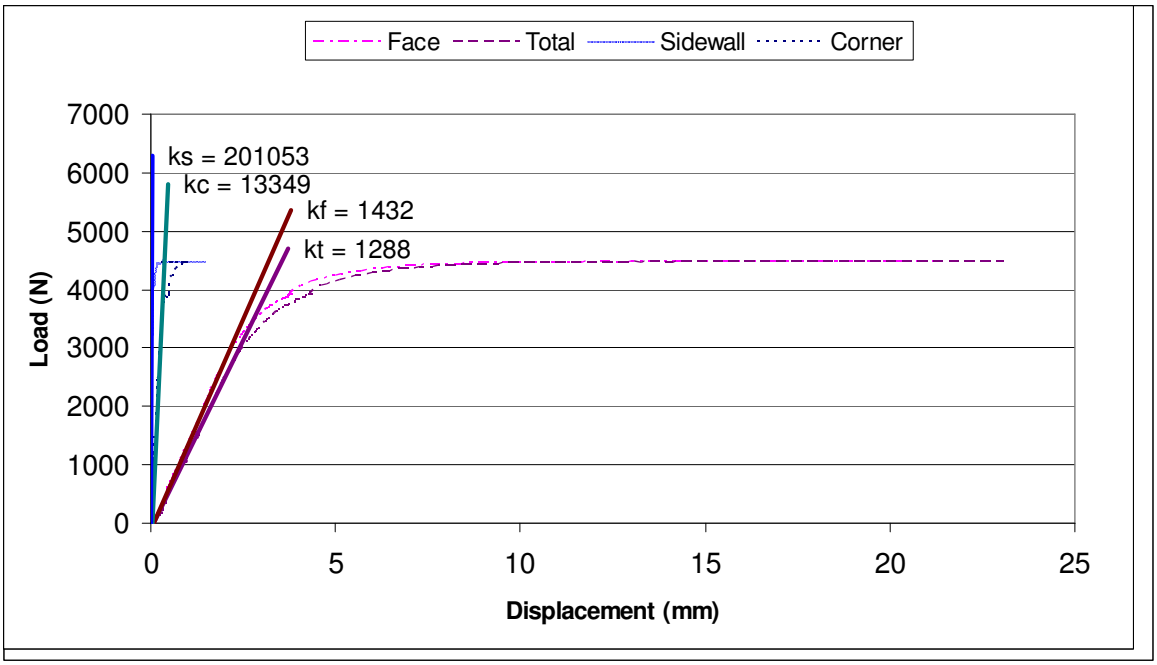

Figure 3.8. Components of deformation of the specimen B2 – test 1

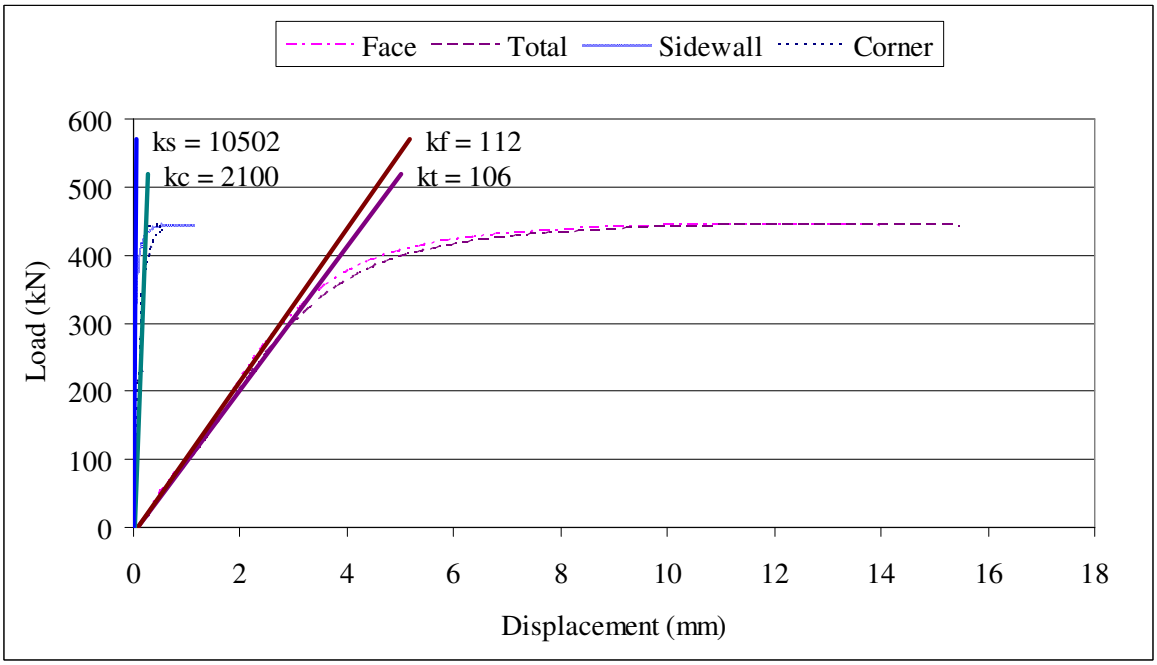

Figure 3.9. Components of deformation of the specimen B2 – test 2

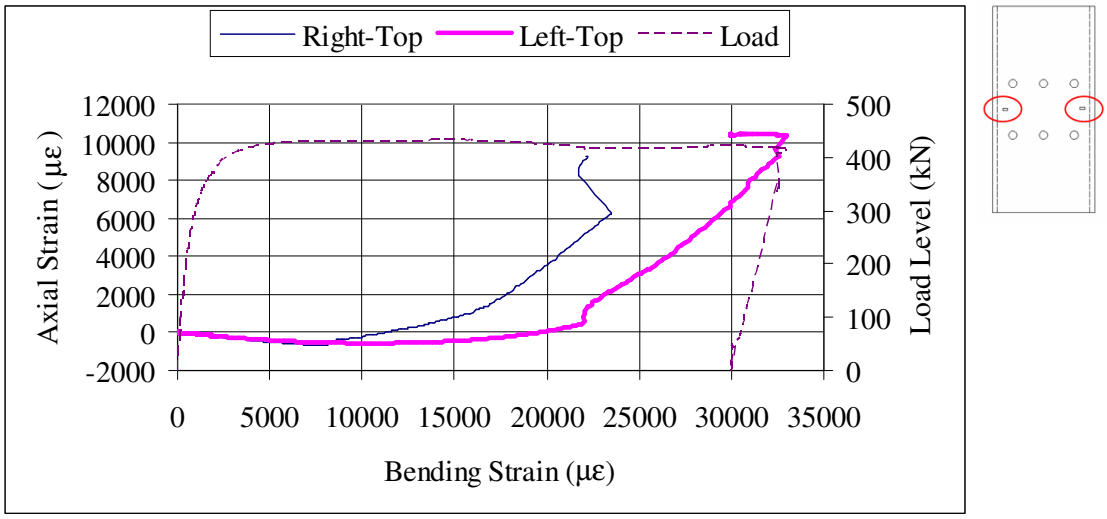

Figure 3.10. Axial and bending strains top face of the specimen B2

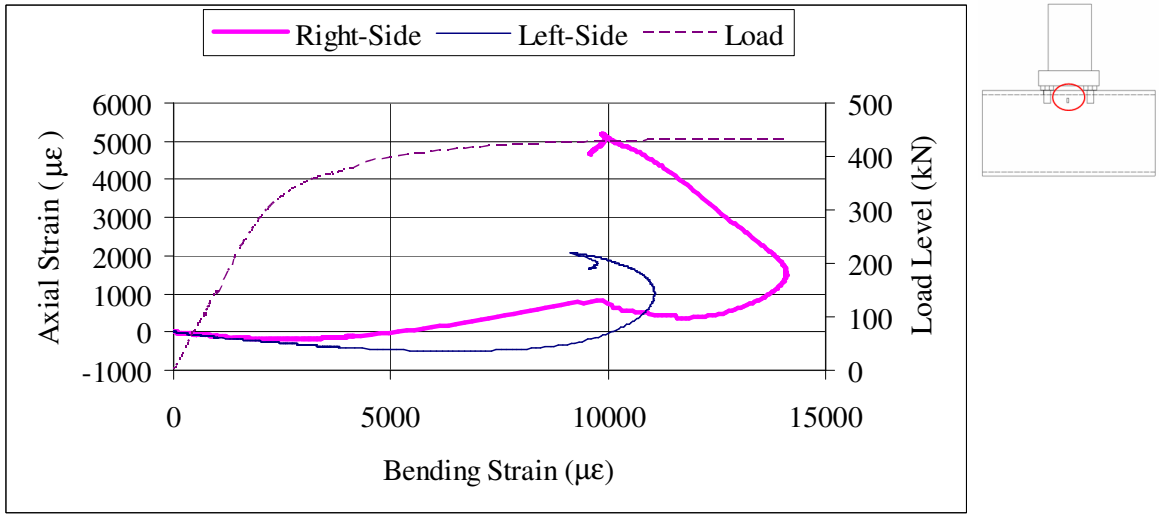

Figure 3.11. Axial and bending strains sidewall of the specimen B2

3.1.3. Test Specimen B3

Two specimens have been successfully tested until rigid plate touched the face of the hollow section. In the first test the rigid plate has been bent in the middle more than expected. In the second test thicker rigid plate has been used. Strain gages were used only

in the first test. Failure mechanisms were bending of the SHS top face inside and sidewalls outside for both of the specimens.

The load vs displacement behaviours of the specimens are given in Figures 3.12 and 3.13. The ultimate load capacities for test one and test two have been recorded in the levels of 366 and 391 kN respectively and the yield loads have been calculated as 298 and 339 kN and the initial stiffness 80 and 68 kN/mm, respectively. Components of the specimen deformation and the initial stiffness values of the components are given in Figures 3.14 and 3.15.

Axial and bending strains at the top corners of the specimen are drawn in Figures 3.16 and 3.17. Bending strains improved more rapidly than axial strains. Considering the strain values, first bending strains at the top corner of the sidewall reached 0.002 strains at the load levels of 210 kN. This is followed by bending strains at the top face corner of the specimen which reached yield level at the load levels of 340 kN. While axial strains at the top face corners of the specimen remained lower than 0.002, at the top corner of the sidewall, axial strains reached yield levels just at ultimate load levels.

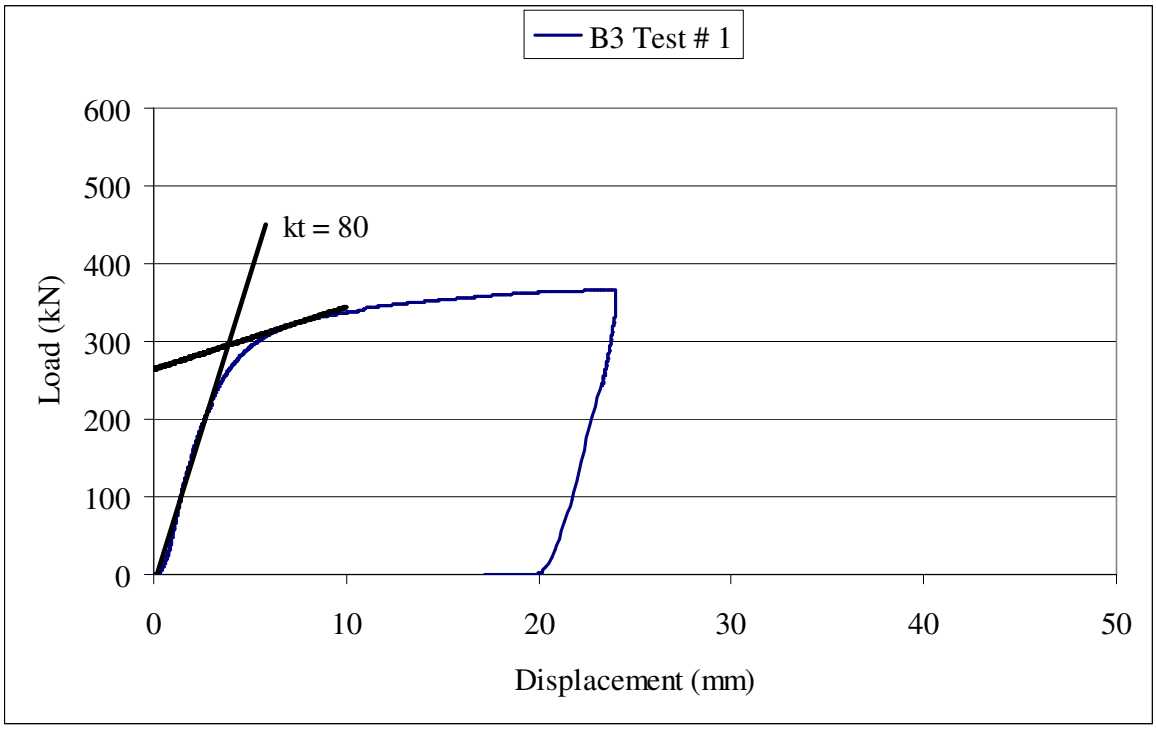

Figure 3.12. Load vs displacement curve of the specimen B3 – test 1

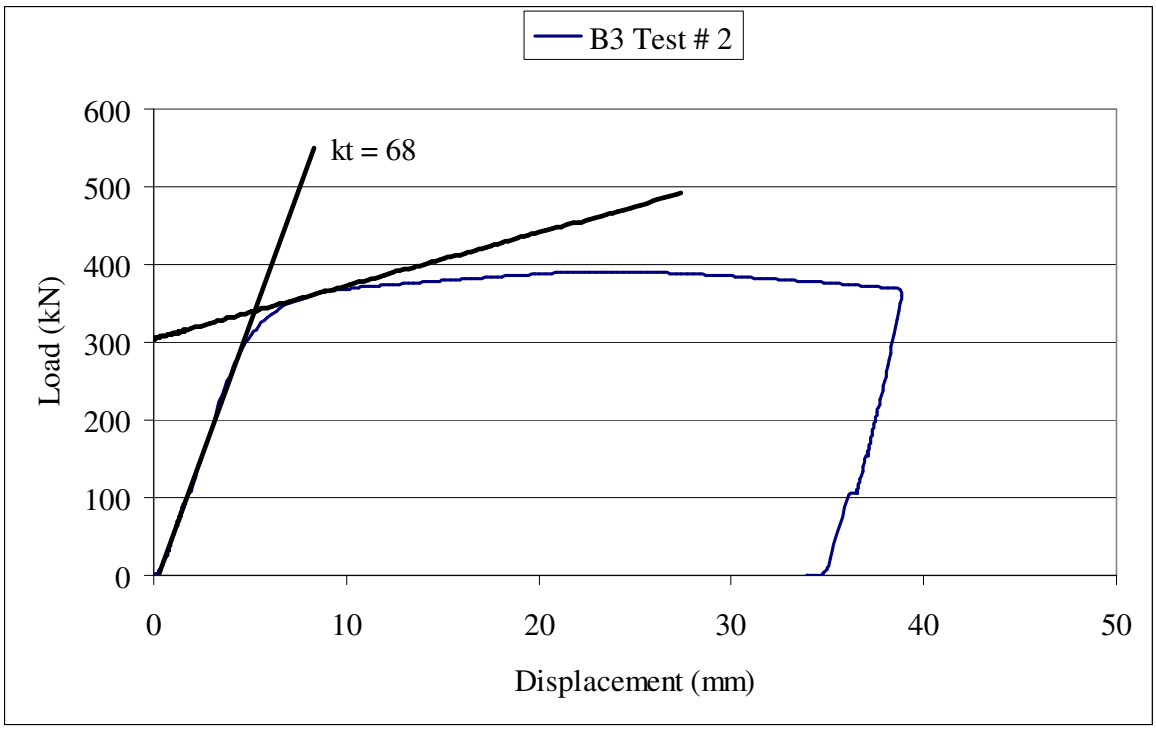

Figure 3.13. Load vs displacement curve of the specimen B3 – test 2

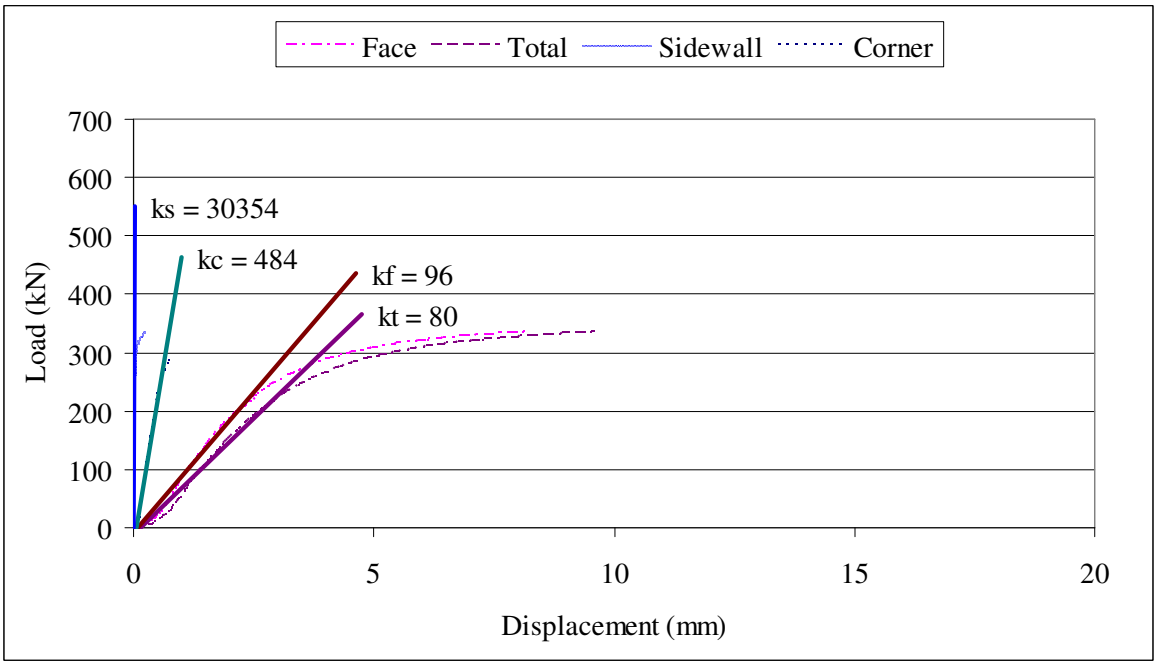

Figure 3.14. Components of deformation of the specimen B3 – test 1

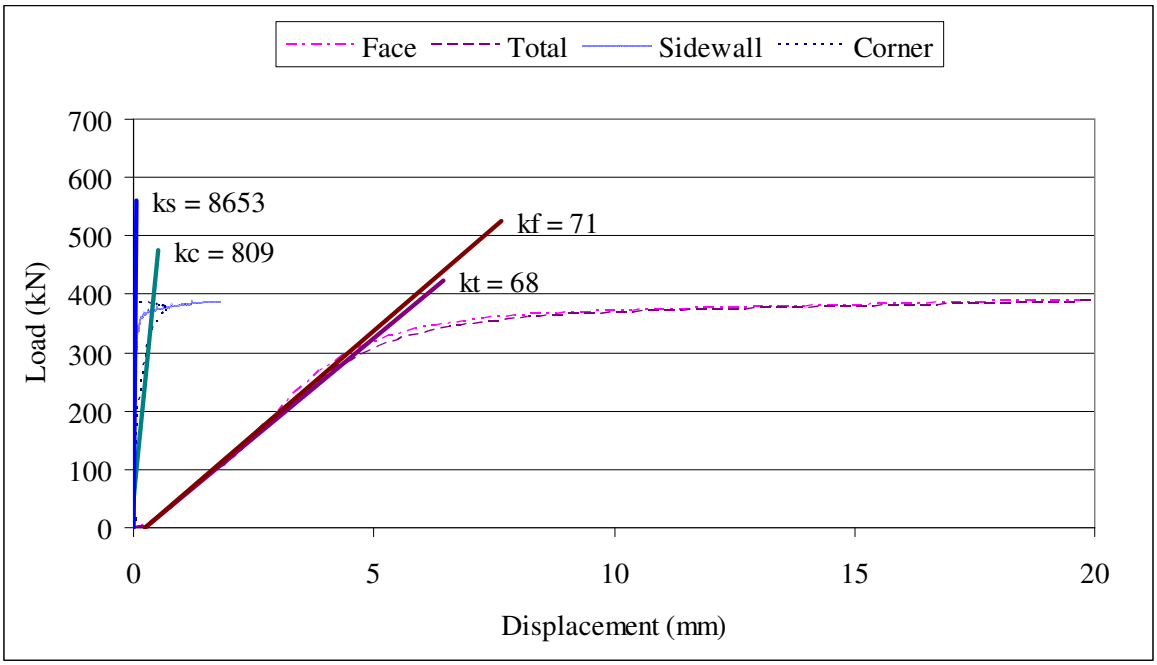

Figure 3.15. Components of deformation of the specimen B3 – test 2

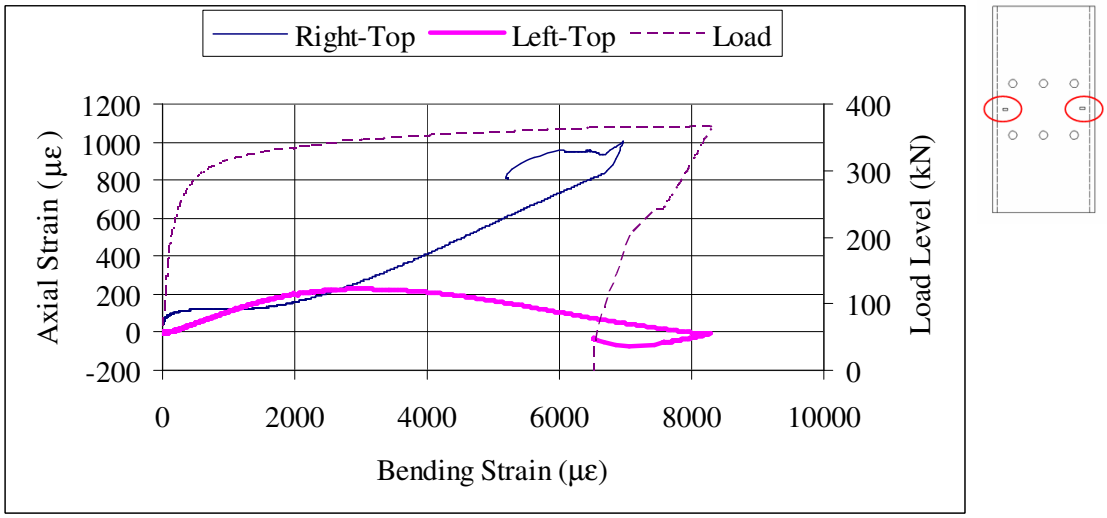

Figure 3.16. Axial and bending strains top face of the specimen B3

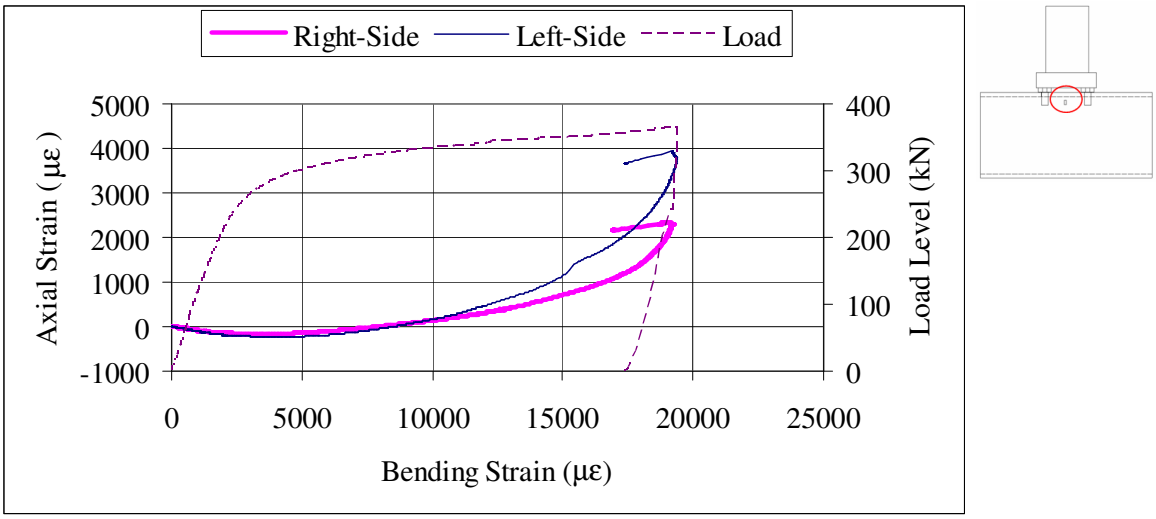

Figure 3.17. Axial and bending strains sidewall of the specimen B3

3.1.4. Test Specimen B4

Two specimens have been successfully tested until rigid plate touched the face of the hollow section. In the first test the rigid plate has been bent in the middle more than expected. In the second test thicker rigid plate has been used. Strain gages were used only in the first test. Failure mechanisms were bending of the SHS top face inside and sidewalls outside for both of the specimens.

The load vs displacement behaviours of the specimens are given Figures 3.18 and 3.19. The ultimate load capacities for test one and test two have been recorded in the levels of 415 and 455 kN respectively and the yield loads have been calculated as 358 and 417 kN and the initial stiffness 108 and 79 kN/mm, respectively. Components of the specimen deformation and the initial stiffness values of the components are given in Figures 3.20 and 3.21.

Axial and bending strains at the top corners of the specimen are drawn in Figures 3.22 and 3.23. Bending strains improved more rapidly than axial strains. Considering the strain values, first bending strains at the top corner of the sidewall reached 0.002 strains at the load levels of 270 kN. This is followed by bending strains at the top

face corner of the specimen which reached yield level at the load levels of 390 kN. All axial strains remained lower than 0.002, even at ultimate load levels.

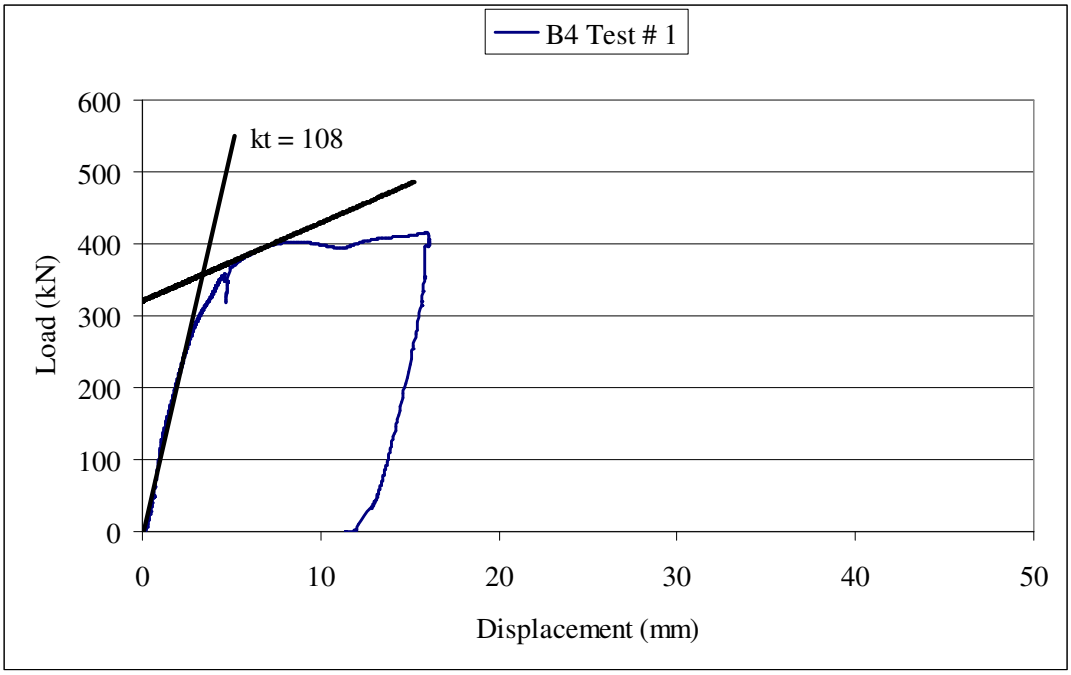

Figure 3.18. Load vs displacement curve of the specimen B4 – test 1

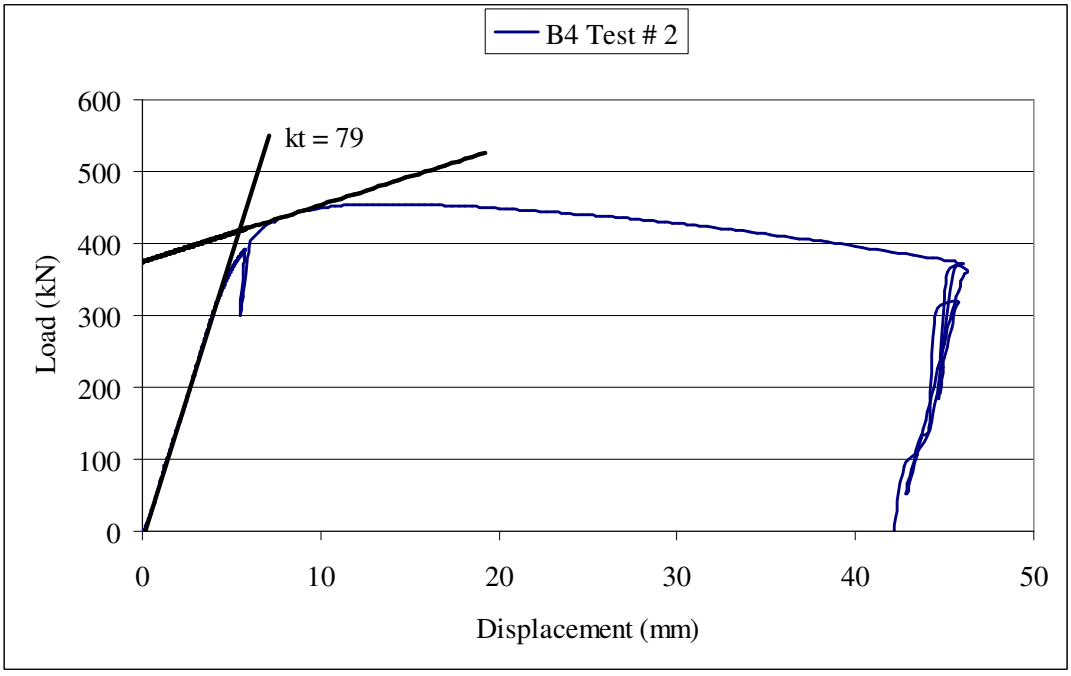

Figure 3.19. Load vs displacement curve of the specimen B4 – test 2

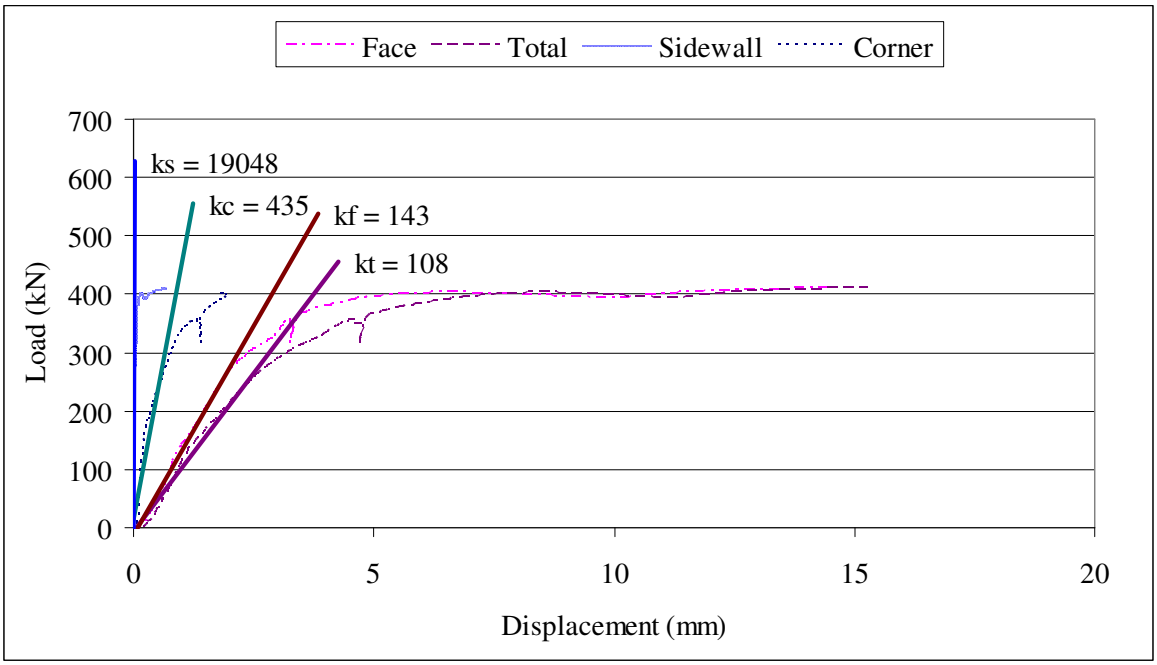

Figure 3.20. Components of deformation of the specimen B4 – test 1

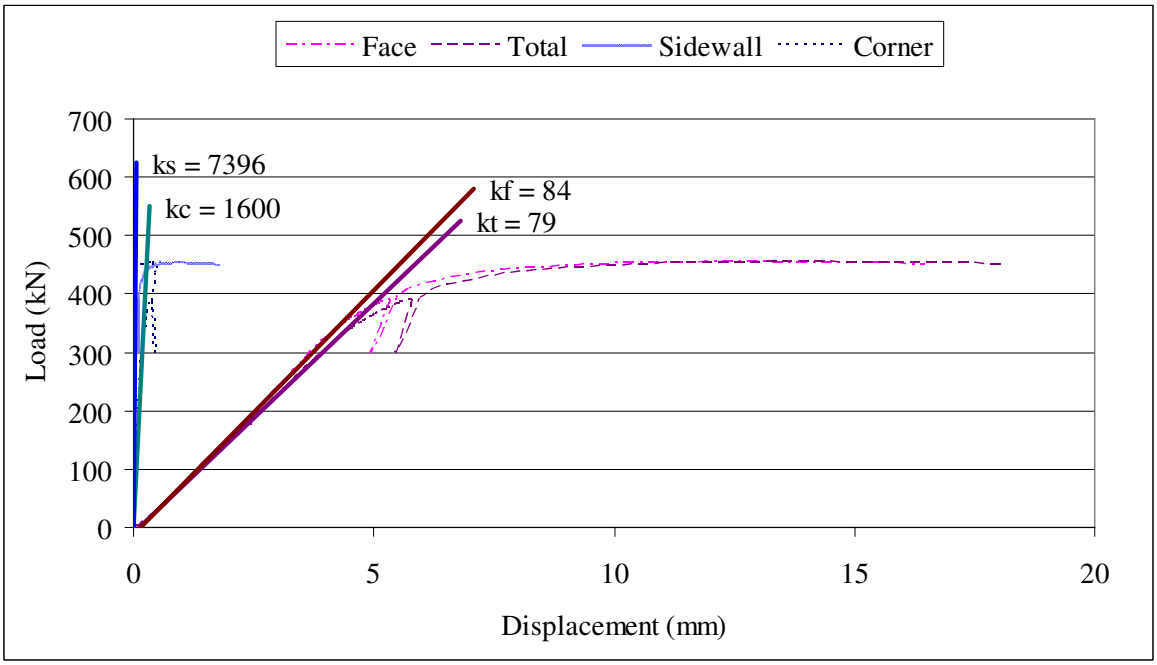

Figure 3.21. Components of deformation of the specimen B4 – test 2

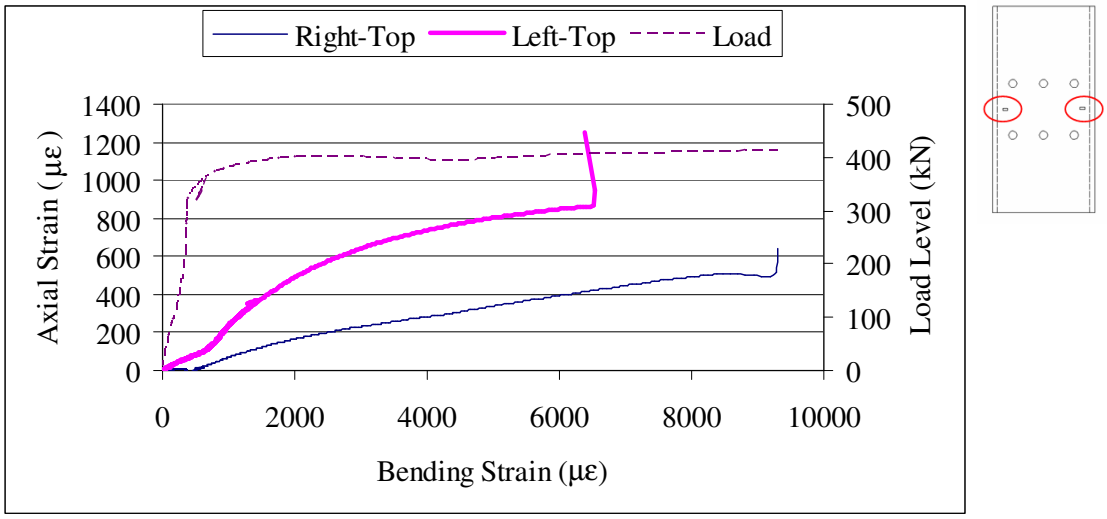

Figure 3.22. Axial and bending strains top face of the specimen B4

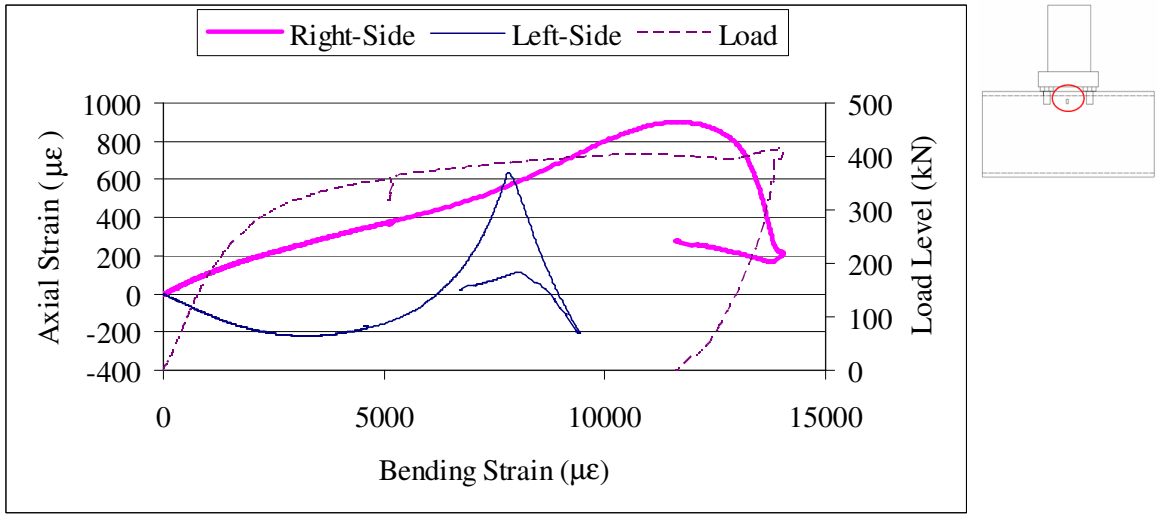

Figure 3.23. Axial and bending strains sidewall of the specimen B4

3.1.5. Test Specimen B5

B5 specimens were former planned to be used in component tests of which the ϕ21.3 mm tubes pass through and connect the holes that were drilled in corresponding faces. After preference of using an alternative setup for compression of tube component, the specimens were decided to be used in face in bending component tests. However the bolt

holes had already been drilled in 20 mm diameter. In the first test M16 bolts were used and observed that M16 did not fit well. Therefore in the second test M20 bolts were preferred. Both specimens have been successfully tested until rigid plate touched the face of the hollow section. During the second test due to a problem at the hydraulic press, the test has been paused and continued after releasing. Strain gages were used in both tests. Failure mechanism of the first test was bending of the SHS top face inside together with leaning of the specimen towards left due to the top disproportionate face bending at the right corner and the second test was failed as usual by bending of the SHS top face inside and sidewalls outside for both of the specimens.

The load vs displacement behaviours of the specimens are given Figures 3.24 and 3.25. The ultimate load capacities for test one and test two have been recorded in the levels of 378 and 449 kN respectively and the yield loads have been calculated as 331 and 381 kN and the initial stiffness 68 and 104 kN/mm, respectively. Components of the specimen deformation and the initial stiffness values of the components are given in Figures 3.26 and 3.27.

Axial and bending strains at the top corners of the specimen are drawn in Figures 3.28 to 3.31. In both tests bending strains improved more rapidly than axial strains. In the first test considering the strain values, first bending strains at the top corners of the sidewalls reached 0.002 strains at the load levels of 170 kN. This is followed by bending strains at the left and right top face corner of the specimen which reached yield level at the load levels of 340 and 360 kN, respectively. While axial strains at the top face corners of the specimen remained lower than 0.002, at the top corner of the sidewall, axial strains reached yield levels at load levels of 355 kN. In the second test considering the strain values, first bending strains at the top corner of the sidewall reached 0.002 strains at the load levels of 250 kN. This is followed by bending strains at the top face corner of the specimen which reached yield level at the load levels of 370 kN. While at the top corner of the sidewall, axial strains reached yield levels at load levels of 395 kN, axial strains at the top face corners of the specimen reached yield levels at load levels of 445 kN.

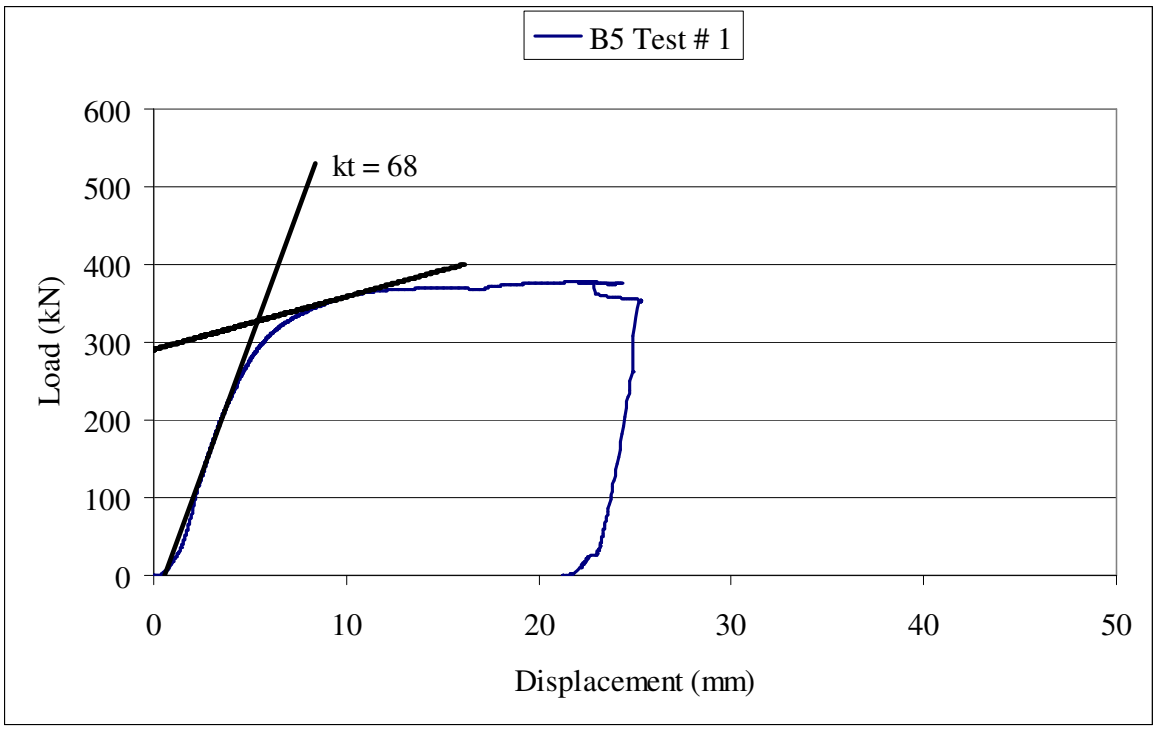

Figure 3.24. Load vs displacement curve of the specimen B5 – test 1

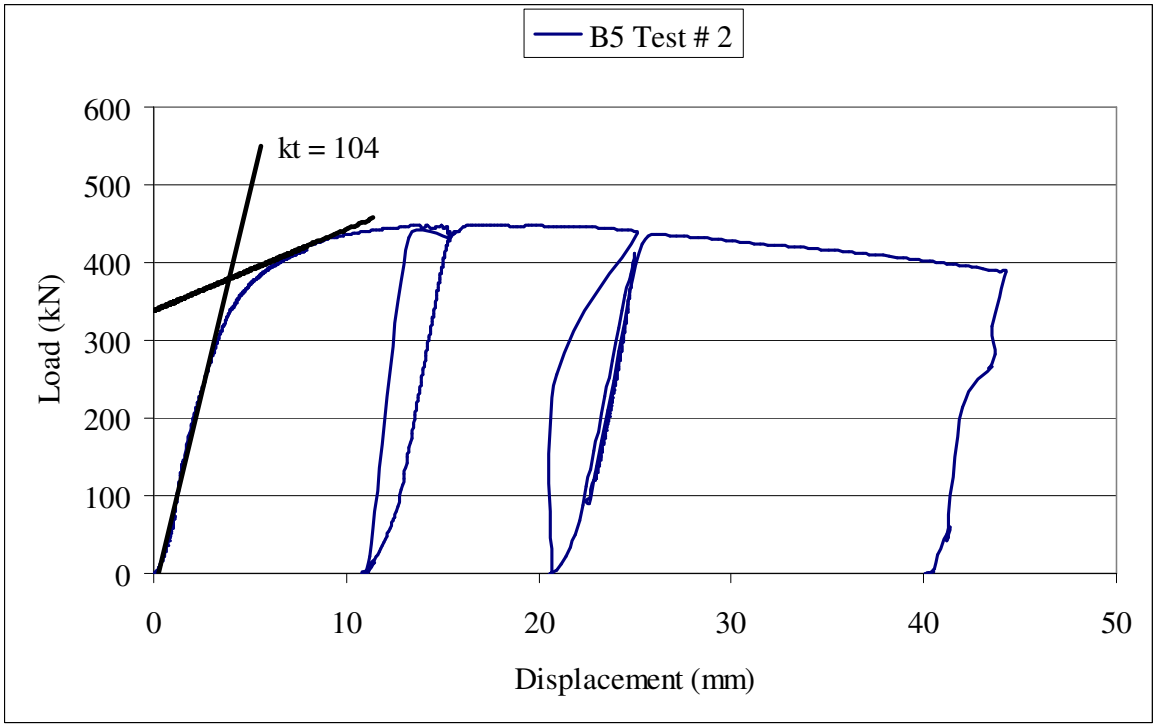

Figure 3.25. Load vs displacement curve of the specimen B5 – test 2

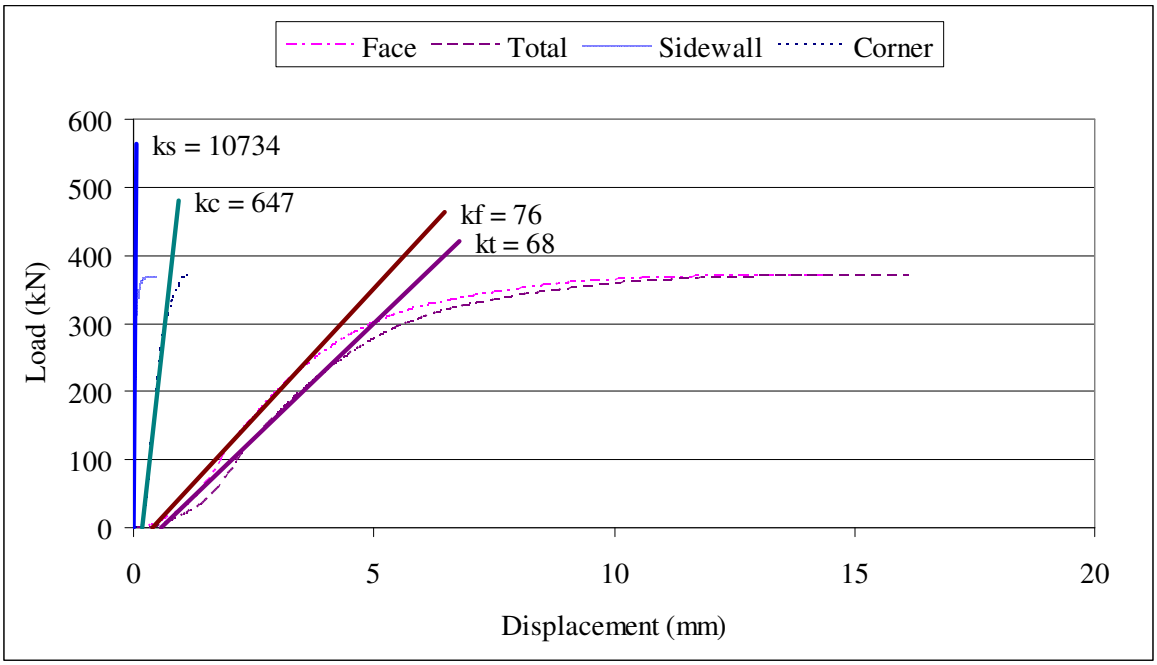

Figure 3.26. Components of deformation of the specimen B5 – test 1

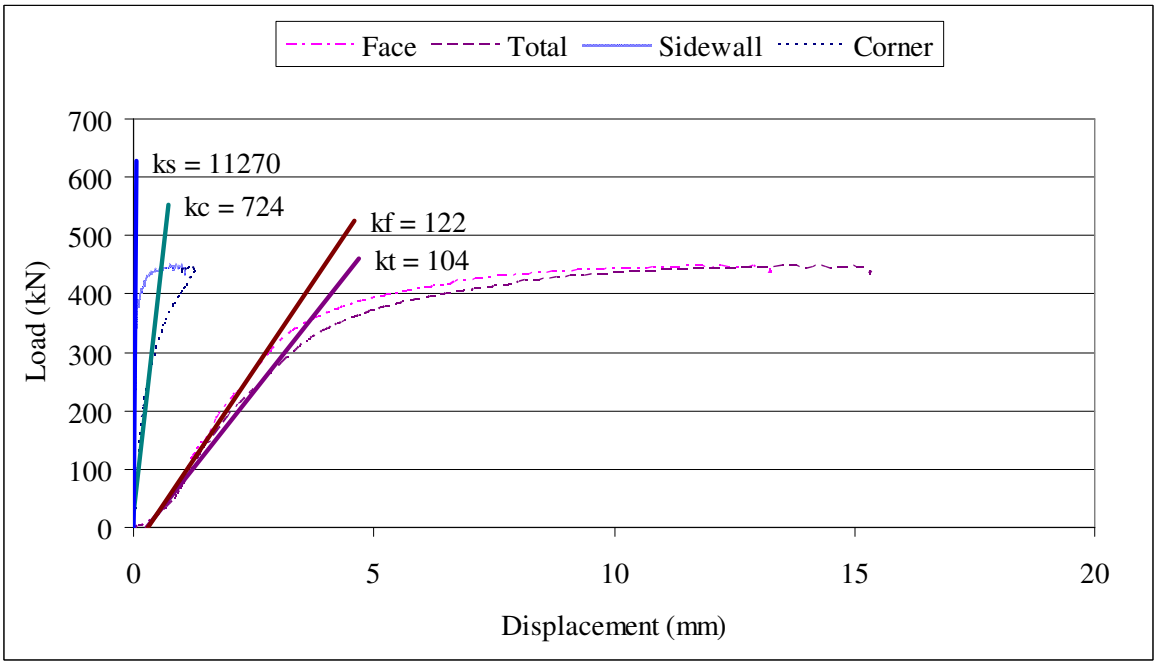

Figure 3.27. Components of deformation of the specimen B5 – test 2

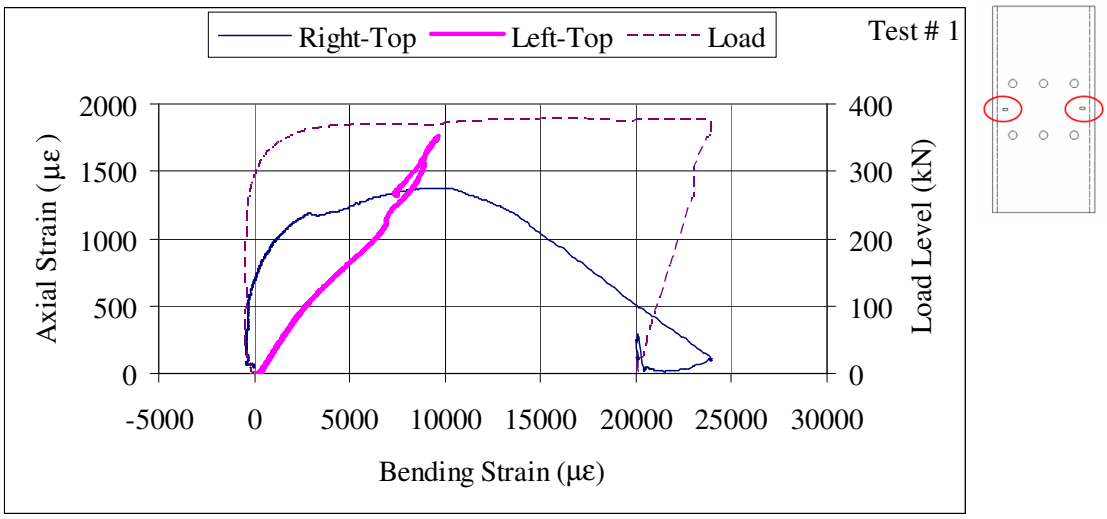

Figure 3.28. Axial and bending strains top face of the specimen B5 – test 1

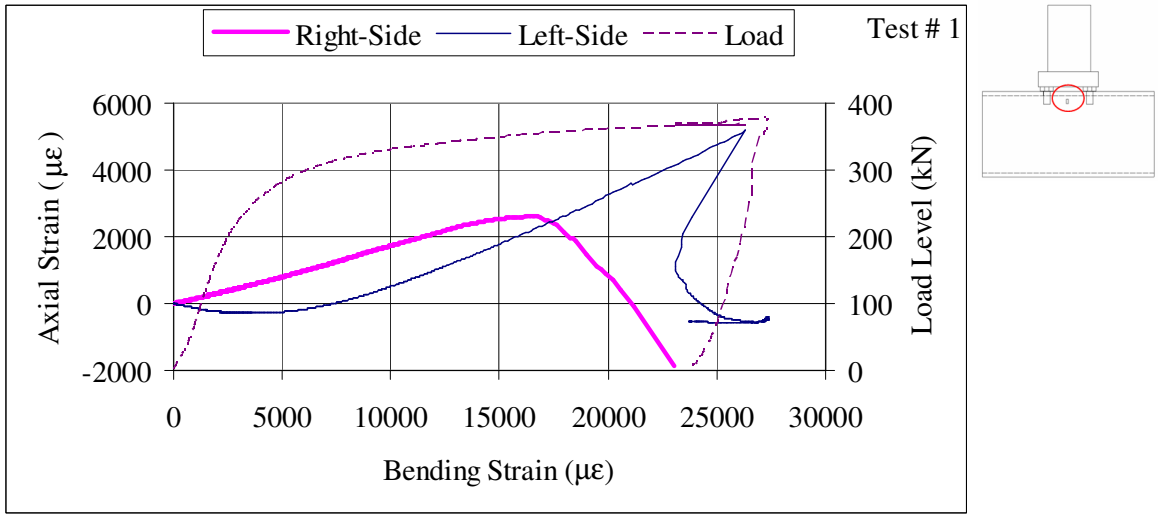

Figure 3.29. Axial and bending strains sidewall of the specimen B5 – test 1

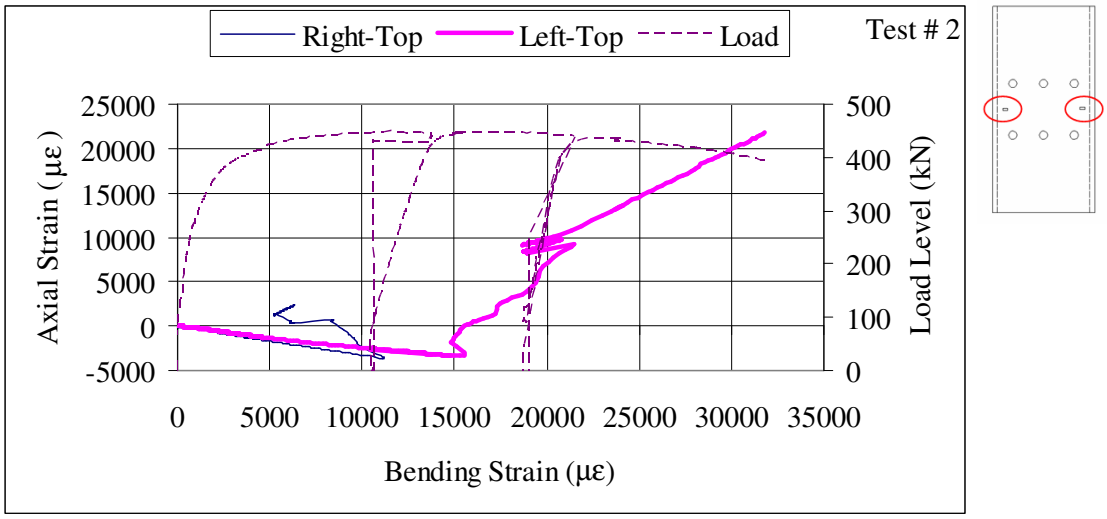

Figure 3.30. Axial and bending strains top face of the specimen B5 – test 2

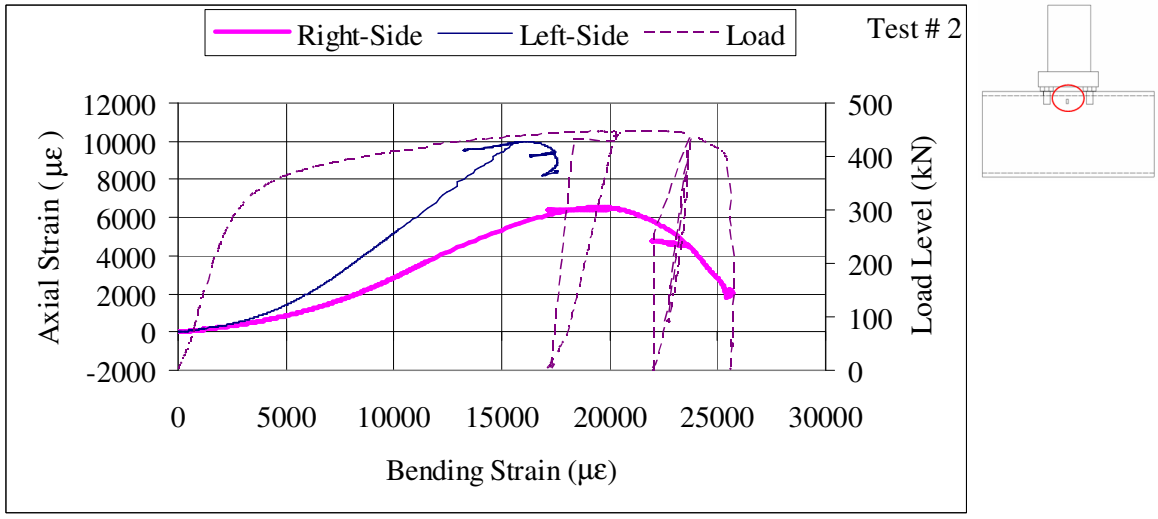

Figure 3.31. Axial and bending strains sidewall of the specimen B5 – test 2

3.1.6. Test Specimen P1

Two specimens have been successfully tested until the limits of dial gages. Strain gages were used only in the first test. Failure mechanisms of both tests were bending of the SHS top face inside together with leaning of the specimen towards right due to the top disproportionate face bending at the left corner.

The load vs displacement behaviours of the specimens are given Figures 3.32 and 3.33. The ultimate load capacities for test one and test two have been recorded in the levels of 555 and 579 kN respectively and the yield loads have been calculated as 504 and 465 kN and the initial stiffness 108 and 216 kN/mm, respectively. Components of the specimen deformation and the initial stiffness values of the components are given in Figures 3.34 and 3.35.

Axial and bending strains at the top corners of the specimen are drawn in Figures 3.36 and 3.37. Bending strains improved more rapidly than axial strains. Considering the strain values, first bending strains at the top corner of the sidewall reached 0.002 strains at the load levels of 300 kN. This is followed by bending strains at the left and right top face corner of the specimen which reached yield level at the load levels of 390 and 460 kN. While at the top corner of the left sidewall, axial strains reached yield levels at load levels of 520 kN, axial strains at the top face corners of the specimen reached yield levels at load levels of 535 kN. Axial strains at top corner of the right sidewall remained lower than 0.002 most probably due to leaning of the specimen towards right.

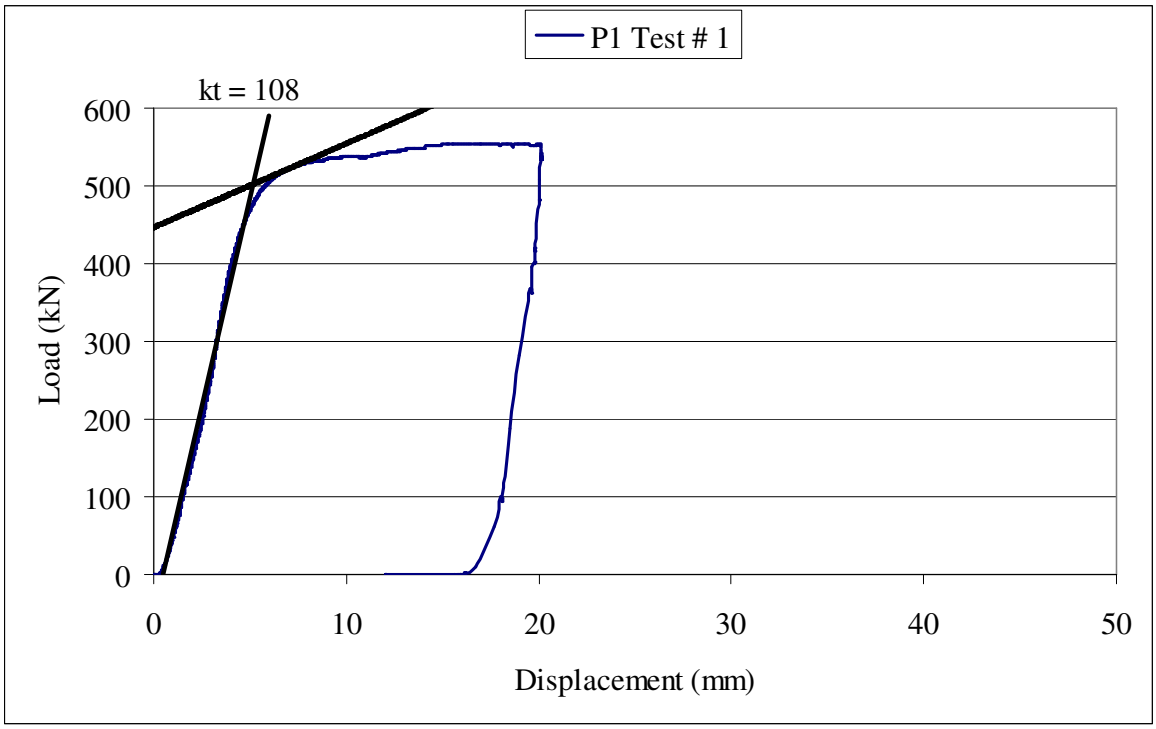

Figure 3.32. Load vs displacement curve of the specimen P1 – test 1

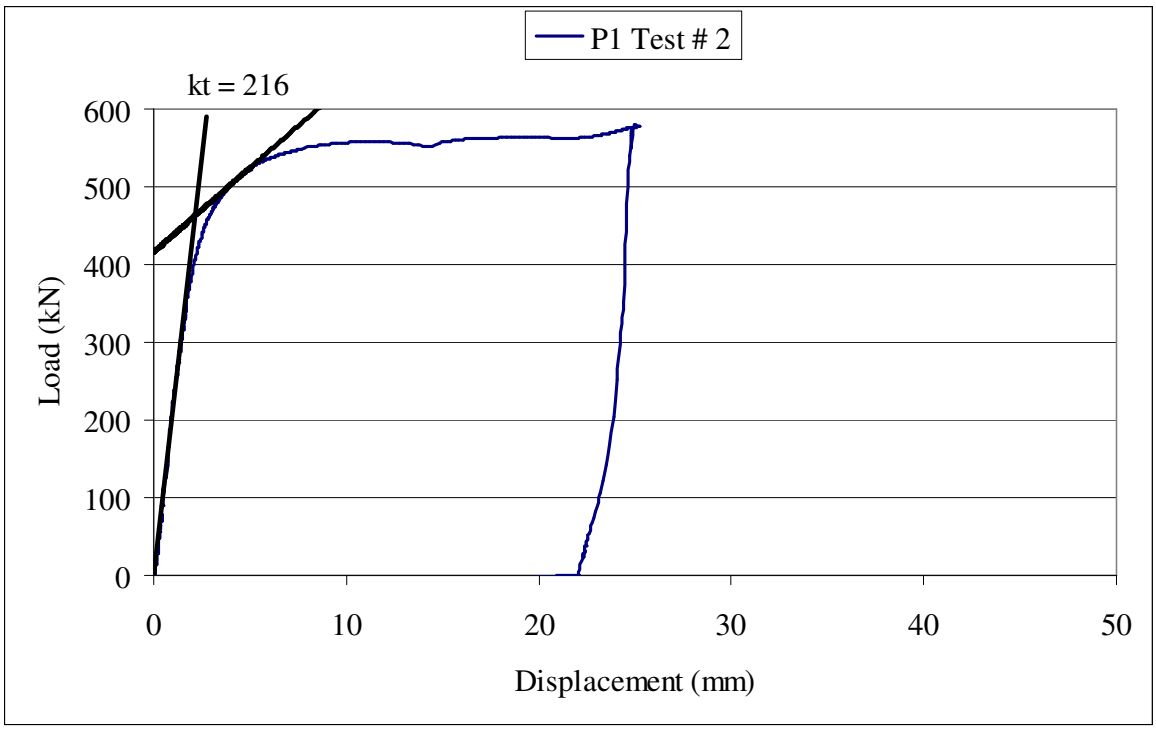

Figure 3.33. Load vs displacement curve of the specimen P1 – test 2

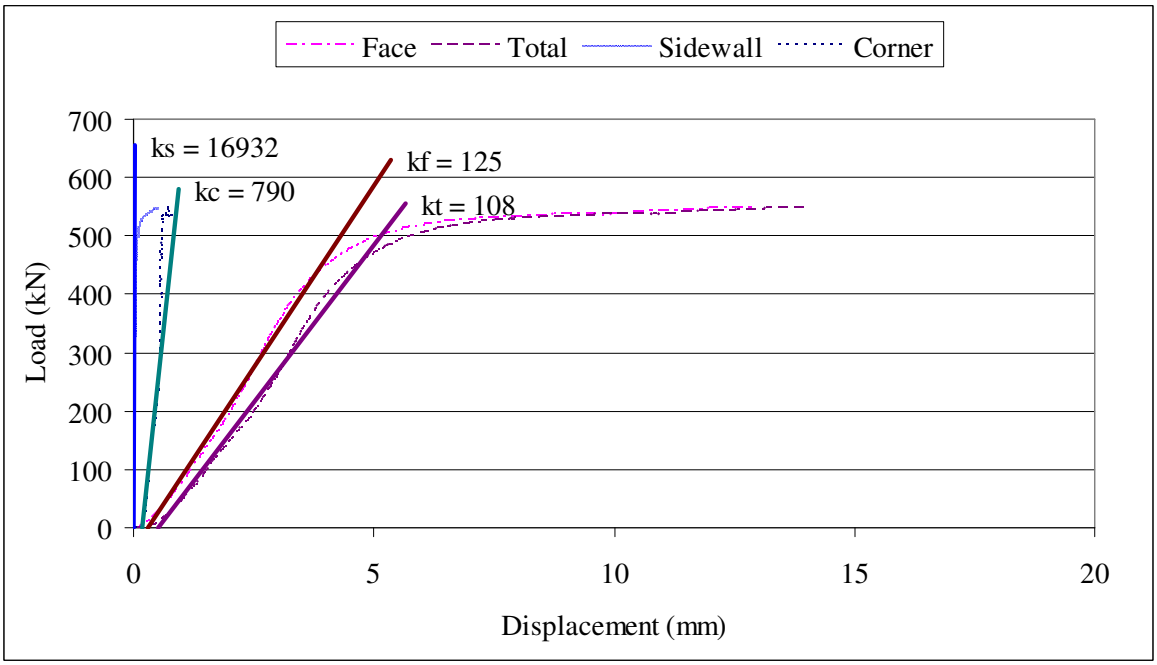

Figure 3.34. Components of deformation of the specimen P1 – test 1

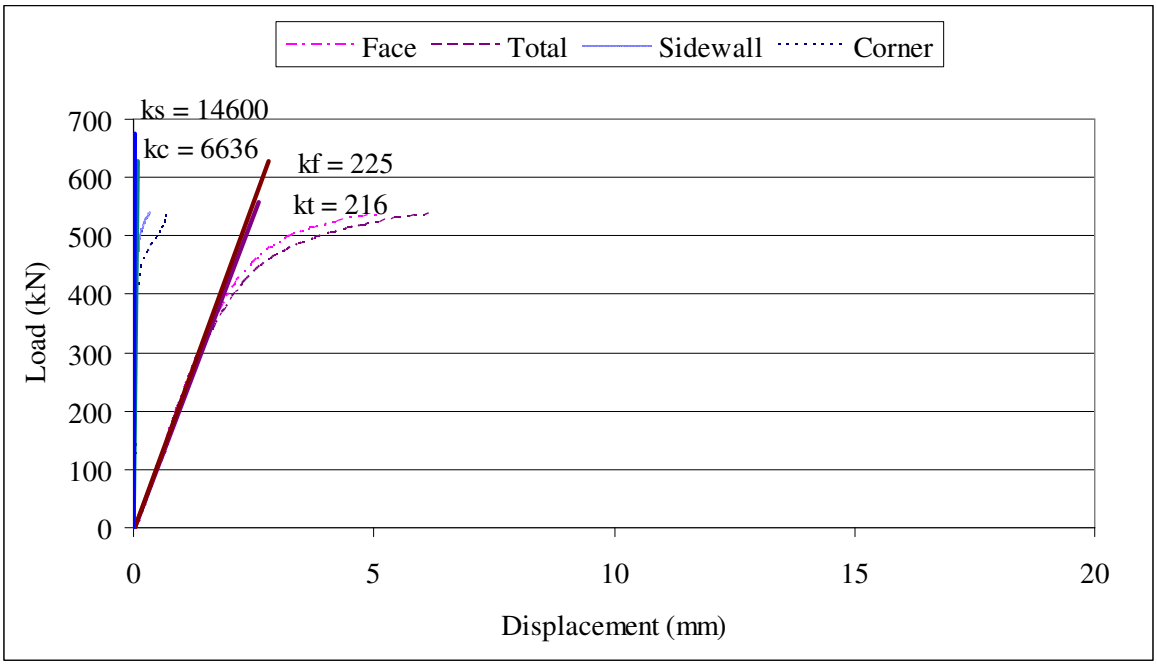

Figure 3.35. Components of deformation of the specimen P1 – test 2

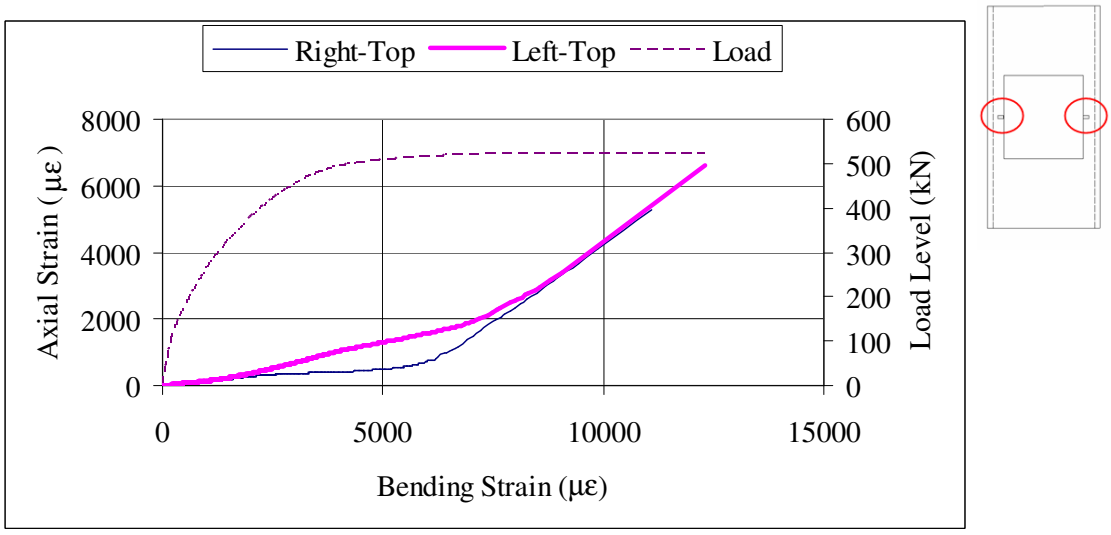

Figure 3.36. Axial and bending strains top face of the specimen P1

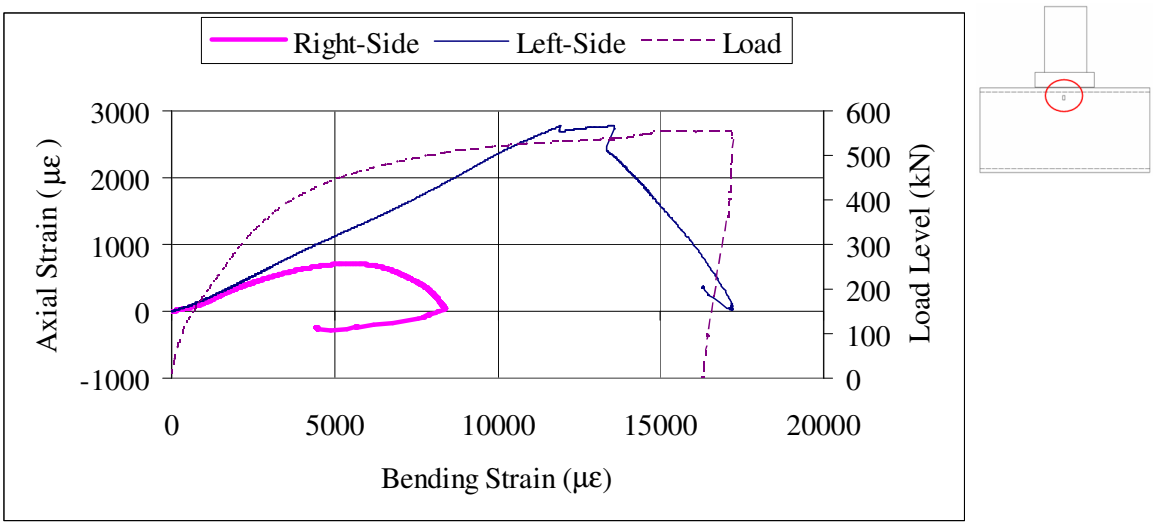

Figure 3.37. Axial and bending strains sidewall of the specimen P1

3.1.7. Test Specimen P2

Two specimens have been successfully tested until the limits of dial gages. In the second test plate dimension was 200 x 140 mm. Rigid plates have been bent in the middle more than expected even thicker plate has been used in the second test. Strain gages were used only in the first test. Failure mechanisms were bending of the SHS top face inside and sidewalls outside for both of the specimens.

The load vs displacement behaviours of the specimens are given Figures 3.38 and 3.39. The ultimate load capacities for test one and test two have been recorded in the levels of 589 and 613 kN respectively and the yield loads have been calculated as 532 and 511 kN and the initial stiffness 213 and 191 kN/mm, respectively. Components of the specimen deformation and the initial stiffness values of the components are given in Figure 3.40.

Axial and bending strains at the top corners of the specimen are drawn in Figure 3.41. Bending strains improved more rapidly than axial strains. Considering the strain values, at the top corners of the sidewalls while bending strains reached 0.002 strains at the load levels of 420 kN, axial strains reached yield levels just at ultimate load levels.

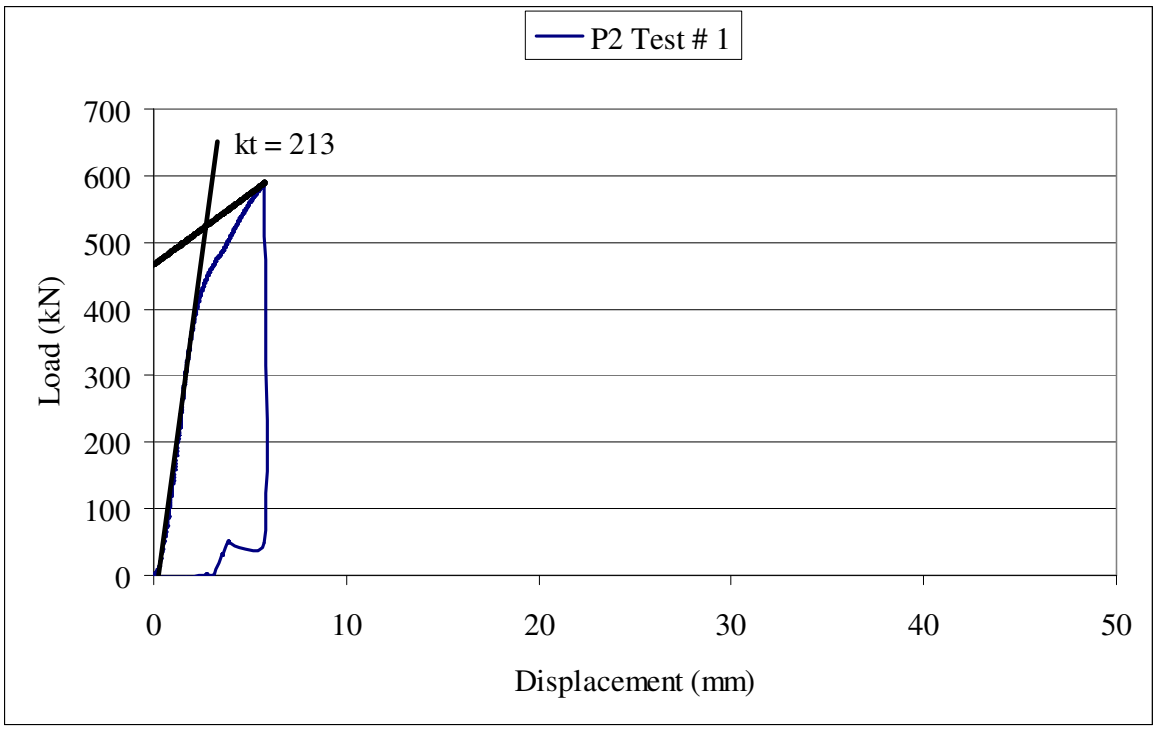

Figure 3.38. Load vs displacement curve of the specimen P2 – test 1

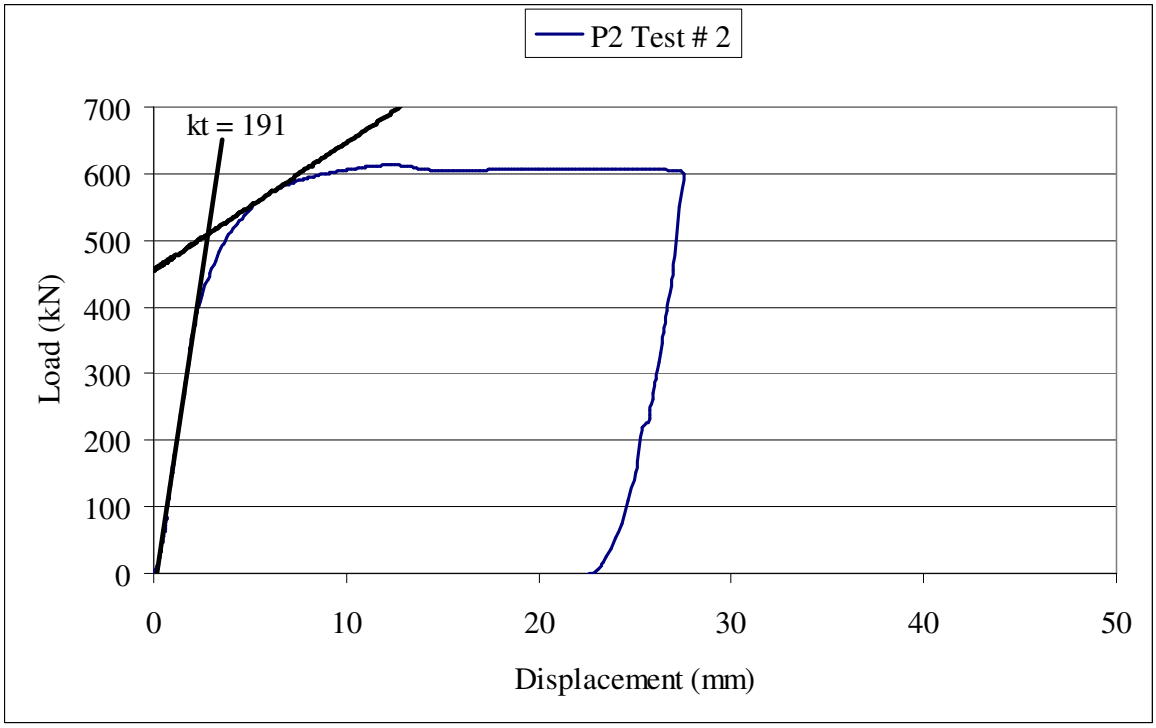

Figure 3.39. Load vs displacement curve of the specimen P2 – test 2

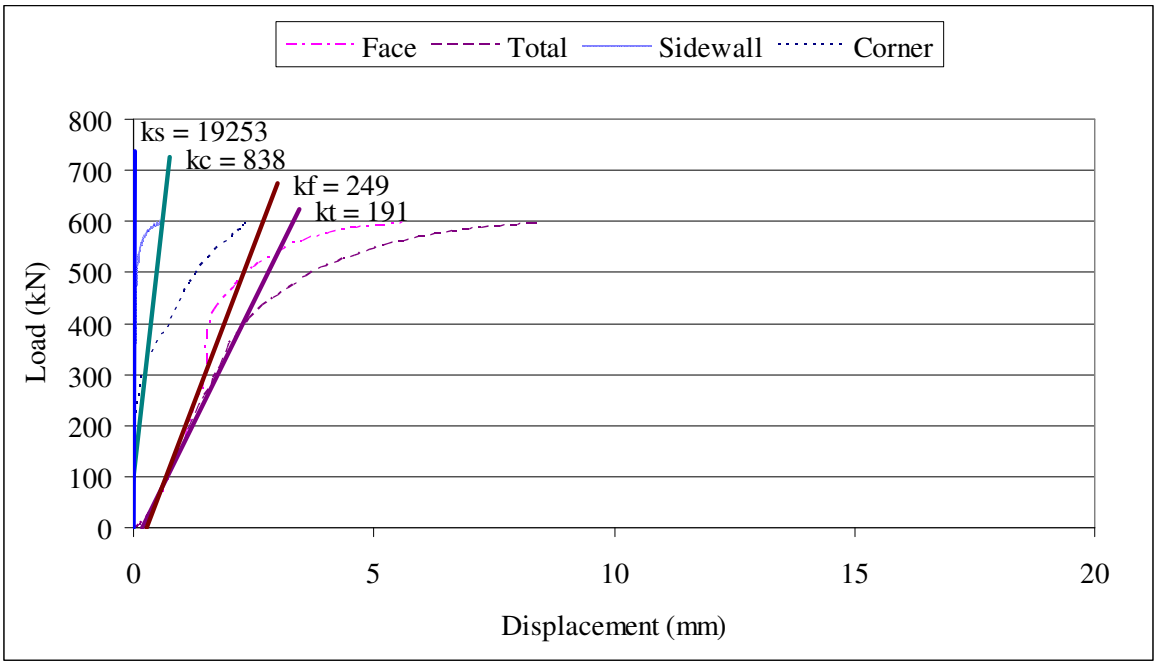

Figure 3.40. Components of deformation of the specimen P2 – test 2

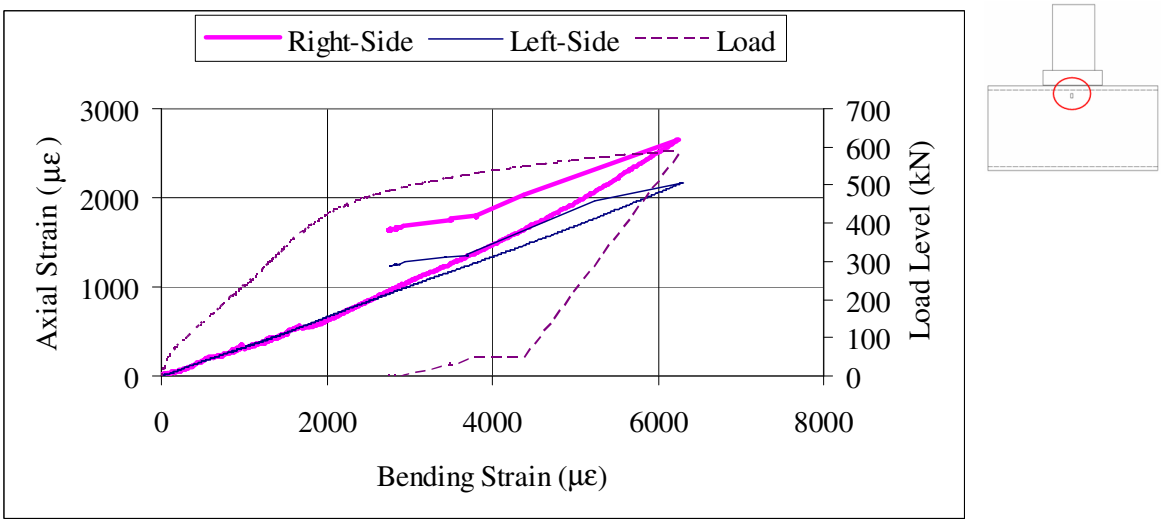

Figure 3.41. Axial and bending strains sidewall of the specimen P2 – test 1

3.1.8. Test Specimen Tube

Four tests have been performed until the tube specimens failed under buckling in the middle. The failure load was very low compared to the capacity of the hydraulic press. That's why it was difficult to control the loading rate. Hopefully in the fourth test the loading rate was slow enough to record more data at the initial stage.

The load vs displacement behaviours and initial stiffness values of the specimens are given Figure 3.42. The ultimate load capacities for specimens in tests one to four were recorded as 34.3, 34.1, 30.8 and 34.3 kN, respectively. Since loading rate of test four was slower than the others, it has lower initial stiffness.

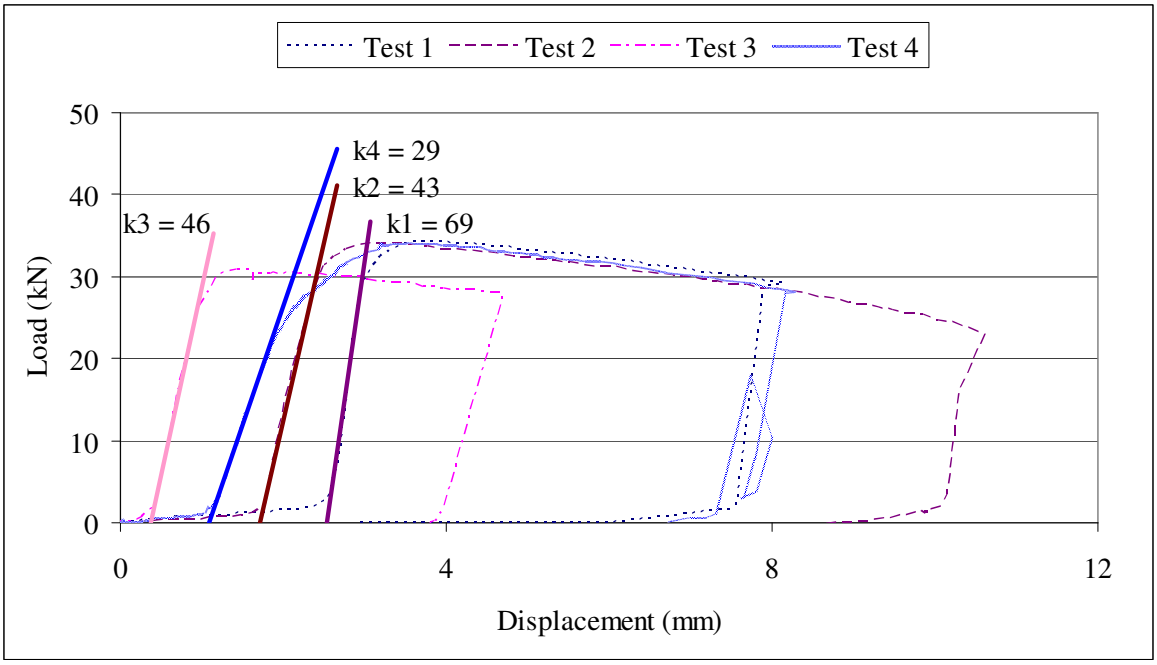

Figure 3.42. Load vs displacement curves of the tubes under compression

3.1.9. Evaluation of Test Results

All tests have been carried on until rigid plate touched the face of the hollow section. Until that time, the loss of strength was in minor levels with almost zero stiffness (perfectly plastic). Although the tests could not be completed until complete failure, the specimens were already deformed more than eight times of their calculated yield displacement without major loss of strength. This ductile behaviour proved high deformation capacity of the hollow sections under this type (face in bending) of loading conditions.

The summary of the test results is given in Table 3.1. The terms k_s, k_f, k_c and k_t refer respectively to initial stiffness of sidewall, face in bending, corner rotation and the total stiffness. F_y and F_u are the yield and ultimate load levels. Since average non-dimensional strength ratios (F_u/F_y) of the whole tests were 1.16, the behaviour of the specimens under this type of loading can also be considered as perfectly plastic. As expected the load carrying capacity and stiffness of plate push thru specimens are higher than the bolt push thru. Considering the stiffness levels, sidewall stiffness can be accepted as rigid compared to others. Although the face deformation behaved very close to the total specimen deformation, deformation due to the corner rotation should not be neglected. Influence of corner stiffness is approximately 10% in average.

In order to make a comparative study on the test results, some parameters have to be defined:

- Non-dimensional strength which is the ratio of ultimate load level and calculated yield load (F_u/F_y)
- Stiffness coefficient which is defined in Eurocode 3 part 1-8 [22]. (k/E, where E is the modulus of elasticity)
- The ratio of the distance between the bolt holes close to opposite sidewalls and the width of the SHS (b_0/L)
- The ratio of the distance between the bolt rows and the width of the SHS (c_0/L)

The influences of b_0/L and c_0/L ratios on the resistance and stiffness coefficients are given in Figure 3.43 to Figure 3.46. The average values at same b_0/L or c_0/L ratios have been plotted. It is observed that b_0/L ratio was more dominant on the behaviour. While b_0/L ratio was increasing, the resistance and the stiffness coefficients have been increased. On the other hand, the effect of c_0/L ratio was in minor levels, especially on the resistance. Besides the stiffness coefficient was decreasing with the increase of c_0/L ratio. It can be concluded that the distance between bolt-rows did not influence the resistance primarily within the scope of this study.

Table 3.1. Phase I - summary of the test results

		Stiffness (kN/mm)				**Strength (kN)**	
	Specimen	**k_s**	**k_c**	**k_f**	**k_t**	**F_y**	**F_u**
Test 1	**B2**	19349	1285	138	124	376.7	431.6
	B3	30354	484	96	80	298.2	365.9
	B4	19048	435	143	108	358.1	415.0
	B5	10734	647	76	68	331.6	378.7
	P1	16932	790	125	108	504.2	554.3
	P2-pilot				213	531.7	588.6
Test 2	**B1**	10597	1065	95	87	309.0	375.7
	B2	10502	2100	112	106	393.4	444.4
	B3	8653	809	71	68	339.4	390.4
	B4	7396	1600	84	79	417.9	454.2
	B5	11270	724	122	104	381.6	448.3
	P1	14600	6636	225	216	465.0	578.8
	P2	19253	838	249	191	511.1	613.1

Table 3.6. Phase I – non-dimensional test results

		Stiffness Coefficient (mm)				Nondimensional Strength	
	Specimen	***ks***	***kc***	***kf***	***kt***	***Fy***	***Fu***
Test 1	**B2**	92.14	6.12	0.66	0.59	1.00	1.15
	B3	144.54	2.31	0.46	0.38	1.00	1.23
	B4	90.71	2.07	0.68	0.52	1.00	1.16
	B5	51.12	3.08	0.36	0.32	1.00	1.14
	P1	80.63	3.76	0.59	0.51	1.00	1.10
	P2-pilot				1.01	1.00	1.11
Test 2	**B1**	50.46	5.07	0.45	0.41	1.00	1.22
	B2	50.01	10.00	0.53	0.50	1.00	1.13
	B3	41.21	3.85	0.34	0.32	1.00	1.15
	B4	35.22	7.62	0.40	0.38	1.00	1.09
	B5	53.67	3.45	0.58	0.50	1.00	1.17
	P1	69.53	31.60	1.07	1.03	1.00	1.24
	P2	91.68	3.99	1.19	0.91	1.00	1.20

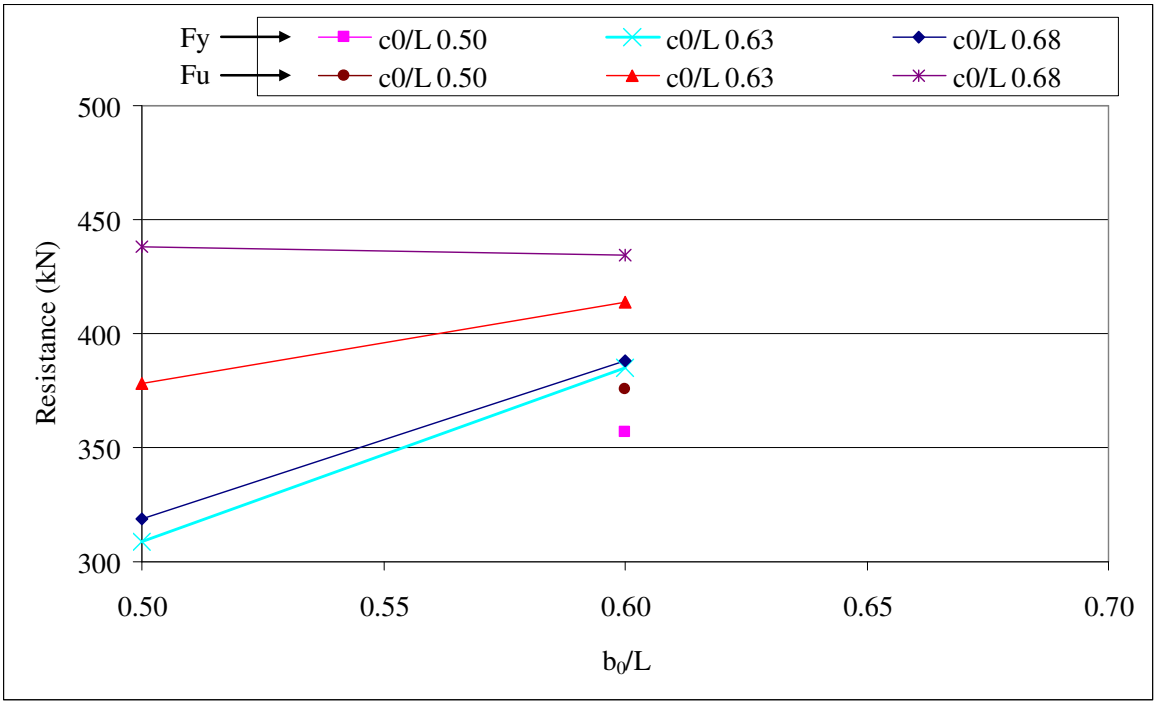

Figure 3.43. Influence of b_0/L ratio on resistance

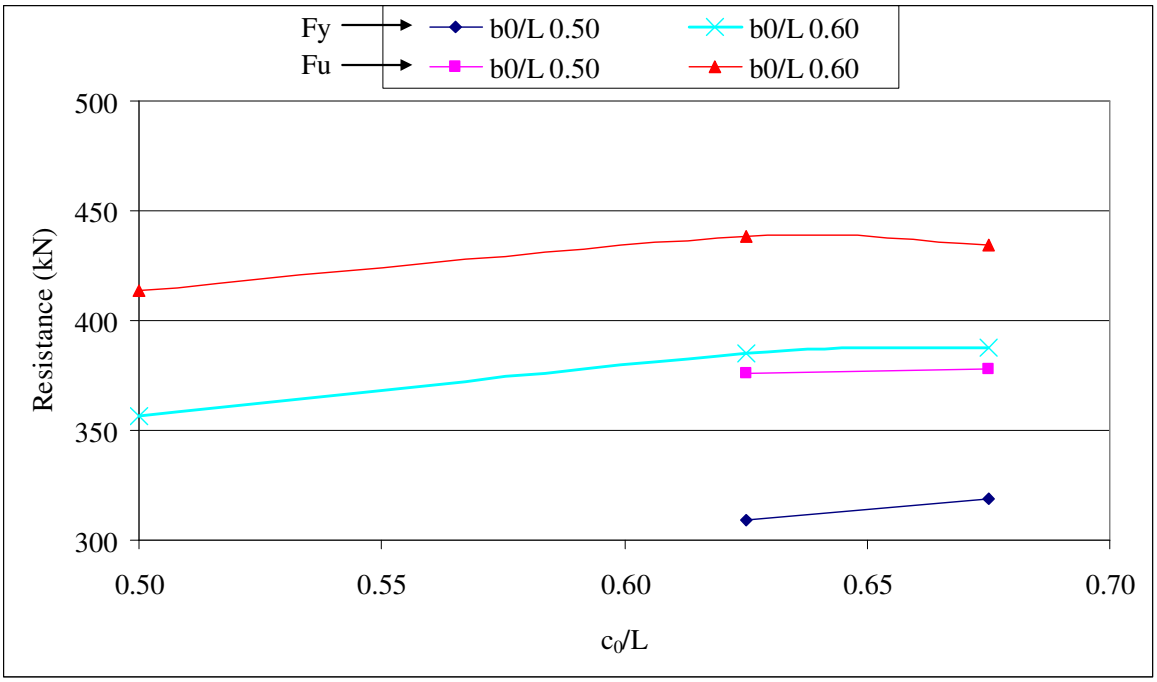

Figure 3.44. Influence of c_0/L ratio on resistance

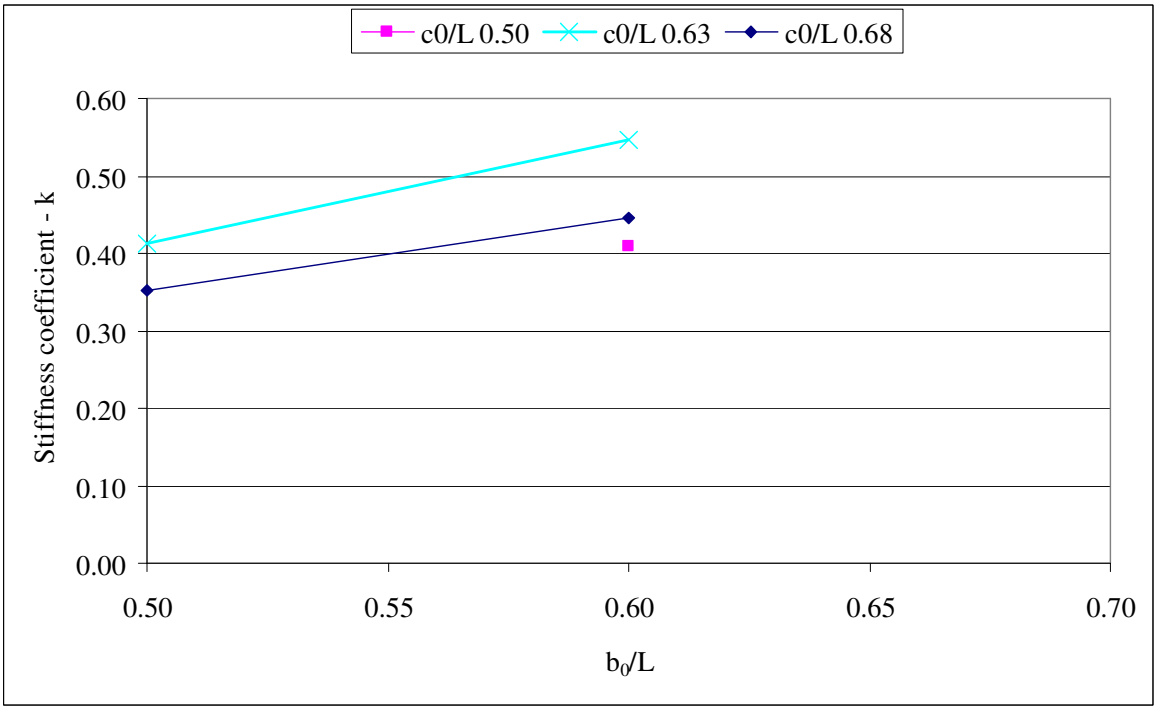

Figure 3.45. Influence of b_0/L ratio on stiffness coefficient (k_t)

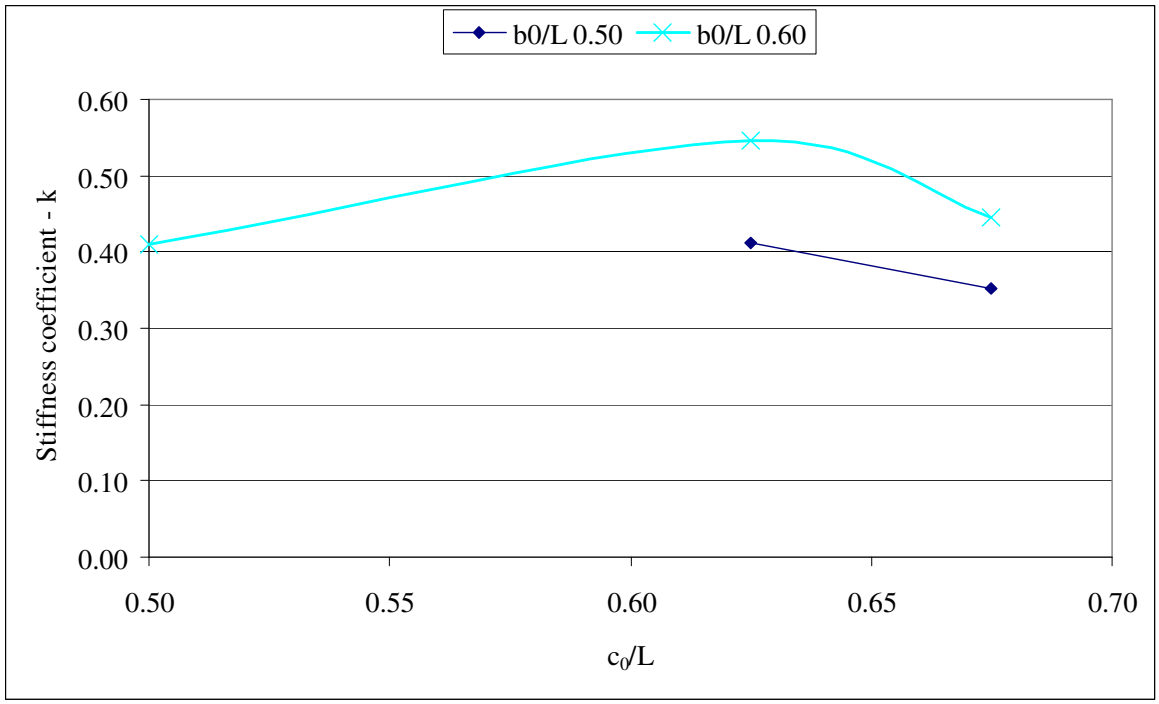

Figure 3.46. Influence of c_0/L ratio on stiffness coefficient (k_t)

Using tubes to link the rear SHS face to the front face could be possible. The average resistance and stiffness levels of the tubes under compression are respectively 33.4 kN and 46.1 kN/mm. Besides during the loading action there would be threaded stud passing through the tubes which would provide resistance against buckling of the tube. Consequently the load could be transferred partially or fully by using adequate number of tubes. This provides the combined action of both rear and front SHS faces which would increase the strength and stiffness of the joint.

3.2. Phase II – Subassemblage Test

Pilot test has been concluded in two steps. With the missing proper out-of-plane frame during the first step of the pilot test, there has been a torsion problem at the loading head of the specimen, especially in the push direction. Therefore, it was decided to continue the test in only one way (pull) cyclic with steps of one fourth of expected yield displacement. The test was stopped at the expected yield displacement in order not to leave

much local plastic deformations. After taking necessary setup improvements like building a proper out-of-plane support system, the pilot specimen have been re-tested.

Slipping plays an important role in the behaviour of these type of bolted connections. Slipping occurs in at the beam-t-stub and column-t-stub interfaces. During the second step of the pilot test, it was observed that the slipping of the partially threaded studs along the bolt line (due to torsion) at the rear face has been observed. This happened at second major shift. The bolt holes at this face were 20 mm in diameter with 4 mm tolerance which was left in order to pass the stain gage cables inside the hole together with the bolt. Availability of thinner cables allowed reducing the bolt hole to 18 mm diameter for the other test specimens. After putting the cables in, 18 mm hole have been narrowed by wrapping round the stud with 0.5 mm thin curved steel sheet. Next was to pay extra attention while tightening the bolts of the other tests. The bolts connecting the t-stub to the beam has been tightened as much as possible. The partially threaded studs connecting the t-stub to the column rear face have been snug tightened (preloading approximately 20-30 % by controlling the strains). Additional bolt preloading in higher levels is not necessary. As soon as the SHS face deforms inside, the stud will loose its pre-tension.

The pilot test was terminated after the sudden rupture of one of the partially threaded studs with a loud noise. The smaller piece of the stud flied off dangerously. For safety reasons, the ends of the studs have been tied with a wire in the other test specimens.

Other phase II specimens have been fabricated considering the necessary adjustments on the specimen immediately after the pilot test. Some photos taken during fabrication stage are given in Appendix C.

A joint is the whole region concerned by the assemblage of the beam(s) with the column. It is composed by the very end portion of the beam(s), the facing adjacent portion of the column, as well as by all the connecting accessories (end plate, cleats, t-stubs, bolts, welds,...) required by a specified type of connection. The deformability of beam-to-column joint consists mainly in two parts [25], which are respectively fed by several contributions:

a) The deformability of the connection area associated to the following phenomena :

- Deformation of the connection elements: end plate or cleats or t-stubs, bolts, rivets, welds,…which is for the case t-stubs.
- Slip and/or hole clearance;
- Deformation of the column web, across its depth, in the so-called tensile and compression zones, i.e. in the regions where the forces carried over by the beam(s) have to diffuse into the column web. Normally in open sections (like HE, IPE profiles) this effect, termed "trapezoidal effect", is the result of the respective lengthening and shortening of the column web depth. However as explained in Section 3.1, for the case this lengthening or shortening of the hollow section sidewall (web) depth is strongly influenced by the deformation of the hollow section face (front or rear face where the connection is). As a result source of deformability results mainly from the out-of-plane deflection of the hollow section sidewall when experiencing the bending moment transmitted by the beam. Therefore this deformation is incorporated with the deformation of column face.
- Deformation of the column face

b) The shear deformation of the column web panel, which is subject to a complex shear stress distribution in the region of the joint.

Consequently, the joint relative rotation φ is composed of the contribution θ of the deformability of the connection area and the shear deformation of the column web (γ). From the Figure 3.47, The shear deformation of the column web is represented by the difference between θ_c and θ_f, where θ_f is the flexural rotation of the column. Regarding the shear force in the column web panel, results from the combined action of equal but opposite forces in the beam flanges (the resultant of which is statically equivalent to the bending moment in the beam) and the shear force resulting from the moment distribution in the column.

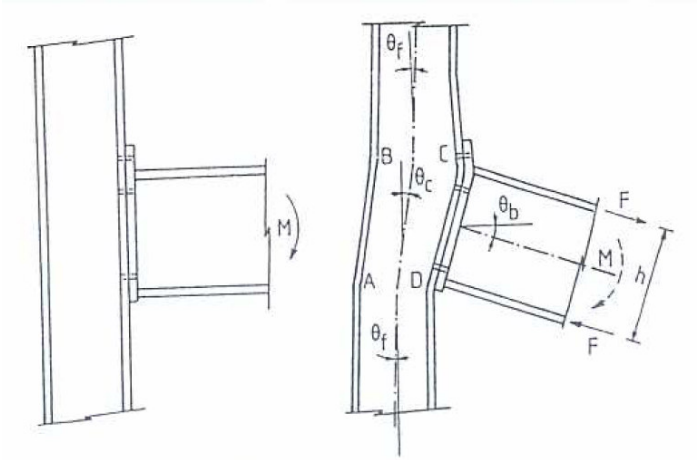

Figure 3.47. Joint deformation behaviour

Because of the appropriate instrumentation, the following characteristic curves associated to the different components of the joint deformability have been recorded for the specimens:

- the joint relative rotation curve
- the connection relative rotation curve
- the column web panel rotation curve

For what concerns especially the deformability of the connection, it is composed by the addition of the following curves:

- the connection slip rotation curves
- the t-stub deformability (including the elongation of the partially threaded studs) rotation curve
- the column face deformability (including the load introduction which is deformation of the column web, across its depth) rotation curve

Photographic views of the specimens before, during and after experiments are presented in Appendix C.

3.2.1. Test Specimen T1M

The specimen has been successfully tested by loading towards the east side of the specimen. Load vs displacement behaviour of the specimen is given in Figure 3.48 which indicates the parameters used to generate the loading history of the cyclic test of specimen T1C. The test continued until sudden and progressive rupture of two partially threaded studs in the west side of the specimen as shown in Figure 3.49. First stud in the south corner ruptured at the moment and rotation levels of 146.6 kNm and 0.080 rad, respectively. Then the second stud in the north corner ruptured at the moment and rotation levels of 133.4 kNm and 0.095 rad, respectively.

Components of joint and connection deformations of the specimen have been given with the initial stiffness values in Figures 3.50 and 3.51, respectively. Although web shear panel zone of the joint performed much stiffer than the connection, the deformation level should also be taken into account. Since the specimen is bolted connection slips plays an important role in the total behaviour of the connection. Slips, especially the slips at the junction of t-stub-beam flange, took place until the levels of 15-20 kNm moment and 0.006 rad rotation. After then bearing resistance of the junction governed and behaved almost linear until failure load. This behaviour was also observed same for the slip at the junction of t-stub-column face but stiffer and in lower deformation levels. The main sources of connection deformation were bending of the column face and the t-stub. Although their stiffness levels were very close, the deformation level of the t-stub was slightly higher.

Strain measurements during test are given in Figures 3.52 to 3.57. Based on the drawings the first yielding started at west t-stub flange of the specimen at the moment level of 75 kNm. (Figure 3.52) Then it was followed by yielding of the column face at slightly higher load levels by also checking the deformability of the connection components. Strains at the t-stub web remained elastic during the test except for the location number three in the Figures 3.53 and 3.54. This was due to deformation after yielding of the t-stub, thus bending of the t-stub web at this location. Unfortunately the triaxial strain gauge which was at position number one in Figure 3.55 was failed during the test. Its shear strain records were unusable. Shear strains at other locations reached 0.002 strains at the moment

level of 110 kNm. Partially threaded studs have been snug-tightened. The average strain level before testing was 822 microstrains. The bolts were ruptured at the strain levels of 0.003-0.0035. The strains of the stud in middle (position two in Figure 3.56) was in low levels even it lose its pretension until the rupture of the bolt in position number one, there after it took the load and prevented the complete sudden failure until the rupture of the other stud in position number three in the figure. As presented in Figure 3.57, the beam flanges remained elastic during the whole test but in levels of yielding at the ultimate load levels, especially the west flange of the beam.

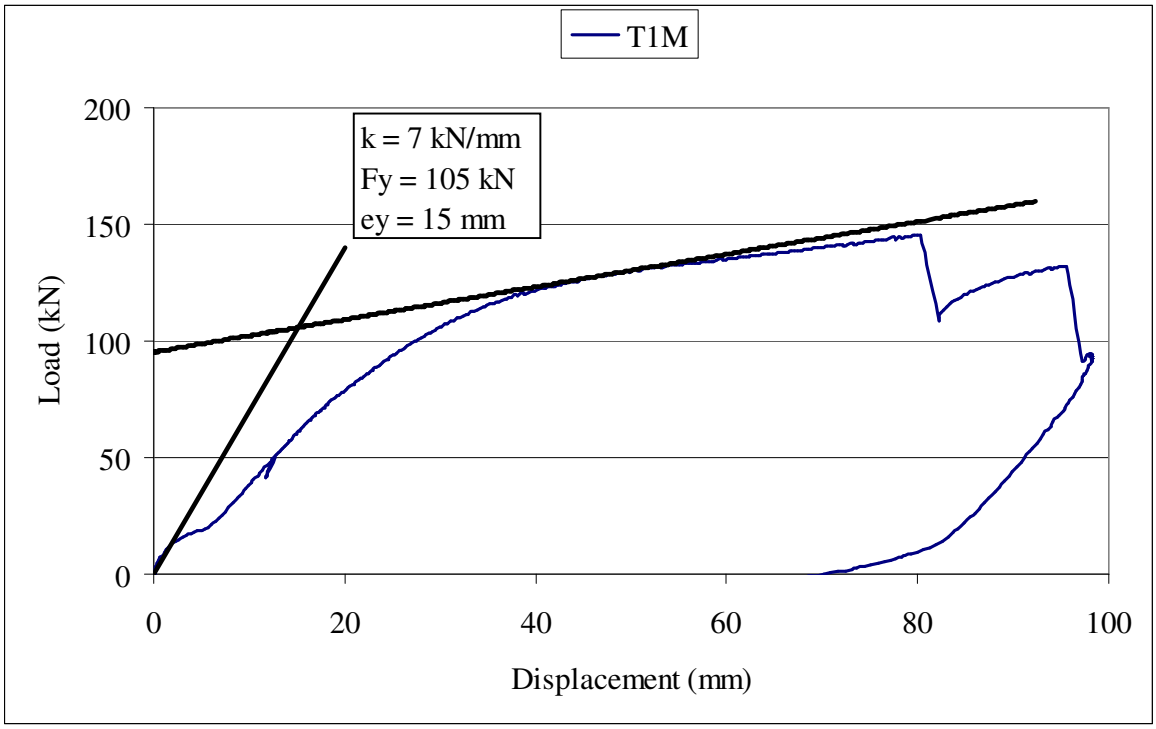

Figure 3.48. Load vs displacement curve of the specimen T1M

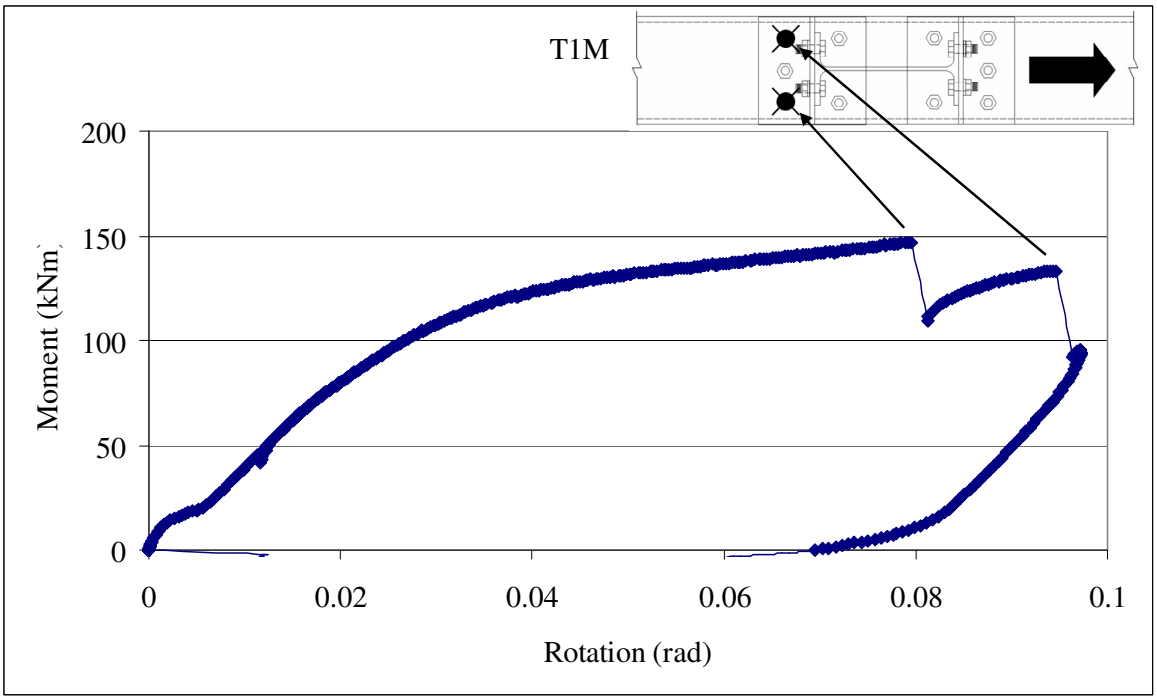

Figure 3.49. Moment vs rotation curve of the specimen T1M

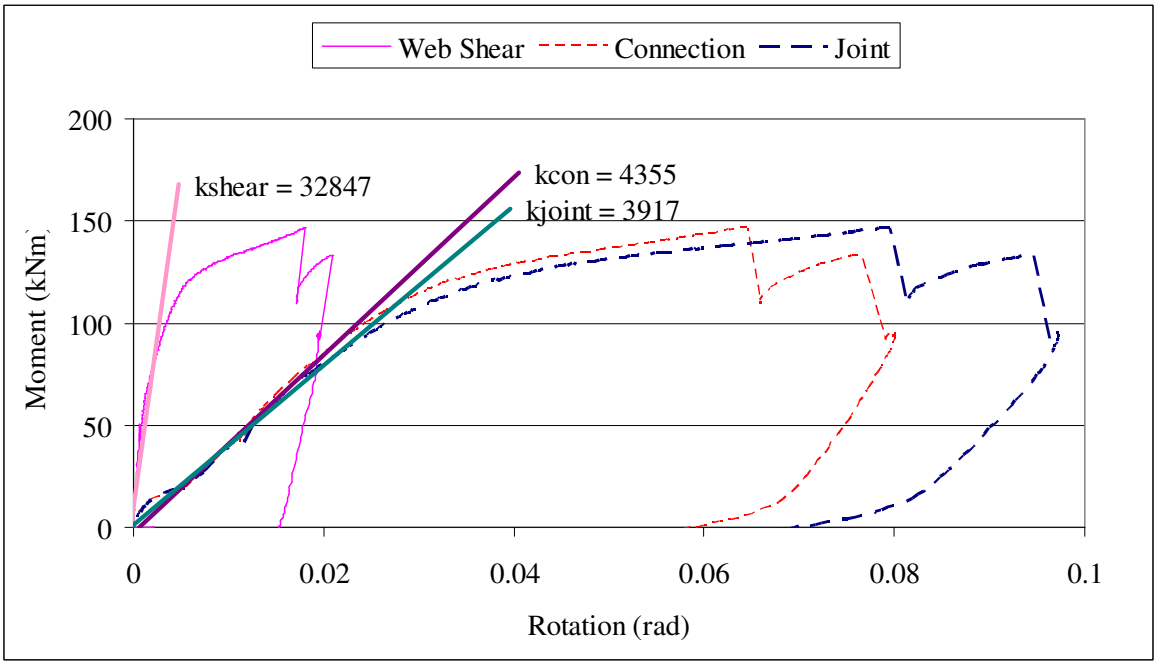

Figure 3.50. Components of joint deformation of the specimen T1M

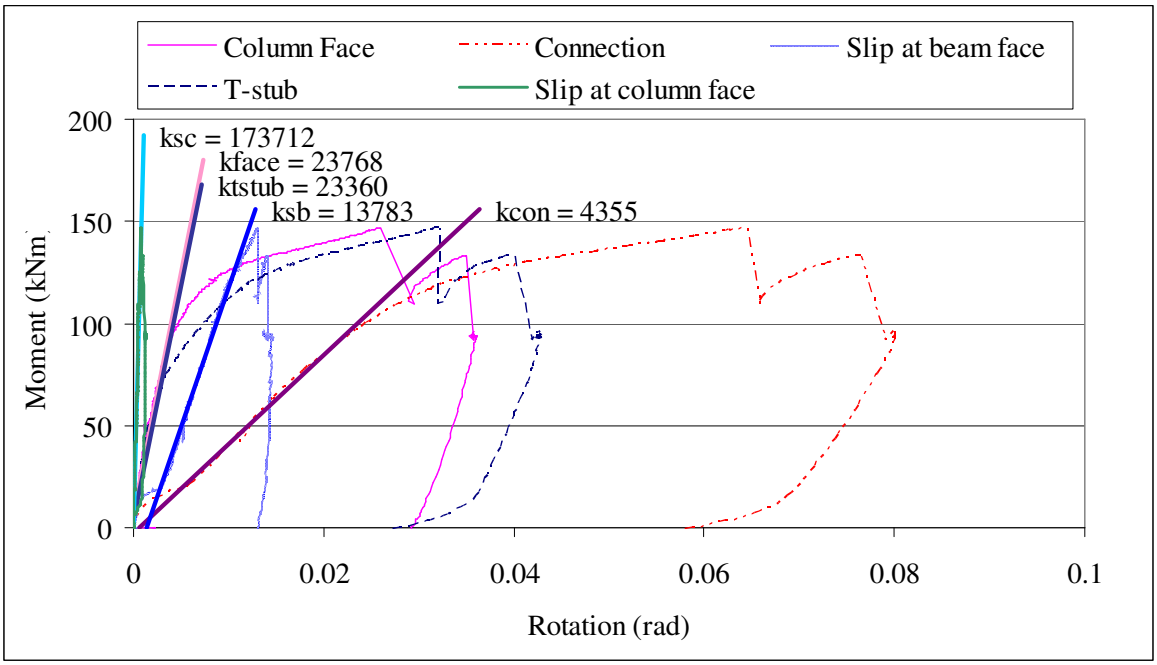

Figure 3.51. Components of connection deformation of the specimen T1M

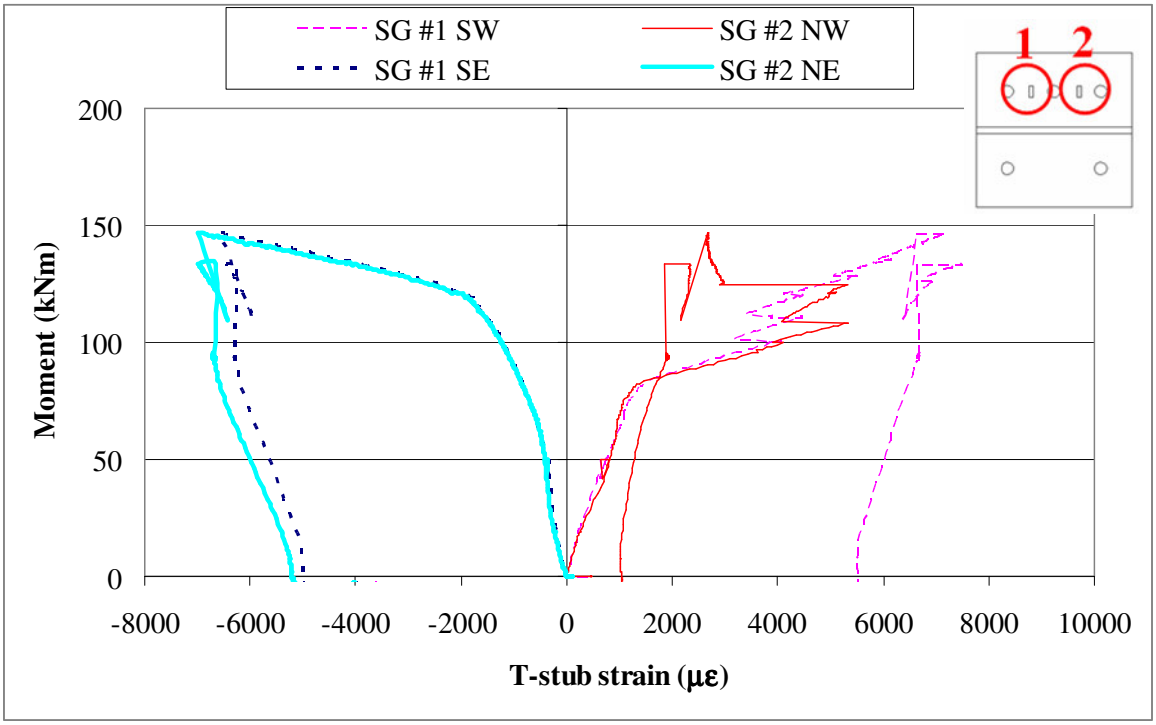

Figure 3.52. Strains at the t-stub flange of the specimen T1M

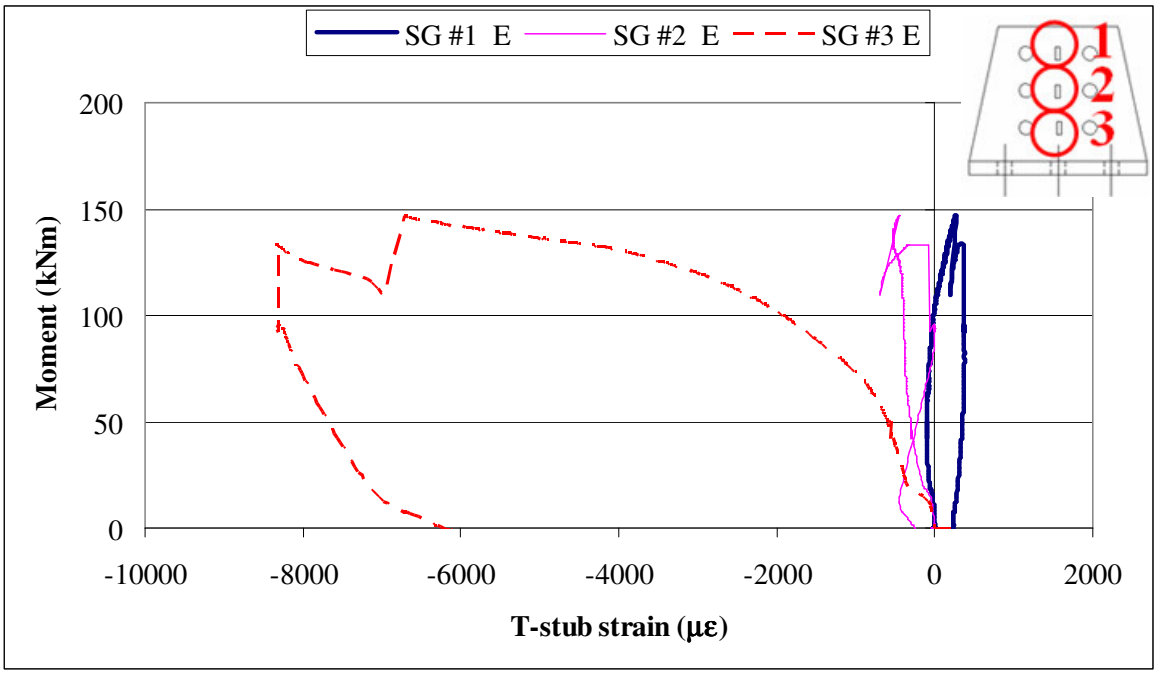

Figure 3.53. Strains at the east t-stub web of the specimen T1M

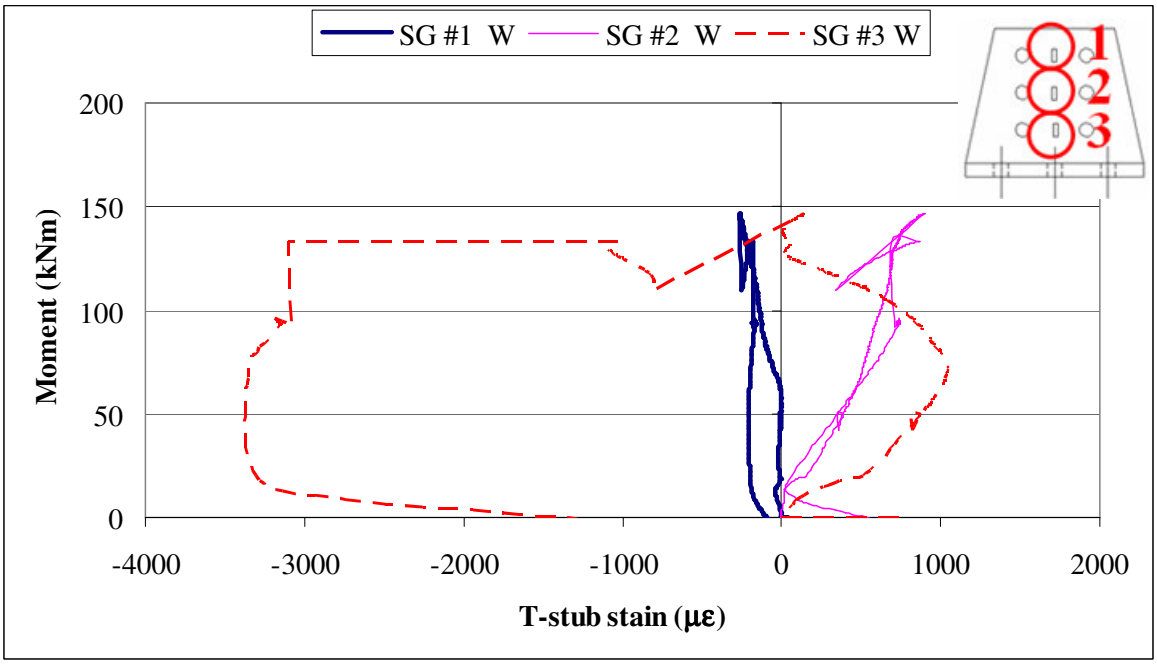

Figure 3.54. Strains at the west t-stub web of the specimen T1M

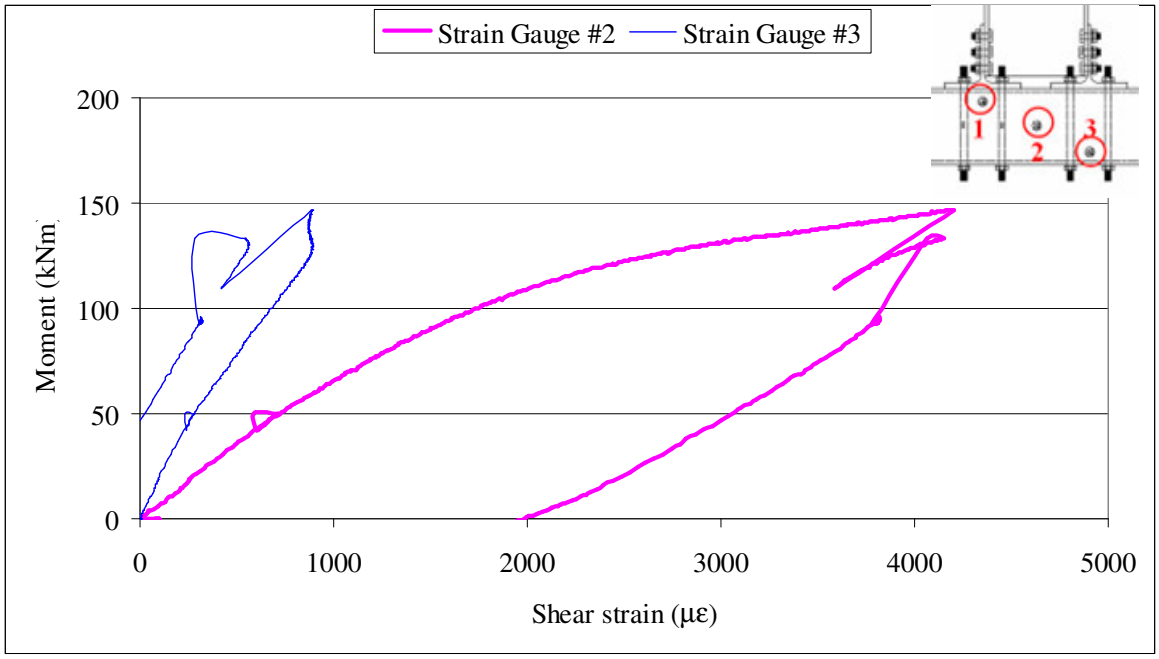

Figure 3.55. Shear strains at the shear panel zone of the specimen T1M

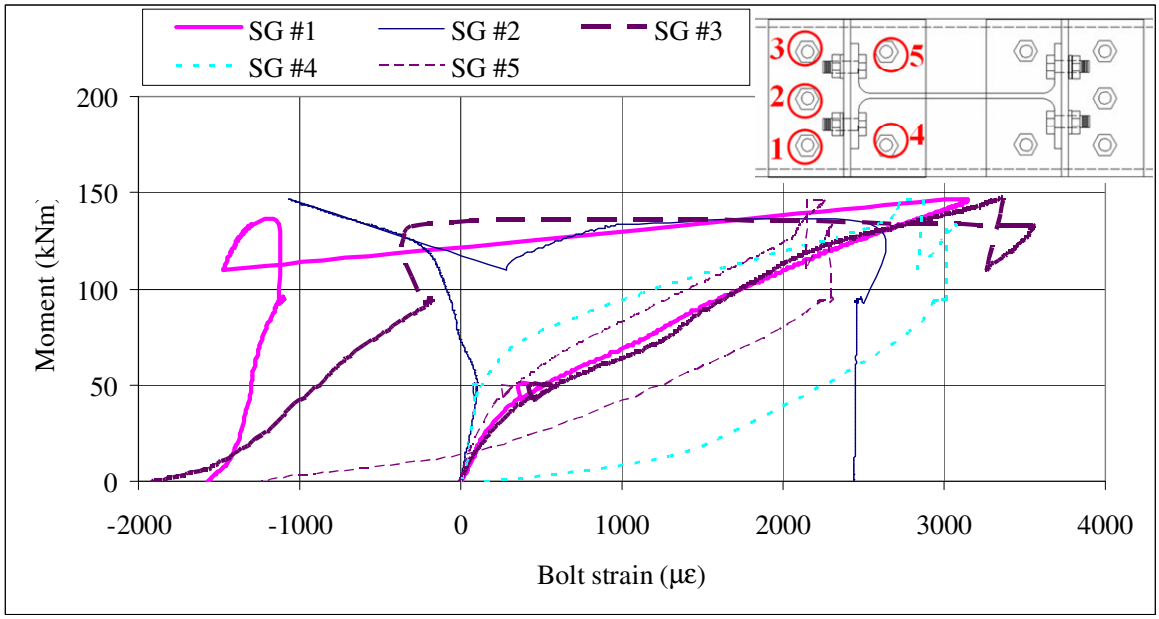

Figure 3.56. Strains on partially threaded studs strains of the specimen T1M

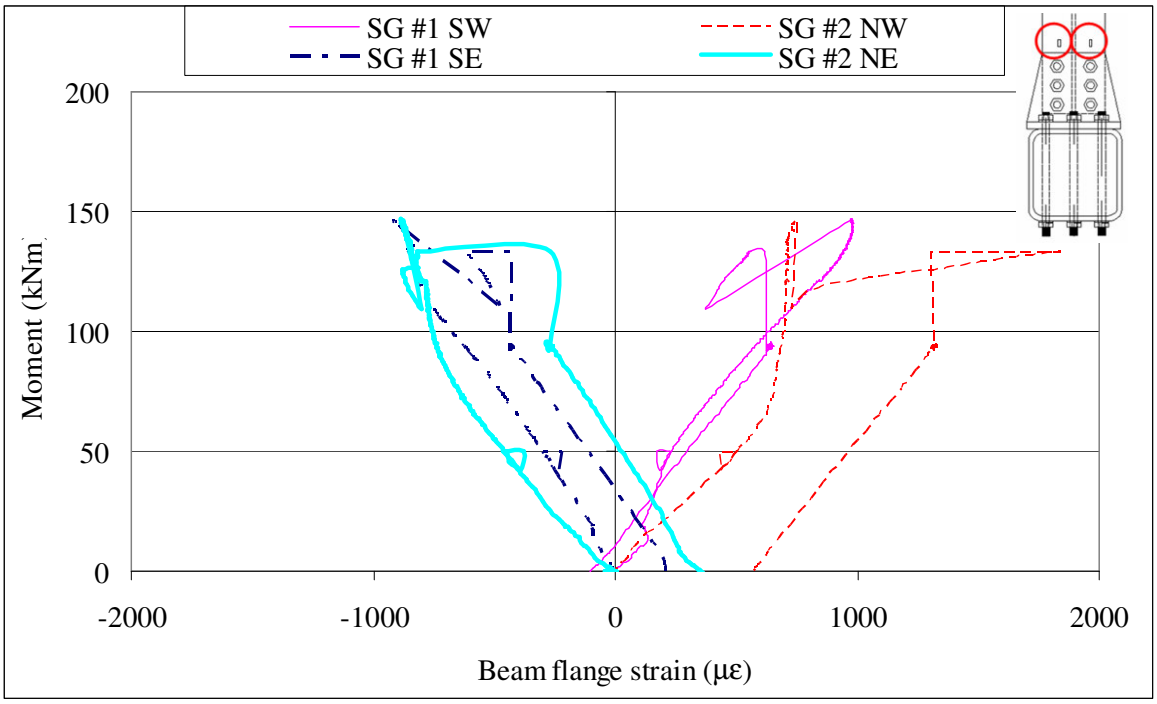

Figure 3.57. Strains at the beam flange of the specimen T1M

3.2.2. Test Specimen T2M

The specimen has been successfully tested by loading towards the east side of the specimen. Load vs displacement behaviour of the specimen is given in Figure 3.58 which indicates the parameters used to generate the loading history of the cyclic test of specimen T2C. The test continued until sudden and progressive rupture of two partially threaded studs in the west side of the specimen as shown in Figure 3.59. First stud in the north corner ruptured at the moment and rotation levels of 161.6 kNm and 0.073 rad, respectively. Then almost at the same instance, the second stud in the south corner ruptured at the moment and rotation levels of 150.2 kNm and 0.075 rad, respectively.

Components of joint and connection deformations of the specimen have been given with the initial stiffness values in Figures 3.60 and 3.61, respectively. Although web shear panel zone of the joint performed much stiffer than the connection, the deformation level should also be taken into account. Since the specimen is bolted connection slips plays an

important role in the total behaviour of the connection. Slips, especially the slips at the junction of t-stub-beam flange, took place until the levels of 20-25 kNm moment and 0.005 rad rotation. After then bearing resistance of the junction governed and behaved almost linear until failure load. This behaviour was also observed same for the slip at the junction of t-stub-column face but stiffer and in lower deformation levels. The main sources of connection deformation were bending of the column face and the t-stub. Although their stiffness levels were very close, the deformation level of the t-stub was slightly higher.

Strain measurements during test are given in Figures 3.62 to 3.67. By checking the deformability of the connection components the first yielding started west t-stub flange of the specimen at the moment level of 80 kNm. Then it was followed by column face in bending at moment level of 125 kNm. (Figure 3.62) Strains at the t-stub web remained elastic during the test except for the location number three in the Figures 3.63 and 3.64. This was due to deformation after yielding of the t-stub, thus bending of the t-stub web at this location. As given in Figure 3.65, shear strains at location number two reached 0.002 strains at the moment level of 130 kNm. Shear strains at other locations remained less than 0.002 strain level. Partially threaded studs have been snug-tightened. The average strain level before testing was 828 microstrains. The studs were ruptured at the strain levels of 0.0025-0.003. The strains of the stud in middle (position two in Figure 3.66) was in low levels even it lose its pretension until the rupture of the bolt in position number one, there after it took the load and prevented the complete sudden failure by the help of the stud in position number four. As presented in Figure 3.67, the beam flanges remained elastic during the whole test but in levels of yielding at the ultimate load levels, especially the west flange of the beam.

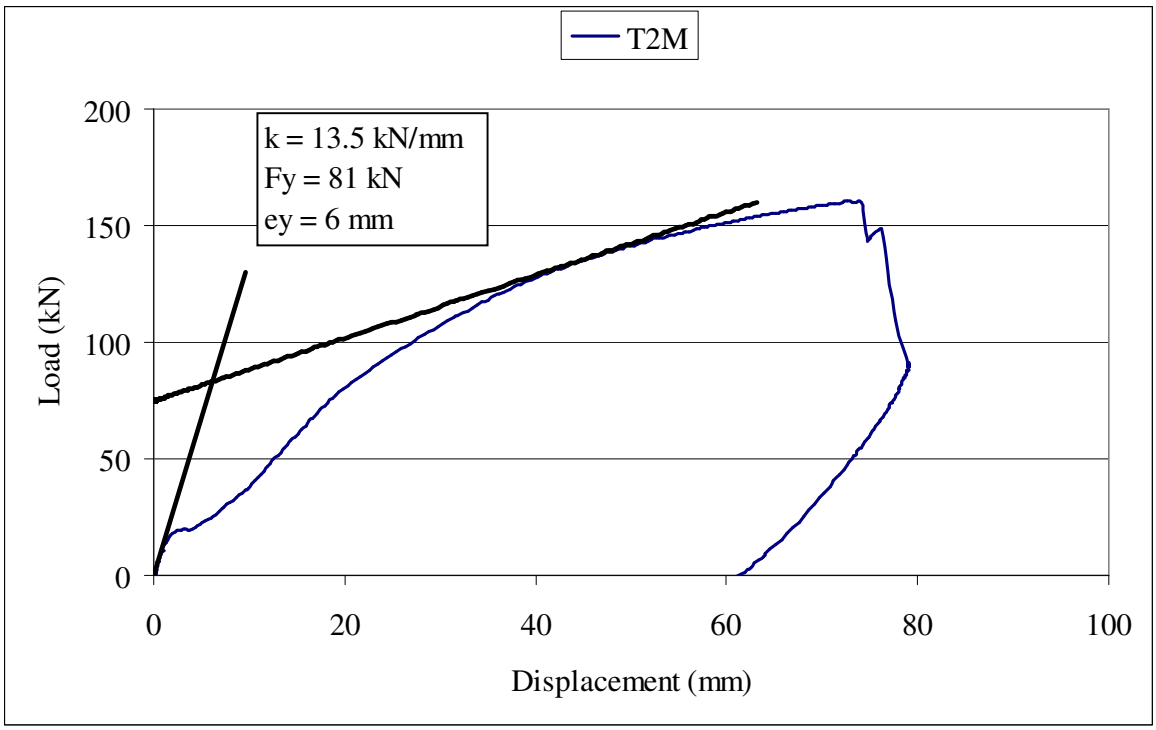

Figure 3.58. Load vs displacement curve of the specimen T2M

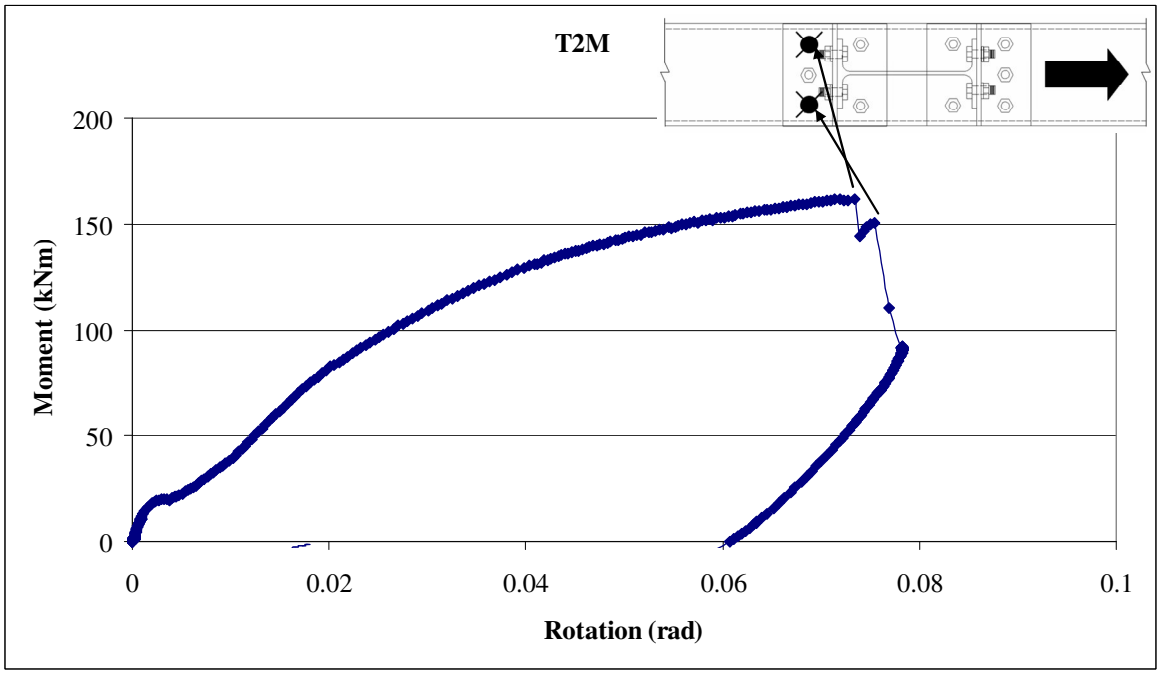

Figure 3.59. Moment vs rotation curve of the specimen T2M

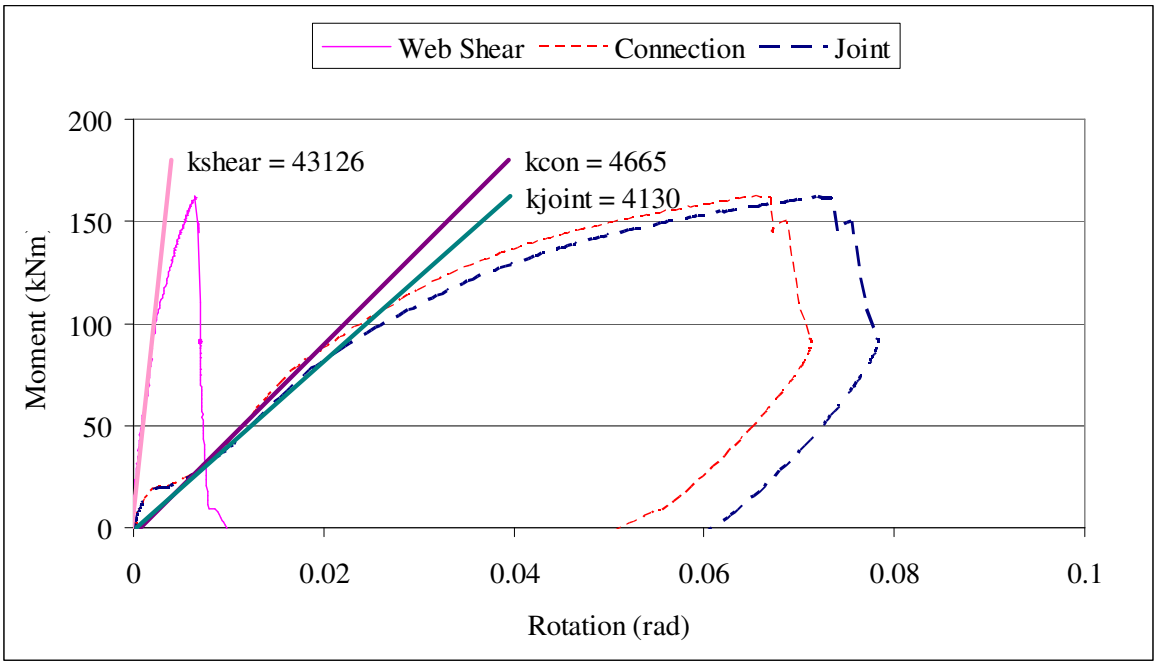

Figure 3.60. Components of joint deformation of the specimen T2M

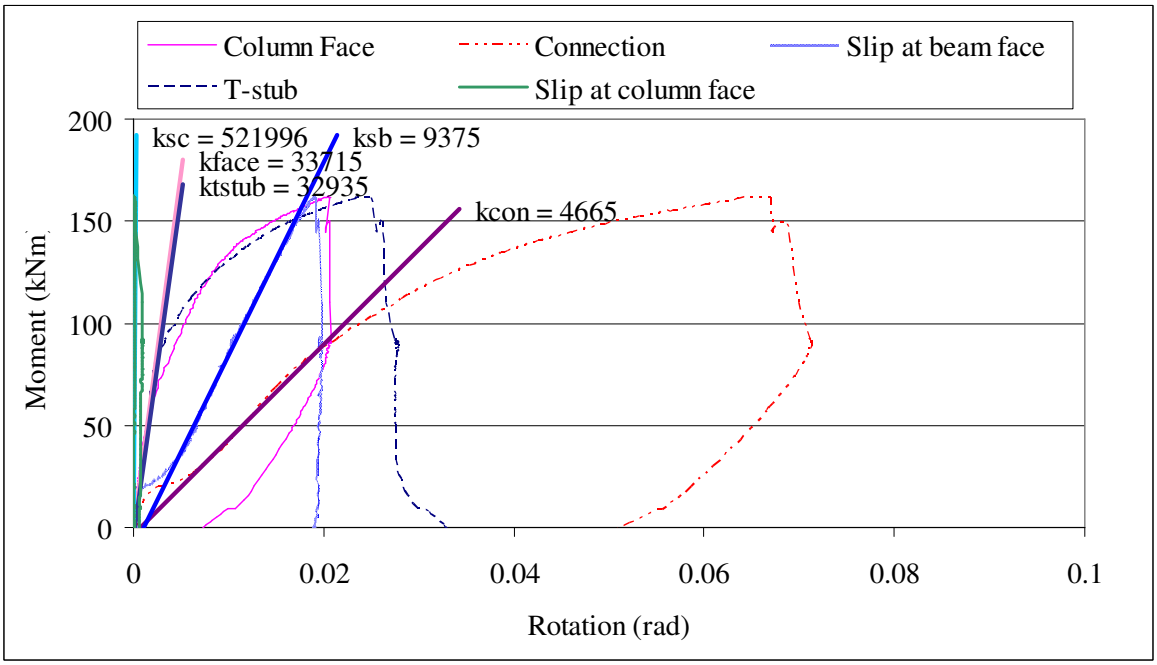

Figure 3.61. Components of connection deformation of the specimen T2M

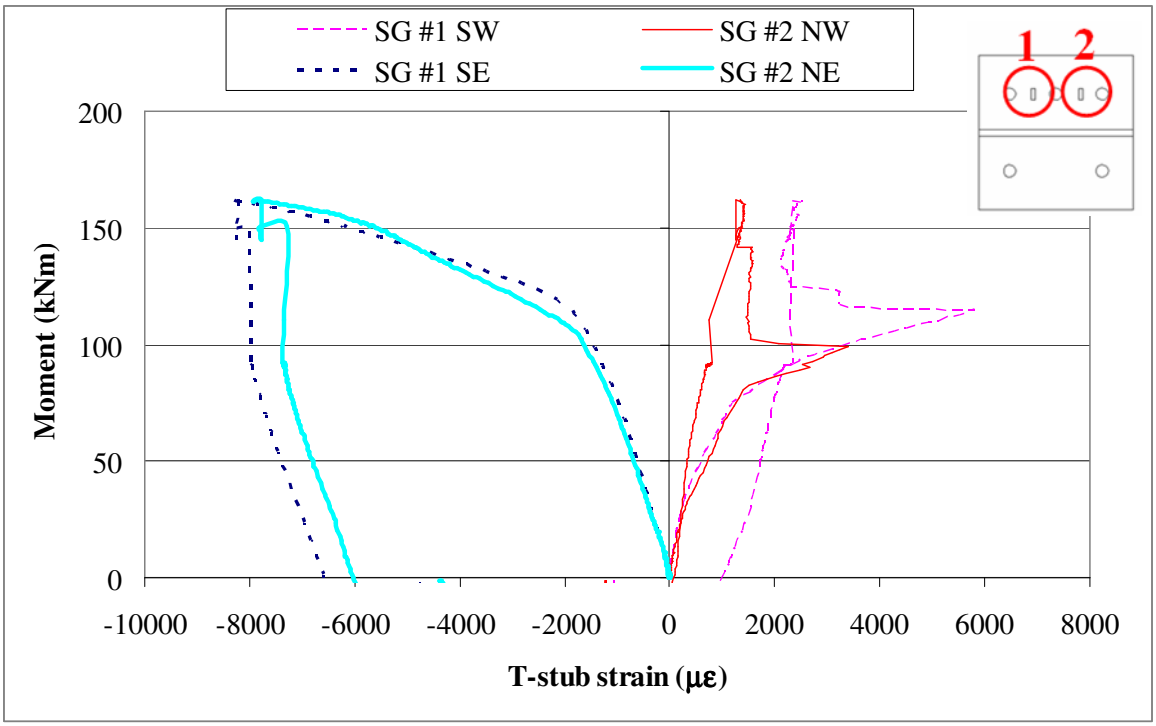

Figure 3.62. Strains at the t-stub flange of the specimen T2M

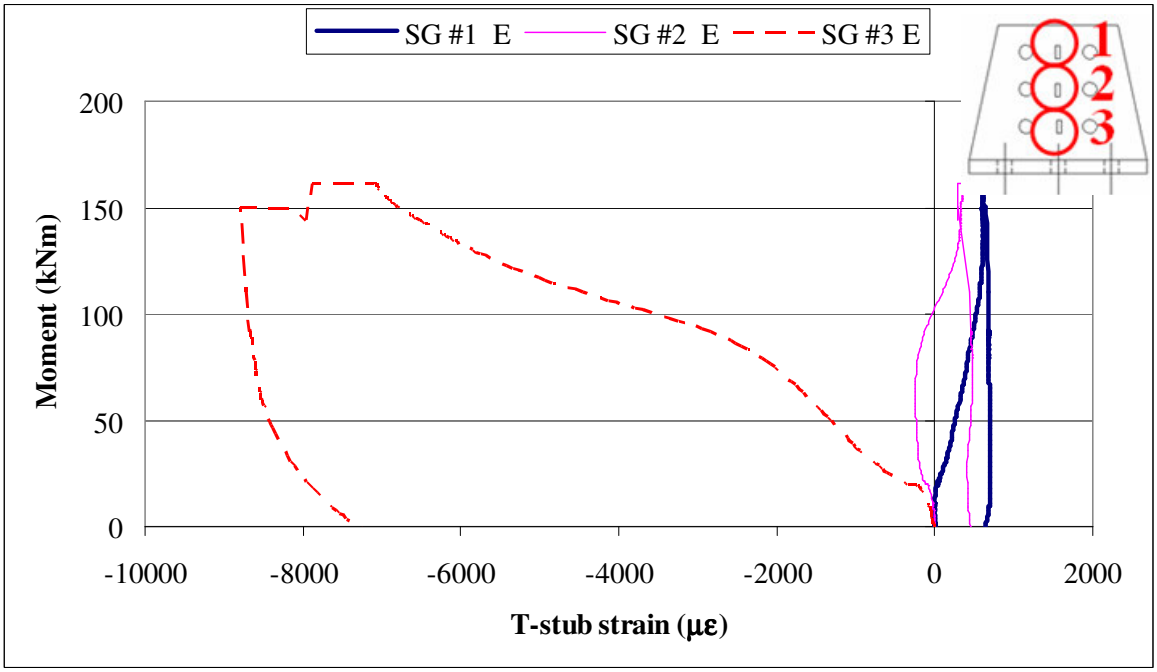

Figure 3.63. Strains at the east t-stub web of the specimen T2M

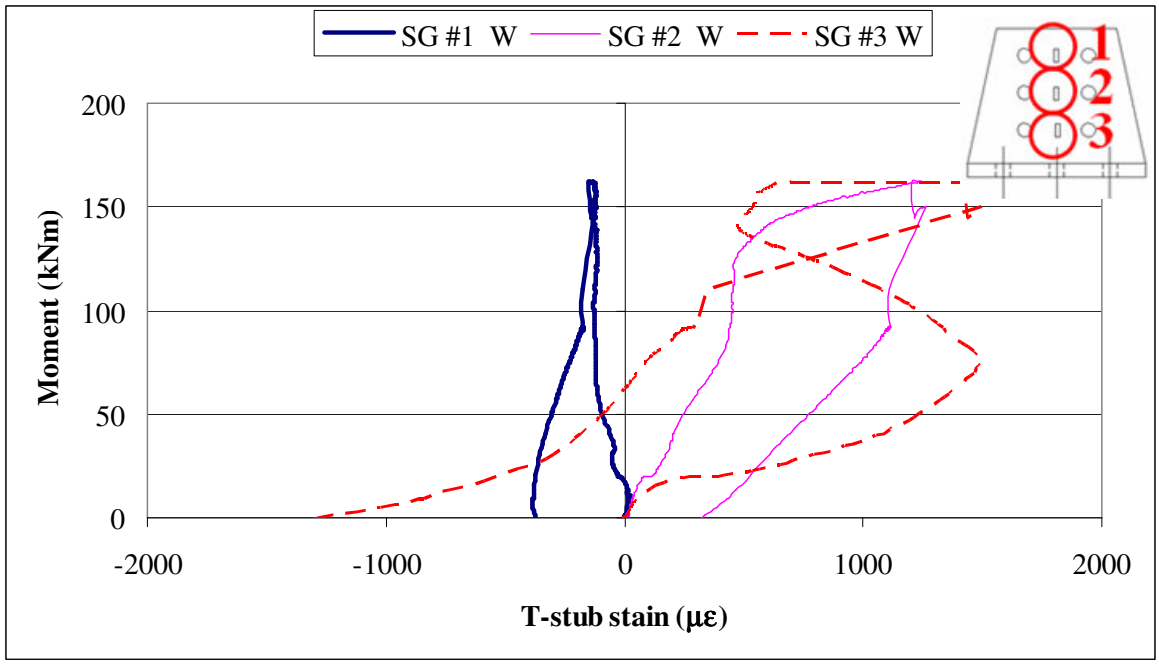

Figure 3.64. Strains at the west t-stub web of the specimen T2M

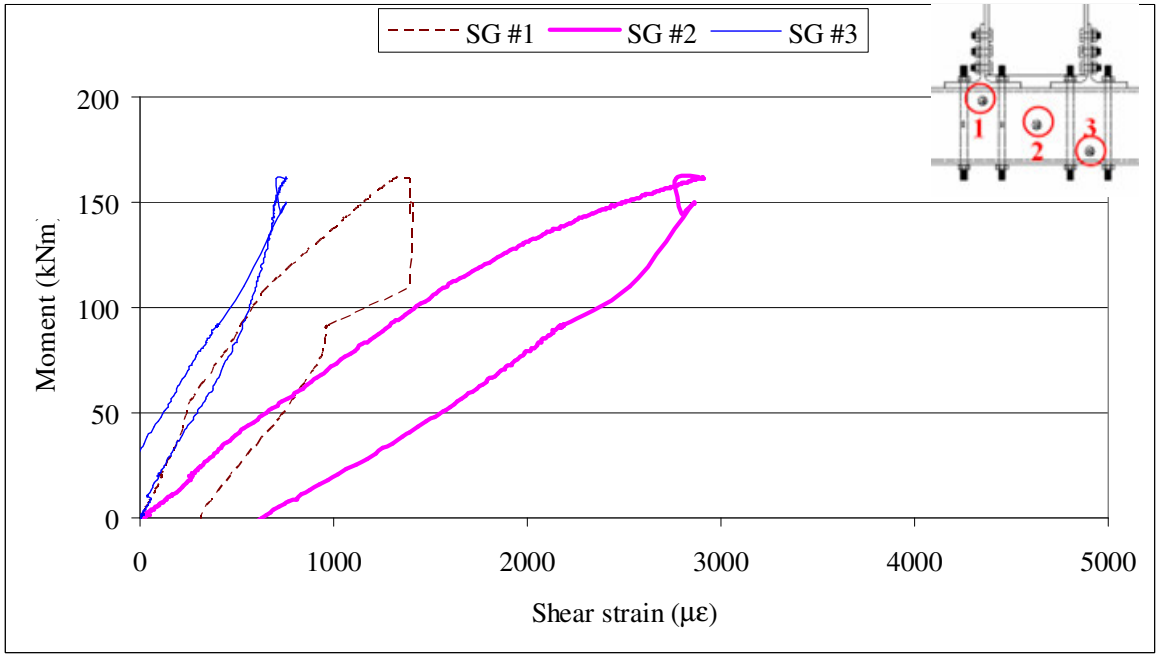

Figure 3.65. Shear strains at the shear panel zone of the specimen T2M

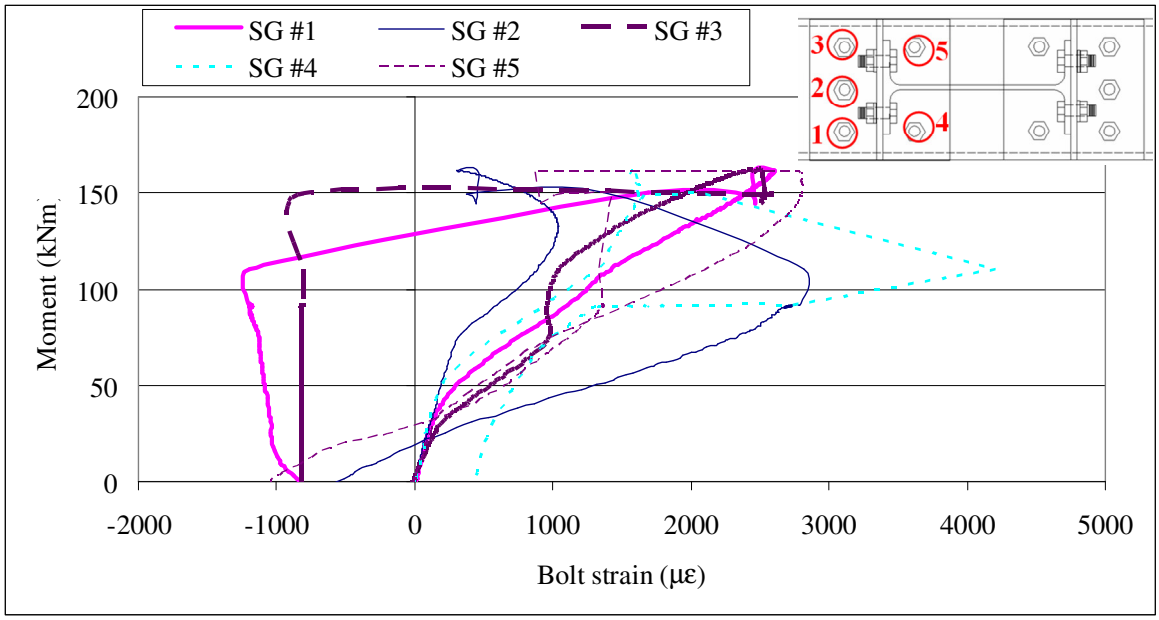

Figure 3.66. Strains on partially threaded studs strains of the specimen T2M

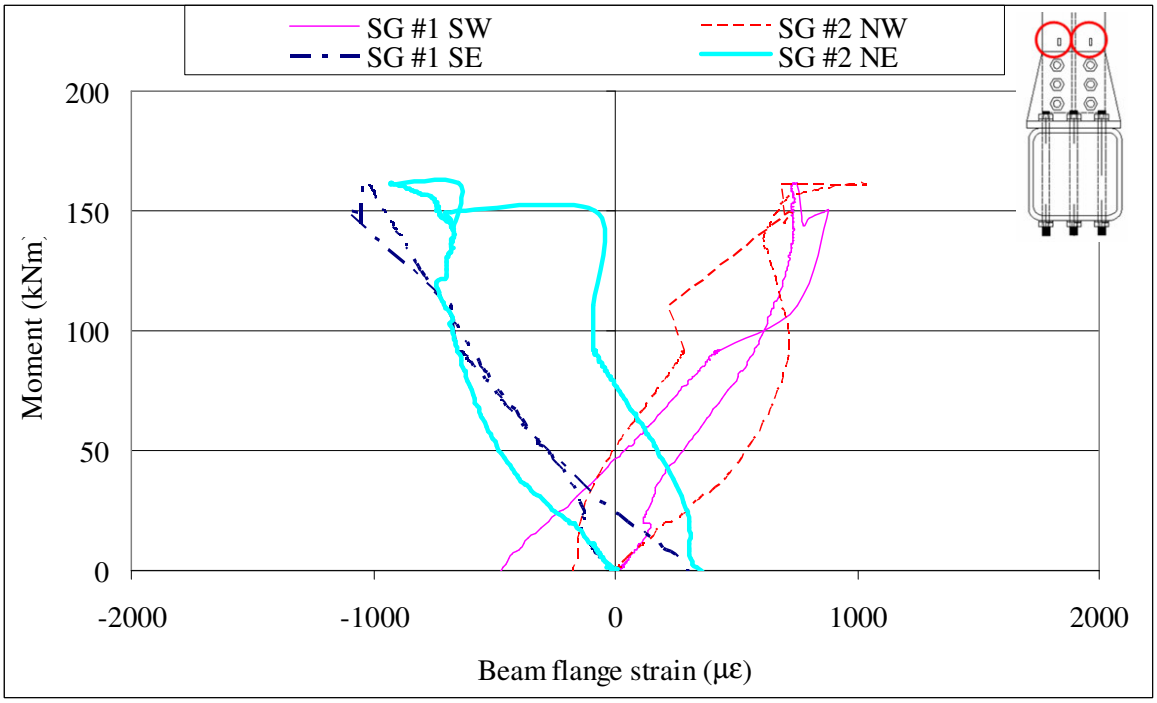

Figure 3.67. Strains at the beam flange of the specimen T2M

3.2.3. Test Specimen T1C

The specimen has been successfully tested by cyclic displacement loading. By generating from the test results of the specimen T1M, the loading history of the specimen T1C is given in Figure 3.68. At 11^{th} cycle maximum positive displacement of the loading actuator has been reached and after then the positive displacement amplitude has remained constant at this limit. After 14^{th} cycle, the test had to be continued at the maximum positive and negative displacement limits of the loading actuator until low cycle fatigue failure. Load vs displacement behaviour of the specimen is given in Figure 3.69. By checking the deformability of the joint and connection components, major yielding took place in the eighth cycle due to deformations of the column face, the t-stub and the web shear panel at almost the same load levels. Since after deformation in the first cycle of the groups, column face did not recover its original position, in second and third cycles of the group no or very little resistance was observed at the column face and web shear panel. The test continued until rupture of west t-stub flange with a loud noise along its stem at the 26th cycle. Moment vs rotation curve and its envelope is given in Figure 3.70.

There were small noises and big noises coming from the specimen during the test. Small noises were especially at the beginning of the cycles while the load was increasing. These were associated with slips at the junction of t-stub-beam flange and occurred in both forward and reverse loadings of the cycles until cycle 12. In the first cycles, these slips took place until 20-30 kNm moment levels where this level dropped down to 5-10 kNm in the tenth cycles. The big noises were frequently and irregular, generally took place when the load was approaching to the peak values. These were associated with slips at the junction of t-stub-column face at the earlier cycles and started happening first at the fifth cycle. Then in latter cycles, big noises due to thread tearing of the partially threaded studs took place after the column face started deforming. At the peak point of the eighth cycle, a very loud noise came out due to unexpected rupture of the bolt at the top south corner of the west t-stub web. Hopefully, this did not affect much the performance of the specimen.

Strain measurements during test are given in Figures 3.71 to 3.75. The strain readings at t-stub flanges are not proper especially in the reverse cycles, this makes it

difficult to evaluate. Hopefully the measurements at t-stub web give an idea about the behaviour. Strains at the t-stub web remained elastic during the test except for the location number three in the Figures 3.72 and 3.73. This was due to deformation after yielding of the t-stub, thus bending of the t-stub web at this location. This yielding first took place in the eighth cycle at 107 kNm moment levels in both forward and reverse loadings. As given in Figure 3.74, shear strains at location number one and two reached yield level at the moment level of 113 kNm of the eighth cycle. Unfortunately the shear strain reading at other location is not proper. Strain readings also verified that in second and third cycles of the group cycles no or very little resistance was observed at web shear panel. As presented in Figure 3.75, the beam flanges remained elastic during the whole test.

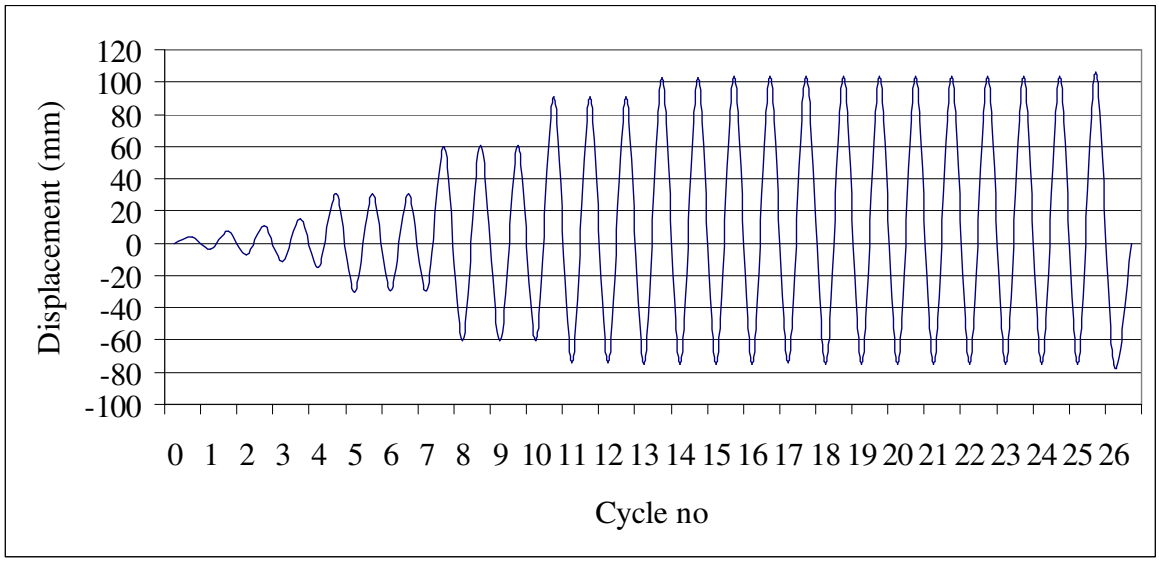

Figure 3.68. Cyclic loading history of the specimen T1C

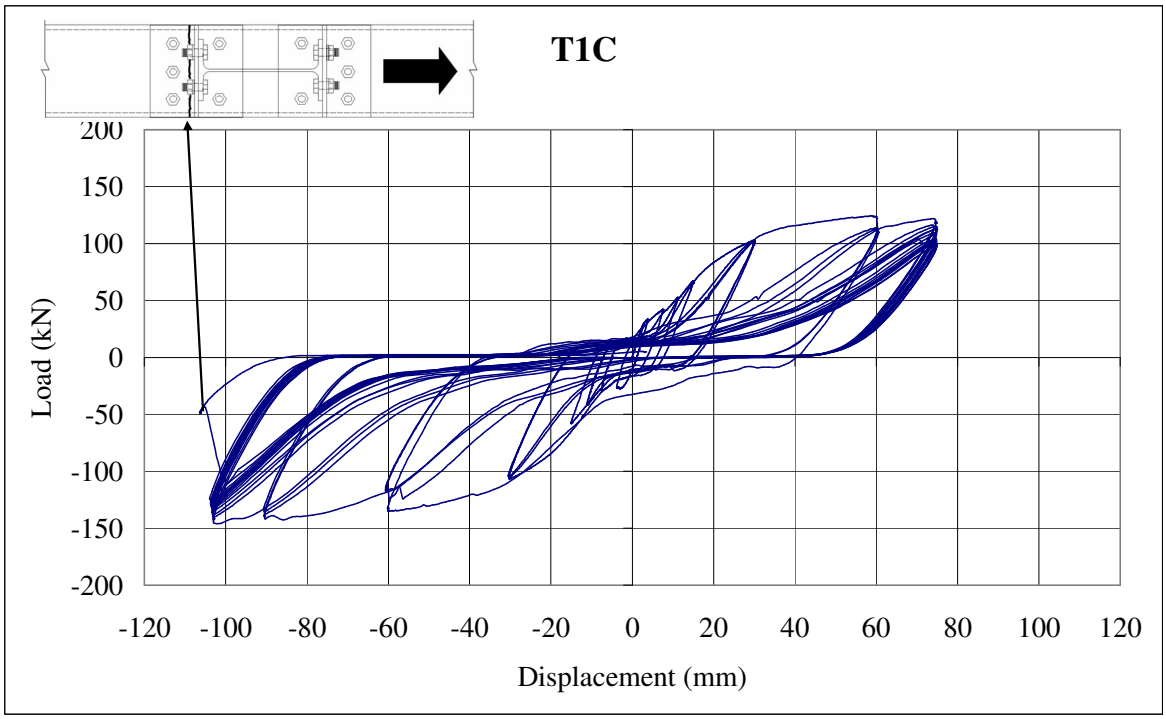

Figure 3.69. Load vs displacement curve of the specimen T1C

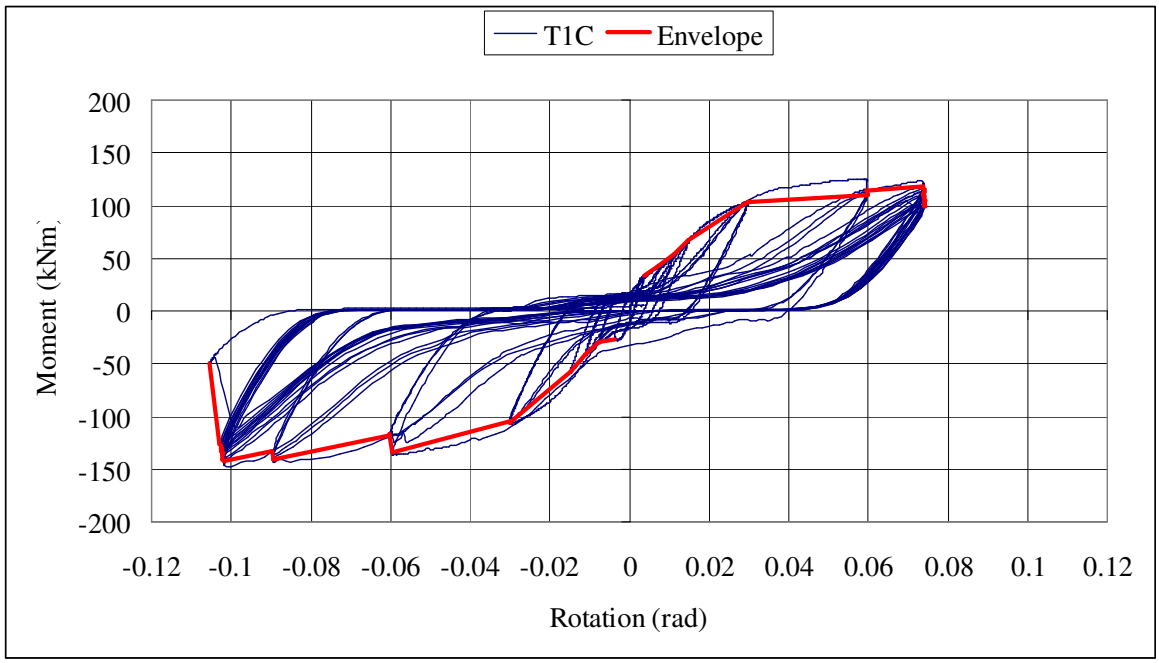

Figure 3.70. Moment vs rotation curve of the specimen T1C

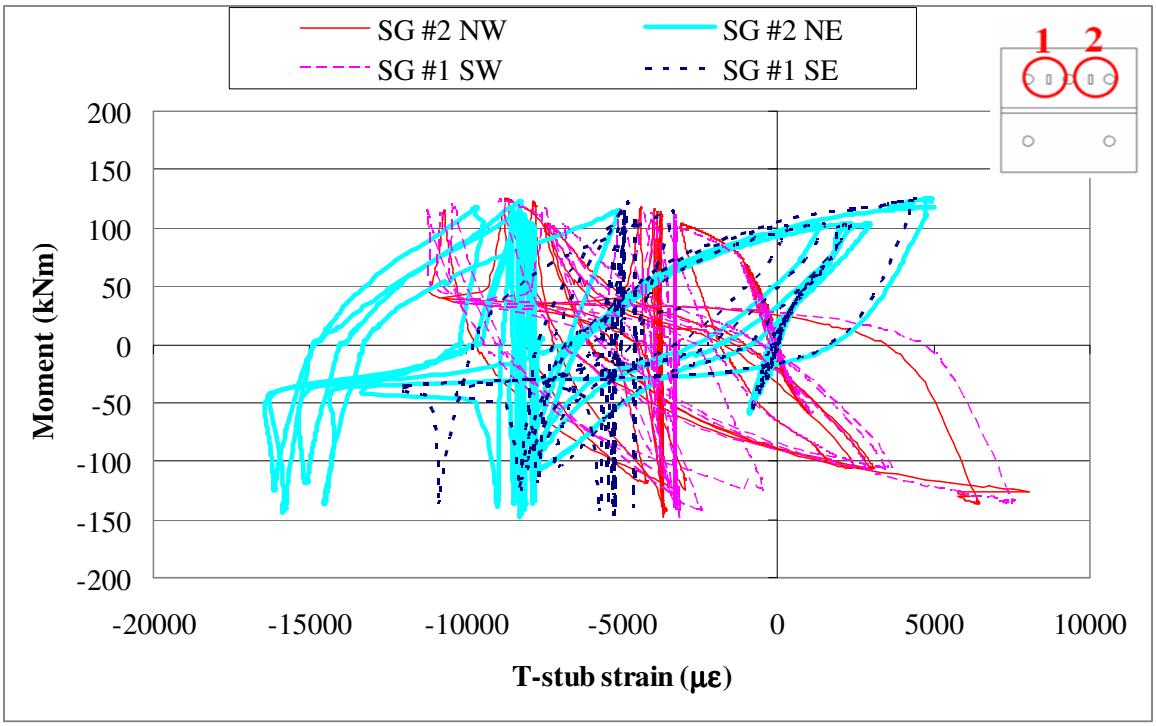

Figure 3.71. Strains at the t-stub flange of the specimen T1C

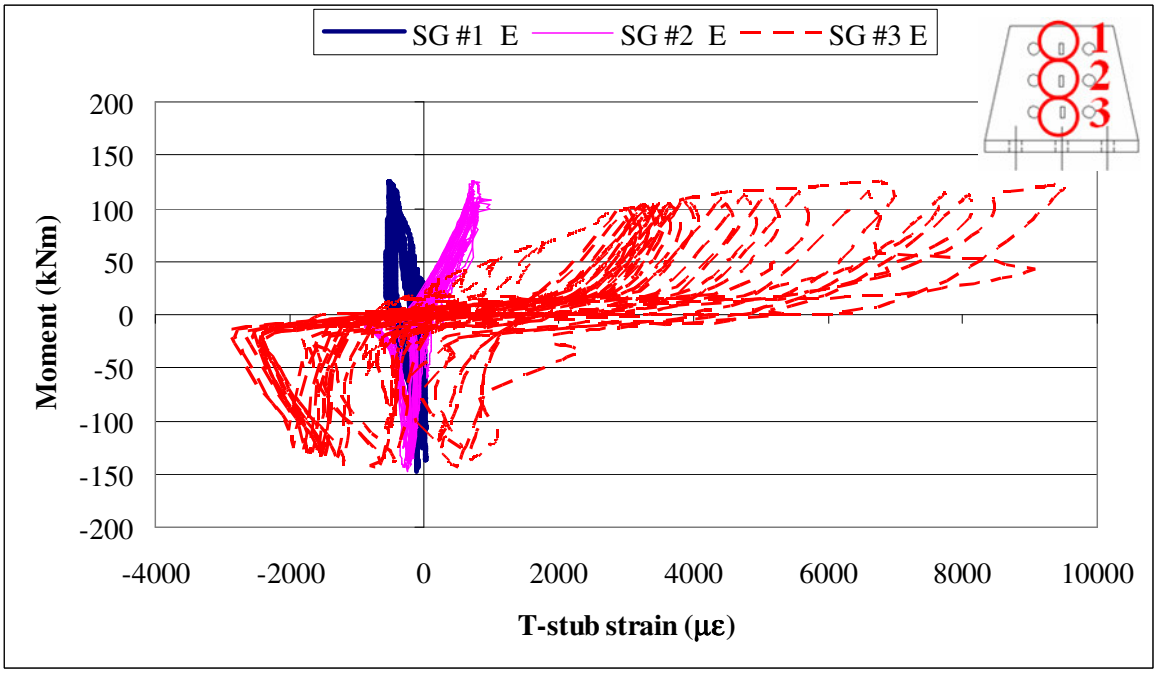

Figure 3.72. Strains at the east t-stub web of the specimen T1C

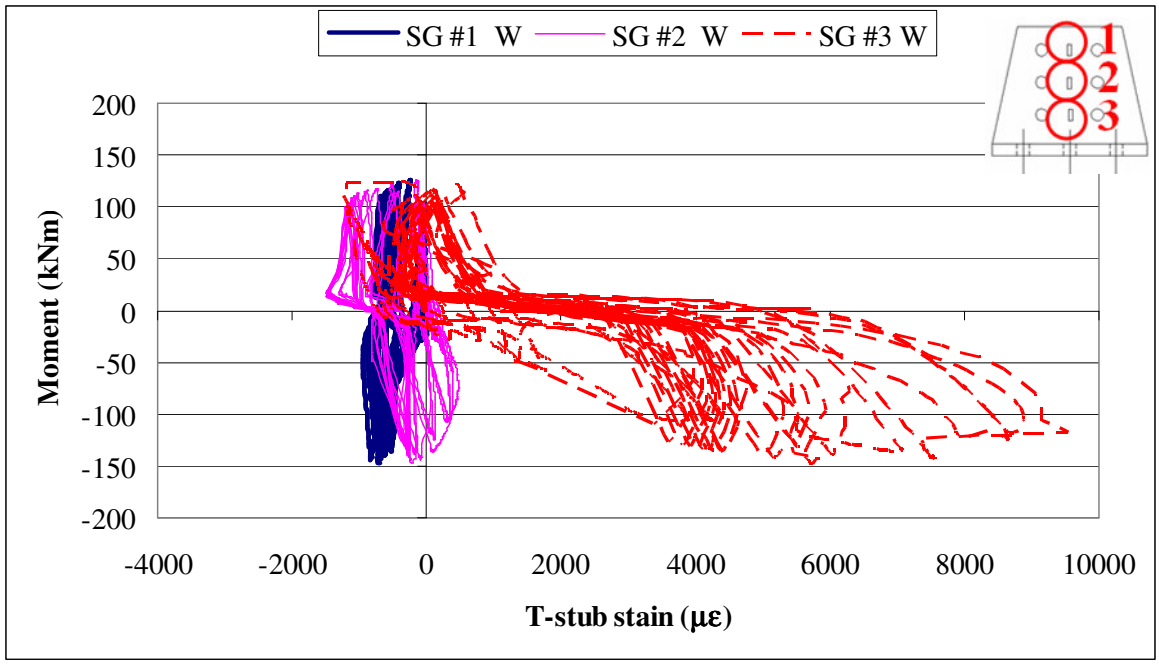

Figure 3.73. Strains at the west t-stub web of the specimen T1C

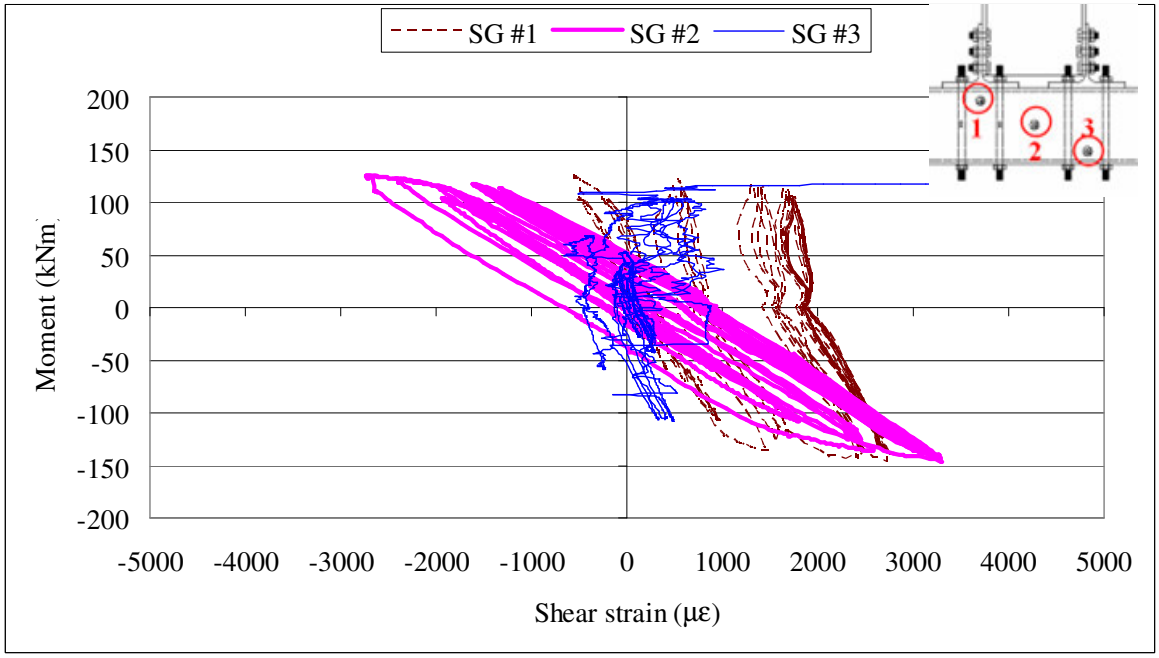

Figure 3.74. Shear strains at the shear panel zone of the specimen T1C

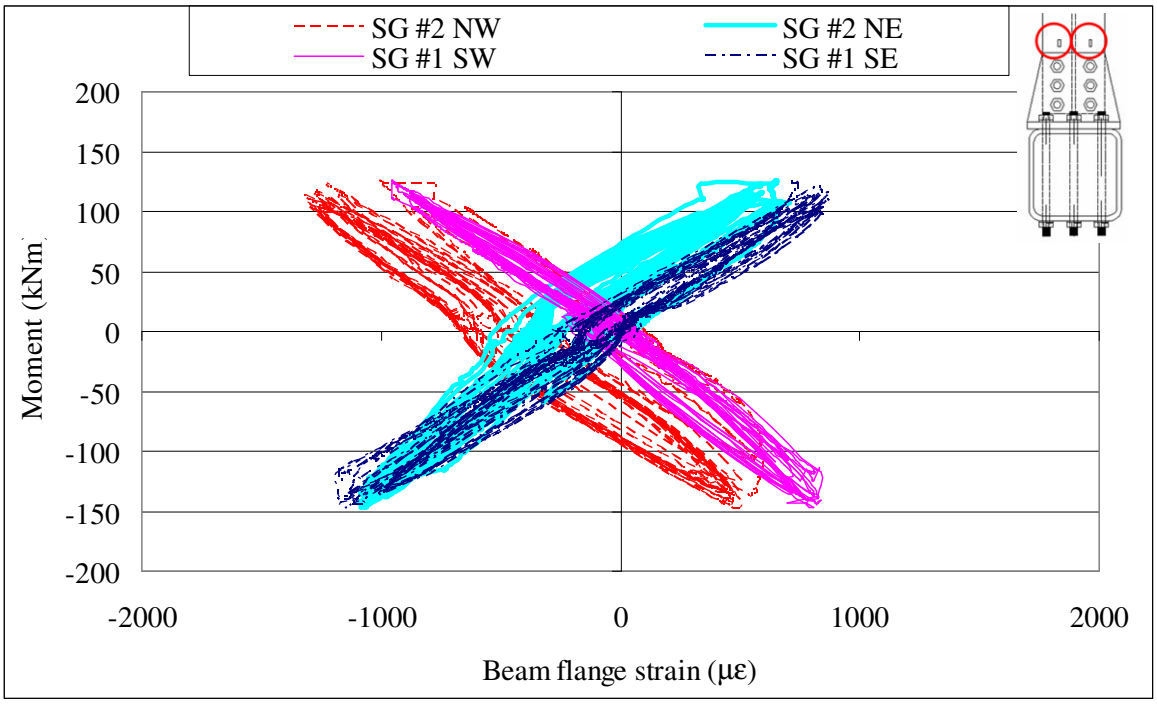

Figure 3.75. Strains at the beam flange of the specimen T1C

3.2.4. Test Specimen T2C

The specimen has been successfully tested by cyclic displacement loading. By generating from the test results of the specimen T2M, the loading history of the specimen T2C is given in Figure 3.76. Load vs displacement behaviour of the specimen is given in Figure 3.77. By checking the deformability of the joint and connection components, at moment levels of 80-90 kNm of the eighth cycle, the trend of the started becoming flatten then after two group cycles in the next loading step which was cycle 11, major yielding took place due to deformations of the column face and the t-stub at almost the same moment levels of 110 kNm.

This was also observed during the test by checking the tightness of the nuts of the partially threaded stud group at the loading direction side at each cycle. When the nuts become loose, this means there is gap opening in between the column face and t-stub, in other words column face has deformed beyond its elastic limit. Until 11th cycle, the nuts

were very tight. After deformation in the first cycle of the groups, column face did not recover to its original position, in second and third cycles of the group no or very little resistance was observed at the column face. At the 20th cycle crack initiation was observed at the east t-stub flange along the its stem starting from the north to south. During the reverse loading of the same cycle similar crack initiation was observed also at the west t-stub flange along the its stem starting from the south to north. At the end of this cycle the crack propagated about 100 mm (half of the t-stub width). 21st cycle was the second group cycle and at peak displacement of the forward loading sudden rupture of one partially threaded stud, which was the south east corner stud of the east stud group, took place. The test continued until complete rupture of the west t-stub flange with a loud noise along its stem at the 27th cycle. Moment vs rotation curve and its envelope is given in Figure 3.78.

There were small noises and big noises coming from the specimen during the test. Small noises were especially at the beginning of the cycles in low load levels while the load was increasing. These were associated with slips at the junction of t-stub-beam flange and occurred in both forward and reverse loadings of the cycles until cycle 13. In the first cycles, these slips took place until 25-35 kNm moment levels where this level dropped down to 5-15 kNm in the tenth cycles. The big noises were frequently and irregular, generally took place when the load was approaching to the peak values. These were associated with slips at the junction of t-stub-column face at the earlier cycles and started happening first at the sixth cycle. Then in latter cycles, big noises due to thread tearing of the partially threaded studs took place mainly after the column face started deforming. These noises continued from eighth cycle till 20th cycle.

Strain measurements during test are given in Figures 3.79 to 3.84. The strain readings at t-stub flanges are not proper especially after 11th cycle and the strain gauges pealed off after 23rd cycle due to excessive deformation at the t-stub flange. At 110 kNm moment levels of 11th cycle strain measurements at the flanges and webs of the t-stub showed yielding at the stem region. As presented in Figure 3.82, the strains on backing plate did not show perfectly yielding behaviour but the trend of the readings became flatten at 70 kNm moment of eighth cycle and 110 kNm moment of 11th cycle. At 130 kNm moment of 17th cycle, it started giving more flatten trend. Again strains at the t-stub web locations of one and two in Figures 3.80 and 3.81, remained elastic during the test. As

given in Figure 3.83, shear strains at location number two and three reached yield level at the moment levels of -130 kNm and +110 kNm of the 11th cycle respectively. Shear strain reading at location one were in the limits of yielding at the moment level of 120 kNm of the 14th cycle. Different than others this strain gauge also showed more resistance in second and third cycles of the group cycles, especially in the forward loadings. As presented in Figure 3.84, the beam flanges remained elastic during the whole test.

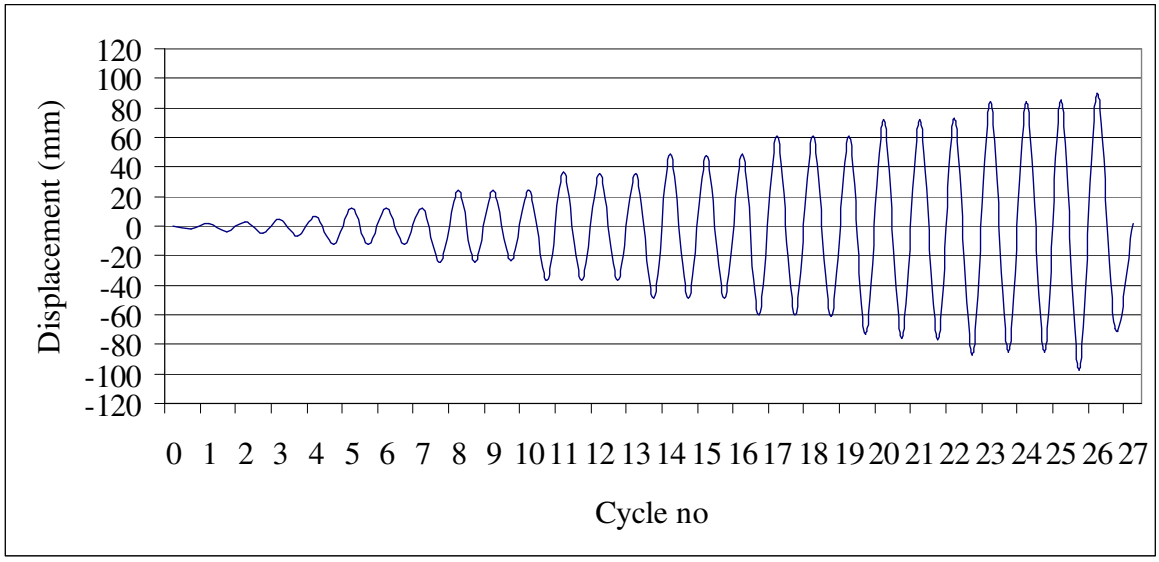

Figure 3.76. Cyclic loading history of the specimen T2C

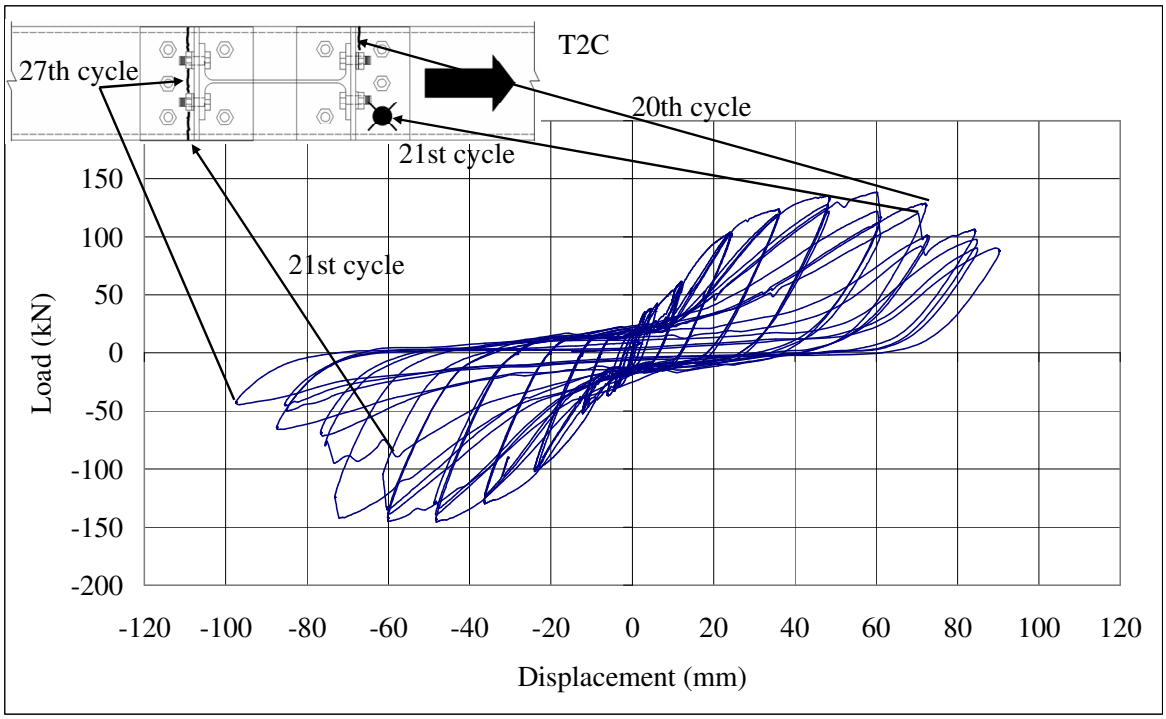

Figure 3.77. Load vs displacement curve of the specimen T2C

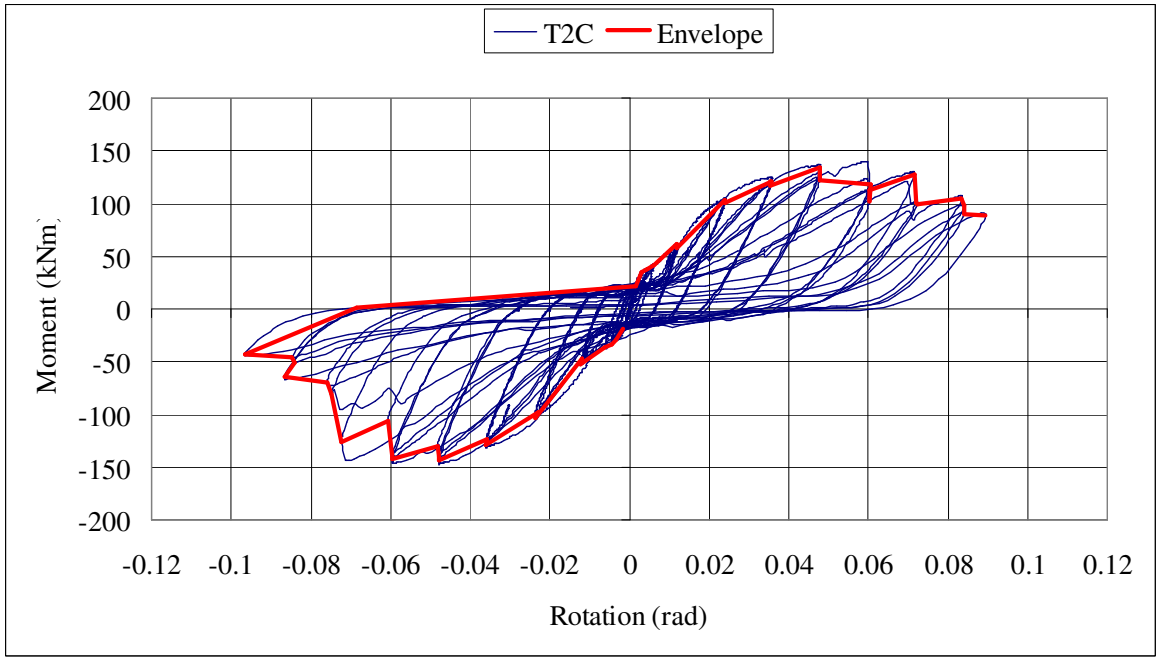

Figure 3.78. Moment vs rotation curve of the specimen T2C

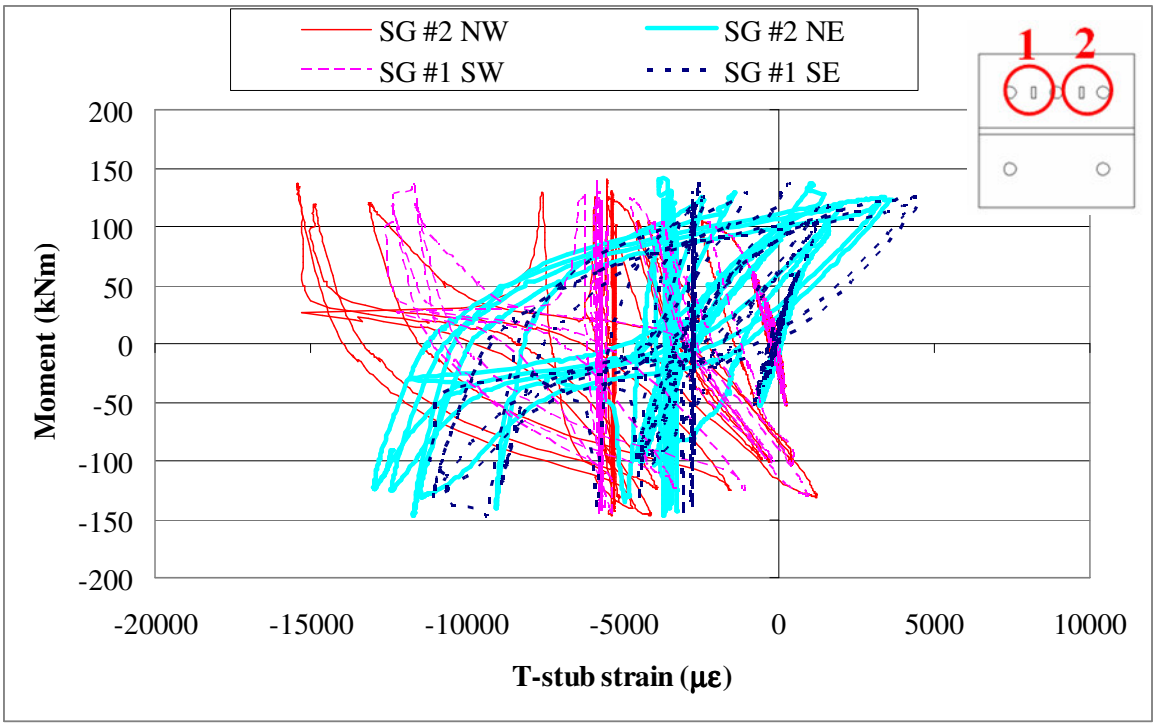

Figure 3.79. Strains at the t-stub flange of the specimen T2C

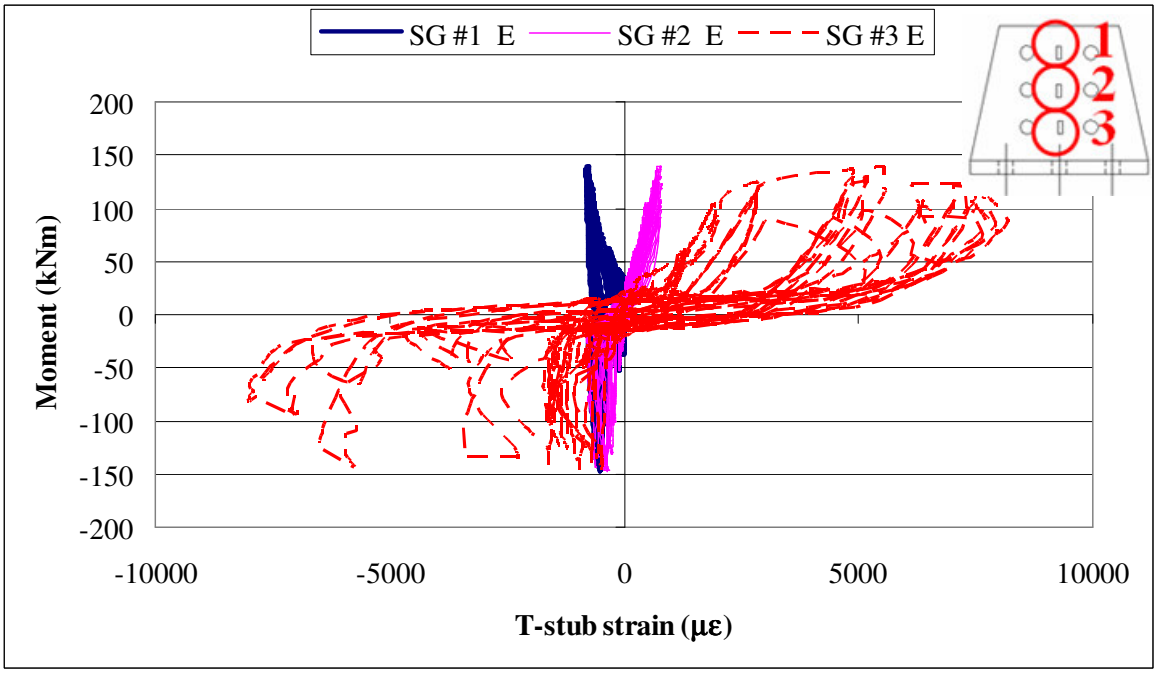

Figure 3.80. Strains at the east t-stub web of the specimen T2C

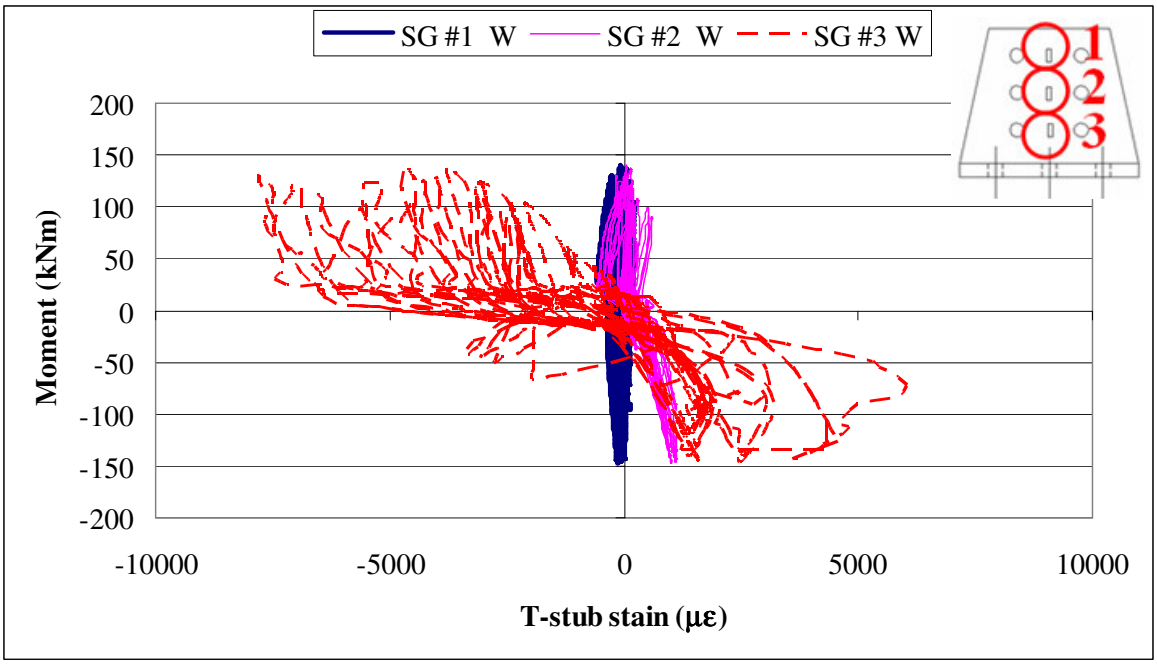

Figure 3.81. Strains at the west t-stub web of the specimen T2C

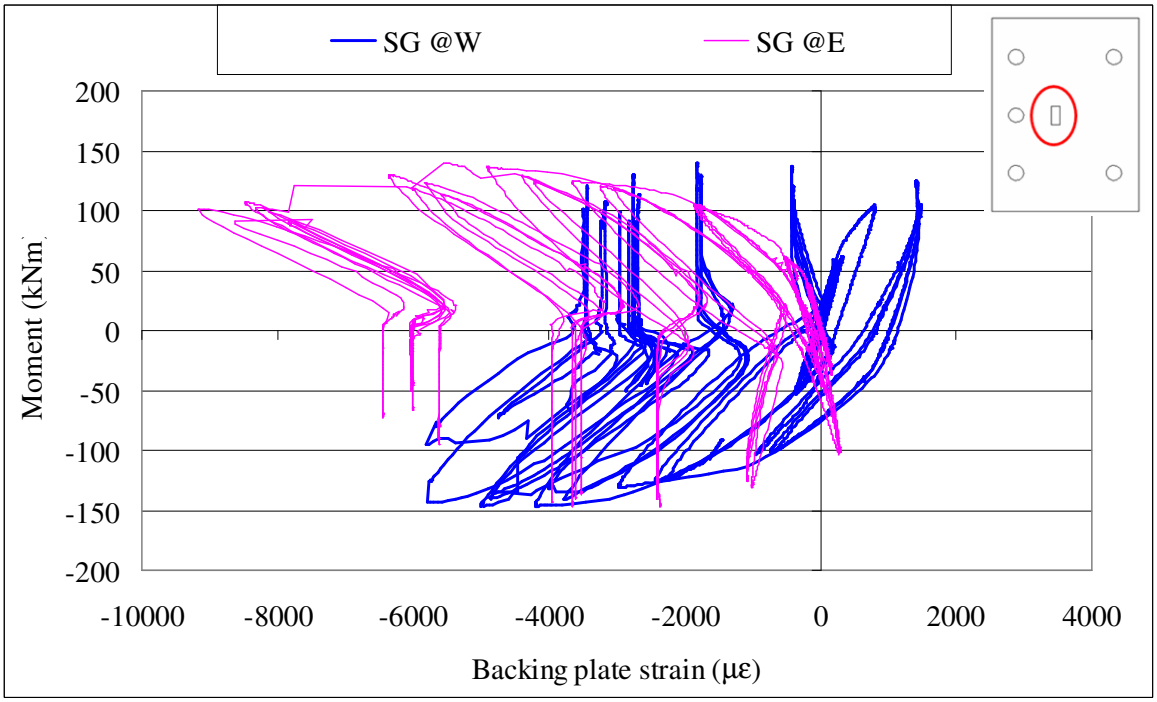

Figure 3.82. Strains at east and west backing plates of the specimen T2C

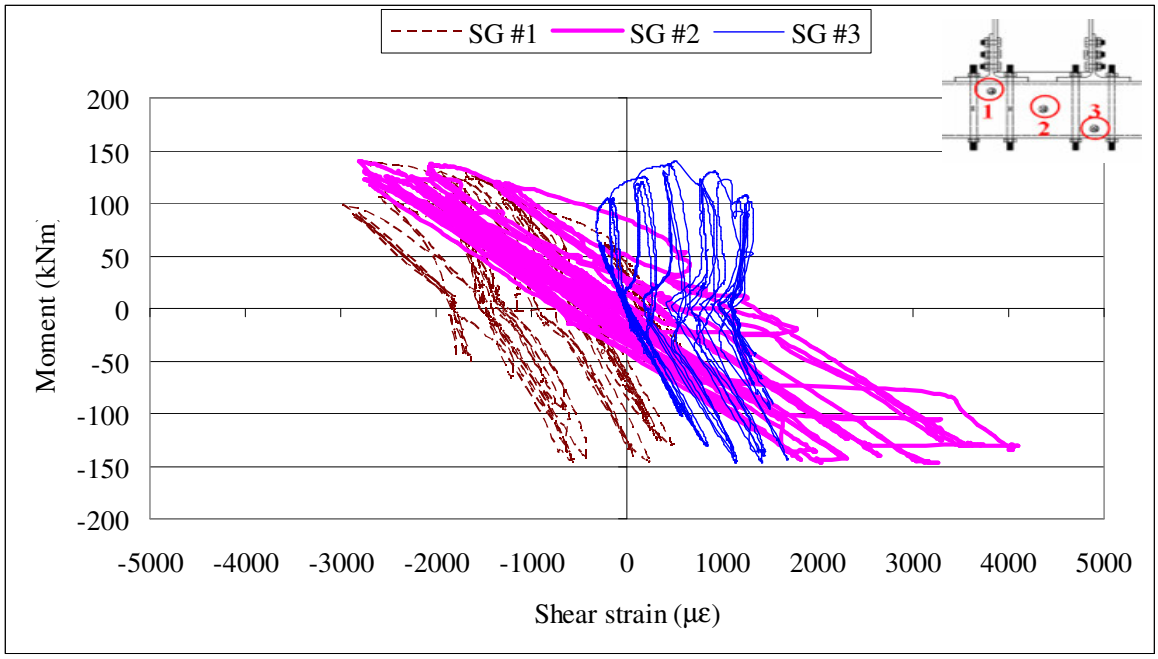

Figure 3.83. Shear strains at the shear panel zone of the specimen T2C

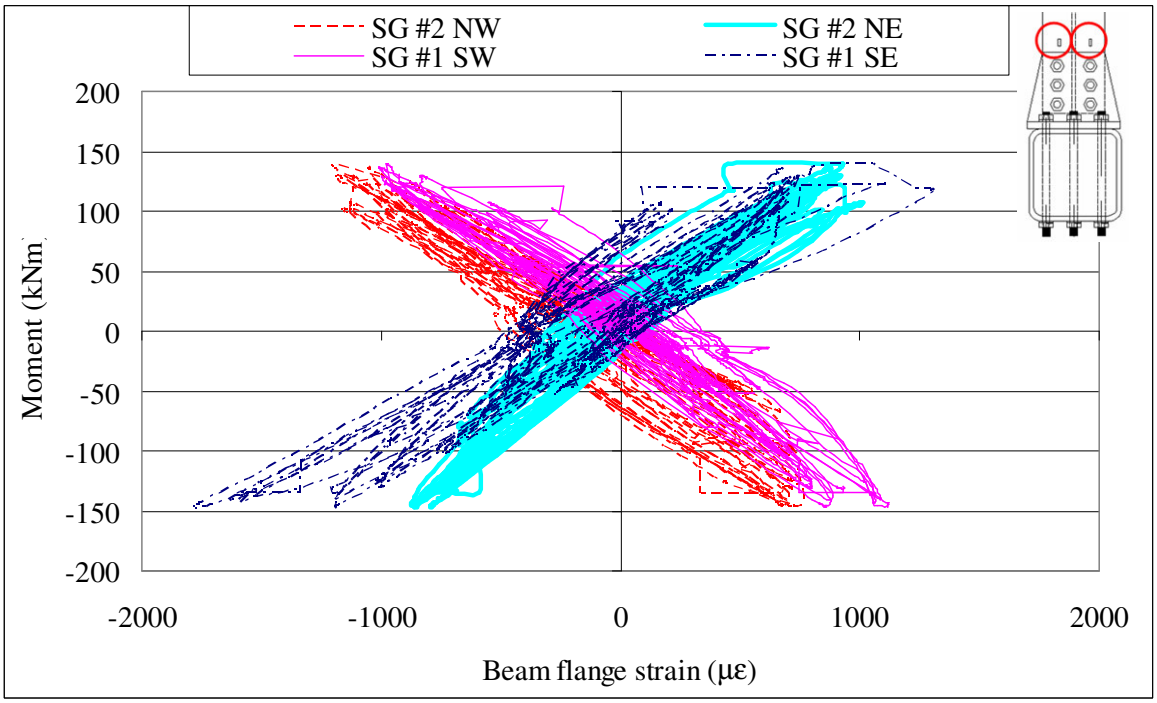

Figure 3.84. Strains at the beam flange of the specimen T2C

3.2.5. Evaluation of Test Results

Frames are classified in Eurocode 3 [22] as braced and unbraced frames according to the structural system providing the strength against lateral displacements. The term “braced frames” is used when a very stiff system of bracing elements is provided in order to reduce the total horizontal displacement by at least 80%. In the opposite case, the term “unbraced frame” is adopted.

In the case of elastic design, the classification by rigidity leads to the three main categories of nominally pinned, rigid and semirigid connections. Nominally pinned connections are assumed to transfer the shear and eventually the normal force from the beam to the column. Moreover, they must be able to rotate without developing significant moments, which might badly affect the resistance of the columns. Rigid connections transmit all end reactions, and their deformation is sufficiently small that their influence on the moment distribution in the structure or on its overall deformation may be neglected. Semirigid connections are designed to provide a predictable degree of interaction between members, based on the design moment-rotation characteristics of the joints.

Semirigid connection is taken into account in the calculation model by a rotational spring, which is characterized by the elastic constant and is usually expressed non-dimensionally as the ratio between the rotational stiffness of the connection and the flexural stiffness (EI_b/L_b) of the connected beam where L_b and I_b are, respectively, the length and the inertia moment of the connected beam. Non-linear behavior ranging from the quasi-perfectly rigid (fully welded, extended end plates) to the flexible (double web angle) is possible. The intermediate positions correspond to a range of semirigidity; some common types are top and bottom flange splices, tee stubs, flush end plate, flange and web angles, and flange angles presented in Figure 3.85.

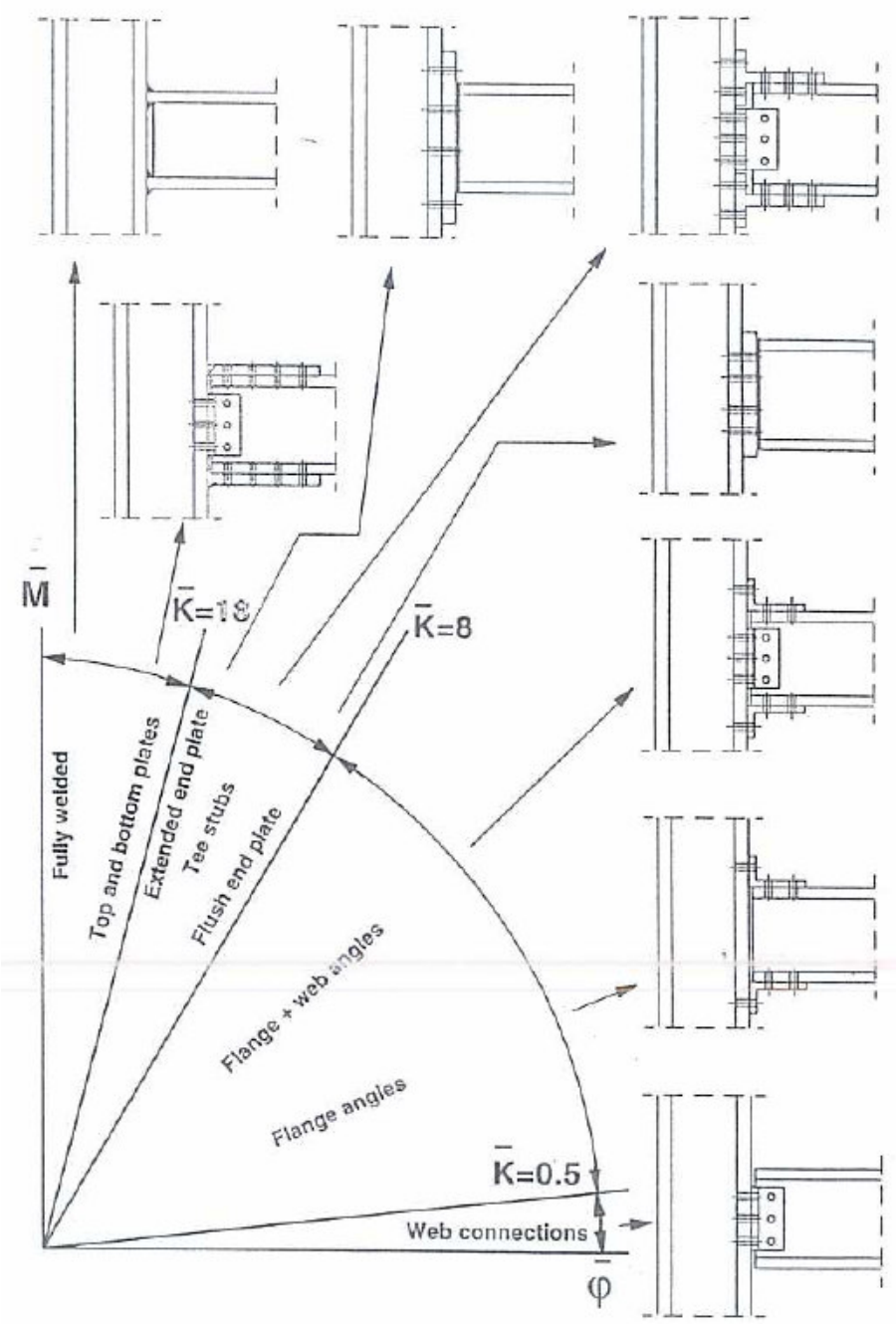

Figure 3.85. Typical values of non-dimensional stiffness of different joints [26]

According to Eurocode 3 [22], the boundary curves of the classification diagram are expressed through the following non-dimensional parameters where K_i is the initial rotational stiffness of the connection, and M_{pb} I_b and L_b are, respectively, the plastic moments, the moment of inertia and the lenght of the connected beam [26]:

$$\overline{K} = \frac{K_i L_b}{EI_b} \tag{3.2}$$

$$\overline{m} = \frac{M_u}{M_{pb}} \tag{3.3}$$

$$\overline{\varphi} = \varphi \frac{EI_b}{M_{pb} L_b} \tag{3.4}$$

With reference to the rotational stiffness, the beam-to-column connections can be classified as

- nominally pinned, for $\overline{K} \leq 0.5$
- semirigid, for $0.5 < \overline{K} < \overline{K}^*$
- rigid, for $\overline{K} \geq \overline{K}^*$.

The value of $\overline{K}^*$ depends on the type of frame, braced or unbraced, and with a value of 8 in the first case and of 25 in the second case according to Eurocode 3. The latter is the situation for moment-resisting frames.

With reference to the flexural resistance, the beam-to-column connections can be classified as

- nominally pinned, for $\overline{m} < 0.25$
- partial strenght, for $0.25 \leq \overline{m} < 1$
- full strengh, for $\overline{m} \geq 1$

The boundary curve between rigid and semirigid connections, according to the Eurocode 3 classification diagram, is a trilinear curve. The first brance is given by Equation (3.5) with $\overline{K}^* = 8$ in the case of braced frames and $\overline{K}^* = 25$ in the case of unbraced frames. The second branch is given by Equations (3.6) and (3.7) for unbraced frames and braced frames, respectively. Finally, the third branch is given by $\overline{m} = 1$ for $\overline{\varphi} >$ 0.12 and $\overline{\varphi} > 0.20$, respectively, for unbraced and braced frames.

$$\bar{m} = \bar{K}^{*}\,\bar{\varphi} \text{ for } \bar{\varphi} \le \frac{2}{3K^{*}} \tag{3.5}$$

$$\bar{m} = \frac{25\varphi + 4}{7} \text{ for } \frac{2}{3\bar{K}^{*}} \le \bar{\varphi} \le 0.12 \tag{3.6}$$

$$\bar{m} = \frac{20\varphi + 3}{7} \text{ for } \frac{2}{3\bar{K}^{*}} \le \bar{\varphi} \le 0.20 \tag{3.7}$$

The three regions spereated by the boundary curves define the rigid, semirigid and nominally pinned (or flexible) connections. The initial linear branch is able to reflect the conditions related to the serviceability limit state, while the horizontal plateau is related to the ultimate limit state conditions. Although the above terms are usually adopted, it would be preferable to use more precise terms, such as rigid-full-strength connections and semirigid-partial-strength connections for the first two regions respectively.

Bijlaard and Steenhuis [27] propose the use of the Eurocode 3 classification by assuming a constant ratio between beam length and beam depth (L_b/d = 25 for unbraced and L_b/d = 20 for braced frames). By choosing the length of the beam according to this proposal, non-dimensional parameters of the specimens T1M and T2M can be calculated as in Table 3.2 and their corresponding non-dimensional monotonic behaviour with the boundary curves of Eurocode 3 are given in Figures 3.86 and 3.87.

In both specimens the bolts which connect the t-stub to beam flange has been tightened as much as possible. That's why both specimens started with very high initial stiffness levels of 7141 kNm/rad and 13771 kNm/rad respectively for T1M and T2M until about 20 kNm moment levels. At this junction, this moment corresponds to about 75 kN couple force which is about 30% of the design slip resistance (44 kN per bolt) calculated according to Eurocode part 1-8. This means that the bolts at this junction should be considered to be snug tightened. However after this slip resistance level has been achieved, the bolts started slipping into bearing and the test has been continued with the reduced stiffness.

Although their stiffness levels are not very high, both specimens failed after reaching plastic moment capacity of the connected beam (142 kNm). Therefore the specimens T1M and T2M can be classified as semi-rigid-full-strength joint according to the joint classification of Eurocode 3.

Table 3.2. Non-dimensional parameters of the specimens

Frame Type	Unbraced (L_b=6750 mm)				Braced (L_b=5400 mm)			
Specimen	T1M		T2M		T1M		T2M	
Before or after slip resistance level at t-stub-beam interface	before	after	before	after	before	after	before	after
Non-dimensional Stiffness	3.96	2.17	7.65	2.29	3.17	1.74	6.12	1.83
Non-dimensional Moment	1.03		1.13		1.03		1.13	

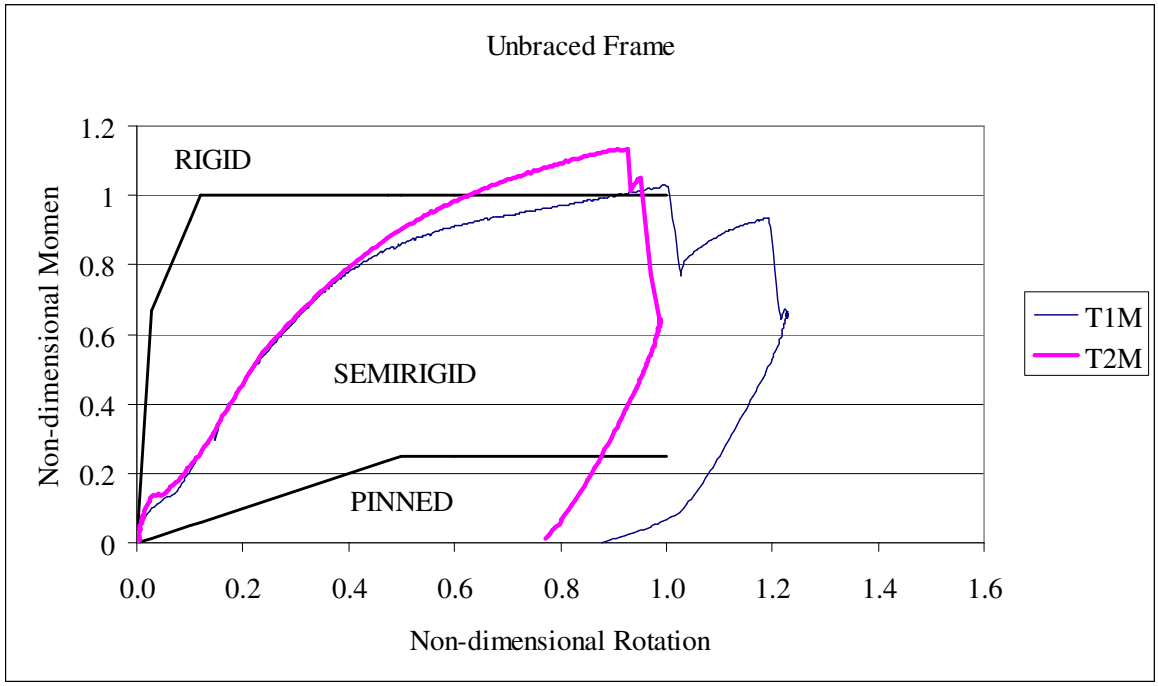

Figure 3.86. Joint classification of the specimens according to Eurocode 3

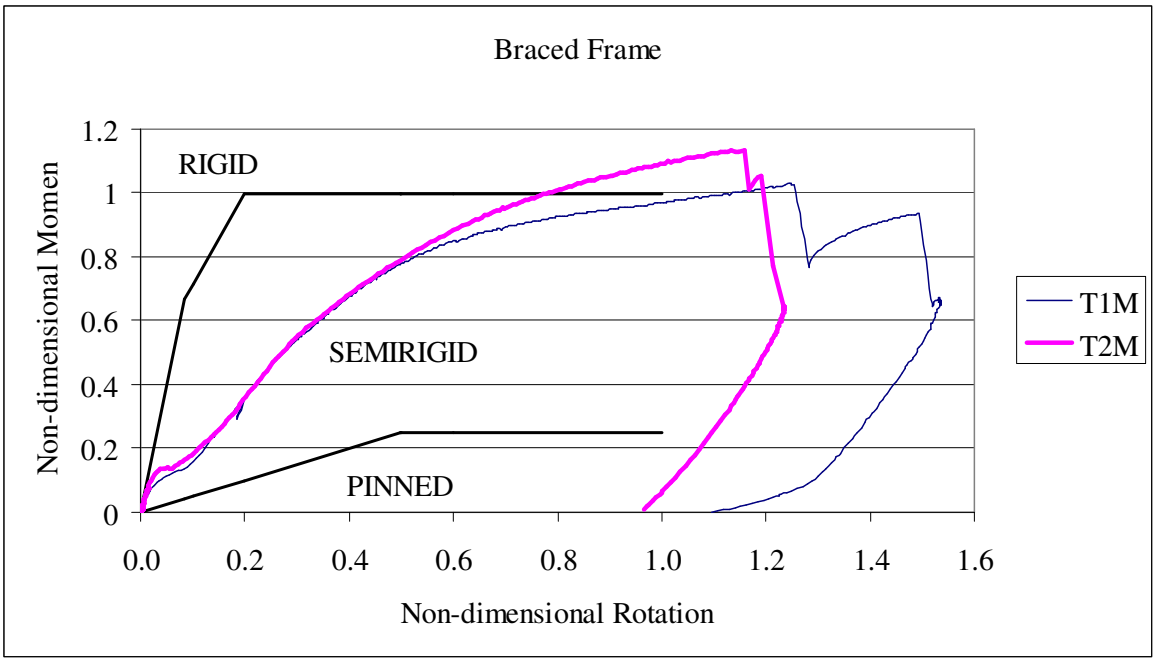

Figure 3.87. Joint classification of the specimens according to Eurocode 3

The only difference between T1 and T2 type of specimens is the additional backing plate for reinforcing the column rear face of the specimens of T2. Considering the joint deformability, shear deformations were much less than the connection deformations due to their stiffness levels. The shear stiffness of the specimen T2M was greater. Mainly connection deformability has been governed by the deformations at the t-stub and at the hollow section column rear face. Although the initial stiffness levels of both t-stub and column face deformations have been come out very close because of the comparable detailing, in higher load levels deformation of the t-stub has been dominant. Especially in T2M backing plate reduced the deformation at the column face successfully. The bearing deformation at the t-stub-beam interface of the specimen T2M is slightly increased comparing to T1M. This might be related to higher stiffness levels of the column face and the t-stub which force this interface to deform more.

Under cyclic loading conditions, the joints can be stable or unstable; it can be considered stable if it exhibits the same behaviour as the monotonic test, even if the number of cycles increases. On the other hand the behaviour can be considered unstable when the stiffness decreases with the number of cycles.

As presented in Figure 3.88, under cyclic loading, joints can be characterized by three types of behavior [26]:

a. Joints that exhibit a stable behavior, characterized by hysteresis loops having the same area inside the curve, which remains constant with increasing number of cycles.
b. Joints that exhibit an unstable behavior due to permanent deformations in holes and bolts, thus reducing the stiffening effect of the tightening force. The slope of the hysteresis curves characterizing the stiffness of the cycle is continuously decreasing.
c. Joints that exhibit again an unstable behavior, characterized by bolt slippage. This phenomenon significantly modifies the shape of the curve by reducing the dissipated energy for the same values of deformations. The increasing deterioration is due to the permanent deformations of holes and shanks.

Both cases b and c lead to collapse due to deterioration of stiffness. Considering the shape of hysteresis loops, the ideal cyclic behaviour of the joint must guarantee sufficient level of strength without stiffness deterioration for a sufficient number of cycles. The evaluation of an acceptable degree of degradation of the design parameters requires a quantitative analysis of their effects on the-overall behaviour of the structure.

It is not possible to say that both specimens exhibited a stable cyclic response and reliable energy-dissipation capacity under repeated loading. Nevertheless strength levels of the specimens were as expected and the strength deterioration was not in significant levels by increasing with the cycle deformation amplitude. On the other hand there was a remarkable stiffness degradation especially after the column rear face of the specimens started deforming due to the opening gab during loading process between t-stub with respect to the column face. Due to the bolted nature of the hysteresis of the joint was influenced by bolt slips at t-stub-beam interface under cyclic loading. As a result hysteretic pinching behaviour was observed. By further considering the flexibility of the hollow section column face, this pinching behaviour became more intense.

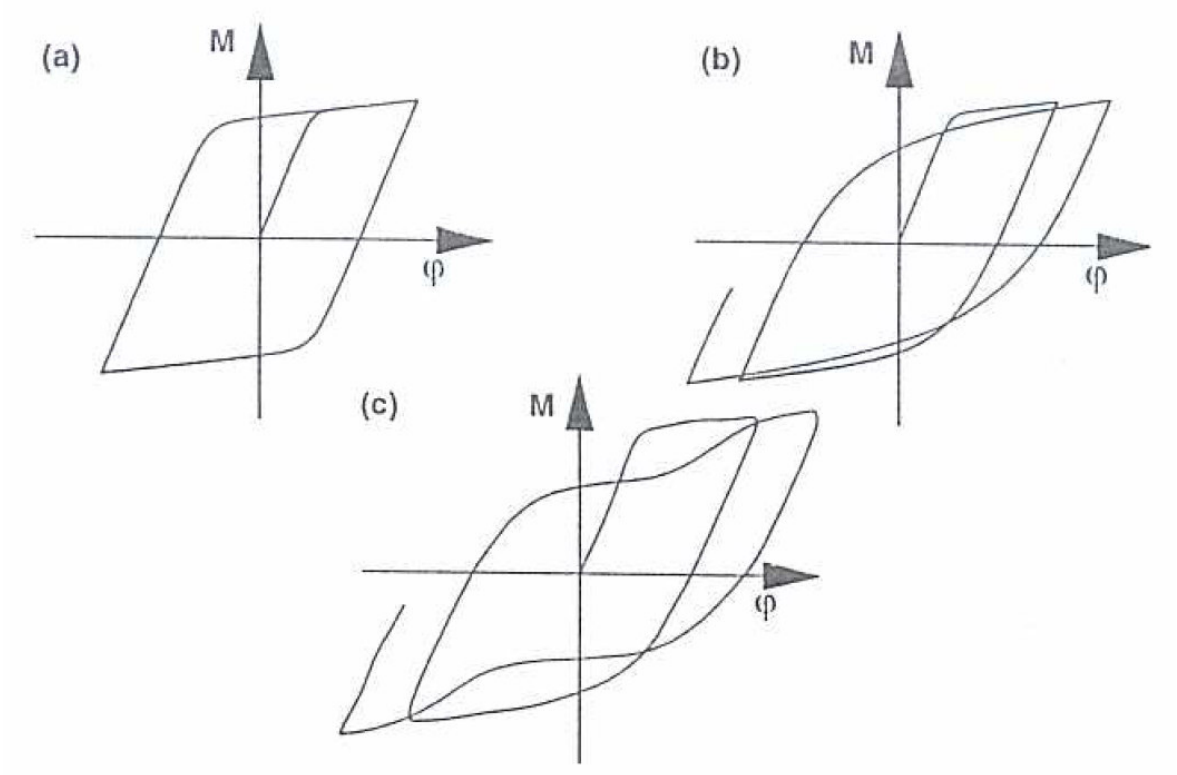

Figure 3.88. Typical hysteresis loops of structural joints [26]

As given in Figure 3.89 and Figure 3.90, both specimens showed similar the initial stiffness levels by comparing their monotonic and cyclic behaviours. Nonetheless the ultimate moment and the corresponding rotation were lower in the case of cyclic actions. The reason is the low-cycle fatigue as well as the fact that plastic excursions due to plastic reversals, from positive to negative range and viceversa, are higher than the ones corresponding to the monotonic loading for the same absolute value of rotation. Strength deterioration phenomena due to cyclic actions were quite limited and remarkable only in the last cycles before specimen failure. Since the monotonic test specimens were loaded until failure, both tests ended with rupture of the partially threaded studs. However in the cyclic tests, the specimens were loaded incrementally which did not stress the studs severely and the tests ended with the failure of the t-stub in adequate amount of cycles. That's why both specimens performed until higher rotation levels.

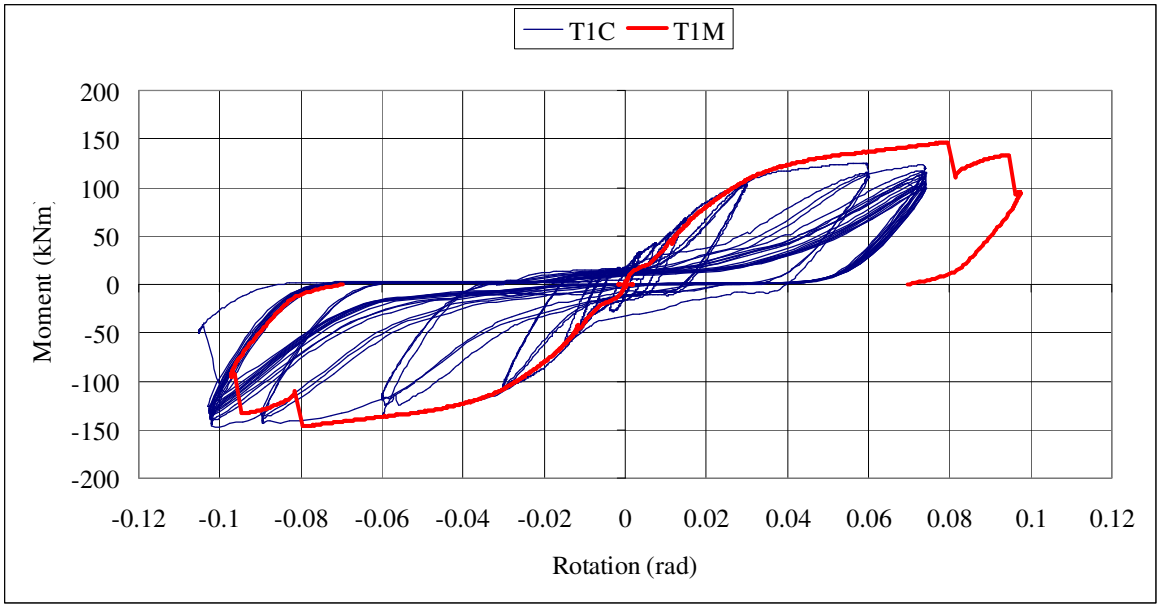

Figure 3.89. Comparison of moment - rotation behaviour of specimens T1M and T1C

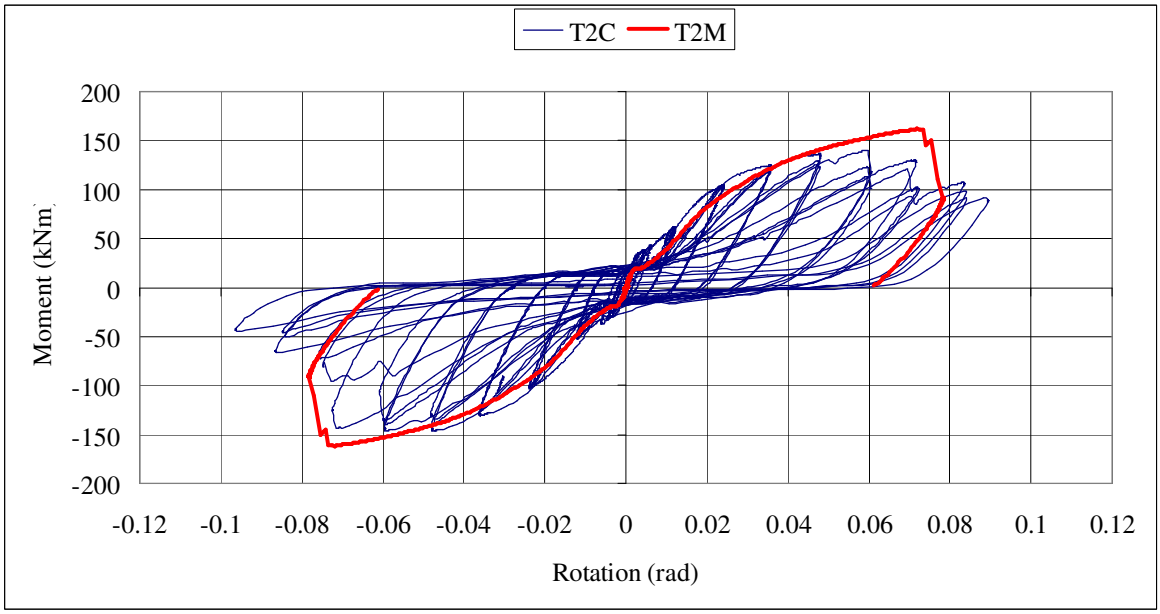

Figure 3.90. Comparison of moment - rotation behaviour of specimens T2M and T2C

In order to quantify the cyclic performance of the specimens, non-dimensional parameters are obtained through limit elastic quantities which are used to compare the generic true cycle given in Figure 3.91 with the ideal elasto-plastic cycle having the same amplitude. According to ECCS Recommendations [24], the experimental cyclic tests shall

be carried out by considering successive groups of cycles with an increasing displacement amplitude and the absolute values of the following quantities shall be deduced from the F-e diagram after each cycle in the range of $e > e_y$.

- the extremes of displacement e_i^+ and e_i^- ;
- the values of the forces F_i^+ and F_i^- corresponding to the extremes of displacement e_i^+ and e_i^- ;
- the extremes of displacements in the positive and negative range of the applied forces, Δe_i^+ and Δe_i^- ;
- the tangent modulus corresponding to the change of the sign of the applied load, $tg\alpha_i^+$ and $tg\alpha_i^-$;
- the areas A_i^+ and A_i^- of the positive and negative half cycles as given in Figure 3.92

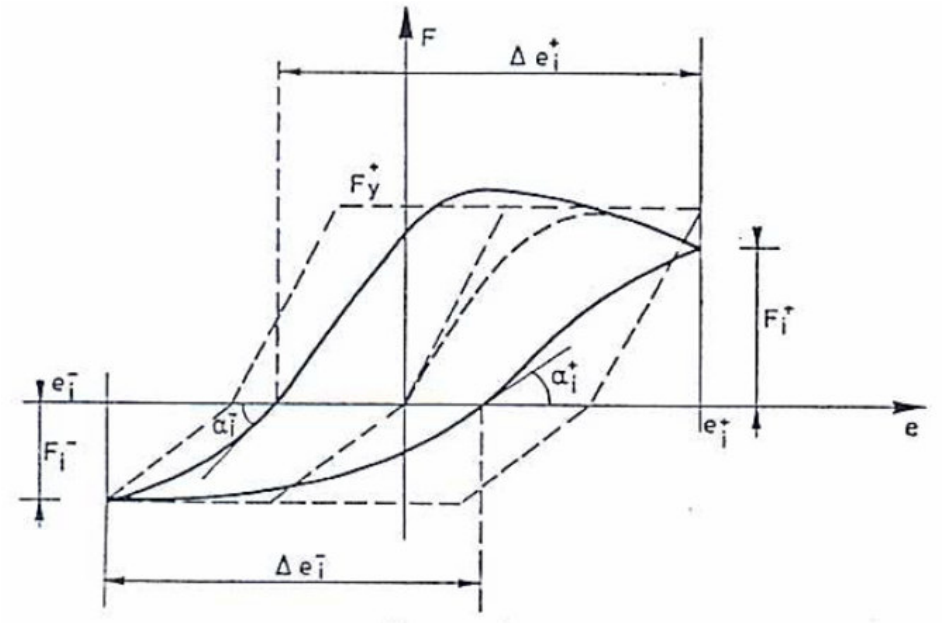

Figure 3.91. Basic data in the ECCS Recommendations for cyclic tests [24]

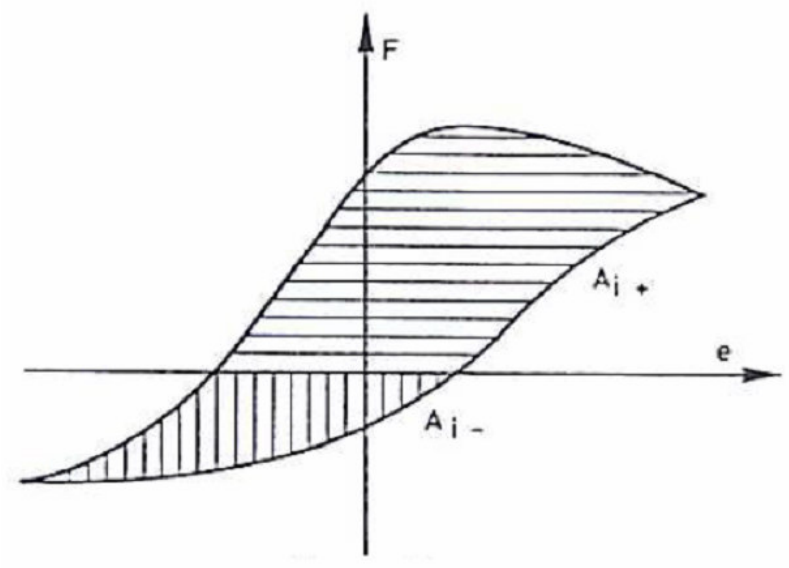

Figure 3.92. Definition of areas used to calculate the dissipated energy ratio [24]

Then following quantities are considered as characterizing parameters to be computed:

- Partial ductility: This parameter represents the ratio between the absolute value of the maximum positive (or negative) displacement in the *i*th cycle and the absolute value of the yield displacement in the corresponding side of the cycle. So, the higher this ratio, the greater is the structure's capacity to withstand large deformations out of the elastic range.

$$\mu_{oi}^{+} = e_i^{+} / e_y^{+},\ \mu_{oi}^{-} = e_i^{-} / e_y^{-} \tag{3.8}$$

- Full ductility (or cyclic ductility): This parameter represents the ratio between the absolute value of the maximum displacement amplitude in the positive force range (or negative) in the *i*th cycle and the corresponding yield displacement. For this parameter the same considerations as for partial ductility apply.

$$\mu_i^{+} = \Delta e_i^{+} / e_y^{+} \qquad \text{and} \qquad \mu_i^{-} = \Delta e_i^{-} / e_y^{-} \tag{3.9}$$

- Full ductility ratio: This parameter represents the ratio between the absolute value of the maximum displacement amplitude in the positive force range (or negative) in the ith cycle and the corresponding displacement in a perfect elasto-plastic behavior. So, the higher this ratio, the greater is the deterioration of the structure (for instance due to loss of stiffness, slip etc.).

$$\psi_i^+ = \Delta e_i^+ / (e_i^+ + (e_i^- - e_y^-)) \qquad \text{and} \qquad \psi_i^- = \Delta e_i^- / (e_i^- + (e_i^+ - e_y^+)) \tag{3.10}$$

- Resistance ratio (or strength degradation ratio): This parameter represents the ratio between the force corresponding to the maximum positive or negative displacement in the *i*th cycle and the yield force in perfect elasto-plastic behavior

$$\varepsilon_i^+ = F_i^+ / F_y^+ \qquad \text{and} \qquad \varepsilon_i^- = F_i^- / F_y^- \tag{3.11}$$

- Rigidity ratio (or stiffness degradation ratio) This parameter is the ratio between the stiffness of the tested structure in the ith cycle mid the initial stiffness. A small value for this ratio (<1) indicates a large loss of stiffness of the structure. This can be caused by global and local buckling phenomena, by the Bauschinger effect exhibited by steel subjected to inelastic load reversals or by the residual curvature during previous cycles.

$$\xi_i^+ = tg\alpha_i^+ / tg\alpha_y^+ \qquad \text{and} \qquad \xi_i^- = tg\alpha_i^- / tg\alpha_y^- \tag{3.12}$$

- Dissipated energy ratio: This parameter represents the ratio between the energy dissipated by the structure in a real half-cycle as defined in Figure 3.92 and the energy dissipated in the half-cycle corresponding to perfect elasto-plastic behavior with the same displacement amplitude.

$$\eta_e^+ = \frac{A_i^+}{F_y^+ .(e_i^+ - e_y^+ + e_i^- - e_y^-)} \qquad \text{and} \qquad \eta_e^- = \frac{A_i^+}{F_y^- .(e_i^- - e_y^- + e_i^+ - e_y^+)} \tag{3.13}$$

Each group of cycles is composed of three cycles having the same displacement amplitude. According to ECCS Recommendations, the behaviour of the specimen is characterized after each group of three cycles by the following parameters. The partial

ductility μ_{oi}^{+}, where i is the index of the last cycle of the group, being taken as the variable, the parameters are :

- $\psi^{+}(\mu_{oi}^{+})$, minimum value of the three ψ_i^{+} evaluated in the group of three cycles.
- $\varepsilon^{+}(\mu_{oi}^{+})$, minimum value of the three ε_i^{+} evaluated in the group of three cycles.
- $\xi^{+}(\mu_{oi}^{+})$, minumum value of the three ξ_i^{+} evaluated in the group of three cycles.
- $\eta^{+}(\mu_{oi}^{+})$, average value of the three η_i^{+} evaluated in the group of three cycles.
- $\varepsilon^{+}*(\mu_{oi}^{+}) = F_i^{+}/F_{i-2}^{+}$, defined as the resistance drop ratio of the group of three cycles in the range of the positive forces.

Similarly, $\psi^{-}(\mu_{oi}^{-})$, $\varepsilon^{-}(\mu_{oi}^{-})$, $\xi^{-}(\mu_{oi}^{-})$are the minimum value of the three ψ_i^{-}, ε_i^{-}, ξ_i^{-} evaluated in the group of 3 cycles. $\eta^{-}(\mu_{oi}^{-})$ is the average of the η_i^{-} of the group. $\varepsilon^{-}*(\mu_{oi}^{-}) = F_i^{-}/F_{i-2}^{-}$ is the resistance drop ratio of the group of three cycles, in the range of the negative forces.

All these parameters are defined as the ratio between the value found in the cyclic testing procedure and that corresponding to a reference test, in which it is assumed to exhibit perfect elasto-plastic behavior. The optimum condition is therefore reached when the behavior of the structure closely follows the ideal perfect elasto-plastic behavior, so when the values of these parameters are near to unity. A small value for these parameters (<1) can be assumed as the end of the test, because this indicates a substantial loss of resistance, stiffness or energy dissipation.

Both specimens completed 26 successful cycles. 27th cycle of test T2C was just half cycle to return the specimen to its original position. Cyclic behaviour parameters of the specimens in function of partial ductility are given in Figure 3.93 and Figure 3.94. According to its definition partial ductility values have to be positive. In order to present the cyclic behaviour parameters of both positive and negative ranges in one figure partial ductility values of negative range of the cycles are given negative in the figures. So, Positive and negative range of the cycles are given respectively, in the right and left hand side of the figures. Since specimen T1C reached limit of the actuator quicker, the partial

ductility level is much less than specimen T2C which performed quite high to bear up large plastic deformations. Full ductility ratios of both specimens exhibited similar behaviour in the levels of 0.80 but decreasing very slightly while number of cycles increases up. The values in negative range are a little higher than the positive range for both specimens. Due to the bolted nature of the connection slips play an important role in the behaviour. During almost all cycles resistance ratios of both specimens are on the level of or higher than the unity until in the last cycles before specimen failure. This proves the strength steadiness of the connection under cyclic loading conditions. The values are even much higher in specimen T2C most probably because of the extra strength provided by the backing plate. Last ten cycles of the specimen T1C had the same displacement amplitude, additionally resistance ratios have been presented in Figure 3.95, which shows steady but slightly decreasing trend close to unity until failure. For both specimens, remarkable stiffness degradation is observed until the cycles of 60 mm displacement amplitude. After this level rigidity of the joint is almost zero. This significant loss of stiffness must be due to the opening gab between t-stub and column face because of the deformations of the column rear face and t-stub after this displacement level. Dissipated energy ratios of both specimens are in the level of 0.30. The trend is quite stable but the level was lower than expected. This is because most of the energy has been dissipated by the t-stub in almost all cycles. However the column face has been active only once (in the first cycles of groups) during group cycles because in next opposite loading, the deformation of the column face could not be recovered.

Total dissipated energies through out the tests T1C and T2C are 107 and 90 kNm, respectively. (Figure 3.96) As given in Figure 3.97, highest level of energies are dissipated in the first cycles of the group cycles. Considering the joint components in Figure 3.98 and Figure 3.99 energy dissipated by deformation of the web shear panel relatively higher about 5% for specimen T2C. This is related to the cyclic loading pattern. Because shear deformations are mainly higher in the first cycles of the group cycles. Since last ten cycle of the test T1C was done in same displacement amplitudes, most of the energy was dissipated by the connection. In Figure 3.100 and Figure 3.101, distribution of the total dissipated energy due to connection deformation on its components. It is obvious that deformations at t-stub played a significant role in dissipation of the energy during both

tests. Especially in test T2C, backing plates stiffened column face and reduced its deformation levels.

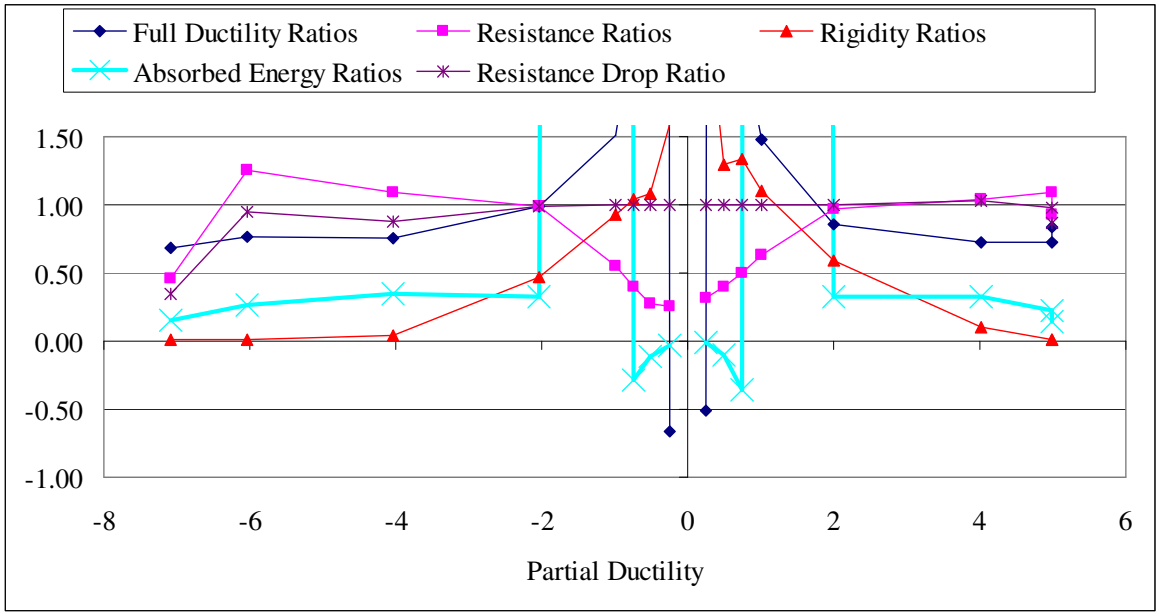

Figure 3.93. Cyclic behaviour parameters of the specimen T1C

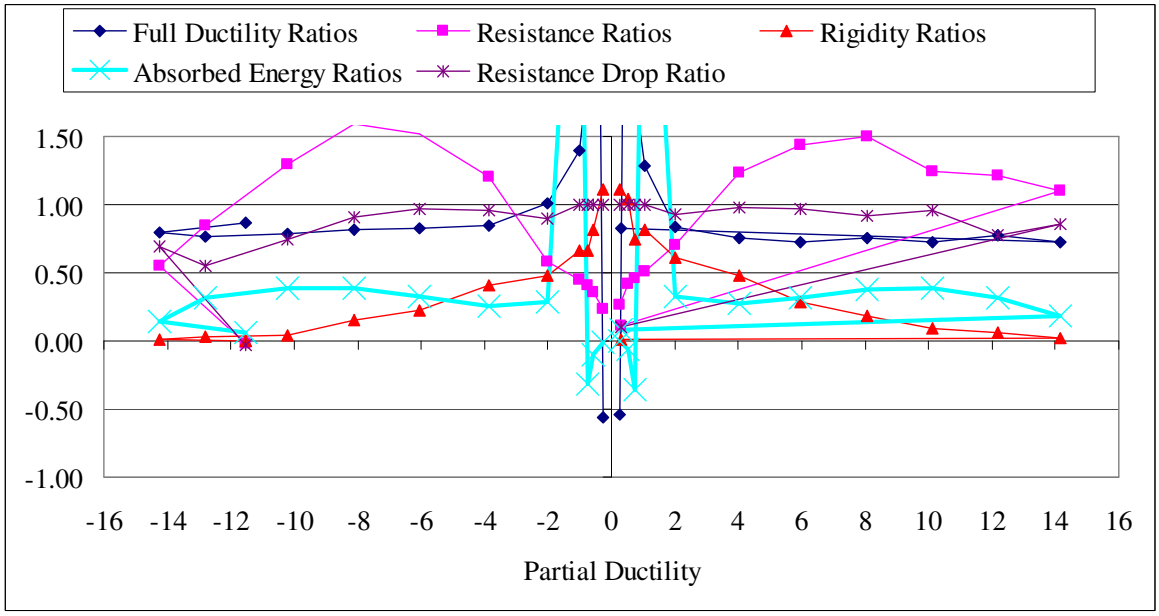

Figure 3.94. Cyclic behaviour parameters of the specimen T2C

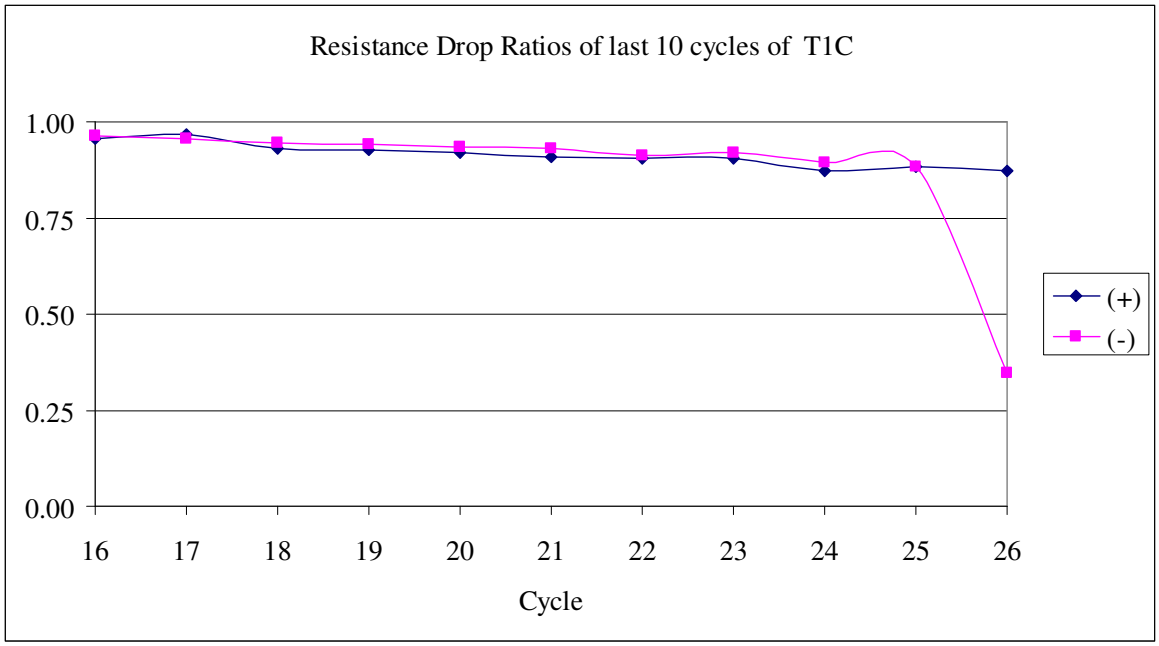

Figure 3.95. Resistance drop ratios of last 10 cycles of the specimen T1C

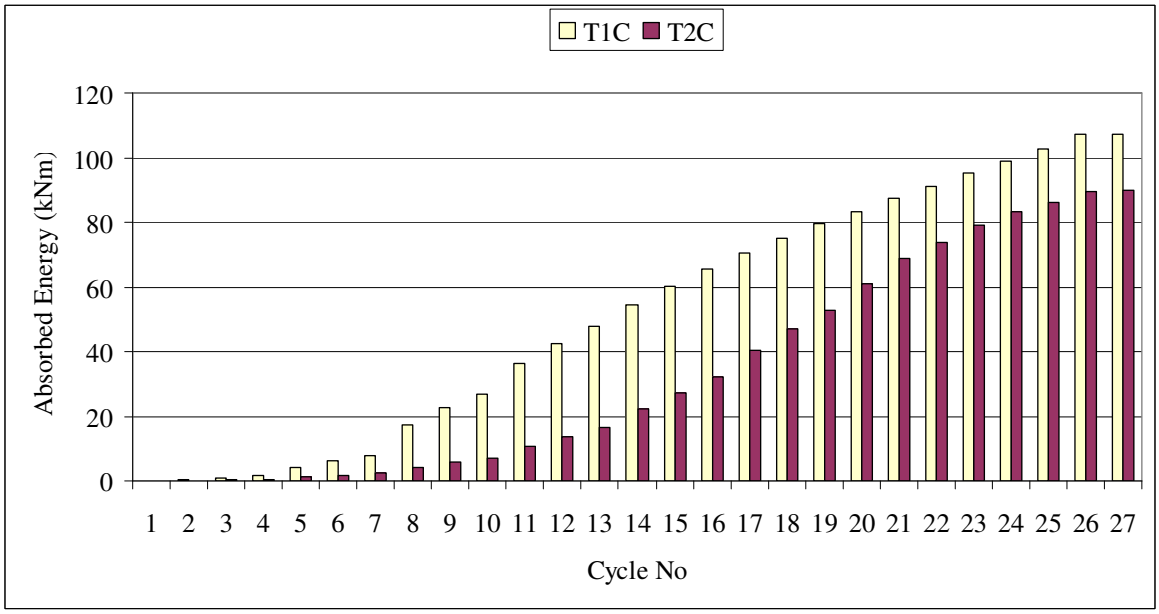

Figure 3.96. Total dissipated energy of specimens T1C and T2C

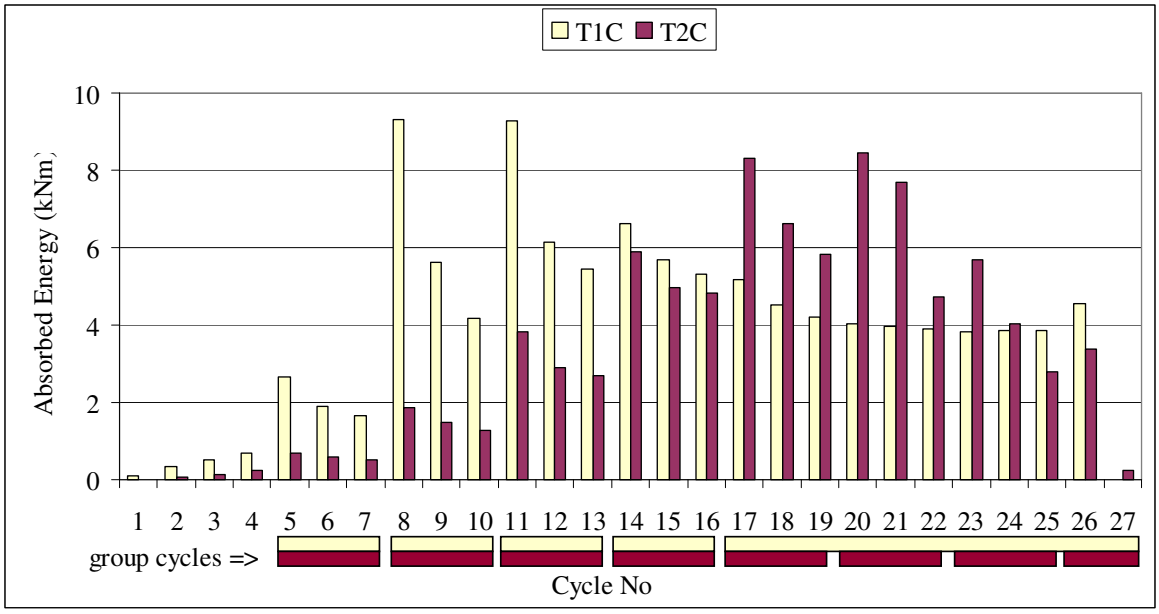

Figure 3.97. Dissipated energy per cycle of specimens T1C and T2C

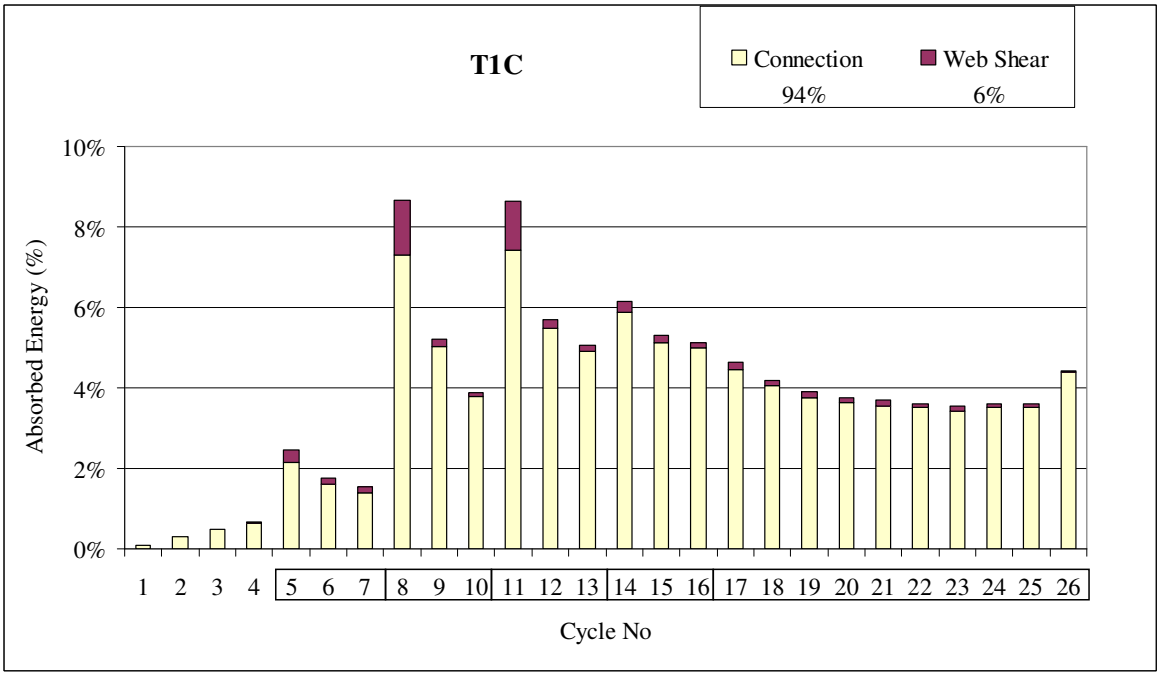

Figure 3.98. Distribution of total dissipated energy on joint components of specimens T1C

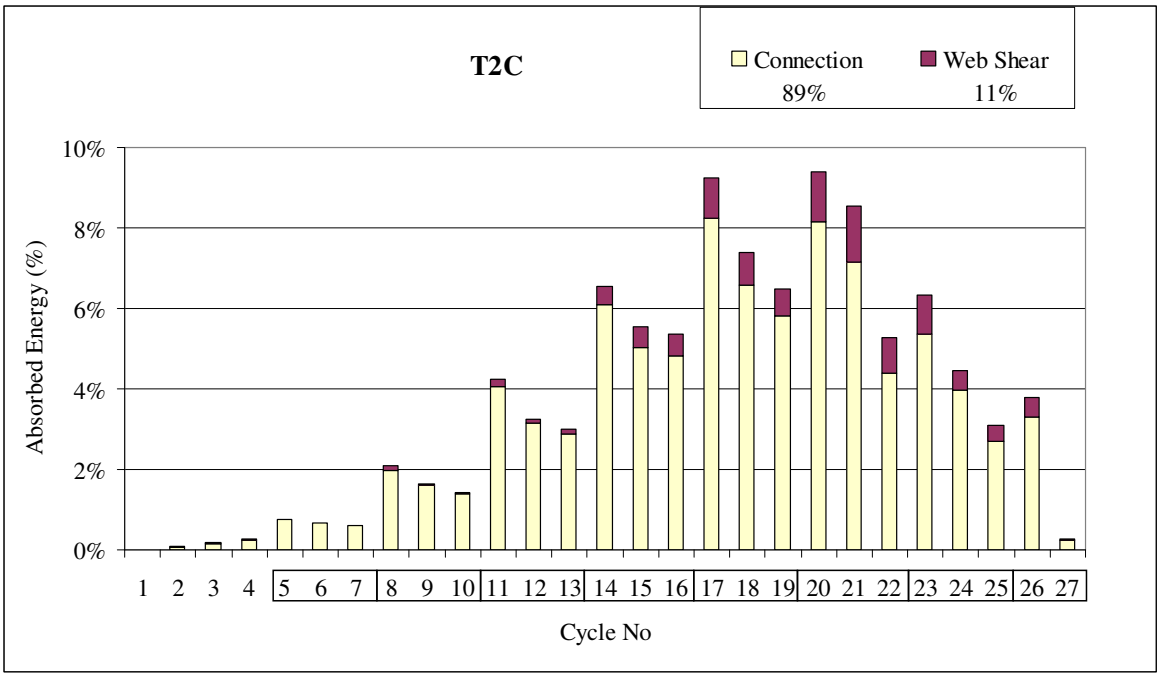

Figure 3.99. Distribution of total dissipated energy on joint components of specimens T2C

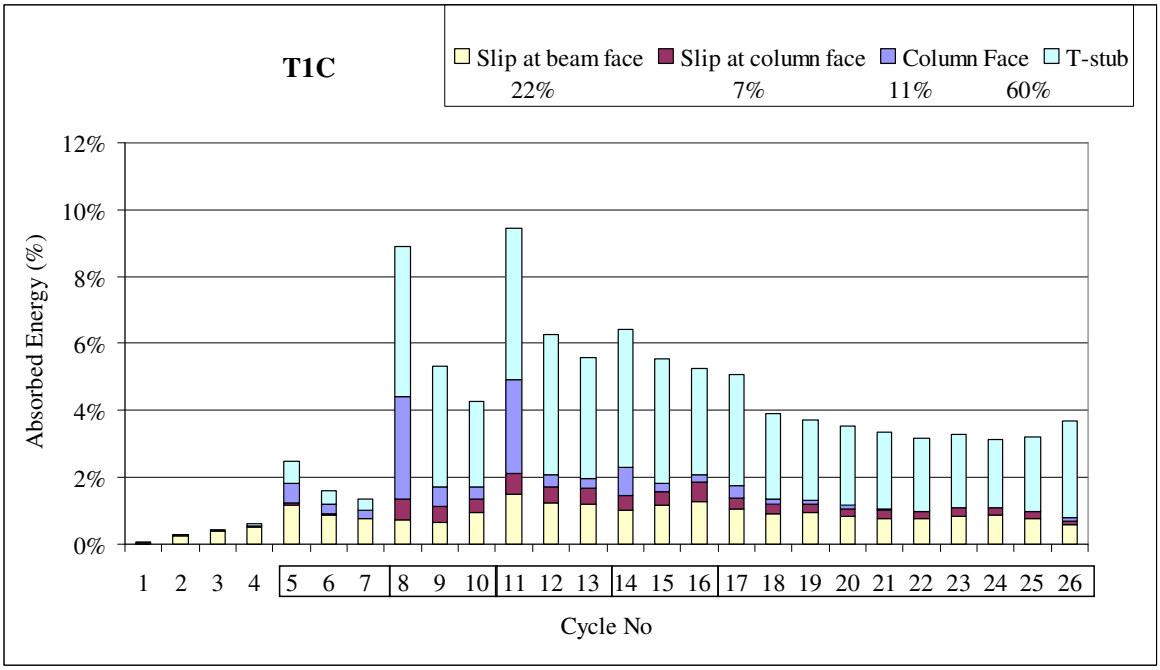

Figure 3.100. Distribution of total dissipated energy of connection on connection components of specimens T1C

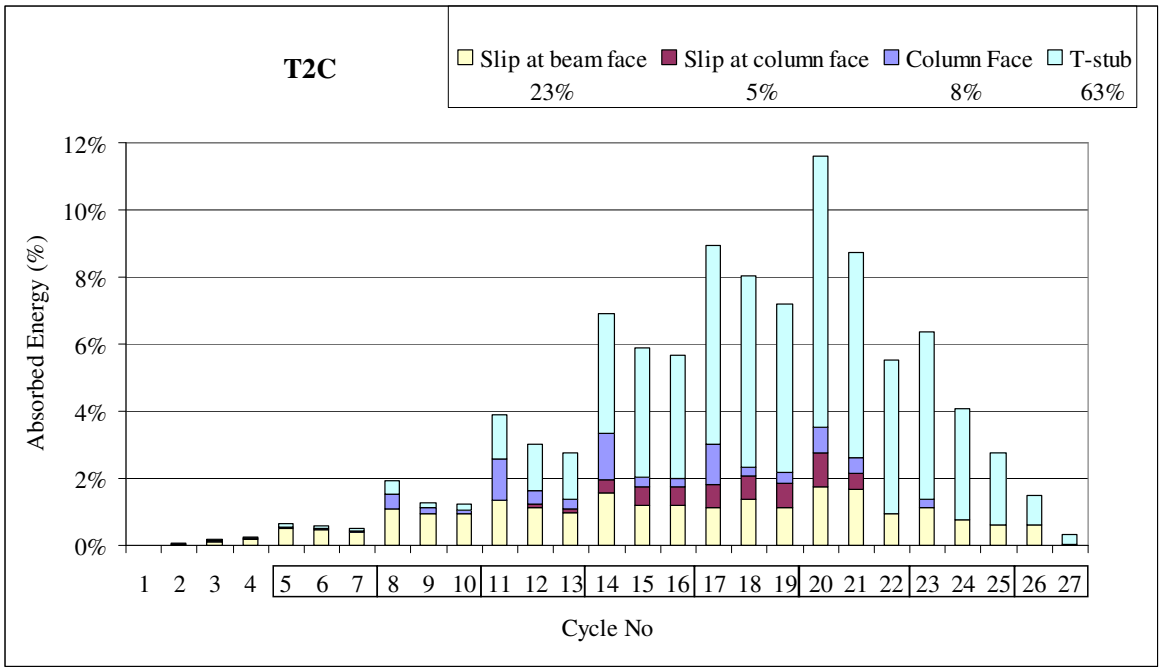

Figure 3.101. Distribution of total dissipated energy of connection on connection components of specimens T2C

In order to compare the behaviour of the proposed joint with other types of joints, non-dimensional strength and non-dimensional dissipated energy parameters can be used [26]. Non-dimensional strength is defined as the ratio between the maximum force F_{max}, applied at the end of the cantilever specimen during the test and the force F_p leading to the yielding of the beam ($F_p = M_{pb}/L_b$, where M_{pb} is the plastic moment of the beam computed on the basis of the actual value of the yield stress of the beam flanges and L the length of the cantilever specimen). The non-dimensional dissipated energy is defined as

$$\overline{E} = \frac{E_{jo\,\mathrm{int}}}{F_p v_p} \tag{3.14}$$

where v_p is the end displacement corresponding to F_p and evaluated for the ideally rigid conditions as follows.

$$v_p = \frac{F_p L_b^3}{3EI_b} \tag{3.15}$$

Non-dimensional strength and non-dimensional dissipated energy parameters of the proposed joint are compared with four typical joints which are described as follows:

- Type A1 which is obtained by three plate splices, which are welded to the column and bolted to the flanges and to the web of the beam [26].
- Type B1 which is made up with angles bolted both to the column and to the beam [26].
- Type C1 which is end plate joint with rigid column stub [26].
- Type D1 which is fully welded joint [26].

As presented in Figure 3.102 and Figure 3.103, non-dimensional strength and non-dimensional dissipated energy of the proposed joints are quite satisfactory when compared with other types of joints; stronger than bolted angle and bolted plate splice joints and acceptable energy dissipation capacity.

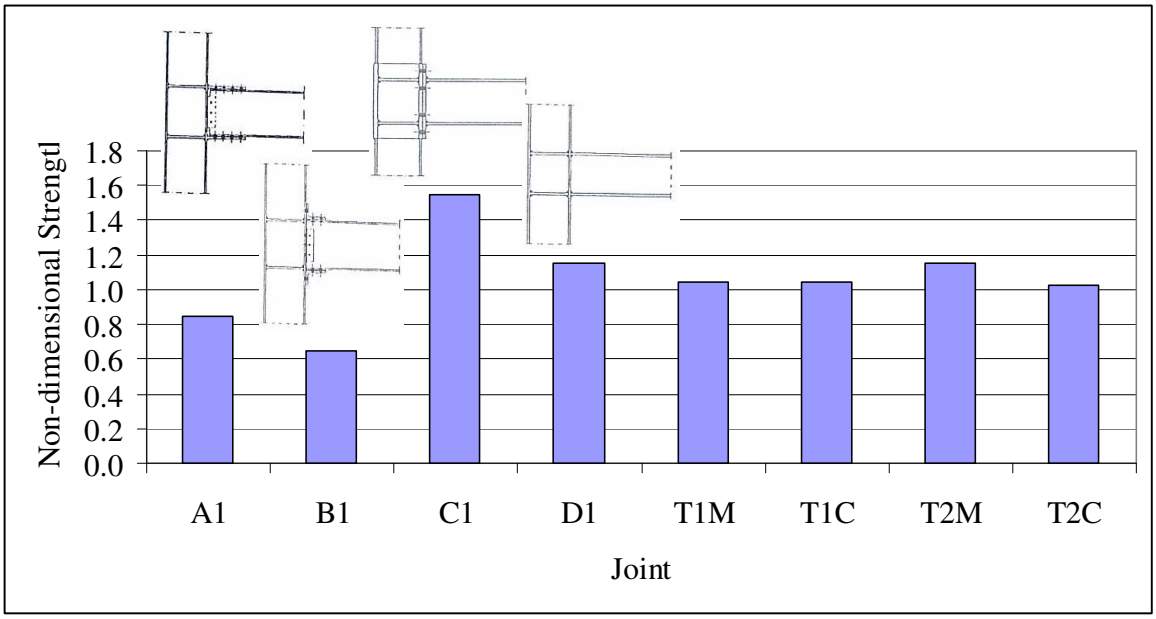

Figure 3.102. Non-dimensional strength of tested joints with other types joints [26]

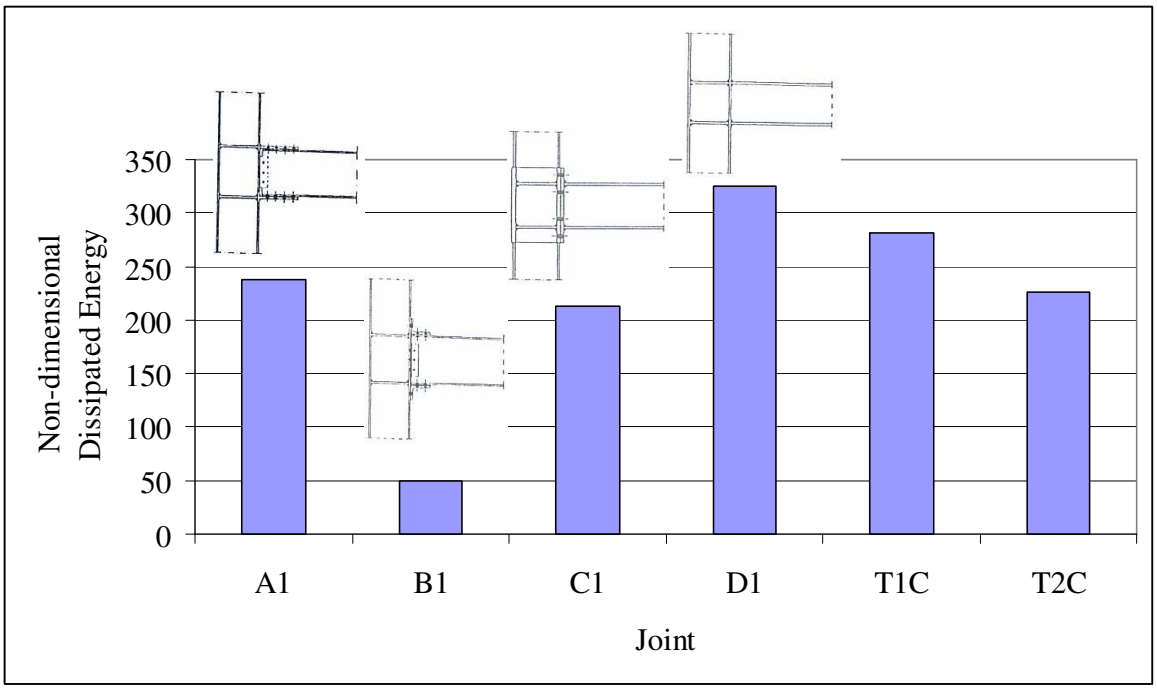

Figure 3.103. Non-dimensional dissipated energy of tested joints with other types joints [26]

4. CONNECTION MODELLING

Mechanical models are based on the simulation of the joint/connection by using a set of rigid and flexible components. Mechanical models are suitable for modelling joint/connection response, provided that a knowledge of the constitutive law of springs is available. These constitutive laws can be obtained through experimental tests or by means of analytical models. In this second case the mechanical model represents only a tool for superimposing the effects of the key deformation sources, so that the global approach is nearer to the analytical one.

4.1. Modeling of SHS Column Face in Bending Component

As described in Section 3.1, the deformability of SHS column face in bending is associated with sidewall deformation, face in bending and corner rotation. In this respect test results of the first phase has been evaluated. In this part resistance and initial stiffness parameters of this component shall be discussed by mechanical modeling approach.

In this part the abbreviations EC, CIDECT and KY refers respectively to Eurocode 3 Part 1-8 [22], CIDECT Report 5BP-4/05 [17] and proposed design approach by this study. For modeling purposes, partial safety factors (γ), if it is indicated in the formulas, are not considered and are taken as unity in calculations.

4.1.1. Resistance of the Component

There are two approaches given hereafter. Resistance calculation based on CIDECT and KY. Both are in the status of proposal to Eurocode 3 Part 1-8 [22].

The calculation method for SHS face in bending according to CIDECT is summarized in Table 4.1. The resistance by applying equivalent rigid rectangle definition in Figure 4.1 and calculating it based on *L* value defined in Figure 4.2 do not give proper solution. The former gives negative square root and must be related with distance in between bolt-rows. When it becomes wider, the bolts response as single bolt rows instead of acting as a group. Using single bolt-row in definition of the equivalent rigid rectangle solves this negative square root problem. However the calculated resistance values are much higher in the level of approximately 17% in average compared to experimental results. This must be related with the definition of the *L* value which might be related to some assumptions in previous literature studies like assuming the corners as rigid. On the other hand in practice the corners of square hollow sections are round and tend to rotate easily. Assuming the definition of *L* as center to center distance of opposite sidewalls (b_c-t_c) and applying equivalent rigid rectangle to single bolt row give more reasonable results as given in Table 4.4 and Figure 4.5 to Figure 4.8.

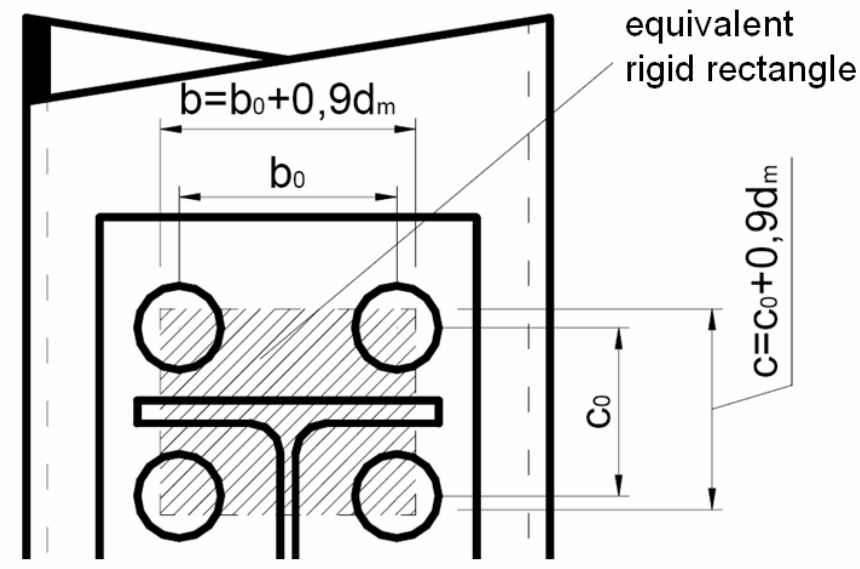

Figure 4.1. Definition of equivalent rectangle of the bolt group [17]

Table 4.1. Resistance of SHS column face in bending component

Component	**Reference**	**Resistance**
SHS in transverse compression - face failure in bending	CIDECT	Load transfer by bolts: Column notations are given in Figure 4.1 and Figure 4.2 but taking L as follows: $L = b_c - t_c$ $b_m = L\left[1 - 0{,}82\frac{t_w^2}{c^2}\left(1 + \sqrt{1 + 2{,}8\frac{c^2}{t_w L}}\right)^2\right]$ If $b_m < b$; $F_{pl,loc} = \beta 4 m_{pl,Rd}\left[\frac{\pi\sqrt{L(a+x)} + 2c}{a+x} + \frac{1{,}5cx + x^2}{\sqrt{3}t_w(a+x)}\right]$ where, $a = L - b$ $\beta = 1$ if $\frac{b+c}{L} \geq 0{,}5$ $\beta = 0{,}7 + 0{,}6\frac{b+c}{L}$ if $\frac{b+c}{L} \leq 0{,}5$ $m_{pl,Rd} = \frac{1}{4}t_w^2 f_y / \gamma_{M0}$ $x = -a + \sqrt{a^2 - 1{,}5ac + \frac{\sqrt{3}t_w}{2}\left[\pi\sqrt{L(a+x_0)} + 4c\right]}$ with $x_0 = L\left[\left(\frac{t_w}{L}\right)^{\frac{2}{3}} + 0{,}23\frac{c}{L}\left(\frac{t_w}{L}\right)^{\frac{1}{3}}\right]\left(\frac{b - b_m}{L - b_m}\right)$

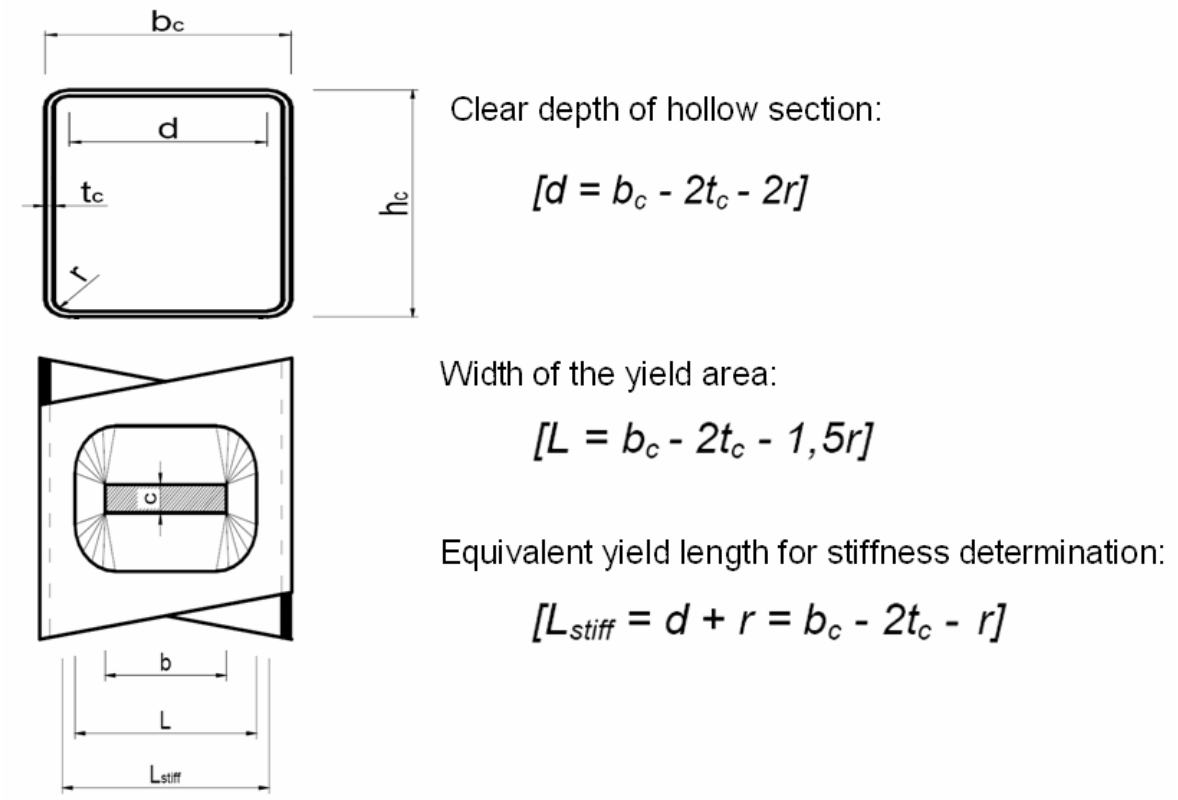

Figure 4.2. Column notations [17]

The calculation method for SHS face in bending according to KY is summarized in Table 4.2. The model is based on the method described in EC with supplementary dimensional definitions. There are no bolts under tension in component tests; therefore mode 1 and mode 3 are not applicable for component modeling of phase I. Since the corners are not as rigid as t-stub stem, it is more reasonable to take m as $b_1 - 0.6\ r$ (b_1 is the distance from bolt hole center to the sidewall as defined in Section 2.3.3 and r is the external corner radius of SHS). The multiplier 0.6 might be related to $1\text{-}t_c/r$ or $1.5t_c$ (t_c is the thickness of SHS). This should be verified in further analytical or experimental studies.

Table 4.2. Resistance of SHS column face in bending component

Component	**Reference**	**Resistance**
SHS in transverse compression - face failure in bending	EC+KY	Considering the deformation similarity, equivalent T-stub is assumed as shown in Figure 4.3 Then necessary dimensions mentioned in Figure 4.4 but taking m as follows: $m = b_1 - 0.6\,r$ Effective length is calculated according to Table 4.3. For Mode 1 (Complete yielding of the flange): Method 1 => $F_{T,1,Rd} = \frac{4M_{pl,1,Rd}}{m}$ Method 2 => $F_{T,1,Rd} = \frac{(8n - 2e_w)M_{pl,1,Rd}}{2mn - e_w(m+n)}$ $M_{pl,Rd} = 0.25\,\Sigma l_{eff}\,t_f^2\,f_y / \gamma_{MO}$ For Mode 2 (Bolt failure with yielding of the flange): $F_{T,2,Rd} = \frac{2M_{pl,2,Rd} + n\Sigma F_{t,Rd}}{m+n}$ For Mode 3 (Bolt failure): $F_{T,2,Rd} = \Sigma F_{t,Rd}$

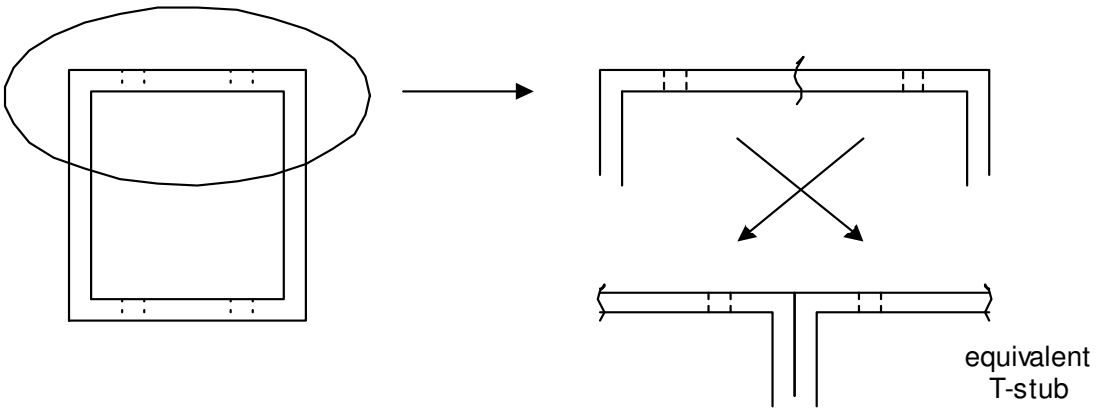

Figure 4.3. Equivalent T-stub behaviour of hollow section face in bending component

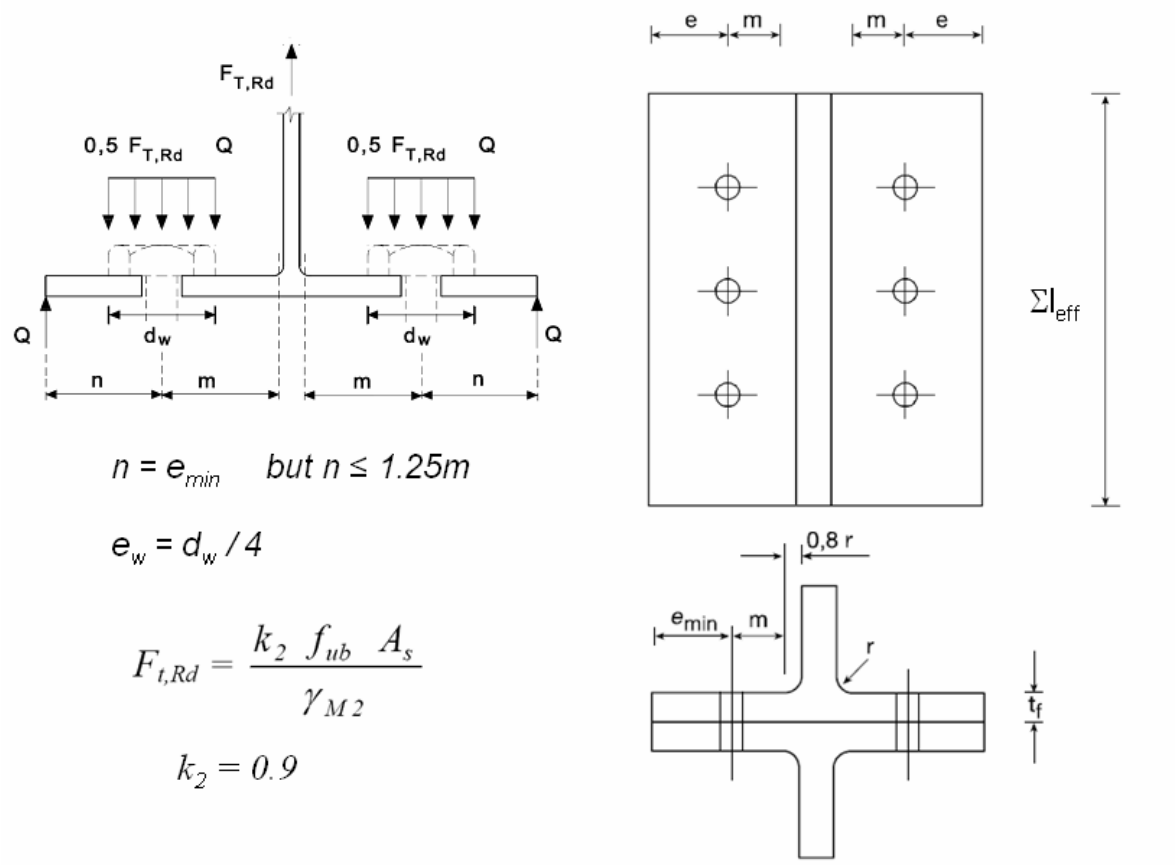

Figure 4.4. Equivalent t-stub [22]

Table 4.3. Effective lengths for an unstiffened column flange [22]

Bolt-row Location	Bolt-row considered individually		Bolt-row considered as part of a group of bolt-rows	
	Circular patterns $\ell_{eff,cp}$	Non-circular patterns $\ell_{eff,nc}$	Circular patterns $\ell_{eff,cp}$	Non-circular patterns $\ell_{eff,nc}$
Inner bolt-row	$2\pi m$	$4m + 1{,}25e$	$2p$	p
End bolt-row	The smaller of: $2\pi m$ $\pi m + 2e_1$	The smaller of: $4m + 1{,}25e$ $2m + 0{,}625e + e_1$	The smaller of: $\pi m + p$ $2e_1 + p$	The smaller of: $2m + 0{,}625e + 0{,}5p$ $e_1 + 0{,}5p$
Mode 1:	$\ell_{eff,1} = \ell_{eff,nc}$ but $\ell_{eff,1} \le \ell_{eff,cp}$		$\sum\ell_{eff,1} = \sum\ell_{eff,nc}$ but $\sum\ell_{eff,1} \le \sum\ell_{eff,cp}$	
Mode 2:	$\ell_{eff,2} = \ell_{eff,nc}$		$\sum\ell_{eff,2} = \sum\ell_{eff,nc}$	

Comparison of the models with the test results are given in Table 4.4 and Figure 4.5 to Figure 4.8. The results in figures are normalized according to yield loads. The results are generated in relation with *b*/*L* and *c*/*L* ratio where *b* and *L* are as given in Table 4.1 and Figure 4.1. As evaluated in Section 3.1.9, the distance between bolt-rows did not influence the resistance primarily within the scope of this study. In both models, resistance is calculated based on single bolt-rows. According to the results, the predictions according to CIDECT and Method 2 of KY are very close to test results in the level of average 1-2 % of the yield load. Method 1 of KY estimates the yield load about 23% lower in average which is expected. Taking into account the perfectly plastic behaviour of the specimens under this type of loading, all yield resistance predictions are under the load deflection curve of the tests. At this moment, it is worthwhile to note that the definitions of *L* and *m* are very important as directly influencing the design resistance.

Table 4.4. Comparison of the modeling results with test results

Specimens of Phase I	b/L	Resistance (kN)				
		Test Results		Modeling Results		
		F_y	F_u	CIDECT	KY (method 1)	KY (method 2)
B1-1	0.66	309.0	375.7	307.0	236.7	280.7
B3-1	0.66	298.2	365.9	307.0	244.0	289.3
B3-2	0.66	339.4	390.4	307.0	244.0	289.3
B2-1	0.76	376.7	431.6	365.7	303.6	390.9
B2-2	0.76	393.4	444.4	365.7	303.6	390.9
B4-1	0.76	358.1	415.0	365.7	313.7	404.0
B4-2	0.76	417.9	454.2	365.7	313.7	404.0
B5-1	0.76	331.6	378.7	365.7	278.3	358.4
B5-2	0.79	381.6	448.3	405.6	278.3	373.7

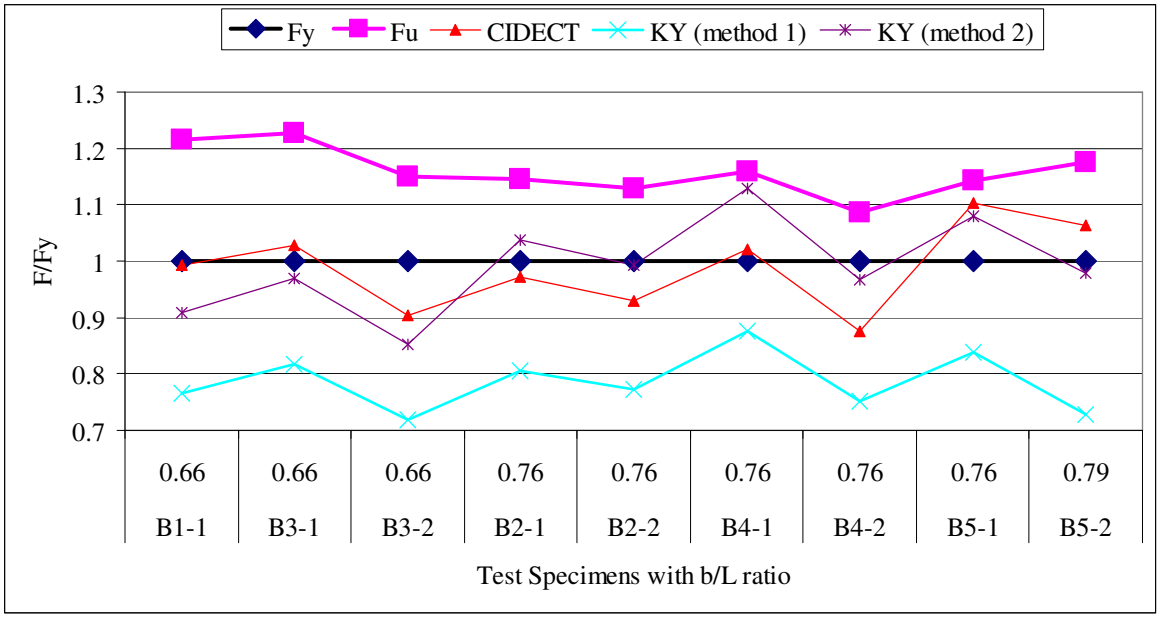

Figure 4.5. Comparison of the modeling results with test results in relation with *b*/*L* ratio

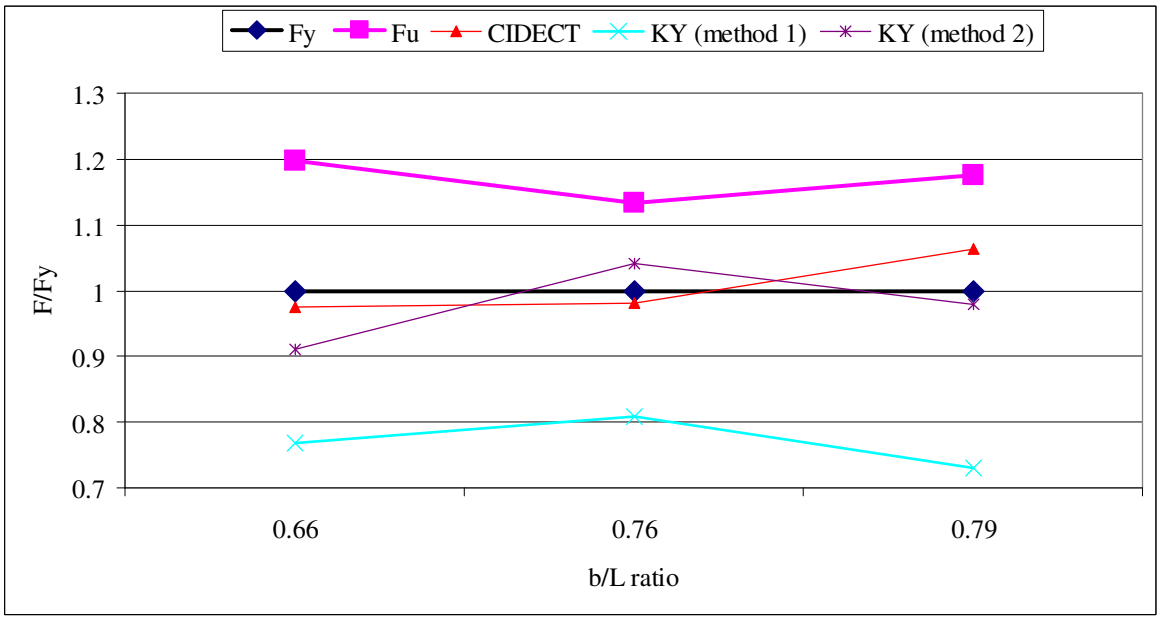

Figure 4.6. Comparison of the average modeling results with average test results in relation with *b*/*L* ratio

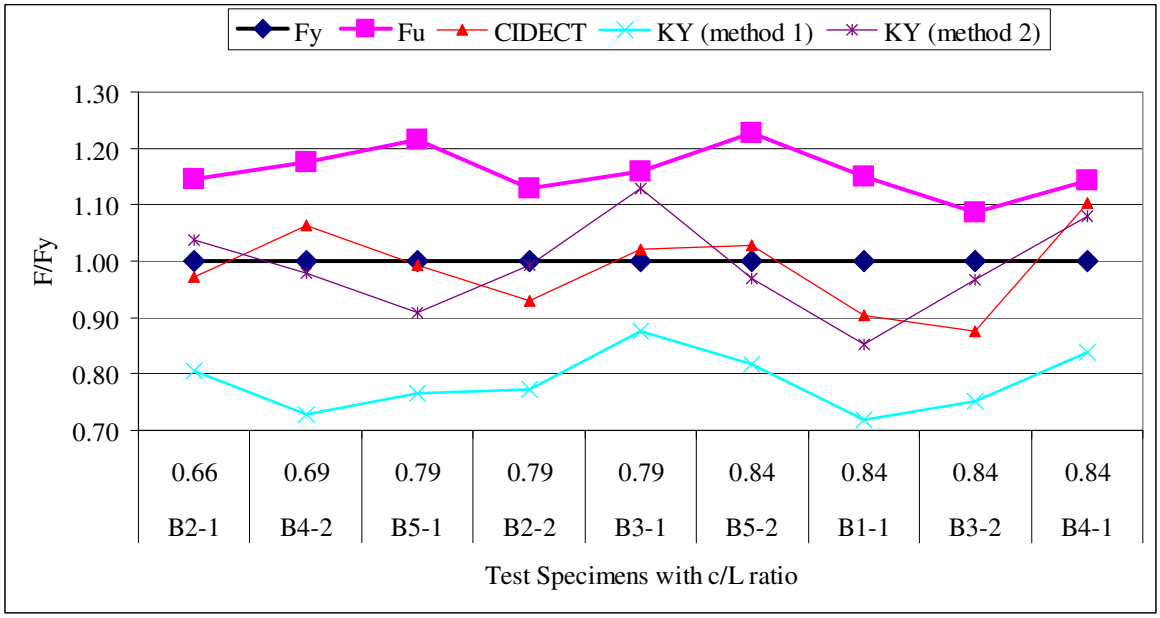

Figure 4.7. Comparison of the modeling results with test results in relation with *c/L* ratio

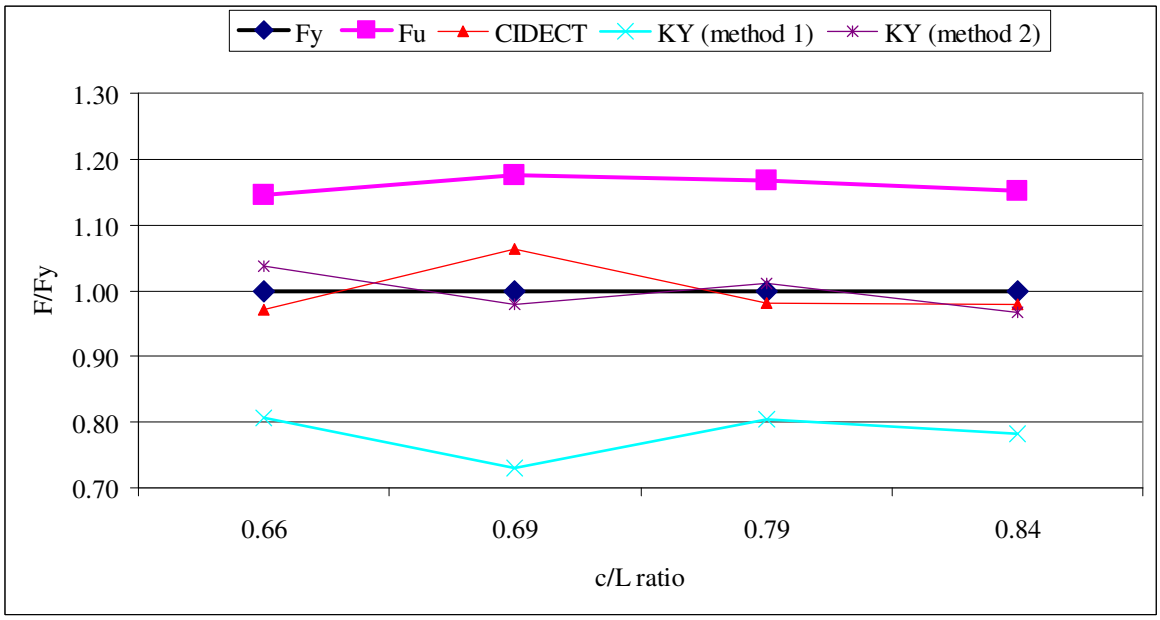

Figure 4.8. Comparison of the average modeling results with average test results in relation with *c/L* ratio

4.1.2. Stiffness coefficients of the Component

There are two approaches given hereafter. Stiffness calculation based on CIDECT and KY. Both are in the status of proposal to Eurocode 3 Part 1-8 [22].

The calculation method for stiffness coefficient of SHS column face in bending according to CIDECT is summarized in Table 4.5. Calculating the coefficient based on L_{stiff} value defined in Figure 4.2 gives extraordinarily high results because of the high values of b/L_{stiff} ratio (greater than 0.75 which is out of validity range of the formula). That's why likewise in Section 4.1.1, L_{stiff} value is taken as L (defined as center to center distance of opposite sidewalls (b_c-t_c)) and single bolt-rows is considered in order also to be within the validity range of the formula. However the calculated stiffness coefficient values are much higher; in average approximately five times the experimental results.

The calculation method for stiffness coefficient of SHS column face in bending according to KY is summarized in Table 4.6. The model is based on the method described in EC with supplementary similar dimensional definitions as Section 4.1.1. The calculated stiffness coefficient values are very much higher; in average approximately 28 times the experimental results.

As described in Section 3.1, the deformability of SHS column face in bending is associated with also sidewall deformation and corner rotation. If the definition is EC is used with a reasonable effective width definition, the sidewall stiffness coefficient in compression can be predicted as given in Table 4.7. The calculated stiffness coefficient values are smaller; in average approximately 6 times less than the experimental results. Besides, considering the results of the component test done under the coverage of this study, the stiffness of sidewall in compression could also be taken as infinity. Similarly stiffness coefficient of corner rotation can be calculated as given in Table 4.8. The calculated stiffness coefficient values are close to the experimental results; in average approximately 24% greater.

Table 4.5. Stiffness coefficient of SHS column face in bending component

Component	Reference	Stiffness coefficient
SHS in transverse compression - face failure in bending	CIDECT	$k_{32} = \frac{t_w^3}{14{,}4\beta L_{stiff}^2}\left(\frac{L_{stiff}^2}{bt_w}\right)^{1{,}25} \frac{\frac{c}{L_{stiff}} + \left(1-\frac{b}{L_{stiff}}\right)\tan\theta}{\left(1-\frac{b}{L_{stiff}}\right)^3 + \frac{10{,}4\left(k_1 - k_2\frac{b}{L_{stiff}}\right)}{\left(\frac{L_{stiff}}{t_w}\right)^2}}$ Single bolt-row has to be considered in the formula and the range of validity is limited by: $10 \le L_{stiff} / t_w \le 50$ $0{,}08 \le b / L_{stiff} \le 0{,}75$ $0{,}05 \le c / L_{stiff} \le 0{,}20$ Dimensions as defined in Section 4.1.1. θ is a parameter determined by: $\theta = 35 - 10\frac{b}{L_{stiff}}$ if $\frac{b}{L_{stiff}} < 0{,}7$ $\theta = 49 - 30\frac{b}{L_{stiff}}$ if $\frac{b}{L_{stiff}} \ge 0{,}7$ Deifinition of θ is given in Figure 4.9. β is the reduction factor which is unity for the case. k_1 =1,5, k_2 =1,6

Table 4.6. Stiffness coefficient of SHS column face in bending component

Component	Reference	Stiffness coefficient
SHS in transverse compression - face failure in bending	EC+KY	By similar idea described in Section 4.1.1. $k_4 = \frac{0{,}9 l_{eff}\, t_{fc}^{\,3}}{m^3}$ $m = b_1 - 0.6\, r$ Effective length is same with the calculated in Section 4.1.1.

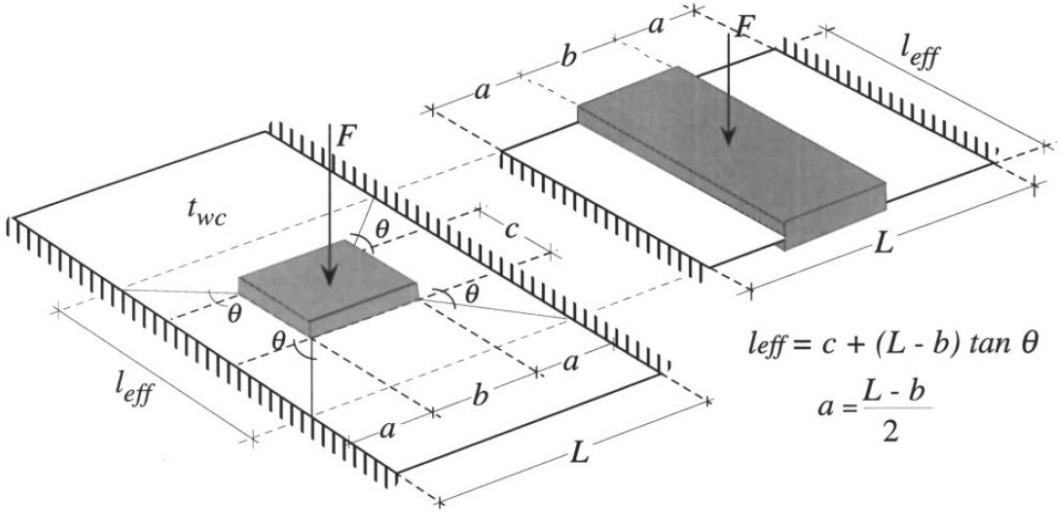

Figure 4.9. Definition of effective length based on angle θ [15]

Table 4.7. Stiffness coefficient of SHS sidewall in compression component

Component	**Reference**	**Stiffness coefficient**
SHS sidewall in compression	EC+KY	$k_2 = \frac{0{,}7\, b_{eff,c,wc}\, t_{wc}}{d_c}$ Effective width could be defined as given in Figure 4.9 ($a = b_1$) with angle θ as defined in Table 4.5. Effective width shall be the smaller of ($8a \tan \theta$) and ($2c + 4a \tan \theta$) where c is the distance between bolt-rows. d_c is the clear depth of the sidewall which can be taken as $d_c = h_c - 2r$ where h_c is the total depth of the section.

Table 4.8. Stiffness coefficient of SHS corner rotation component

Component	**Reference**	**Stiffness coefficient**
SHS corner rotation	EC+KY	$k = \frac{0.9 l_{eff} t_c^3}{r^3}$ Effective length could be defined as given in Figure 4.9 ($a = b_1 - r$) with angle θ as defined in Table 4.5. Effective width shall be the smaller of ($8a \tan\theta$) and ($2c + 4a \tan\theta$) where c is the distance between bolt-rows.

Comparison of the models with the test results are given in Table 4.9. The results in figures are normalized according to stiffness coefficients of test results. The results are generated in relation with b/L and c/L ratio where b and L are as given in Table 4.1 and Figure 4.1. In both models, stiffness coefficients are calculated based on single bolt-rows. Since CIDECT is not defining stiffness coefficients for sidewall in compression and corner in rotation, the model proposed in this study is incorporated with column face in bending stiffness coefficient of CIDECT to compare with the total stiffness coefficient level. In order to present comparative results in one figure, SHS column face in bending coefficient of KY ($k_{f,EC+KY}$) is plotted based on secondary axis where the other are plotted based on primary axis in Figure 4.10 and Figure 4.11. Except for the sidewall stiffness in compression, all other predictions are greater than the test results. During tests sidewall behaved much stiffer than what is predicted. The calculated stiffness level is in average 15-16% of the test results. Further study has to be done to improve the model by also taking into account the out of plane deformation of the sidewall during loading though inside at the top face. For the time being sidewall in compression stiffness coefficient could be taken as infinity considering the test results. Corner in rotation stiffness coefficient is estimated in average 24% greater than the test results. Looking into the column face in bending stiffness coefficient, although the estimation of CIDECT is roughly 5-6 times better than the prediction of KY, it is approximately five times the test results. After calculating the total stiffness coefficients KY and CIDECT predicts total stiffness respectively in the order of 5.5 and 3 times the test results in average. The predictions of SHS column face in bending stiffness coefficient, thus the total stiffness coefficient in

smaller *b*/*L* ratio are more closer to the test results. Further analytical and experimental study is necessary especially in higher values of *b*/*L* ratios. Again it is worthwhile to note that the definitions of *L* and *m* are also significant as directly influencing the design stiffness coefficients. In both model *L* and *m* are chosen to be in correspondence with the resistance calculations.

Table 4.9. Comparison of the modeling results with test results

Specimens of Phase I	b/L	c/L	Stiffness Coefficients (mm)									
			Test Results				Modeling Results					
							CIDECT		EC+KY			
			k_s	k_c	k_f	k_t	k_f	k_t	k_f	k_c	k_s	k_t
B1-1	0.66	0.79	50.46	5.07	0.45	0.41	1.57	1.12	6.87	6.42	10.40	2.52
B3-1	0.66	0.84	144.54	2.31	0.46	0.38	1.57	1.12	7.08	6.42	10.40	2.54
B3-2	0.66	0.84	41.21	3.85	0.34	0.32	1.57	1.12	7.08	6.42	10.40	2.54
B2-1	0.76	0.79	92.14	6.12	0.66	0.59	2.59	1.27	17.28	3.65	7.88	2.18
B2-2	0.76	0.79	50.01	10.00	0.53	0.50	2.59	1.27	17.28	3.65	7.88	2.18
B4-1	0.76	0.84	90.71	2.07	0.68	0.52	2.59	1.27	17.86	3.65	7.88	2.19
B4-2	0.76	0.84	35.22	7.62	0.40	0.38	2.59	1.27	17.86	3.65	7.88	2.19
B5-1	0.76	0.66	51.12	3.08	0.36	0.32	2.59	1.27	15.84	3.65	7.88	2.15
B5-2	0.79	0.69	53.67	3.45	0.58	0.50	3.54	1.46	15.84	3.65	7.88	2.15

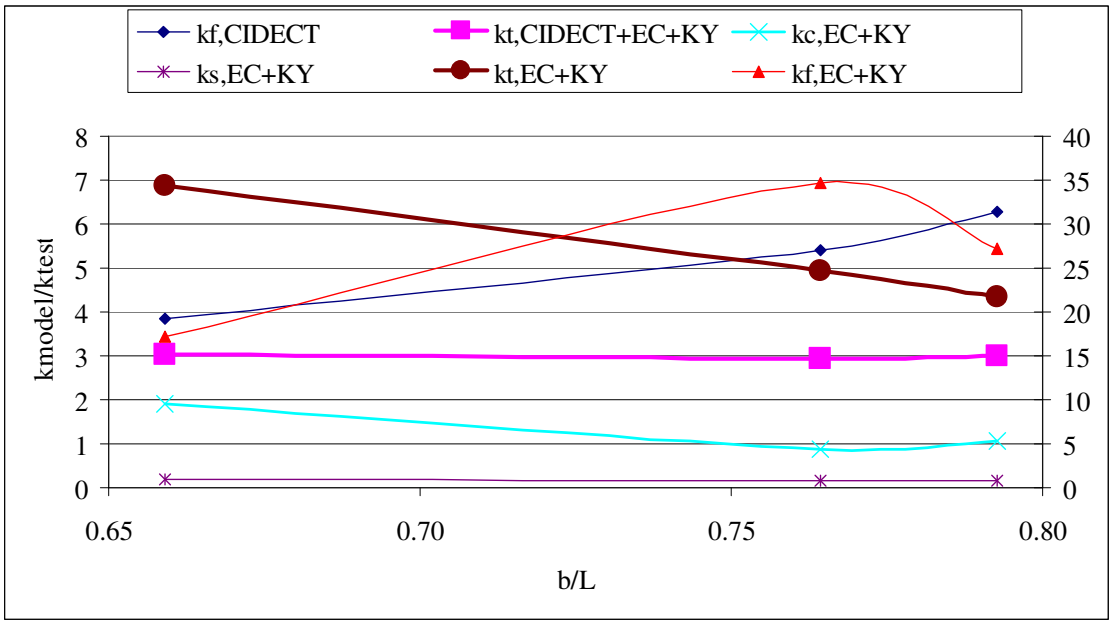

Figure 4.10. Average normalized modeling results in relation with *b*/*L* ratio

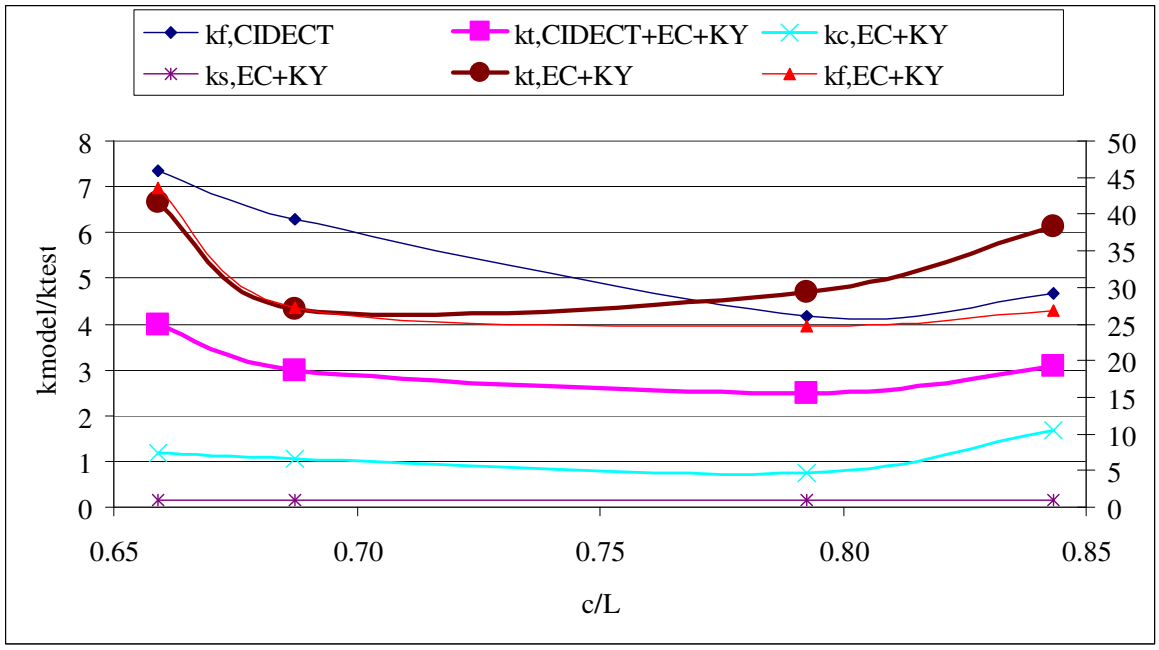

Figure 4.11. Average normalized modeling results in relation with *c/L* ratio

Based on the test results of the specimen T1M given in Section 3.2.1, the SHS column face stiffness level is 23768 kNm/rad. This corresponds to stiffness coefficient of 1.44 mm ($k=K/Ez^2$, where z is the lever arm and E is the modulus of elasticity) which is approximately 2.5-3 times the stiffness levels of B-type of specimens. This might be related to the length of the specimens. In order to observe the influence of the length on the stiffness a simple linear finite element model has been developed by using finite element solver SAP2000. Just the face has been modeled with shell elements in two groups. In the first group opposite sides are restrained fixed where in the second group hinged. These represent the upper and lower bound restraint conditions of the real corner behaviour which is in between. The other sides are free. As given in Figure 4.12, in order to optimize the model half of the face has been modeled by adding rollers in one side where the load is applied at two locations representing the bolt locations. The rollers allow displacement in the direction of the load. Parameters are the width (b_c) and the distance from the loading point to the opposite end (e_1). Displacement (δ) records have been taken in the middle of the side where the load is applied. The normalized force (F) over displacement values which is directly proportional to the stiffness are given in Figure 4.13. The ratios e_1/b_c of the B-type of specimens are in the range of 0.66 to 0.75 where in specimen T1M this ratio

is in the level of 6.5. It can be concluded that the column face in bending stiffness of T-type of specimens could be even 2-2.5 times of B-type of specimens.

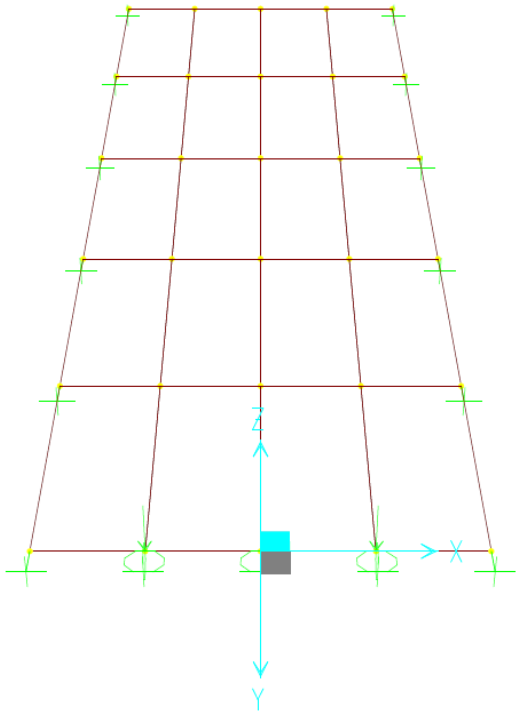

Figure 4.12. Linear finite element model generated in SAP2000

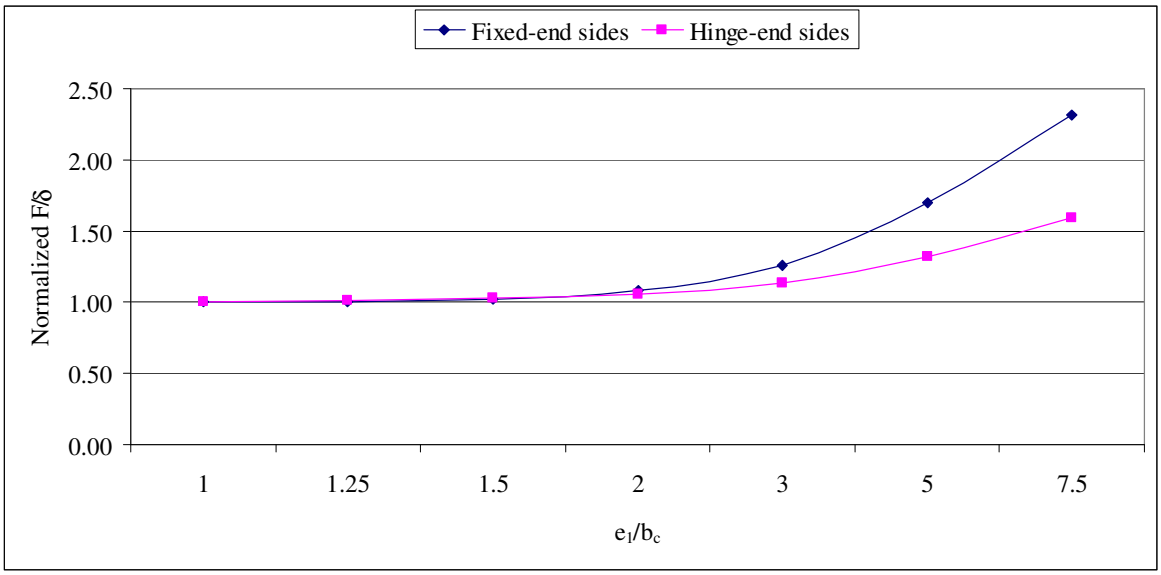

Figure 4.13. Normalized force over displacement values of the model

4.2. Modeling of Tubes under Compression Component

As evaluated in Section 3.1.9, the load could be transferred partially or fully by using adequate number of tubes that connect the rear SHS face to the front and allow partially threaded stud to pass through. This provides the combined action of both rear and front SHS faces which would increase the strength and stiffness of the joint. In this part resistance and initial stiffness parameters of this component shall be discussed by mechanical modeling approach.

4.2.1. Resistance of the Component

Resistance of the tubes under compression is mainly governed by its stability, thus a buckling problem. At present, a large number of design codes exist and the recommended procedures are often very similar. Eurocode 3 part 1-1 [28] is referred to in the following.

For hollow sections, the only buckling mode to be considered is flexural buckling. It is not required to take account of lateral-torsional buckling, since very large torsional rigidity of a hollow section prevents any torsional buckling.

The design buckling resistance capacity ($N_{b,Rd}$) of a compression member is given by;

$$N_{b,Rd} = \kappa.A.\frac{f_y}{\gamma_M} \tag{4.1}$$

where is A is the area of the cross section, κ is the reduction factor of the relevant buckling curve dependent on the non-dimensional slenderness of a column, f_y is the yield strength of the material used, γ_M is the partial safety factor on the resistance side (taken unity for capacity calculation).

The reduction factor κ is can be described analytically (for computer calculations) by following equation:

$$\kappa = \frac{1}{\Phi + \sqrt{\Phi^2 - \overline{\lambda^2}}}, \text{ but } \kappa \le 1 \text{ with } \Phi = 0.5\left[1 + \alpha(\overline{\lambda} - 0.2) + \overline{\lambda^2}\right] \quad (4.2)$$

where the imperfection factor α is 0.13, 0.21, 0.34, 0.49, 0.76 for the corresponding buckling curves of a_o, a, b, c, d respectively. For cold formed hollow sections buckling curve c is recommended. The non-dimensional slenderness $\overline{\lambda}$ is determined by

$$\overline{\lambda} = \frac{\lambda}{\lambda_E} \quad \text{with } \lambda = \frac{l_b}{i} \quad \text{and} \quad \lambda_E = \pi.\sqrt{\frac{E}{f_y}} \quad (4.3)$$

where l_b is the effective buckling length, i is the radius of gyration and E is the modulus of elasticity.

The buckling resistance of the tube 21.3 x 2 mm is calculated in Table 4.10 as 26.8 kN which is approximately 20% lower than the average test results (33.4 kN). Test results in Section 3.1.8 are not yield but ultimate load capacity of the tubes. That's why it is normal to have such difference. As a result the buckling resistance calculated based on Eurocode 3 can acceptably used to calculate the resistance of the tube under compression component.

Table 4.10. Buckling resistance of the tube 21.3 x 2 mm under compression

Component	**Reference**	**Resistance**
Resistance of the tube under compression	Eurocode 3 Part 1-1	<u>For tube 21.3 x 2 mm,</u> f_y = 235 MPa, l_b = 200 mm, A = 121 mm^2, i = 6.86 mm λ = 200 / 6.86 = 29.15 $\lambda_E = \pi \sqrt{(210000/235)} = 93.91$ => $\bar{\lambda}$ = 29.15 / 93.91 = 0.31 α=0.49 for buckling curve c. $\Phi = 0.5 (1+0.49(0.31-0.2)+0.31^2) = 0.575$ => $\kappa = 1/(0.575+\sqrt{(0.575^2-0.31^2)}) = 0.944$ $N_{b,Rd}$ = 0.944 x 121 x 235 = 26.8 kN

4.2.2. Stiffness coefficients of the Component

The stiffness of compression members is directly proportional with EA/l_b of the section where E is the modulus of elasticity, A is the cross-section area of the tube and l_b is the buckling length of the tube. Hence the stiffness coefficient can be proposed as follows:

$$k = \rho \frac{A}{l_b} \tag{4.4}$$

where ρ is the calibration factor which can be defined according to test results.

According the test results given in Section 3.1.8, average stiffness level is 46.1 kN/mm which corresponds to stiffness coefficient of 0.22 mm. The area and buckling length of the tube 21.3 x 2 mm are respectively 121 mm^2 and 200 mm. As a result the stiffness coefficient can be calculated as 0.605ρ where ρ should be in the level of 0.36 by calibrating with the average test results.

Considering the value of the calibration factor, it can be associated with $\bar{\lambda}$ which is defined and calculated in Section 4.2.1. If $\bar{\lambda}$ is directly used as calibration factor, the stiffness coefficient prediction will be slightly lower than the average test results.

Further analytical and/or experimental study is necessary by using different tube sizes and tube lengths to verify the calibration factor.

4.3. Component Modeling of the Joint

Simply the model of the studied joint is characterized by three linear springs, namely the column face in bending spring (including load introduction and corner rotation), connection spring and the shear spring as presented in Figure 4.14. The first one accounts for the deformation due to the load transmitted by the beam to rear face of the column, the second one is for deformation connect components (deformations of t-stub, bolt slips and bearing) and the third one simulates the shear deformation of the panel zone. In this case new sources of deformation are taken into account by means of additional springs, namely connection springs.

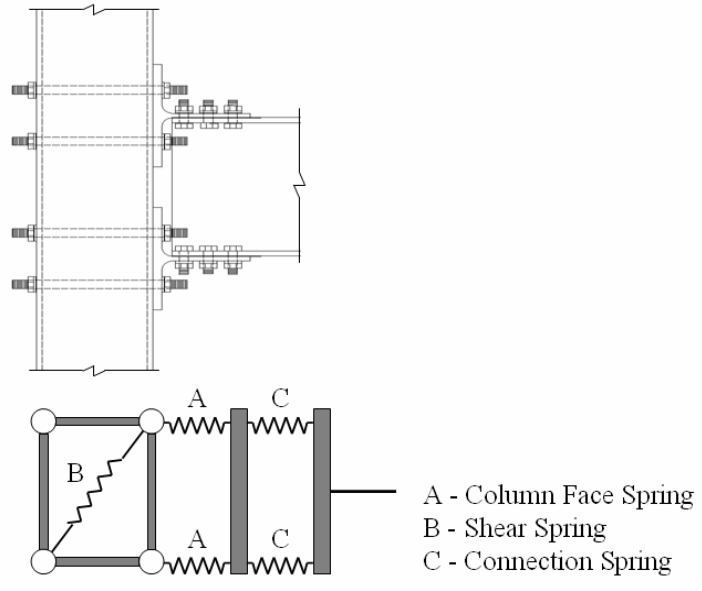

Figure 4.14. Mechanical model of the bolted joint

Several tests have been carried out to define the characteristics of the springs, in order to use the model to provide the response of all combinations of beams and columns made by European rolled sections. Eurocode 3 covers most of the components mainly related to open sections (H or I profiles). However component properties of joints with hollow sections are still not yet covered. There is an ongoing analytical study proposing properties of the components related to hollow section connections. In the following part, comparative component modeling of the studied joint shall be done by using as basis the existing knowledge, plus adapting some new approaches. In Table 4.11 two models that are developed and the list of components related to the studied joint are given. The reference column abbreviations EC, CIDECT and KY refers respectively to Eurocode 3 Part 1-8 [22], CIDECT Report 5BP-4/05[17] and proposed design approach by this study. In the first model resistance and stiffness parameters of SHS column face in bending component are calculated based on CIDECT whereas in the second model it is based on KY. Except for component A32 of CIDECT, all components of CIDECT are referring to Eurocode 3 Part 1-8.

Table 4.11. The two models and list of their related joint components

Component	**Model 1**		**Model 2**	
	T1M	**T2M**	**T1M**	**T2M**
SHS column web panel in shear	CIDECT	CIDECT	CIDECT	CIDECT
SHS column sidewall (web) in transverse compression	EC+KY	EC+KY	EC+KY	EC+KY
SHS in transverse compression - face failure in bending	CIDECT	CIDECT+KY	EC+KY	EC+KY
Backing plate in bending	-	KY	-	EC+KY
T-stub in bending	EC	EC	EC	EC
Bolts (partially threaded studs) in tension	EC	EC	EC	EC
Bolts in shear	EC	EC	EC	EC
Plate in bearing (plate in general, beam flange or web, column flange or face, end-plate, cleat or base plate)	EC	EC	EC	EC

4.3.1. Geometrical and Mechanical Data

Main joint data and detailed characteristics of the materials are given in Table 4.12 to Table 4.15. Drawings of the connections details and dimensions have been already given in Section 2.4.3.

Table 4.12. Main joint data

Configuration	I Beam-to-SHS column joint configuration
Column	SHS 200x200x10 S235
Beam	IPE 270 S275
Type of connection	T-stub connection with 5 partially threaded studs
T-stub	Split HEB 200 S275
Partially threaded studs	M16, 8.8
Bolts	M16, 8.8

Table 4.13. Detailed Characteristics of column and beam elements

Column SHS 200x200x10 mm		
Depth	*hc*	200 mm
Width	*bc*	200 mm
Thickness of the SHS section	*tc*	10 mm
External corner radius	*rc*	25 mm
Area	*A*	72.60 cm²
Inertia	*I*	4251 cm4
Yield strength	*fyc*	253 N/mm2
Ultimate strength	*fuc*	409 N/mm2

Beam IPE 270		
Depth	*hb*	270 mm
Thickness of the web	*twb*	6.60 mm
Width	*bb*	135 mm
Thickness of the flange	*tfb*	10.20 mm
Root radius	*rb*	15.00 mm
Area	*A*	45.95 cm²
Inertia	*I*	5790.00 cm4
Plastic section modulus	*Wpl,y.b*	484.00 cm³
Yield strength	*fyb*	294.00 N/mm²
Ultimate strength	*fub*	435.00 N/mm²

Table 4.14. Detailed Characteristics of column and beam elements

T-stub - Split HEB 200		
Depth	h_b	200 mm
Thickness of the web	t_{wt}	9.00 mm
Width	b_b	200 mm
Thickness of the flange	t_{ft}	15.00 mm
Root radius	r_t	18.00 mm
Yield strength	f_{yb}	302.00 N/mm²
Ultimate strength	f_{ub}	443.00 N/mm²
At column interface		
Direction of load transfer (1)		
Number of bolts rows	n_1	2
Edge to first bolt row distance	e_{11}	50.00 mm
Pitch between bolt row 1 and 2	p_1	100.00 mm
last bolt row to edge distance	e_{1n}	50.00 mm
Direction perpendicular to Load transfer (2)		
Number of bolts rows	n_2	3
Edge to first bolt row distance	e_{21}	40.00 mm
Pitch between bolt row 1 and 2	p_2	120.00 mm
Edge to second bolt row distance	e_{22}	100.00 mm
Pitch between bolt row 2 and 3	p_2	60.00 mm
last bolt row to edge distance	e_{23}	40.00 mm
At beam interface		
Direction of load transfer (1) web		
Number of bolts rows	n_1	3
Edge to first bolt row distance	e_{11}	30.00 mm
Pitch between bolt row 1 and 2	p_1	42.00 mm
Edge to second bolt row distance	e_{12}	72.00 mm
Pitch between bolt row 2 and 3	p_2	42.00 mm
Last bolt row to edge distance	e_{13}	114.00 mm
Direction perpendicular to Load transfer (2)		
Number of bolts rows	n_2	2
Edge to first bolt row distance	e_{21}	32.00 mm
Pitch between bolt row 1 and 2	p_2	72.00 mm
last bolt row to edge distance	e_{22}	32.00 mm

Table 4.15. Detailed Characteristics of backing plate and connecting accessories

Backing Plate 15 mm		
Length	h_c	150 mm
Width	b_c	200 mm
Thickness of the SHS section	t_c	15 mm
Yield strength	f_{yc}	266 N/mm2
Ultimate strength	f_{uc}	416 N/mm2

Partially treaded studs and bolts M16		
Gross area	A	201.00 mm²
Resistant area	A_s	157.00 mm²
Diameter of the shank	d	16.00 mm
Diameter of the holes	d_0	17.00 mm
Largest width of the nut	d_1	30.00 mm
Smallest width of the nut	d_2	26.00 mm
Mean diameter of bolt/nut head $(d_1+d_2)/2$	d_m	28.00 mm
Height of the nut	h_{nut}	13.00 mm
Height of the head	h_{head}	10.00 mm
Thickness of the washer	t_{washer}	4.00 mm
Yield strength	f_{yb}	640.00 N/mm²
Ultimate strength	f_{ub}	800.00 N/mm²

4.3.2. Resistance of the Components

Resistance of the basic joint components are calculated in following tables. In the reference column abbreviations EC, CIDECT and KY refers respectively to Eurocode 3 Part 1-8 [22], CIDECT Report 5BP-4/05 [17] and proposed design approach by this study. For modeling purposes, partial safety factors (γ) are not considered and are taken as unity in calculations.

Table 4.16. Resistance of column web in shear component

Component	Reference	Resistance		
Column web in shear	EC CIDECT	$V_{wp,Rd} = \frac{0,9 f_{y,wc} A_{vc}}{\sqrt{3}\,\gamma_{M0}}$	and	$A_v = \frac{Ah}{(b+h)}$
		A_{vc} is the shear area of the column. A_{vc} = 7260 x 200 / (200 + 200) = 3630 mm^2 $V_{wp,Rd}$ = 0.9 x 253 x 3630 / √3 = 477.2 kN		

Table 4.17. Resistance of SHS column for sidewall crushing and punching shear failure modes at rear face

Component	Reference	Resistance
SHS column (sidewall) web under transverse compression and punching shear (at upper beam flange)	CIDECT	Definition of the compression zone for bolt groups is given in Figure 4.1. Design resistance is given in Figure 4.15 <u>Load transfer by partially threaded studs</u>: $b_i = b$ = 120 + 0.9 x 28 = 145.2 mm < b_0-2t_0 (180 mm) => punching shear failure mode $t_i = c$ = 100 + 0.9 x 28 = 125.2 mm $b_{e,p}$ = 10 x 145.2 / (200/10) = 72.6 mm < b_i (145.2 mm) OK ! $N_{1,Rd}$ = 253 x 10 (2 x 125.2 + 2 x 72.6) / √3 = 577.9 kN <u>Load transfer by partially threaded studs and backing plate</u>: Load is transferred by dispersion at 45^O through the backing plate; $b_i = b$ = 120 + 0.9 x 28 + 2 x 15 = 175.2 mm < b_0-2t_0 (180 mm) => punching shear failure mode $t_i = c$ = 100 + 0.9 x 28 + 2 x 15 = 155.2 mm < width of the backing plate (150 mm) => t_i = 150 mm. $b_{e,p}$ = 10 x 175.2 / (200/10) = 87.6 mm < b_i (175.2 mm) OK ! $N_{1,Rd}$ = 253 x 10 (2 x 150 + 2 x 87.6) / √3 = 694.1 kN

Table 4.18. Resistance of SHS column for sidewall crushing failure mode at front face

Component	**Reference**	**Resistance**
SHS column (sidewall) web in transverse compression (at lower beam flange)	CIDECT	Design resistance is given in Figure 4.15 <u>Load transfer by t-stub</u>: b_i = 200 mm > b_0-2t_0 (180 mm) => sidewall crushing failure mode t_i = 2 x 0.6 r_t + 2 t_{ft} t_i = 2 x 0.6 x 18 + 2 x 15 = 51.6 mm $N_{1,Rd}$ = 253 x 10 (2 x 51.6 + 10 x 10) = 514.1 kN

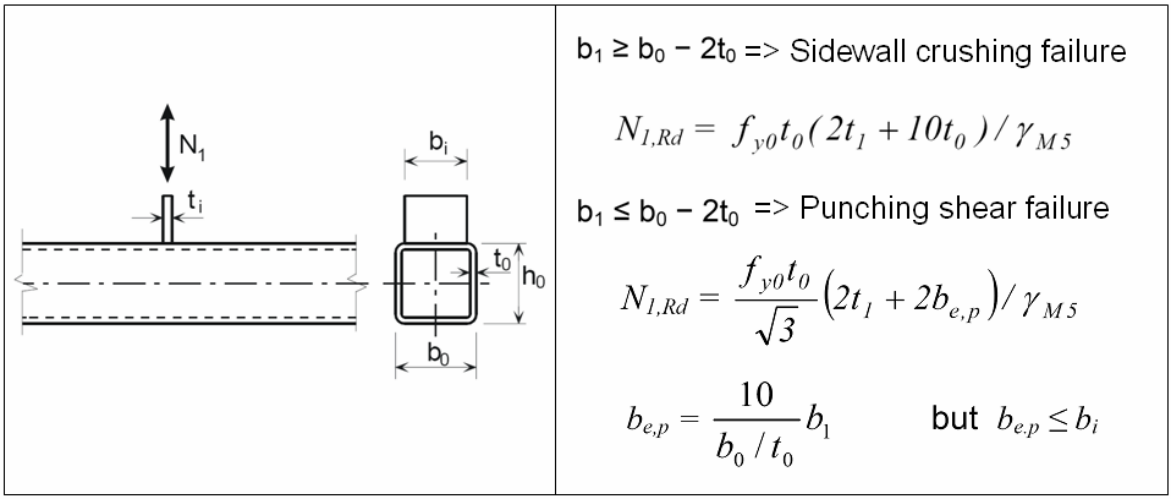

Figure 4.15. Resistance of SHS column for sidewall crushing and punching shear failure modes [22]

Table 4.19. Resistance of column face in bending component

Component	Reference	Resistance
SHS in transverse compression - face failure in bending	CIDECT	Load transfer by partially threaded studs: $b_m = L\left[1 - 0{,}82\frac{t_w^2}{c^2}\left(1+\sqrt{1+2{,}8\frac{c^2}{t_w L}}\right)^2\right]$ Column notations are given in Figure 4.2. But referring to Section 4.1.1, L is taken as 190 mm. c = 0.9 x 28 = 25.2 mm for single bolt-row. b_m = 49.7 mm < b (= 120 + 0.9 x 28 = 145.2 mm) => $F_{pl,loc} = \beta 4 m_{pl,Rd}\left[\frac{\pi\sqrt{L(a+x)}+2c}{a+x}+\frac{1{,}5cx+x^2}{\sqrt{3}t_w(a+x)}\right]$ where, $a = L - b$ = 190 – 145.2 = 44.8 $\beta = 1$ if $\frac{b+c}{L} \geq 0{,}5$ $\beta = 0{,}7 + 0{,}6\frac{b+c}{L}$ if $\frac{b+c}{L} \leq 0{,}5$ $m_{pl,Rd} = \frac{1}{4}t_w^2 f_y / \gamma_{M0}$ $x = -a + \sqrt{a^2 - 1{,}5ac + \frac{\sqrt{3}t_w}{2}\left[\pi\sqrt{L(a+x_0)}+4c\right]}$ with $x_0 = L\left[\left(\frac{t_w}{L}\right)^{\frac{2}{3}} + 0{,}23\frac{c}{L}\left(\frac{t_w}{L}\right)^{\frac{1}{3}}\right]\left(\frac{b-b_m}{L-b_m}\right)$ (25.2 + 145.2) / 190 > 0.5 => β = 1 $m_{pl,Rd}$ = 10^2 x 253 / 4 = 6325 Nmm/mm x_0 = 19.64 => x = 12.96 => $F_{pl,loc}$ = 182.9 kN for single bolt row and $F_{pl,loc}$ = 182.9 x 2 = 365.7 kN for bolt group in tension zone.

Table 4.20. Resistance of SHS column face in bending component with backing plate

Component	**Reference**	**Resistance**
SHS in transverse compression - face failure in bending	CIDECT+ KY	The influence of backing plate can be introduced by transferring the load by dispersion at 45^O through the backing plate. <u>Load transfer by partially threaded studs and backing plate</u>: Column notations are given in Figure 4.2. Referring to Section 4.1.1, L is taken as 190 mm. c = 0.9 x 28 + 15 + (25-0.9x28/2)= 52.8 mm for single bolt-row considering the limits of the backing plate. b_m = 130.6 mm < b (= 120 + 0.9 x 28 +30 = 175.2 mm) => $a = L - b$ = 190 – 175.2 = 14.8 (52.8 + 175.2) / 190 > 0.5 => β = 1 $m_{pl,Rd}$ = 10^2 x 253 / 4 = 6325 Nmm/mm x_0 = 23.45 => x = 22.61 => $F_{pl,loc}$ = 340.4 kN for single bolt row and $F_{pl,loc}$ = 340.4 x 2 = 680.8 kN for bolt group in tension zone.

Table 4.21. Resistance of SHS column face in bending component

Component	Reference	Resistance
SHS in transverse compression - face failure in bending	EC+KY	As explained in Section 4.1.1 necessary dimensions mentioned in Figure 4.4 are as follows: e = 60 mm, m = 40 – 15 = 25 mm (referring to Section 4.1.1) n = 1.25 x 25 = 31.5 mm, p = 100 mm d_w = 30 mm => e_w = 30/4 = 7.5 mm <u>For Mode 1 (Complete yielding of the flange):</u> Referring to Section 4.1.1, method 2 is used as follows: Σl_{eff}=275 mm as given in Table 4.22. Both bolt-rows are end bolt-rows. $M_{pl,Rd} = 0.25\ \Sigma l_{eff}\ t_f^2\ f_y\ /\ \gamma_{MO}$ = 0.25x275x10^{2}x253= 1.7 kNm $F_{T,1,Rd}$ = 358.4 kN <u>For Mode 2 (Bolt failure with yielding of the flange):</u> $F_{t,Rd}$ = 0.9 x 880 x 157 = 124,3 kN For 5 bolts => $\Sigma F_{t,Rd}$ = 621.7 kN $F_{T,2,Rd}$ = 407.2 kN <u>For Mode 3 (Bolt failure):</u> $F_{T,2,Rd} = \Sigma F_{t,Rd}$ = 621.7 kN

Table 4.22. Effective length calculation for SHS column face

Bolt-row location	Bolt row considered individually		Bolt row considered as a part of a group of bolt rows	
	Circular pattern ($l_{eff,cp}$)	Non-circular pattern ($l_{eff,nc}$)	Circular pattern ($l_{eff,cp}$)	Non-circular pattern ($l_{eff,nc}$)
End bolt-row	157	175	179	138
For Mode 1	$l_{eff,1}$	157	$\Sigma l_{eff,1}$	275
For Mode 2	$l_{eff,2}$	175	$\Sigma l_{eff,2}$	275
For Mode 1	For 2 bolt-rows $\Sigma l_{eff,1}$		275	
For Mode 2	For 2 bolt-rows $\Sigma l_{eff,2}$		275	

Table 4.23. Resistance of SHS column face in bending component with backing plate

Component	**Reference**	**Resistance**
SHS in transverse compression - face failure in bending	EC+KY	<u>For Mode 1 (Complete yielding of the flange) – Method 2</u>: Resistance with backing plate is as follows: $F_{T,1,Rd} = \frac{(8n - 2e_w)M_{pl,1,Rd} + 4nM_{bp,Rd}}{2mn - e_w(m+n)}$ Referring to Table 4.21 and Table 4.22; Σl_{eff}=275 mm for SHS face but for backing plate Σl_{eff}=150 mm since e_1 = 25 mm t_{bp} = 15 mm, $f_{y,bp}$ = 266 N/mm^2 $M_{bp,Rd}$ =0.25Σl_{eff} t_{bp}^2 $f_{y,bp}/\gamma_{MO}$ =0.25x150x15^{2}x266= 2.2 kNm $F_{T,1,Rd}$ = 604.3 kN <u>For Mode 2 (Bolt failure with yielding of the flange):</u> Same as calculated in Table 4.21 => $F_{T,2,Rd}$ = 407.2 kN <u>For Mode 3 (Bolt failure):</u> Same as calculated in Table 4.21 => $F_{T,2,Rd}$ = 621.7 kN

It is important to note that CIDECT+KY do not take into account the failure mode of bolt failure with yielding of the hollow section column face in bending. That's why while calculating the resistance of SHS column face in bending component with backing plate, it gives greater resistance than EC+KY.

Table 4.24. Resistance of t-stub in bending component

Component	**Reference**	**Resistance**
T-stub in bending	EC	As explained in Section 4.1.1, necessary dimensions mentioned in Figure 4.4 are as follows: e = 50 mm, m = 50 – 9/2 – 0.8 x 18 = 31.1 mm n = 1.25 x 31.1 = 38.9 mm, p = 60 mm d_w = 30 mm => e_w = 30/4 = 7.5 mm As given in Table 4.33, effective length of the t-stub is; Σl_{eff} = 200 mm For Mode 1 (Complete yielding of the flange) – Method 2: $F_{T,1,Rd} = \frac{(8n - 2e_w) M_{pl,1,Rd}}{2mn - e_w (m + n)}$ $M_{pl,Rd} = 0.25 \Sigma l_{eff} t_f^2 f_y / \gamma_{MO}$ = 0.25 x 200 x 15^2 x 302 $M_{pl,Rd}$ = 3.4 kNm => $F_{T,1,Rd}$ = 531.2 kN For Mode 2 (Bolt failure with yielding of the flange): $F_{T,2,Rd} = \frac{2M_{pl,2,Rd} + n\Sigma F_{t,Rd}}{m + n}$ $F_{t,Rd}$ = 0.9 x 880 x 157 = 124.3 kN For 5 bolts => $\Sigma F_{t,Rd}$ = 621.7 kN $M_{p2,Rd} = 0.25 \Sigma l_{eff} t_f^2 f_y / \gamma_{MO}$ = 0.25 x 200 x 15^2 x 302 $M_{p2,Rd}$ = 3.4 kNm => $F_{T,2,Rd}$ = 442.5 kN For Mode 3 (Bolt failure): $F_{T,2,Rd} = \Sigma F_{t,Rd}$ = 621.7 kN

Table 4.25. Effective length calculation for t-stub

Bolt-row location	Bolt row considered individually		Bolt row considered as a part of a group of bolt rows	
	Circular pattern ($l_{eff,cp}$)	Non-circular pattern ($l_{eff,nc}$)	Circular pattern ($l_{eff,cp}$)	Non-circular pattern ($l_{eff,nc}$)
Inner bolt-row	195	187	120	60
End bolt-row	178	133	140	70
End bolt-row	178	133	140	70
For Mode 1	$l_{eff,1}$	133	$\Sigma l_{eff,1}$	400
For Mode 2	$l_{eff,2}$	133	$\Sigma l_{eff,2}$	200
For Mode 1	For 3 bolt-rows $\Sigma l_{eff,1}$	454		200
For Mode 2	For 3 bolt-rows $\Sigma l_{eff,2}$	454		200

Table 4.26. Resistance of partially threaded studs in tension

Component	**Reference**	**Resistance**
Bolts (partially threaded studs) in tension	EC	$F_{Rd,2} = n \times min[F_{t,Rd}; B_{p,Rd}]$ where n is the number of bolts in the tension zone of the joint Tension resistance of the partially threaded stud: $F_{t,Rd} = \frac{k_2 \ f_{ub} \ A_s}{\gamma_{M2}}$ where k_2 = 0,63 for countersunk bolt, k_2 = 0,9 otherwise $F_{t,Rd}$ = 0.9 x 880 x 157 = 124,3 kN per bolt Punching shear resistance of the partially threaded stud: $B_{p,Rd} = 0,6 \pi d_m t_p f_{up} / \gamma_{M2}$ $B_{p,Rd}$ = 0.6π x 28 x 10 x 409 = 216 kN per bolt For 5 bolts => $\Sigma F_{Rd.2}$ = 621.7 kN

Table 4.27. Resistance of bolts in shear

Component	Reference	Resistance
Bolts in shear	EC	$F_{v,Rd} = \frac{\alpha_v \ f_{ub} \ A}{\gamma_{M2}}$ where the shear plane passes through the unthreaded portion of the bolt (A is the gross cross section of the bolt): $\alpha_v = 0,6$ Shear resistance of the bolts: $F_{v,Rd}$ = 0.6 x 880 x 201 = 106.2 kN per shear plane. For 6 bolts => $\Sigma F_{v,Rd}$ = 637 kN

Table 4.28. Resistance calculation of plate in bearing

Component	Reference	Resistance
Plate in bearing (plate in general, beam flange or web, column flange or face, end-plate, cleat or base plate)	EC	The design resistance of bolts in bearing shall be determined as follows: $F_{b,Rd} = \frac{k_1 \ a_b \ f_u \ d \ t}{\gamma_{M2}}$ where α_b = min [α_d ; f_{ub}/f_u ; 1.0] in the direction of load transfer: • for end bolts : $\alpha_d = e_1 / 3d_0$ • for inner bolts: $\alpha_d = (p_1 / 3d_0) - 0.25$ perpendicular to the direction of load transfer: • for edge bolts: k_1 = min [(2.8 e_2/d_0)–1.7 ; 2.5] • for inner bolts: k_1 = min [(1.4 p_2/d_0)–1.7 ; 2.5] d_0 is the hole diameter and d is the bolt diameter.

Table 4.29. Resistance of beam flange in bearing

Component	**Reference**	**Resistance**
Beam flange in bearing	EC	Bearing resistance of the beam flange: t = 10.2 mm, f_u = 435 MPa, d_0 = 17 mm, d = 16 mm f_{ub}/f_u = 880 / 435 = 2.02 There are 3 bolt-rows; Bolt-row 1 (e_1 = 20 mm, e_2 = 32 mm): α_d = 20 / 3x17 = 0.39 => α_b = 0.39 k_1 = min [(2.8x32/17)–1.7 ; 2.5] = 2.5 $F_{b,1}$ = 2.5x0.39x435x16x10.2 = 69.2 kN $\Sigma F_{b,1}$ = 2 x 69.2 = 138.4 kN for bolt-row 1 Bolt-rows 2 and 3 (p_1 = 42 mm, e_2 = 32 mm): α_d = (42/ 3x17) - 0.25 = 0.57 => α_b = 0.57 k_1 = min [(2.8x32/17)–1.7 ; 2.5] = 2.5 $F_{b,2,3}$ = 2.5x0.57x435x16x10.2 = 101.2 kN $\Sigma F_{b,2,3}$ = 4 x 101.2 = 404.7 kN for bolt-rows 2 and 3 For 6 bolts => $\Sigma F_{b,Rd}$ = 138.4 + 404.7 = 543.1 kN

Table 4.30. Resistance of t-stub web in bearing

Component	**Reference**	**Resistance**
Beam t-stub web in bearing	EC	Bearing resistance of the t-stub: t = 9 mm, f_u = 443 MPa, d_0 = 17 mm, d = 16 mm f_{ub}/f_u = 880 / 443 = 1.99 There are 3 bolt-rows; Bolt-row 1 (e_1 = 30 mm, e_2 = 37.8 mm): α_d = 30 / 3x17 = 0.59 => α_b = 0.59 k_1 = min [(2.8x37.8/17)–1.7 ; 2.5] = 2.5 $F_{b,1}$ = 2.5x0.59x443x16x9 = 94.1 kN $\Sigma F_{b,1}$ = 2 x 94.1 = 188.2 kN for bolt-row 1 Bolt-rows 2 (p_1 = 42 mm, e_2 = 46 mm): α_d = (42/ 3x17) - 0.25 = 0.57 => α_b = 0.57 k_1 = min [(2.8x46/17)–1.7 ; 2.5] = 2.5 $F_{b,2}$ = 2.5x0.57x443x16x9 = 90.9 kN $\Sigma F_{b,2}$ = 2 x 90.9 = 181.8 kN for bolt-rows 2 Bolt-rows 3 (p_1 = 42 mm, e_2 = 54.2 mm): α_d = (42/ 3x17) - 0.25 = 0.57 => α_b = 0.57 k_1 = min [(2.8x54.2/17)–1.7 ; 2.5] = 2.5 $F_{b,3}$ = 2.5x0.57x443x16x9 = 90.9 kN $\Sigma F_{b,3}$ = 2 x 90.9 = 181.8 kN for bolt-rows 3 For 6 bolts => $\Sigma F_{b,Rd}$ = 188.2 + 181.8 + 181.8 = 551.8 kN

4.3.3. Moment Resistance of the Joint

According to both approaches, the weakest links and corresponding resistance values are given in Table 4.31. Plastic moment resistance (M_{Rd}) and elastic moment resistance (M_e) have been calculated based on Equation (4.5). The lever arm of the studied joint has been taken according to the definitions given in Figure 4.16 as the distance from the centre of compression to a point midway between two bolt-rows in tension and measured as 279 mm.

$$M_{Rd} = F_{Rd}\, z \qquad \text{and} \qquad M_e = (2/3)\, x\, M_{Rd} \tag{4.5}$$

Table 4.31. Moment resistance of the joint

Modeling by	Specimen	Weakest component	F_{Rd} (kN)	M_{Rd} (kNm)	M_e (kNm)
Model 1	T1M	SHS face in bending	365.7	102.0	68.0
	T2M	T-stub in bending	442.5	123.5	82.3
Model 2	T1M	SHS face in bending	358.4	100.0	66.7
	T2M	SHS face in bending	407.2	113.6	75.7

Type of connection	Centre of compression	Lever arm	Force distributions
a) Welded connection 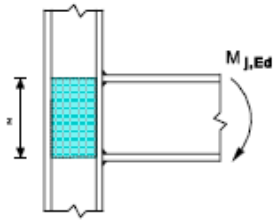	In line with the mid thickness of the compression flange	$z = h - t_{fb}$ h is the depth of the connected beam t_{fb} is the thickness of the beam flange	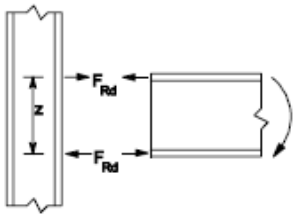
b) Bolted connection with angle flange cleats 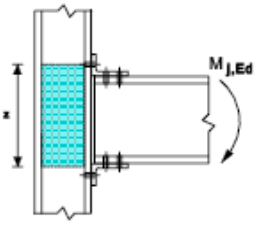	In line with the mid-thickness of the leg of the angle cleat on the compression flange	Distance from the centre of compression to the bolt-row in tension	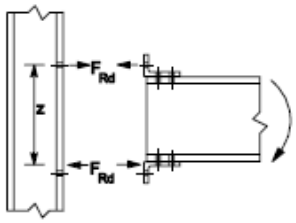
c) Bolted end-plate connection with only one bolt-row active in tension 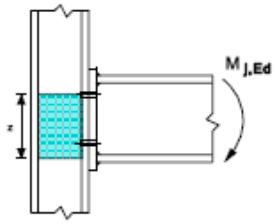	In line with the mid-thickness of the compression flange	Distance from the centre of compression to the bolt-row in tension	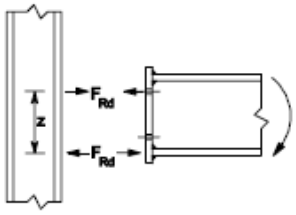
d) Bolted extended end-plate connection with only two bolt-rows active in tension 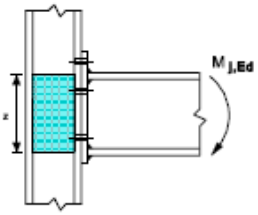	In line with the mid-thickness of the compression flange	Conservatively z may be taken as the distance from the centre of compression to a point midway between these two bolt-rows	
e) Other bolted end-plate connections with two or more bolt-rows in tension 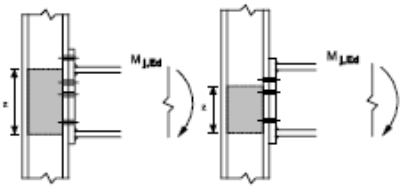	In line with the mid-thickness of the compression flange	An approximate value may be obtained by taking the distance from the centre of compression to a point midway between the farthest two bolt-rows in tension	A more accurate value may be determined by taking the lever arm z as equal to z_{eq} obtained using the method given in C.1.1.1.1.

Figure 4.16. Centre of compression, lever arm z and force distributions for deriving the design moment resistance [22]

4.3.4. Stiffness coefficients of the Components

Stiffness coefficients of the joint components are calculated in following tables. In the reference column abbreviations EC, CIDECT and KY refers respectively to Eurocode 3 Part 1-8 [22], CIDECT Report 5BP-4/05[17] and proposed design approach by this study.

Table 4.32. Stiffness coefficient of SHS column web in shear component

Component	**Reference**	**Stiffness coefficient**
SHS column web in shear	EC CIDECT	$k_1 = \frac{0{,}38 A_{vc}}{\beta z}$ z is the lever arm and β is the transformation parameter which is unity for single sided joints[30]. A_{vc} is the shear area of the column. A_{vc} = 7260 x 200 / (200 + 200) = 3630 mm^2 k_1 = 0.38 x 3630 / 279 = 4.9 mm

Referring to Section 4.1.2, stiffness coefficient of SHS column face in bending component shall be calculated in combination with SHS sidewall in compression and SHS corner rotation for both CIDECT and KY. Although EC does not recommend to take into account the influence of the backing plate, it can be introduced by again using the same idea of load transfer path by dispersion at 45^O through the backing plate while calculating the effective dimensions.

Table 4.33. Stiffness coefficient of SHS column face in bending component

Component	**Reference**	**Stiffness coefficient**
SHS in transverse compression - face failure in bending (upper beam flange level)	EC+KY	Refering to Section 4.1.2, the configuration is same as specimen B5. SHS column face in bending : $k_4 = \frac{0{,}9 l_{eff}\, t_{fc}^{\,3}}{m^3}$ $m = b_1 - 0.6\, r = 40 - 0.6\text{x}25 = 25$ mm Effective length is same with the calculated in Section 4.3.2. $l_{eff} = 137.5$ mm $k_4 = 7.92$ mm per bolt-row. SHS sidewall in compression : $k_2 = \frac{0{,}7\, b_{eff,c,wc}\, t_{wc}}{d_c}$ Effective width is defined as given in Section 4.3.2. $b_{eff} = 84.4$ mm $d_c = b_c - 2r = 200 - 2\text{x}25 = 150$ mm $k_2 = 3.94$ mm per bolt-row. SHS corner rotation : $k = \frac{0.9 l_{eff} t_c^3}{r^3}$ Effective length is defined as given in Section 4.3.2. $l_{eff} = 31.66$ mm $k = 1.82$ mm per bolt-row. $k_{4,t} = [(1/7.92) + (1/3.94) + (1/1.82)]^{-1} = 1.07$ mm including sidewall in compression and corner rotation.

Table 4.34. Stiffness coefficient of SHS column face in bending component with backing plate

Component	**Reference**	**Stiffness coefficient**
SHS in transverse compression - face with backing plate failure in bending	EC+KY	Referring to Table 4.33, SHS column face in bending : k_4 = 7.92 mm per bolt-row for SHS face. Effective length for backing plate is same with the calculated effective length in Section 4.3.2 : l_{eff} = 75 mm $k_{4,bp}$ = 0.9x75x15^3/25^3 = 14.58 mm per bolt-row $k_{4,face}$ = 7.92 + 14.58 = 22.5 mm per bolt-row. SHS sidewall in compression : Additional to the effective width definition given in Section 4.3.2, load transfer path by dispersion at 45^O through the backing plate but limited with the edge. So on one side b_{eff} is limited with 25 mm but on the other side by additional 15 mm. => b_{eff} = 25 + (84.4/2 +15) = 82.2 mm k_2 = 0.7x82.2x10/150 = 3.84 mm per bolt-row. SHS corner rotation : Additional to the effective width definition given in Section 4.3.2, load transfer path by dispersion at 45^O through the backing plate but limited with the edge. So, on one side b_{eff} is limited with 25 mm but on the other side by additional 15 mm l_{eff} = = 25 + (31.66/2 +15) = 55.83 mm k = 0.9x55.83x10^3/25^3 = 3.22 mm per bolt-row. $k_{4,t,bp}$ = [(1/22.5) + (1/3.84) + (1/3.22)]$^{-1}$ = 1.62 mm including sidewall in compression and corner rotation.

Table 4.35. Stiffness coefficient of SHS column face in bending component

Component	Reference	Stiffness coefficient
SHS in transverse compression - face failure in bending (upper beam flange level)	CIDECT	Referring to Section 4.1.2, the configuration is same as specimen B5; SHS column face in bending : $k_{32} = \frac{t_w^3}{14{,}4\beta L_{stiff}^2}\left(\frac{L_{stiff}^2}{bt_w}\right)^{1{,}25} \frac{\frac{c}{L_{stiff}} + \left(1-\frac{b}{L_{stiff}}\right)\tan\theta}{\left(1-\frac{b}{L_{stiff}}\right)^3 + \frac{10{,}4\left(k_1 - k_2\frac{b}{L_{stiff}}\right)}{\left(\frac{L_{stiff}}{t_w}\right)^2}}$ $L_{stiff} = L = b_c\text{-}t_c$ = 200-10 = 190 mm b = 145.2 mm, c = 25.2 mm, $\theta = 26^O$ k_{32} = 1.30 mm per bolt-row. SHS sidewall in compression : Same with Table 4.34; k_2 = 3.94 mm per bolt-row. SHS corner rotation : Same with Table 4.34; k = 1.82 mm per bolt-row. $k_{32,t} = [(1/1.30) + (1/3.94) + (1/1.82)]^{-1}$ = 0.63 mm including sidewall in compression and corner rotation.

Table 4.36. Stiffness coefficient of SHS column face in bending component with backing plate

Component	**Reference**	**Stiffness coefficient**
SHS in transverse compression - face with backing plate failure in bending	CIDECT KY	Referring to Table 4.35, SHS column face in bending : $L_{stiff} = L = b_c - t_c$ = 200-10 = 190 mm Additional to the b and c values defined in Section 4.1.2, load transfer path by dispersion at 45^O through the backing plate but limited with the edge. b = 175.2 mm, c = 52.8 mm, $\theta = 21^O$ k_{32} = 22.02 mm per bolt-row. SHS sidewall in compression : Same with Table 4.33; k_2 = 3.84 mm per bolt-row. SHS corner rotation : Same with Table 4.33; k = 3.22 mm per bolt-row. $k_{32,t,bp} = [(1/22.02) + (1/3.84) + (1/3.22)]^{-1}$ = 1.62 mm including sidewall in compression and corner rotation.

Table 4.37. Stiffness coefficient of t-stub in bending component

Component	Reference	Stiffness coefficient
T-stub in bending	EC	T-stub in bending : $k_6 = \frac{0{,}9 l_{eff}\, t_a^{\,3}}{m^3}$ As given in Section 4.3.2, e = 50 mm, m = 50 – 9/2 – 0.8 x 18 = 31.1 mm n = 1.25 x 31.1 = 38.9 mm, p = 60 mm min effective length of the t-stub: l_{eff} = 60 mm k_6 = 0.9 x 60 x 15^3 / 31.1^3 = 6.06 mm per bolt-row.

Table 4.38. Stiffness coefficient of SHS sidewall in compression at lower flange

Component	Reference	Stiffness coefficient
SHS column (sidewall) web in transverse compression (at lower beam flange)	EC KY CIDECT	SHS sidewall in compression: $k_2 = \frac{0{,}7\, b_{eff,c,wc}\, t_{wc}}{d_c}$ By using a similar calculation method with the resistance calculation given in Table 4.18; Load transfer by t-stub: b_i = 200 mm > b_0-2t_0 (180 mm) => sidewall crushing failure mode t_i = 2 x 0.6 r_t + 2 t_{ft} t_i = 2 x 0.6 x 18 + 2 x 15 = 51.6 mm b_{eff} = 2 t_i + 10t_0 = (2 x 51.6 + 10 x 10) = 203.2 mm d_c = b_c – 2r = 200 – 2x25 = 150 mm k_2 = 0.7 x 203.2 x 10 / 150 = 9.48 mm

Table 4.39. Stiffness coefficient of partial threaded studs in tension component

Component	Reference	Stiffness coefficient
Partial threaded studs in tension	EC	$k_{10} = 1{,}6 A_s / L_b$ L_b is the bolt elongation length, taken as equal to the grip length (total thickness of material and washers), plus half the sum of the height of the bolt head and the height of the nut. For the case L_b should include width of the hollow section. L_b = 200 + 15 + 2 x 4 + 13 = 236 mm k_{10} = 1.6 x 157 / 236 = 1.06 mm

Table 4.40. Stiffness coefficient of bolts in shear component

Component	Reference	Stiffness coefficient
Bolts in shear	EC	$k_{11} = \frac{16 n_b d^2 f_{ub}}{E d_{M16}}$ d_{M16} is the nominal diameter of an M16 bolt; n_b is the number of bolt-rows in shear. k_{11} = (16 x 3 x 16^2 x 800) / (210000 x 16) = 2.92 mm

Table 4.41. Stiffness coefficient of beam flange and t-stub web in bearing component

<table>
<tr><th>Component</th><th>Reference</th><th colspan="2">Stiffness coefficient</th></tr>
<tr><td rowspan="3">Plate in bearing</td><td rowspan="3">EC</td><td>$k_{12} = \frac{24 n_b k_b k_t d f_u}{E}$</td><td rowspan="2">$e_b$ is the distance from the bolt-row to the free edge of the plate in the direction of load transfer;
p_b is the spacing of the bolt-rows in the direction of load transfer;
n_b is the number of bolt-rows in shear.</td></tr>
<tr><td>$k_b = k_{b1}$
but $k_b \leq k_{b2}$
$k_{b1} = 0{,}25\, e_b / d + 0{,}5$
but $k_{b1} \leq 1{,}25$
$k_{b2} = 0{,}25\, p_b / d + 0{,}375$
but $k_{b2} \leq 1{,}25$
$k_t = 1{,}5\, t_j / d_{M16}$
but $k_t \leq 2{,}5$</td></tr>
<tr><td colspan="2">There are 3 bolt-rows.
<u>For beam flange</u>, t_j = 10.2 mm, f_u = 435
Bolt-row 1 (e_b = 20 mm, p_b = 42 mm, d = 16 mm):
k_{b1} = 0.81, k_{b2} = 1.03, k_t = 0.96
k_{12b1} = 24 x 3 x 0.81 x 0.96 x 16 x 435 / 210000 = 1.85 mm
Bolt-row 2 (e_b = 62 mm, p_b = 42 mm, d = 16 mm):
k_{b1} = 1.46, k_{b2} = 1.03, k_t = 0.96
k_{12b2} = 24 x 3 x 1.03 x 0.96 x 16 x 435 / 210000 = 2.35 mm
Bolt-row 3 (e_b = 104 mm, p_b = 42 mm, d = 16 mm):
k_{b1} = 2.13, k_{b2} = 1.03, k_t = 0.96
k_{12b3} = 24 x 3 x 1.03 x 0.96 x 16 x 435 / 210000 = 2.35 mm
<u>For t-stub</u>, t_j = 9 mm, f_u = 443
Bolt-row 1 (e_b = 30 mm, p_b = 42 mm, d = 16 mm):
k_{b1} = 0.96, k_{b2} = 1.03, k_t = 0.84
k_{12b1} = 24 x 3 x 0.96 x 0.84 x 16 x 443 / 210000 = 1.95 mm
Bolt-row 2 (e_b = 72 mm, p_b = 42 mm, d = 16 mm):
k_{b1} = 1.6, k_{b2} = 1.03, k_t = 0.84
k_{12b2} = 24 x 3 x 1.03 x 0.84 x 16 x 443 / 210000 = 2.09 mm
Bolt-row 3 (e_b = 114 mm, p_b = 42 mm, d = 16 mm):
k_{b1} = 1.6, k_{b2} = 1.03, k_t = 0.84
k_{12b3} = 24 x 3 x 1.03 x 0.84 x 16 x 443 / 210000 = 2.09 mm</td></tr>
</table>

4.3.5. Initial Design Stiffness of the Joint

According to Eurocode 3 part 1-8 [30], provided that the axial force in the connected member does not exceed 5% of the design resistance of its cross-section, the rotational stiffness S_j of a beam-to-column joint, for a moment M_e less than the design moment resistance $M_{j,Rd}$ of the joint, may be obtained with sufficient accuracy from Equation (4.6) where k_i is the stiffness coefficient for basic joint component i, z is the lever arm and μ is the stiffness ratio $S_{j,ini} / S_j$. Note that the initial rotational stiffness $S_{j,ini}$ of the joint is given by expression with $\mu = 1.0$.

$$S_j = \frac{Ez^2}{\mu \sum_i \frac{1}{k_i}} \tag{4.6}$$

In the studied joint, two bolt rows are in tension. Therefore k_{eq} should be calculated from column web in compression (k_3), column face in bending (k_4 or k_{32}), t-stub in bending (k_6) and bolts in tension (k_{10}). According to simplified method [22] each of these modified values should be taken as twice the corresponding value for a single bolt row of the t-stub. Two k_{11} coefficients (one for each flange, so top and bottom) and four k_{12} coefficients (one for each top and bottom beam flange and one for each top and bottom t-stub and each bolt rows in bearing) have to be considered. For the case summation of the stiffness coefficients can be written as in Equation (4.7) and Equation (4.8) for Model 1 and Model 2 solutions respectively.

$$\sum_i \frac{1}{k_i} = \frac{1}{k_1} + \frac{1}{k_2} + \frac{1}{2k_3} + \frac{1}{2k_{32}} + \frac{1}{2k_6} + \frac{1}{2k_{10}} + \frac{1}{k_{11top}} + \frac{1}{k_{12top}} + \frac{1}{k_{11bottom}} + \frac{1}{k_{12bottom}} \tag{4.7}$$

$$\sum_i \frac{1}{k_i} = \frac{1}{k_1} + \frac{1}{k_2} + \frac{1}{2k_3} + \frac{1}{2k_4} + \frac{1}{2k_6} + \frac{1}{2k_{10}} + \frac{1}{k_{11top}} + \frac{1}{k_{12top}} + \frac{1}{k_{11bottom}} + \frac{1}{k_{12bottom}} \tag{4.8}$$

According to the equation above, the initial stiffness value of the specimen T1M is calculated as 2026.8 kNm/rad and 2112.4 kNm/rad by Model 1 and Model 2 respectively

and the initial stiffness value of the specimen T2M is calculated as 2156.5 kNm/rad by both Model 1 and Model 2.

4.3.6. Rotation capacity of the Joint

According to Eurocode 3 part 1-8 [22], a joint with either a bolted end-plate or angle flange cleat connection may be assumed to have sufficient rotation capacity for plastic analysis, provided that both of the following conditions are satisfied:

a) the design moment resistance of the joint is governed by the design resistance of either the column flange in bending or the beam end-plate or tension flange cleat in bending.

b) the thickness t of either the column flange or the beam end-plate or tension flange cleat (not necessarily the same basic component as in (a)) less than or equal to $0.36d\sqrt{(f_{ub}/f_y)}$ where f_y is the yield strength of the relevant component and f_{ub} is the tensile strength of the bolt.

Since in the studied joint t-stub governed the design of the moment resistance and wall thickness of SHS (10 mm) is less than 10.2 mm, it can assumed that the studied joint has sufficient rotation capacity for plastic analysis.

4.3.7. Comparison of the Joint Model with the Test Results

Bilinear model described in Eurocode 3 part 1-8 [22] is used to draw calculated moment rotation of the joint. According the model, after elastic moment level, the initial stiffness is reduced to its half until plastic moment capacity of the joint. The comparison of the model with the test result T1M and T2M are given respectively in Figure 4.17 and Figure 4.18. In two different models, the only difference is the calculation approach of the column face in bending component. Thus other components remained same. The minimum

component resistances of both models are mainly by SHS column face in bending except for the specimen T2M of Model 1 which is by t-stub in bending. Both models did not reach to peak moment capacity because the joint is assumed to be yielded elasto-plasticly as soon as the first component yields in bilinear modeling approach. However if model proceeds step by step with the next yielding point by eliminating the yielded components, peak moment resistance would be achieved considering the resistance levels of the other components. On the other hand the stiffness approach is also different but gives very close stiffness coefficient values. As a result both models give almost the same moment-rotation trend and conservatively lower estimate comparing with test results of the specimens. The main reason of this is that the stiffness is mainly governed by flange and t-stub bearing components in the models. The related bolts were snug-tightened. In order to improve the model, the stiffness coefficients with related component stiffness of the test results can be compared.

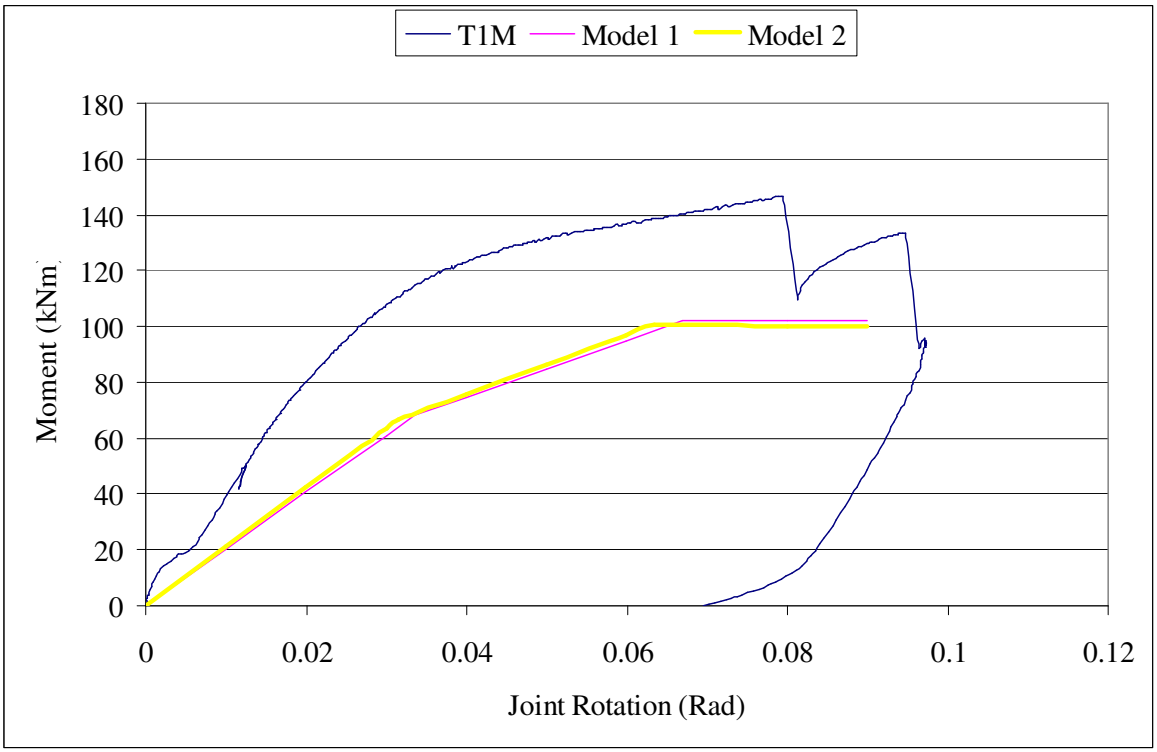

Figure 4.17. Comparison of mechanical models with test result of T1M

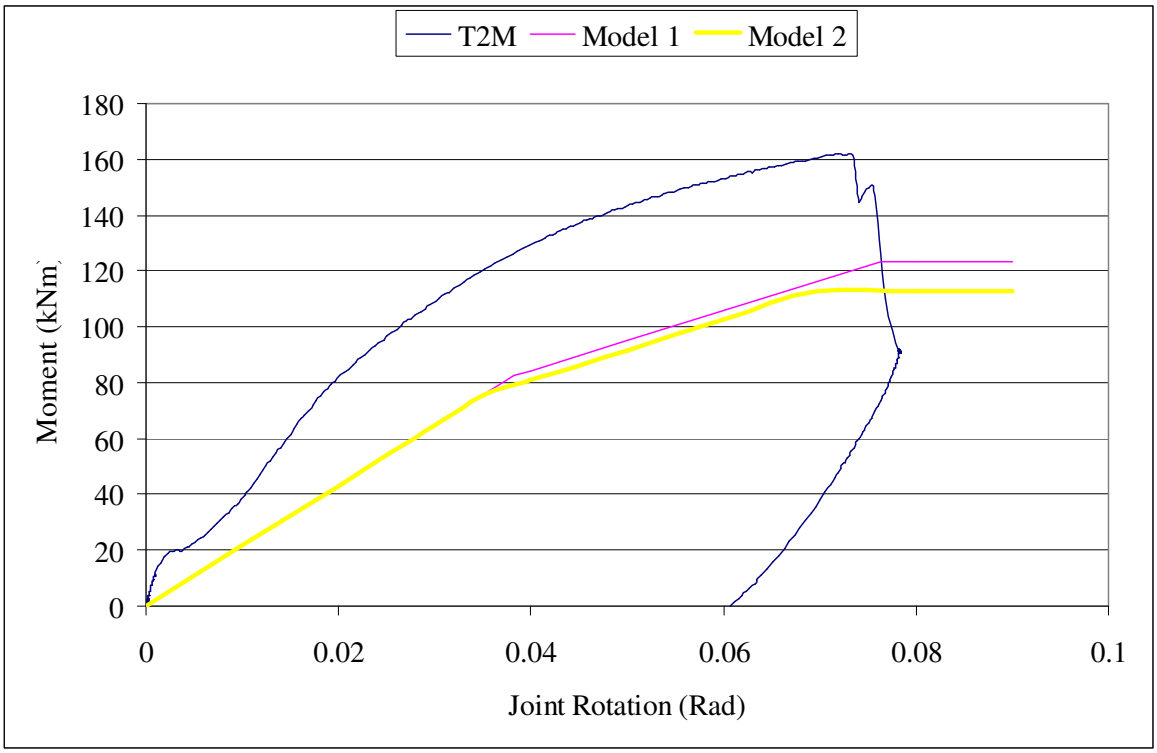

Figure 4.18. Comparison of mechanical models with test result of T2M

Based on the test results of the specimen T1M and T2M given in Section 3.2, the SHS column face stiffness level is 23768 and 33715 kNm/rad. This corresponds to stiffness coefficient of 1.44 mm and 2.05 mm ($k=K/Ez^2$, where z is the lever arm and E is the modulus of elasticity). The stiffness coefficients calculated by Model 1 are slightly lower for T1M but higher for T2M. On the other hand Model 2 predicts influence of the backing plate very close to the test results, but overestimates stiffness levels of both T1M and T2M by about 50%.

In both models stiffness coefficients of t-stub in bending and SHS column web in shear components are same and calculated according to Eurocode 3 part 1-8. Based on the test results average stiffness coefficient of t-stub in bending component can be calculated as 1.71 mm which is about 30% of the prediction of the models. The models estimate the stiffness coefficient of SHS column web in shear component as 4.9 mm which is approximately twice the average test results. (2.31 mm)

The bolts connecting t-stub to the beam flange were snug-tightened (approximately 30% preloaded). That's why at the very initial stage of the tests, the specimens behaved stiffer until slip resistance level achieved. Under these conditions, plate bearing and bolts in shear components have to be taken into account in stiffness calculations according to Eurocode 3 part 1-8. The models underestimate the total bearing and bolt shear stiffness coefficients as 0.22 mm which is 30% of the average test results. (0.70 mm) This stiffness coefficient builds a weakest link in the stiffness calculation of the models and governs. The very initial stage of the tests until slip resistance level can be modeled by assuming preloaded case in stiffness calculations. In this case stiffness coefficients of plate bearing and bolt in shear components are taken infinity. Accordingly, initial stiffness values of Model 1 and Model 2 are 9862 kNm/rad and 12280 kNm/rad respectively for T1M and 13947 (same by both models) for T2M. The predictions overestimate the stiffness more than 35% for T1M, on the other hand are very close to test results of T2M.(7141 kNm/rad for T1M and 13771 kNm/rad for T2M) The comparisons of moment rotation behaviours are given in Figure 4.19 and Figure 4.20.

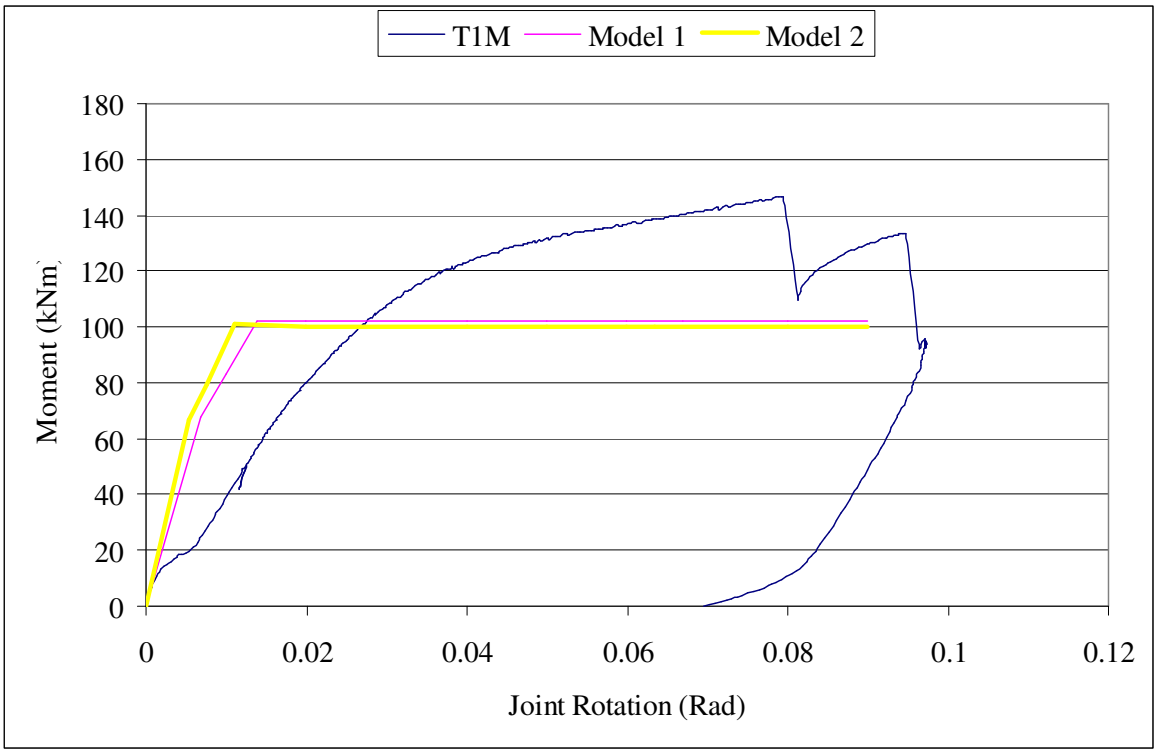

Figure 4.19. Comparison of mechanical models (preloaded bolts) with test result of T1M

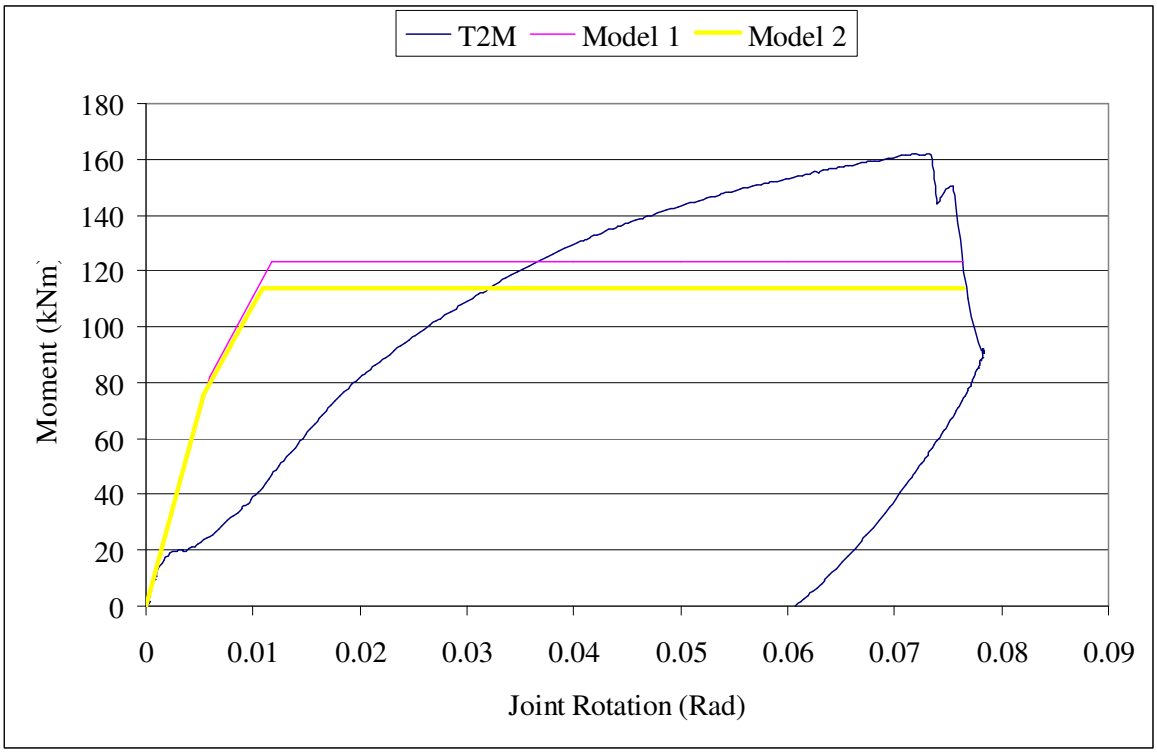

Figure 4.20. Comparison of mechanical models (preloaded bolts) with test result of T2M

5. CONCLUSIONS

Advantages of these bolted connections over welded connections lie in the fact that brittle fracture can be avoided by using sufficiently tough material for the beams, splice plates and diaphragms. The beam flanges at the bolted connections sustained plastic deformation largely in a plane stress state, suggesting that the flanges would fail by plastic instability rather than brittle fracture. Additionally, no welded joints exist at the stub-beam ends where the beam moments become highest. Thus, the demand for skilled welding is less for the new bolted connections. Further the cyclic behaviour of the bolted connections shows a pinched form because bolts slip. However, the hysteresis loops show significant hardening envelopes after the bolts slip into bearing until very large rotation of the joint is achieved. That's why it is easy to achieve a cumulative plastic deformation factor greater than 100 for these type of connections, examples of which are drastically improved over conventional welded ones.

Even all specimens reached beam plastic load level, this took place under high deformation levels. Besides reversed cyclic tests showed that the studied connections behaved in a manner suitable for use as either pinned or semirigid partial strength connections for simply designed braced steel frames in seismic areas or for unbraced steel frames in less seismic areas.

Reinforcing the hollow section column rear face by backing plate has provided an increase of strength and initial stiffness but a reduction of energy dissipation capacity of the joint.

The desired failure mechanism of such a joint is first to have a failure in component strength hierarchy. For this joint type, it was proved that this could be under controlled by the designer. However considering the cyclic performance, the desired failure should be such that the hollow section column face would participate more in energy dissipation of the joint. This can only be possible by the deformation of the face in both inward and outward directions during cycles. Although energy dissipation capacity of the joint was acceptable, it was mainly governed by deformability of the t-stub. Column face only acted

at the first cycles of the group cycles when the specimen was loaded to the next displacement step. Reinforcing the holes of the partially threaded studs with tubes passing through the hollow section might be effective to make column face to participate by resisting at the other group cycles. Increasing the thickness of the SHS column or by adding concrete inside the SHS column which prevents column face deformation towards inside can also improve the strength of the joint but not much the energy dissipation capacity as energy is dissipated mainly at the t-stub. By using much stronger t-stub (thicker t-stub flange), much stiffer joint can be designed with more energy dissipation capacity.

Almost all specimens of phase I, exhibited elasto-plastic behaviour although it is expected to have higher post-limit stiffness based on the available literature. This might be related to the loading condition. The load is applied on the SHS face towards inside which creates a stability problem.

There is good agreement between the test results and the proposed models in resistance point of view. However the stiffness predictions are not satisfactorily well.

According to the definition in FEMA 355D [29], the first plastic rotation is the plastic rotation which can be achieved with a given yield mechanism and connection type without a sudden loss in resistance or deterioration in the behavior of the connection. The second plastic rotation, is the plastic rotation at which the connection is expected to lose its capacity to support gravity loads. This second plastic rotation is more often based upon judgment and extrapolation of experimental results, since few experiments were conducted having deformations of the magnitude required for this level of behavior. Based on the performed cyclic tests first and second plastic rotation levels can be respectively 0.1 rad (same for both) for T1C; and 0.06 rad and 0.085 rad for T2C.

6. RECOMMENDATIONS FOR FUTURE WORK

Considering the cyclic performance, in order hollow section face to participate in energy dissipation, the deformation of the face in both inward and outward directions during cycles has to be maintained. If this action is provided by additional simple fittings, the cyclic performance of this type of joint shall be improved. This can be achieved by reinforcing column face by placing tubes through the hollow section and passing the partially threaded stud inside the tubes. In the present study, a model based on limited number of tests has been given to support this idea. In order to check its effectiveness, following a finite element model further experimental tee joint cyclic tests could be done.

The mechanical model, which was proposed in this research, was adapted by using limited number of test results. This model could be generalized by considering the available test results in the literature and additional analytical, numerical and/or experimental studies. Further by using other hollow sections in different dimensions as a parameter the study could be enhanced. The dimensions of this reinforcing backing plate is also important to study extensively because it is directly in relation with deformability of the column rear face. The effect of axial loading is not a parameter in this study. However the stability of the tubular column under compressive stresses might be influenced due to these plastic deformations that take at the hollow section column face.

There is still missing design knowledge to mechanically model this type of bolted connections connecting I beams to hollow sections. For example further research is needed to define stiffness of the sidewall in compression or tension component. There is also very limited research on the deformability and stiffness levels of the components to put in the design.

Corners of the rectangular and square hollow sections are round. That’s why it should not be considered that much stiff as modeled in several researches. Roundness of the corners influences the location of the yield line and the length of the stiffness, thus influences the design while modeling the joint.

APPENDIX A: EVALUATION OF DISPLACEMENTS OF PHASE I – COMPONENT TESTS

As given in Figure A.1, the deformation of face has been measured at the alignment of the bolts which were at the corners by Ch 20 to Ch 23. The displacement of the hydrolic press has also been measured by Ch 24. As given in Equation (A.1), the average of these five reading gives the face displacement.

$$\delta_{face} = \frac{[Ch20] + [Ch21] + [Ch22] + [Ch23] + [Ch24]_{net}}{5} \tag{A.1}$$

where,

$$[ch24]_{net} = [ch24] - \delta_{plate} \tag{A.2}$$

Deformations at the rigid plate are calculated by the Equation (A.3) according to Figure A.2.

$$\delta_{plate} = \frac{\frac{[ch8] \times a_2}{a_1 + a_2} + \frac{[ch9] \times a_3}{a_3 + a_4}}{2} \tag{A.3}$$

Relative horizontal and vertical displacements of the corners are much smaller compared to the face deformation. By neglecting the corner displacements, the displacement due to rotation of the corner can be calculated from the related measurement presented in Figure A.1 as given in Equation (A.4). The values of b1 and b4 are defined in Section 2.3.3.

$$\delta_{corner} = \frac{[ch15] + [ch16] + [ch17]_{net} + [c18]_{net}}{4} \tag{A.4}$$

where

$$[Ch17]_{net} = [Ch17] - \delta_{sidewall} - \delta_{plate} - \delta_{face} \cdot \frac{b_{[ch17]}}{b_4} \tag{A.5}$$

$$[Ch18]_{net} = [Ch18] - \delta_{sidewall} - \delta_{plate} - \delta_{face} \cdot \frac{b_{[ch18]}}{b_1} \tag{A.6}$$

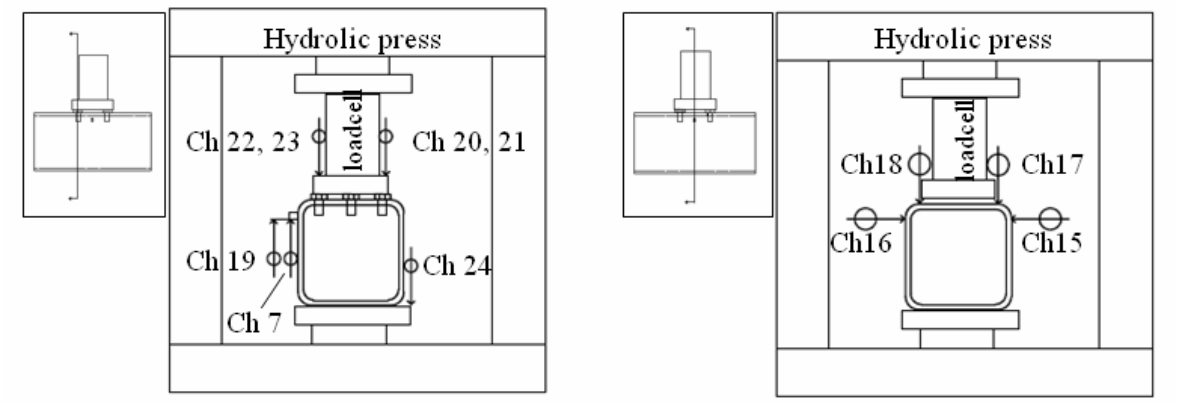

Figure A.1. Measurement of the face and corner deformations

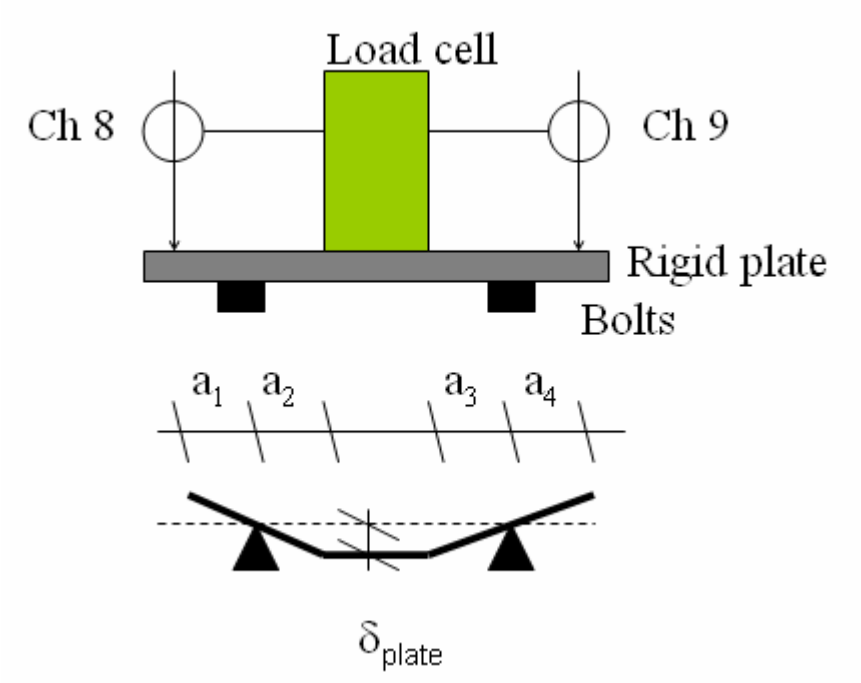

Figure A.2. Measurement of the rigid plate deformation

According to the geometry shown in Figure A.3, sidewall displacement is calculated as follows:

$$\theta = \frac{[ch19]-[ch7]}{d_{7,19}} \tag{A.7}$$

$$x' = x.\cos\theta \quad \text{and} \quad y' = \sqrt{y^2 - (x.\sin\theta)^2} \tag{A.8}$$

$$\delta_{Sidewall} = 200 - x' - y' \tag{A.9}$$

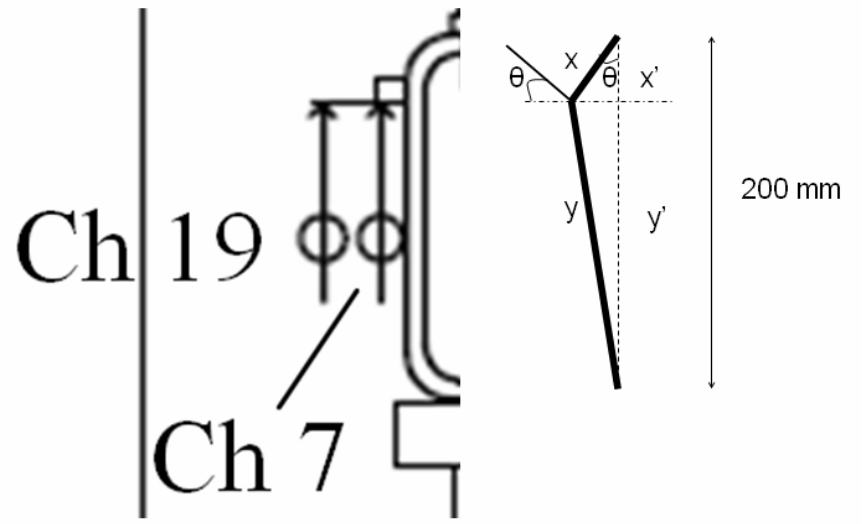

Figure A.3. Measurement of sidewall displacement

APPENDIX B: EVALUATION OF DISPLACEMENTS AND STRAINS OF PHASE II – SUBASSEMBLAGE TEST

In view to compute the rotation of the beam, of the column, and of the joint and connection components totally 22 measurements have been made. The channel numbering is given in Figures B.1 and B.2. Formulation of the measurements is presented in Tables B.1 to B.3.

Two displacement measurements (Ch2 and Ch3) have been taken at the level of loading. Support settlements are followed by Ch 5, Ch 15 and Ch 24. Necessary corrections have been done related to these settlements. Dial gauges Ch 6 and Ch 12 on the column flange have been located symmetrically to the axis of this column. In order to measure the flexural rotation of the column Ch7, Ch11, Ch17 and Ch20 have been used. Their spacing was as large allowed by the beam depth. Ch 4 and Ch 8 have been located inside the web as close as possible to the connection.

The measurements of the rotation resulting from the slip at the interface between the t-stub and the beam flange have been made by measuring the relative displacement between two points (Ch 16 and Ch 19) located at, respectively on the t-stub and on the both flanges of the beam.

Deformation of the column face has been measured by Ch 13 and Ch 14 which were located symmetrically to the axis of this column and point at the geometrical center of the bolt holes locations. This measurement includes load introduction which is deformation due to compression of the sidewall. The deformation of the t-stub including elongation of the partially threaded studs and deformation of the column face has been measured by Ch 22 and Ch23.

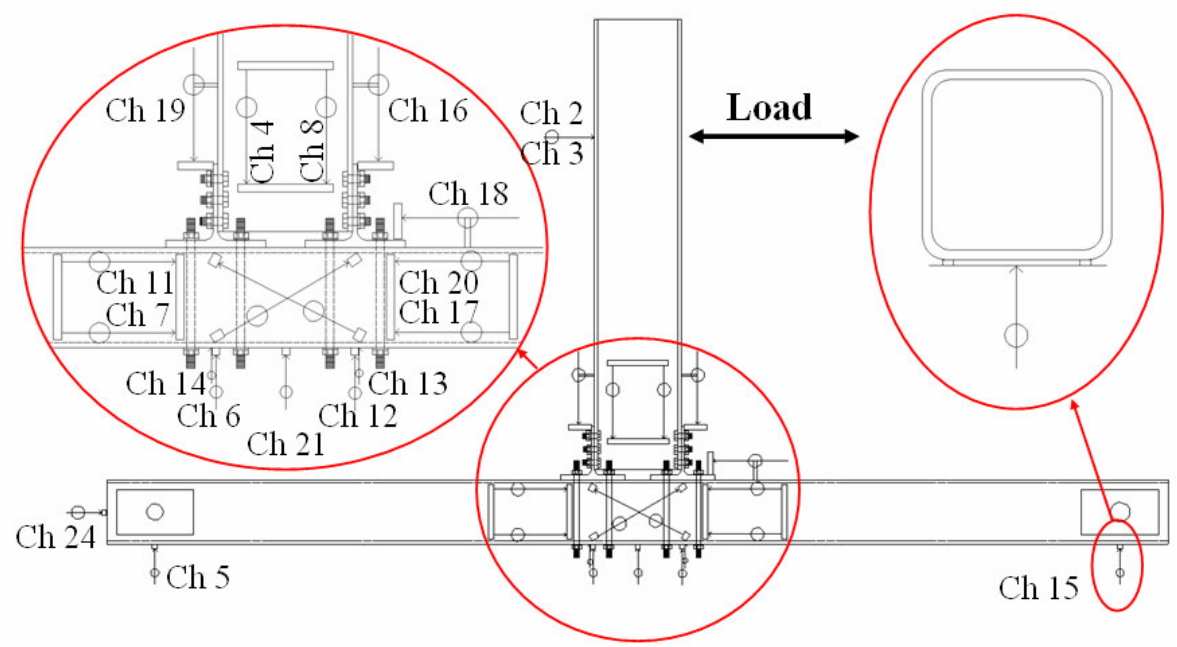

Figure B.1. Instrumentation of the specimen

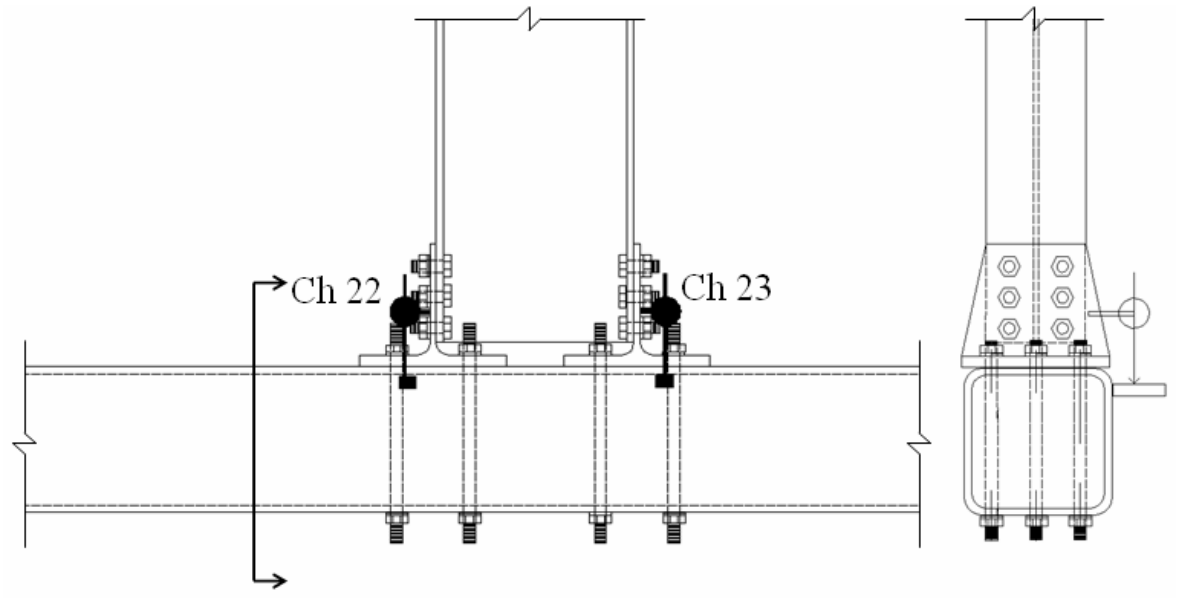

Figure B.2. Instrumentation of the specimen – t-stub

Table B.1. Formulas to measure components of joint deformability

	Rotations	Formulas
Components of Joint deformability	Joint rotation	$\phi = \dfrac{\dfrac{[ch2]+[ch3]}{2} - [ch24] - [ch5 - ch15] \times \dfrac{L_b}{L_c}}{L_b}$
	Shear deformation	$\gamma = \theta_c - \dfrac{\theta_{fwest} + \theta_{feast}}{2}$ $\theta_c = \dfrac{[ch6]_{net} - [ch12]_{net}}{d_{6,12}}$ $\gamma = \dfrac{[ch6]_{net} - [ch12]_{nst}}{d_{6,12}} - \dfrac{\dfrac{[ch7]-[ch11]}{d_{7,11}} + \dfrac{[ch17]-[ch20]}{d_{17,20}}}{2}$ Shear strains: $\gamma_{xy} = 2\varepsilon_{45^o} - (\varepsilon_{0^o} + \varepsilon_{90^o})$
	Connection Rotation	$\phi = \theta + \gamma \Rightarrow \theta = \phi - \gamma$

Table B.2. Formulas to measure components of connection deformability

	Rotations	Formulas
Components of Connection deformability	Slips at beam face	$\theta_{sb} = \dfrac{[ch19]-[ch16]}{d_{16,19}} - \dfrac{[ch8]-[ch4]}{d_{4,8}}$
	Slips at column face	$\theta_{sc} = \dfrac{[ch18]}{L_b}$
	Deformations of column face inluding load introduction	$\theta_{face} = \dfrac{[ch14]_{net} - [ch13]_{net}}{d_{13,14}} - \theta_c$
	Deformations of t-stub including bolt elangation	$\theta_{tstub} = \dfrac{[ch22] - [ch23]}{d_{22,23}} - \theta_{face}$

Table B.3. Formulas to eliminate support settlements

Dial gauge corrections by eliminating support settlements	$$[ch12]_{net} = [ch12] - \left([ch21] - \frac{[ch21] - [ch15]}{L_{c/2}} \times d_{12,21} \right)$$ $$[ch6]_{net} = [ch6] - \left([ch21] - \frac{[ch21] - [ch15]}{L_{c/2}} \times d_{6,21} \right)$$ $$[ch13]_{net} = [ch13] - \left([ch21] - \frac{[ch21] - [ch15]}{L_{c/2}} \times d_{13,21} \right)$$ $$[ch14]_{net} = [ch14] - \left([ch21] - \frac{[ch21] - [ch15]}{L_{c/2}} \times d_{14,21} \right)$$

APPENDIX C: PHOTOGRAPHIC VIEW OF TEST SET-UP AND SPECIMENS BEFORE, DURING AND AFTER TESTING

Figure C.1. Fabrication of the specimens

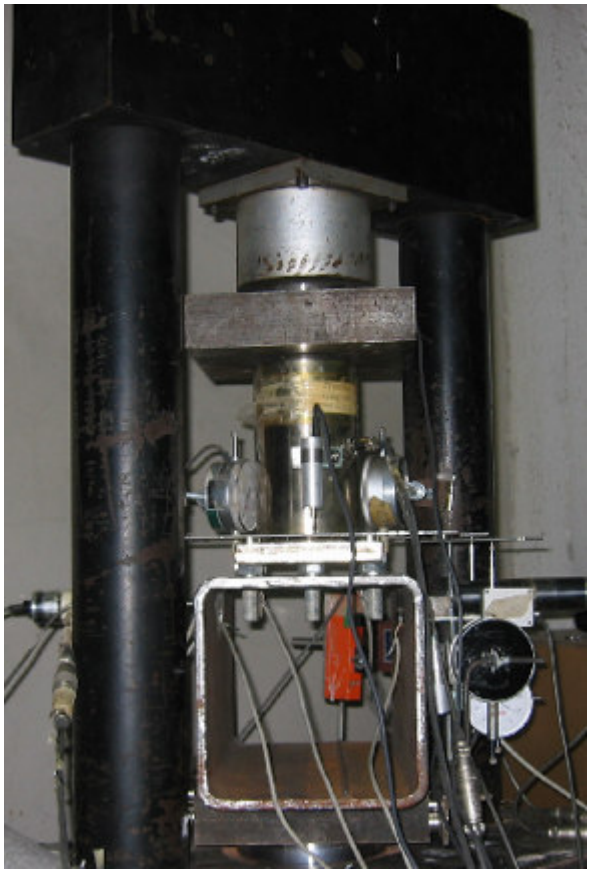

Figure C.2. Test setup of phase I – component tests

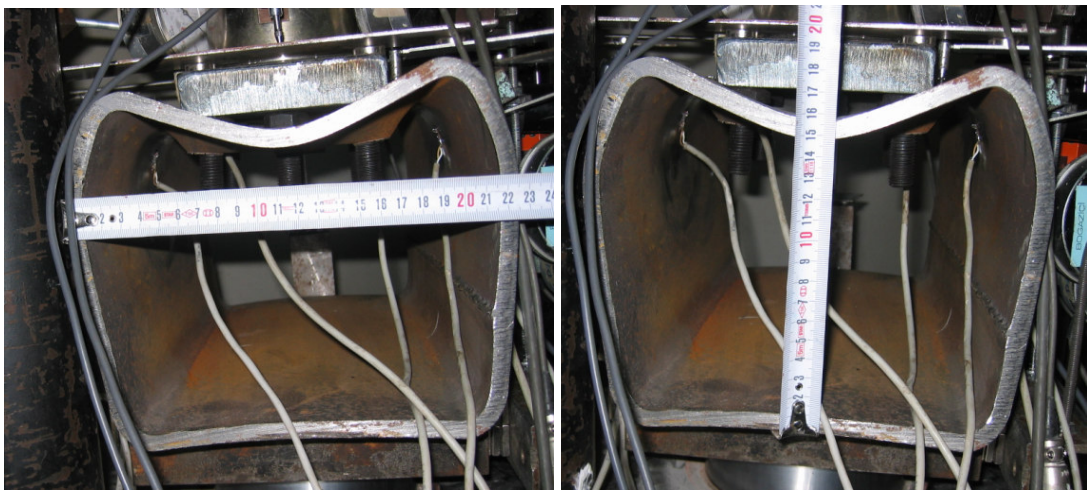

Figure C.3. Deformations after test of specimen B1 – test#2

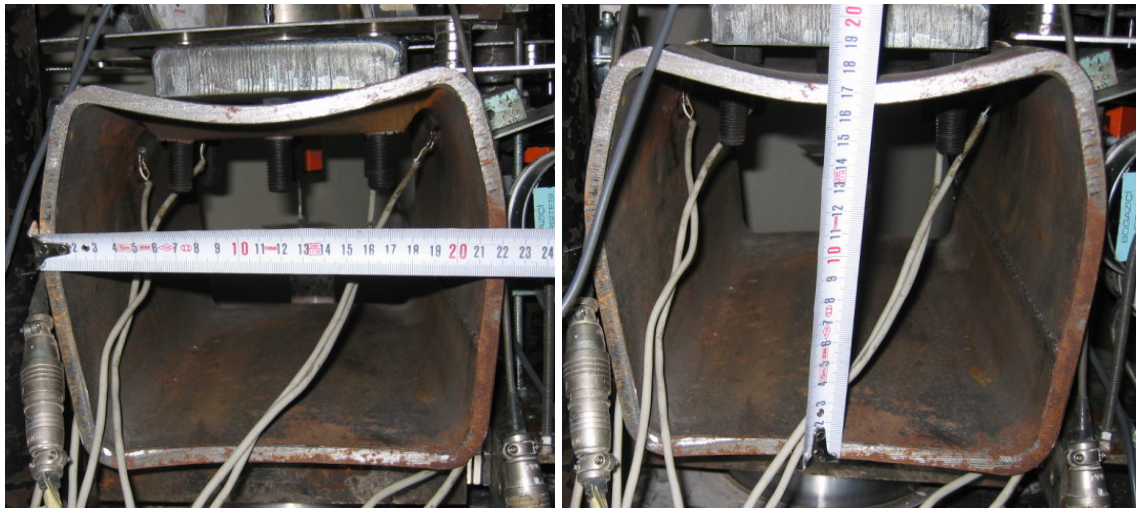

Figure C.4. Deformations after test of specimen B2 – test#1

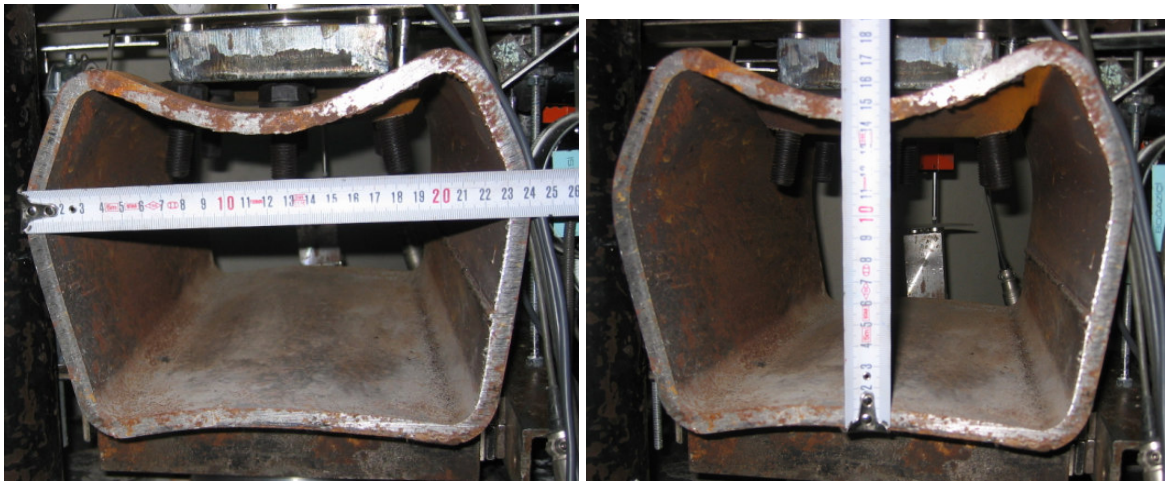

Figure C.5. Deformations after test of specimen B2 – test#2

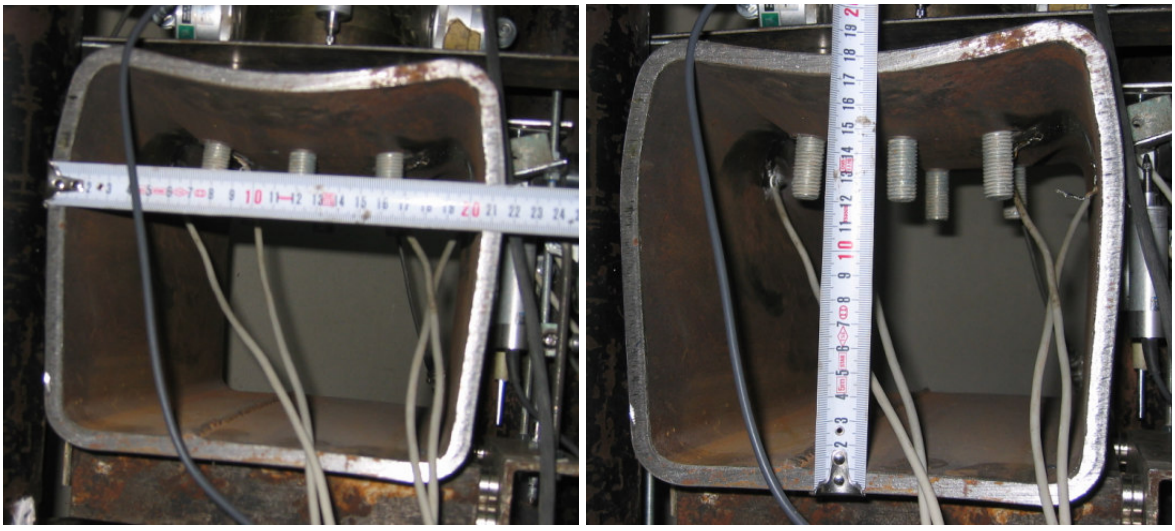

Figure C.6. Deformations after test of specimen B3 – test#1

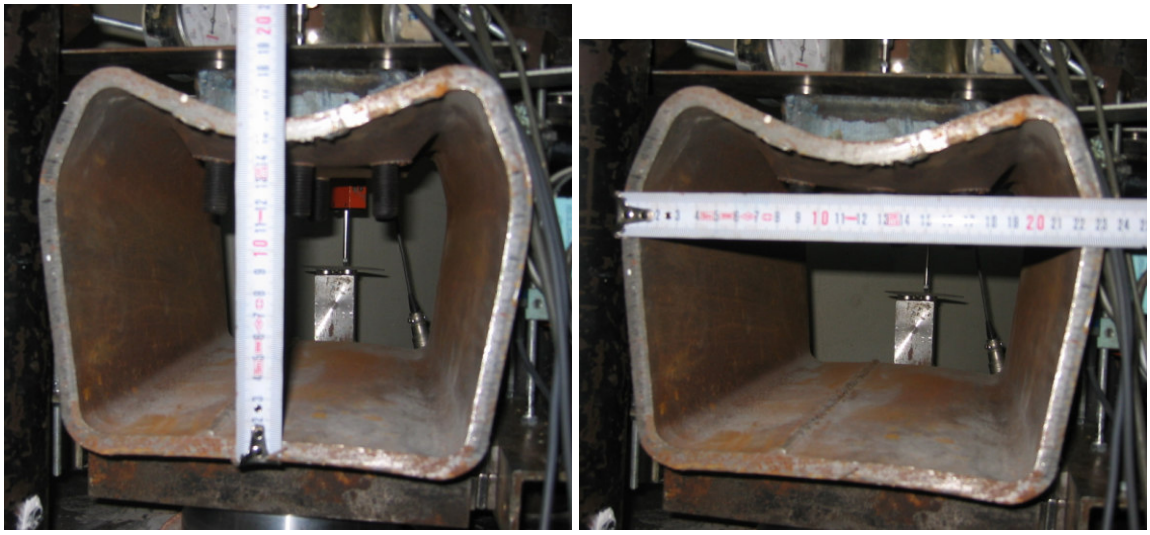

Figure C.7. Deformations after test of specimen B3 – test#2

Figure C.8. Deformations after test of specimen B4 – test#1

Figure C.9. Deformations after test of specimen B4 – test#2

Figure C.10. Deformations after test of specimen B5 – test#1

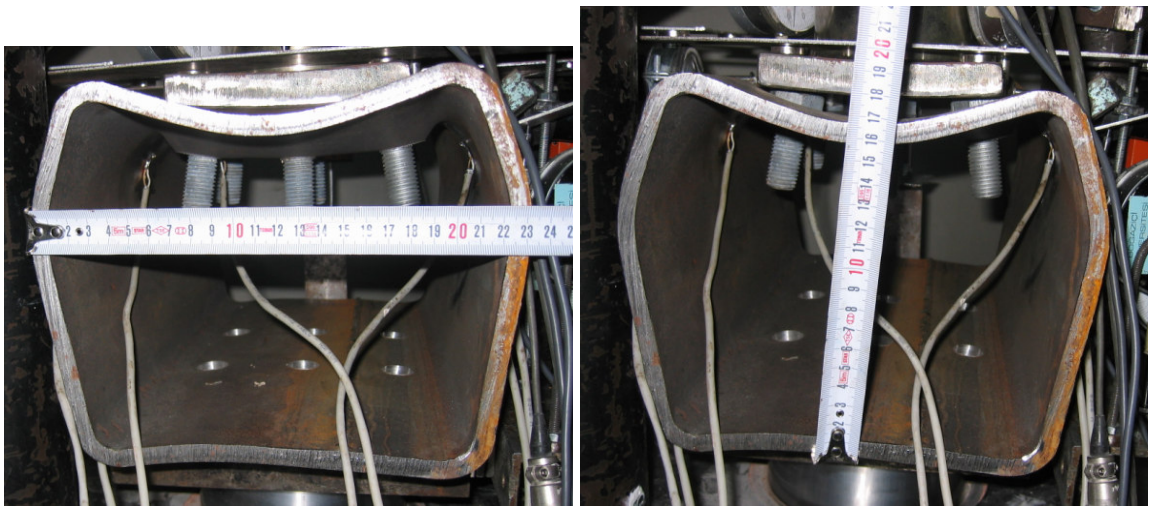

Figure C.11. Deformations after test of specimen B5 – test#2

Figure C.12. Deformations after test of specimen P1 – test#1

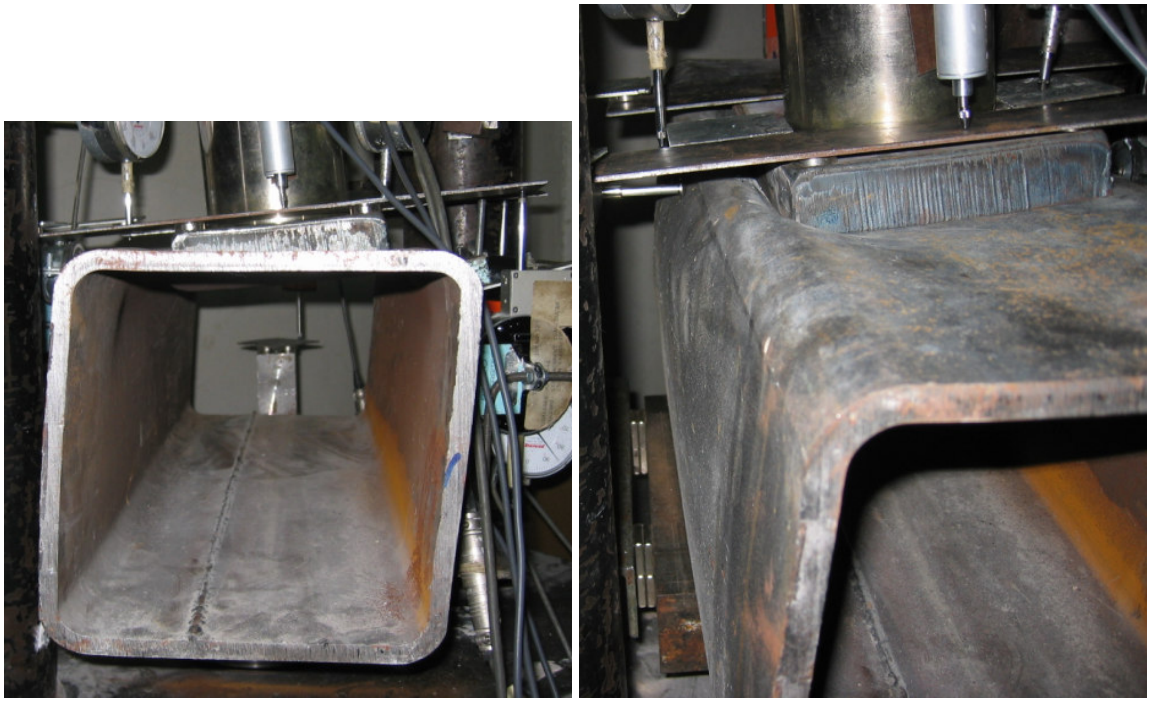

Figure C.13. Deformations after test of specimen P1 – test#2

Figure C.14. Deformations after test of specimen P2 – test#2

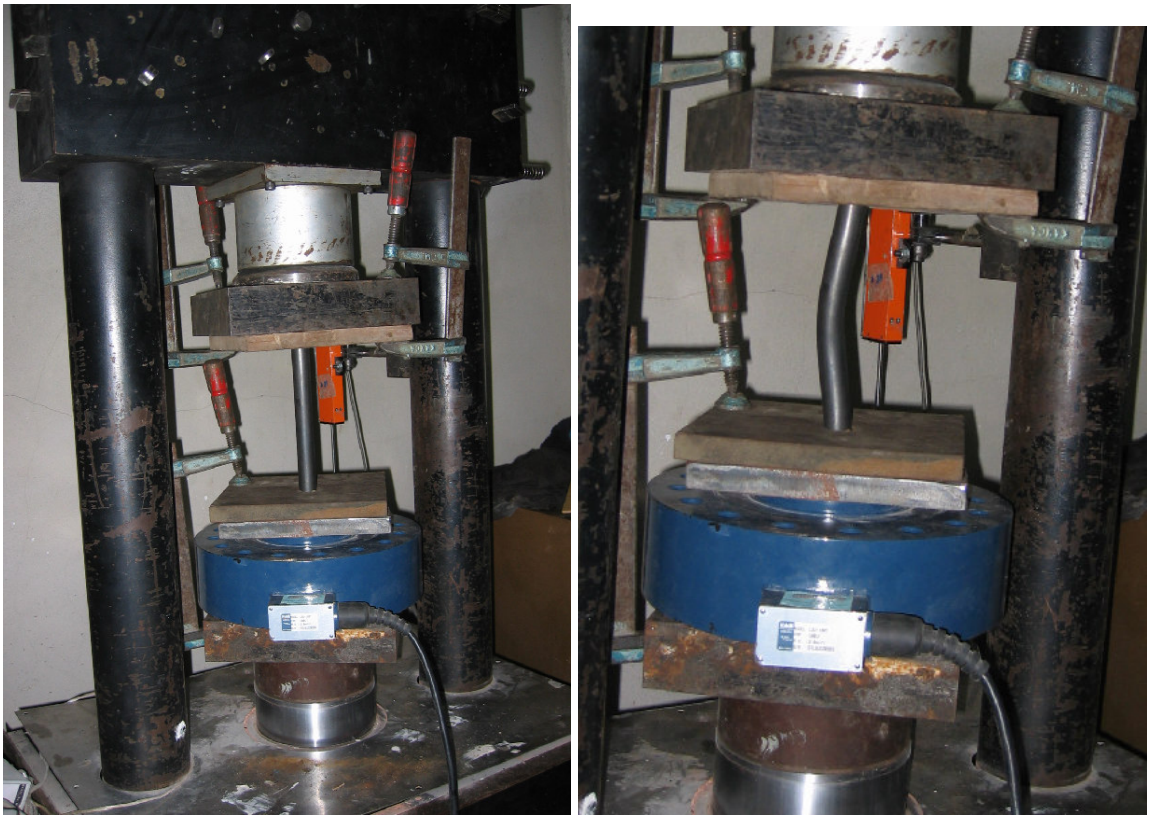

Figure C.15. Test set-up and deformations after test of specimen tubes

Figure C.16. Test set-up of T-type of specimens

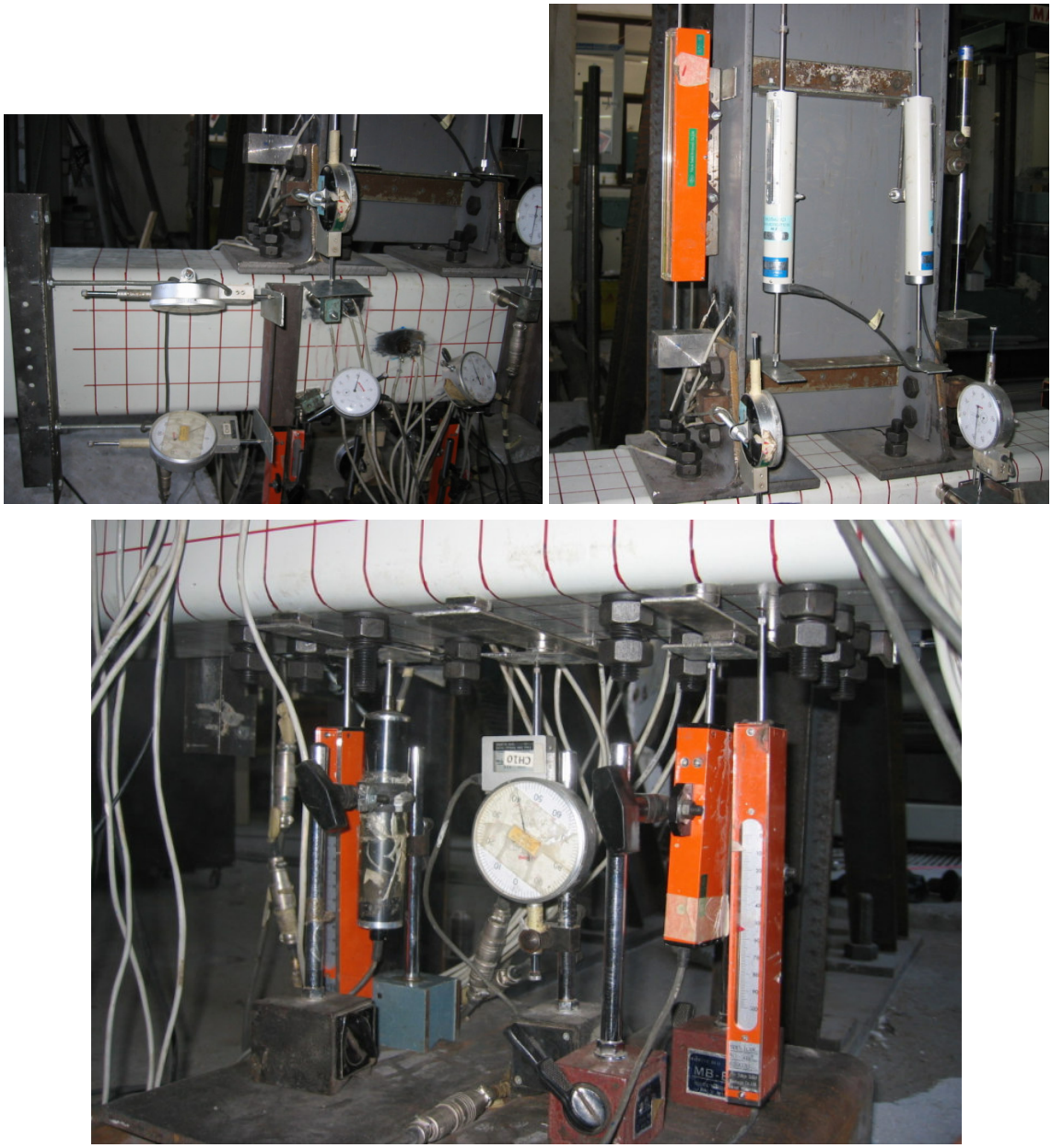

Figure C.17. Instrumentation of T-type of specimens

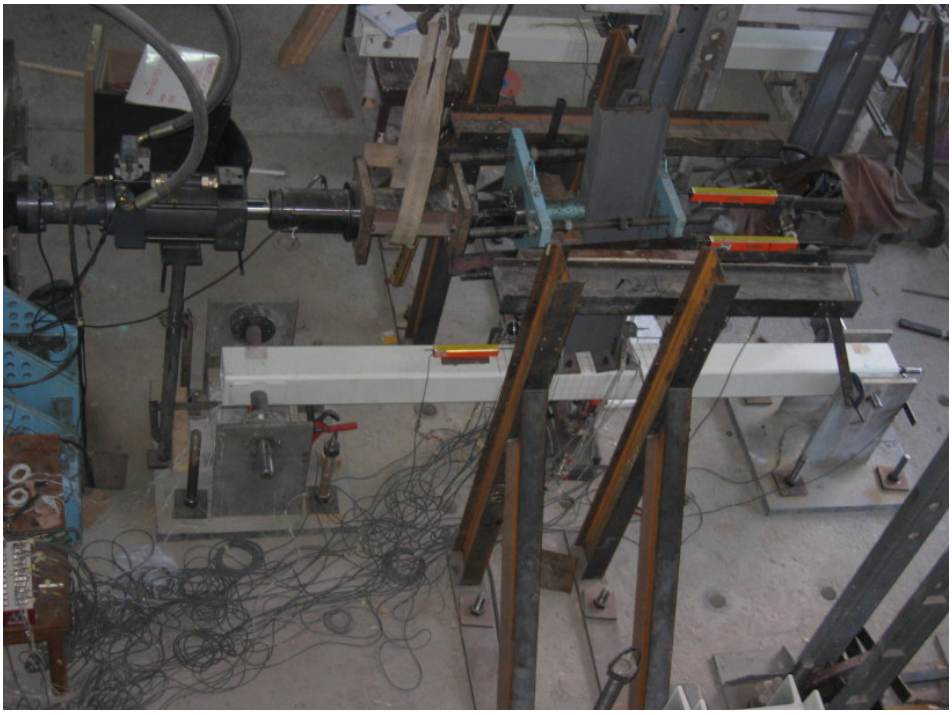

Figure C.18. Deformations after test of specimen T1M

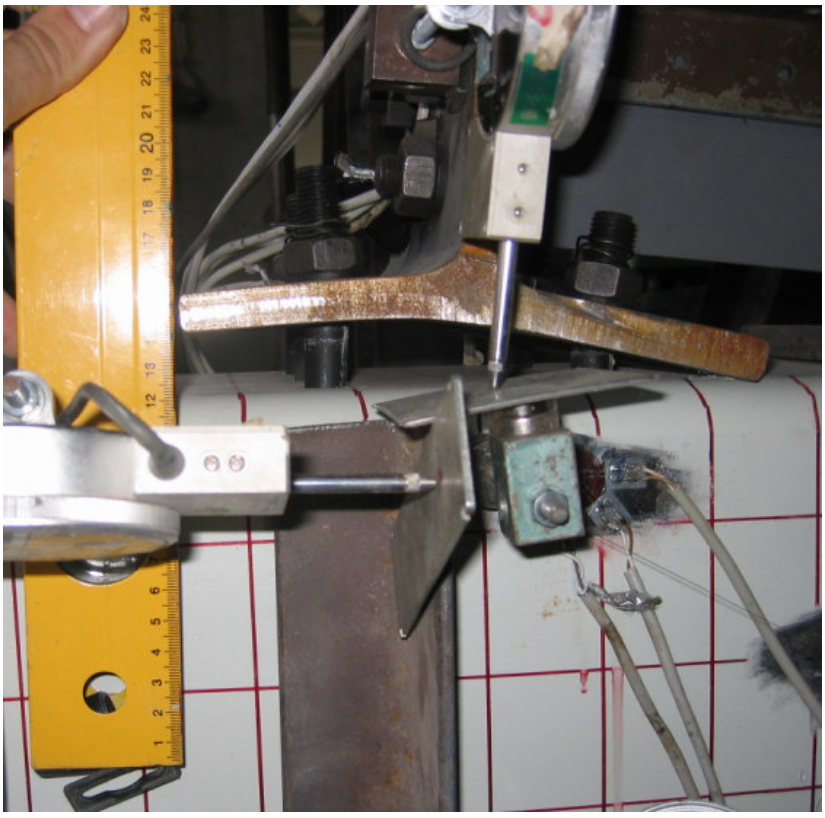

Figure C.19. Deformations after test of specimen T1M

Figure C.20. Deformations after test of specimen T1M

Figure C.21. Deformations after test of specimen T1M

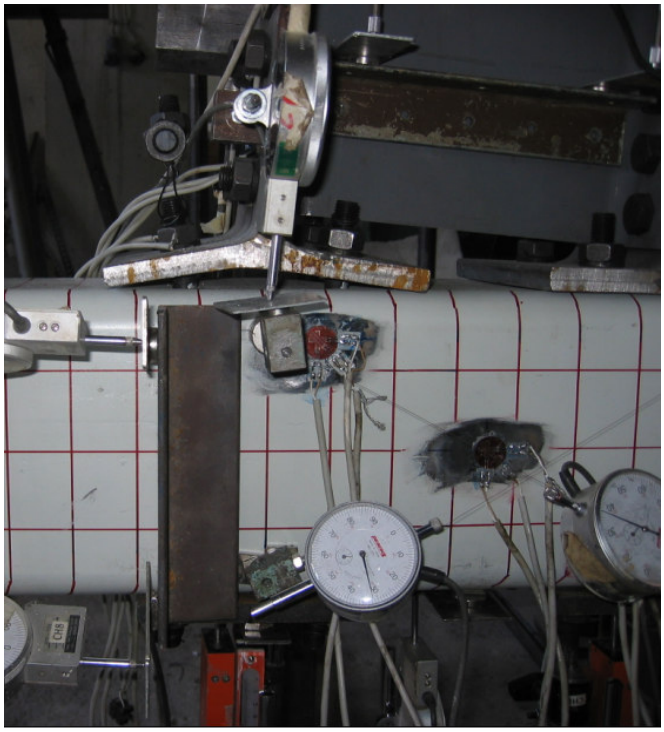

Figure C.22. Deformations after test of specimen T2M

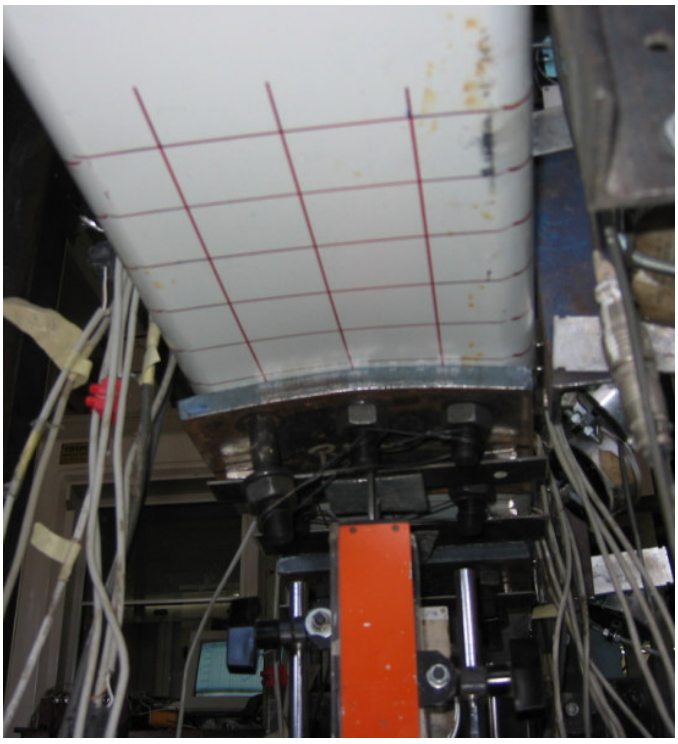

Figure C.23. Deformations after test of specimen T2M

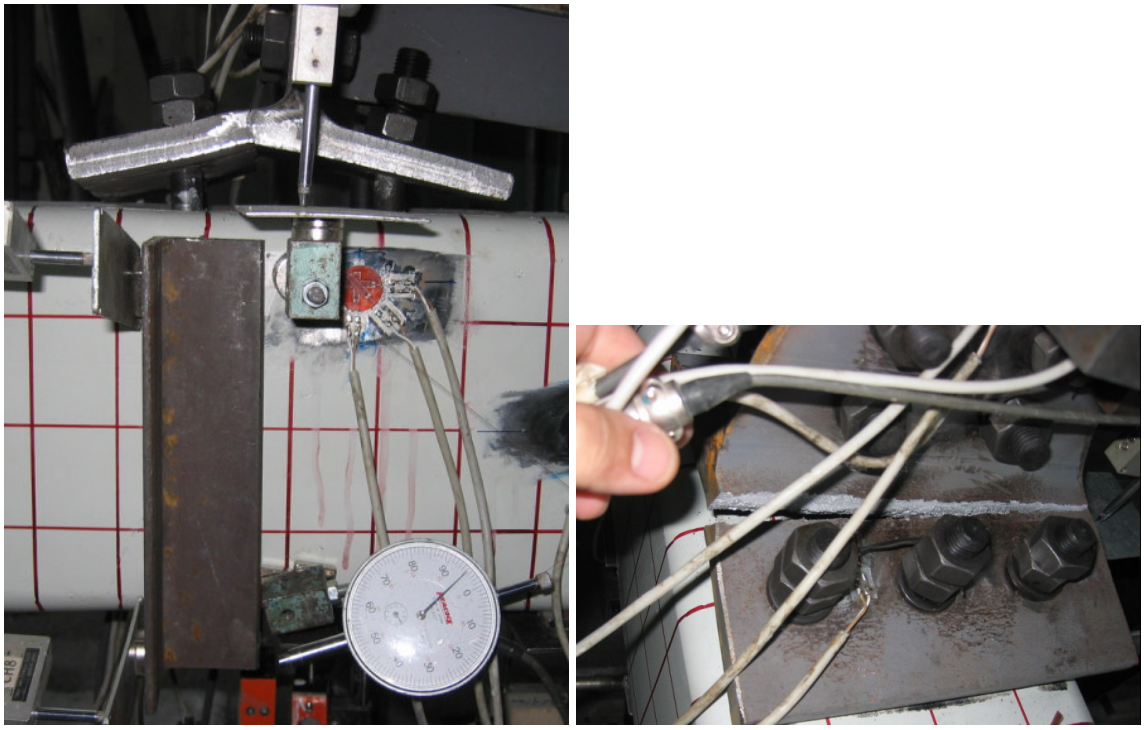

Figure C.24. Failure of the t-stub stem of specimen T1C

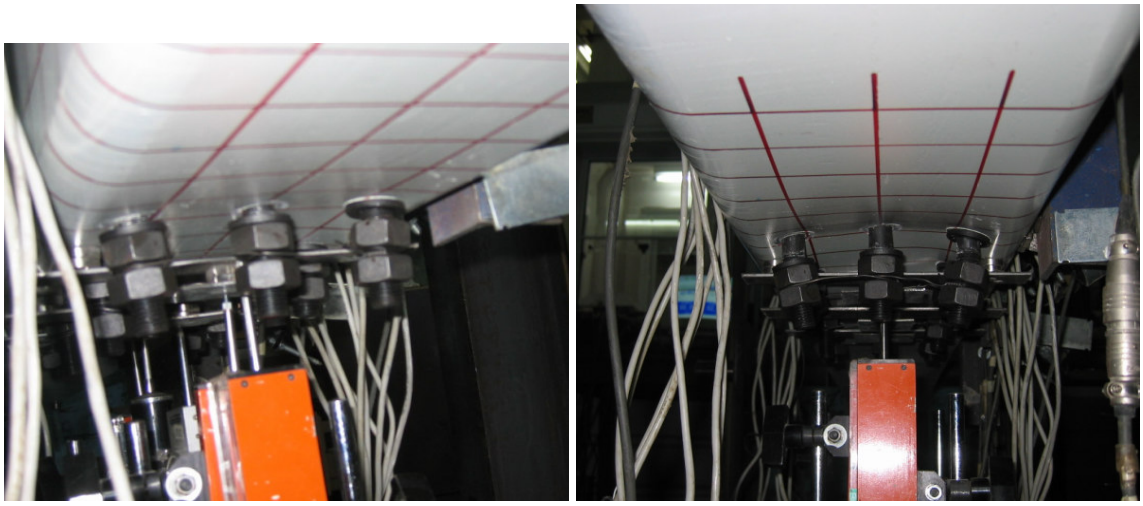

Figure C.25. Release of the partially threaded studs while loading towards opposite direction of specimen T1C

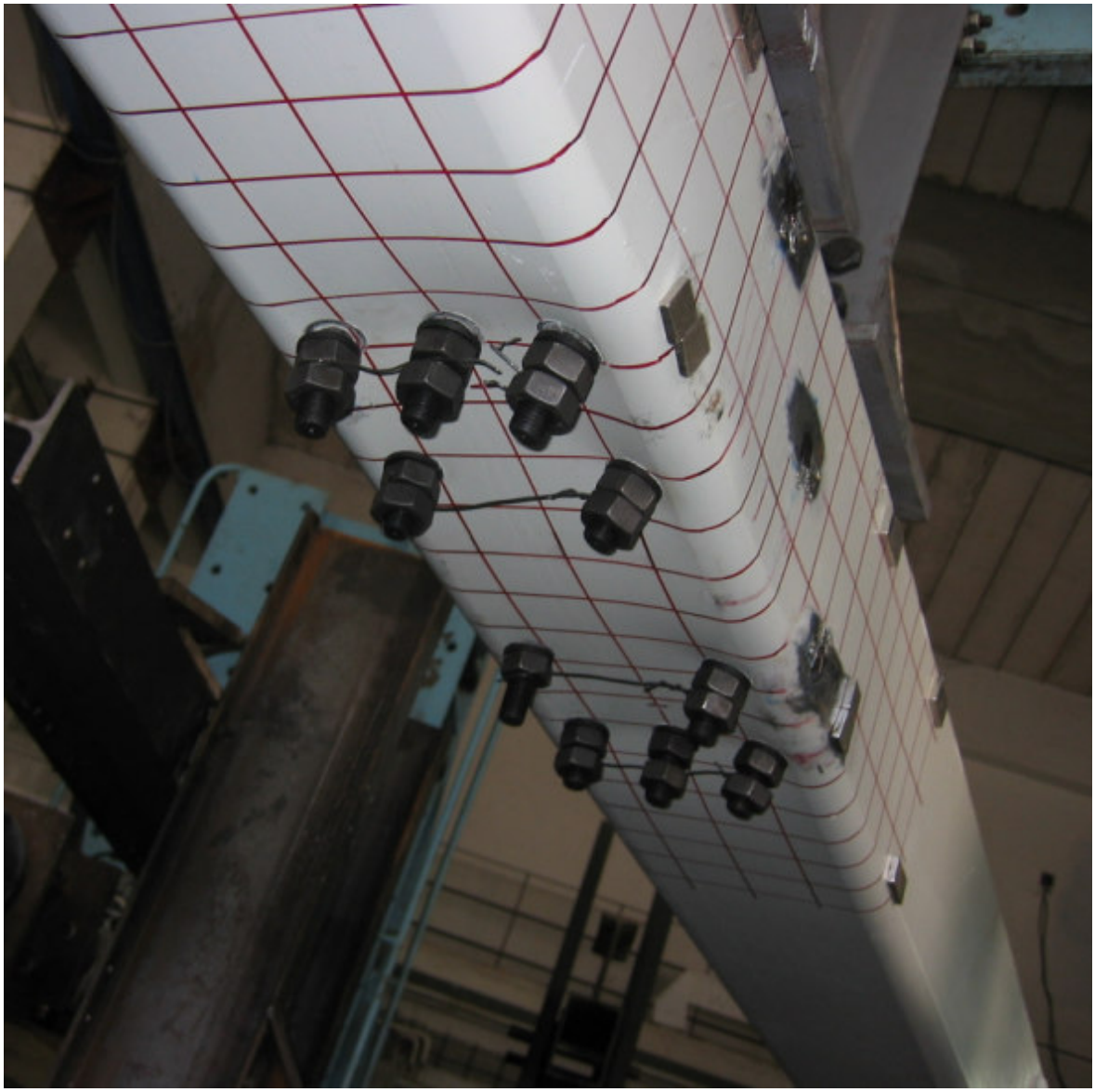

Figure C.26. Deformations at SHS rear face after test of specimen T1C

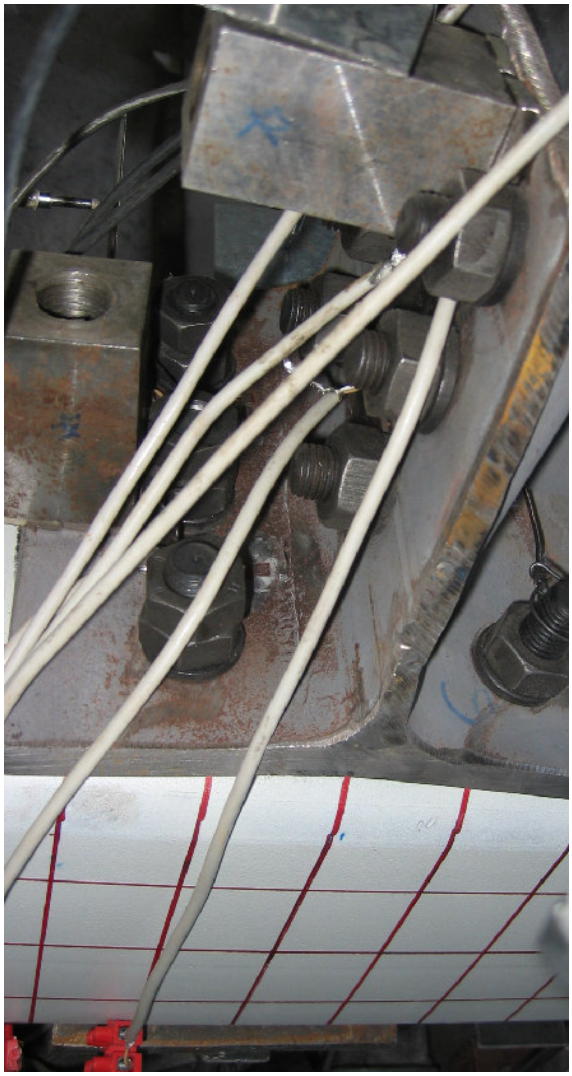

Figure C.27. Crack initiation at t-stub during test of specimen T2C

Figure C.28. Crack propagation at t-stub during test of specimen T2C

Figure C.29. Complete failure of t-stub stem during test of specimen T2C

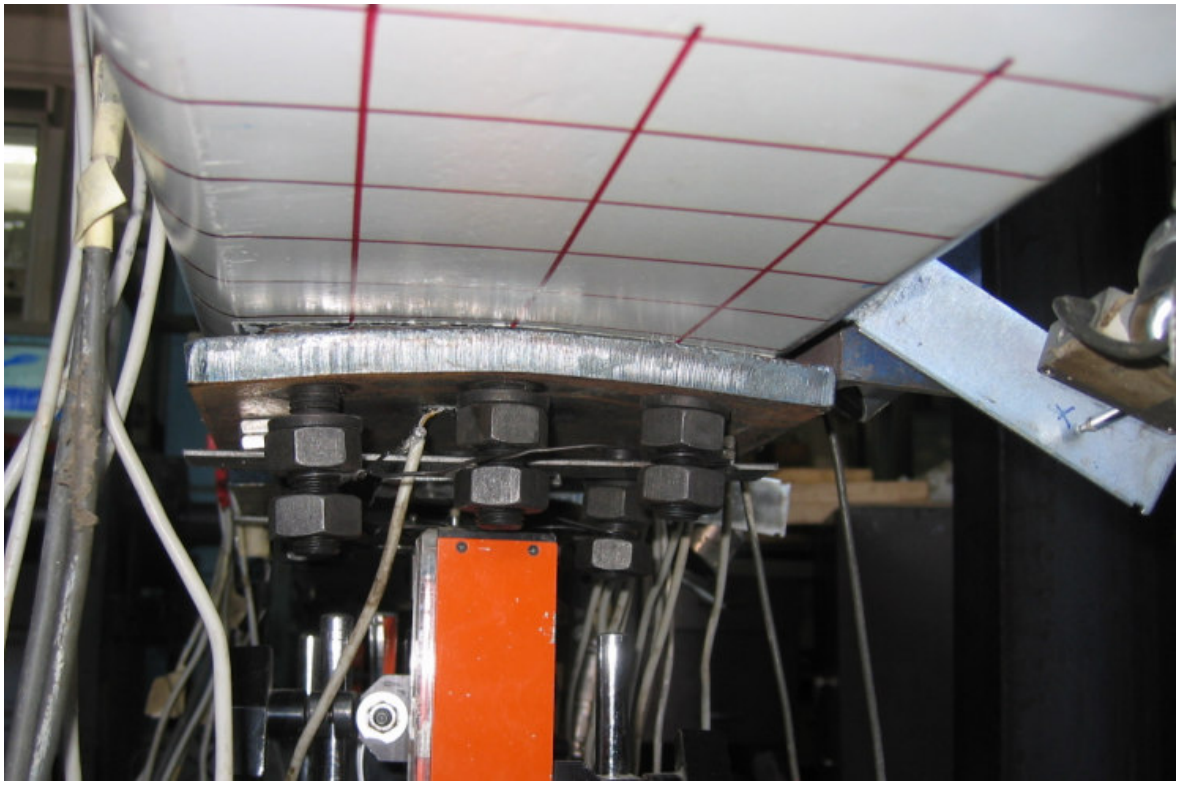

Figure C.30. Release of the partially threaded studs while loading towards opposite direction of specimen T2C

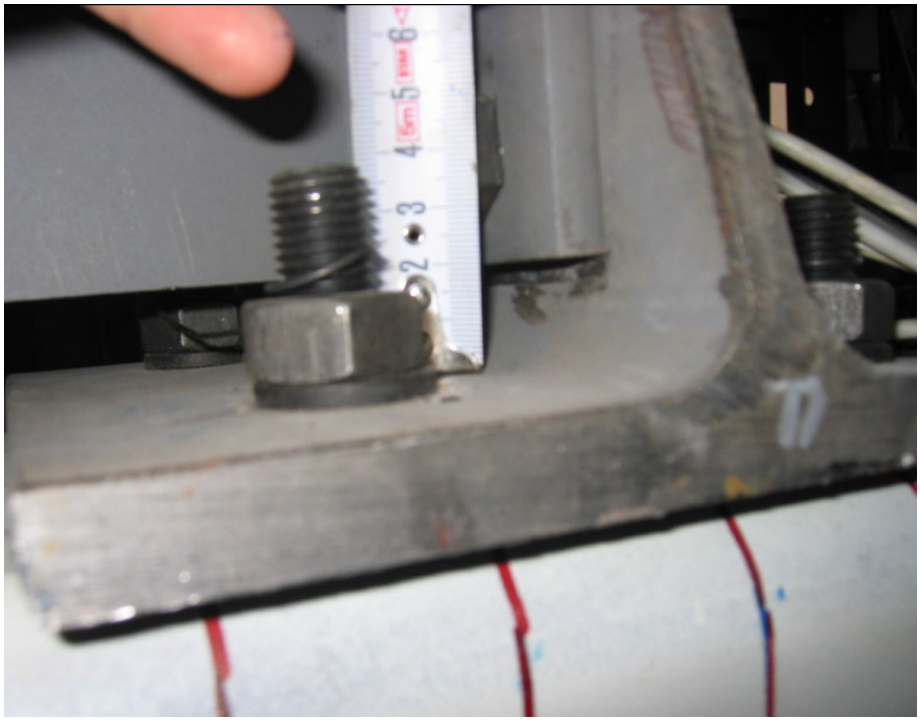

Figure C.31. Slips at t-stub beam interface

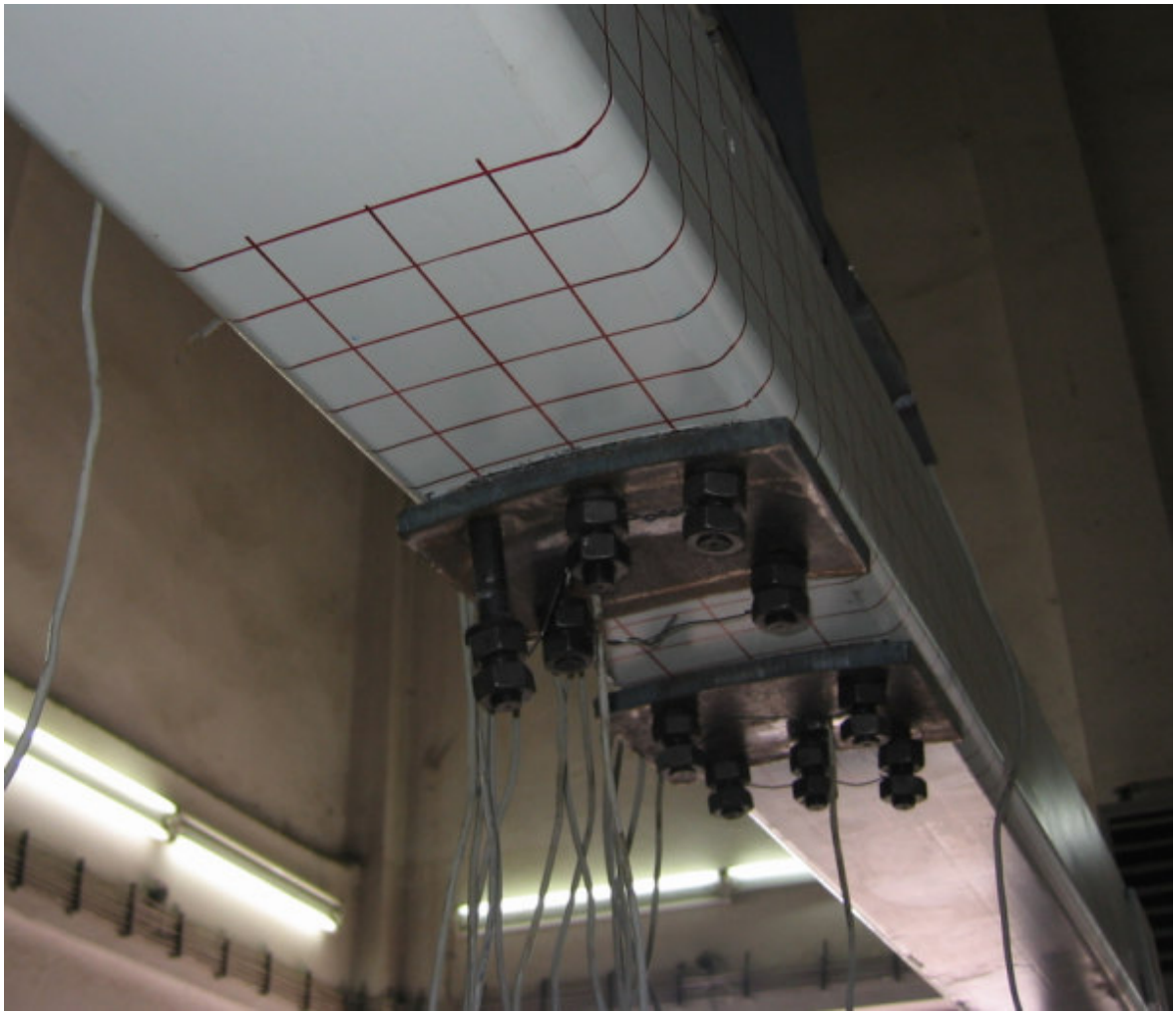

Figure C.32. Deformations at SHS rear face after test of specimen T2C

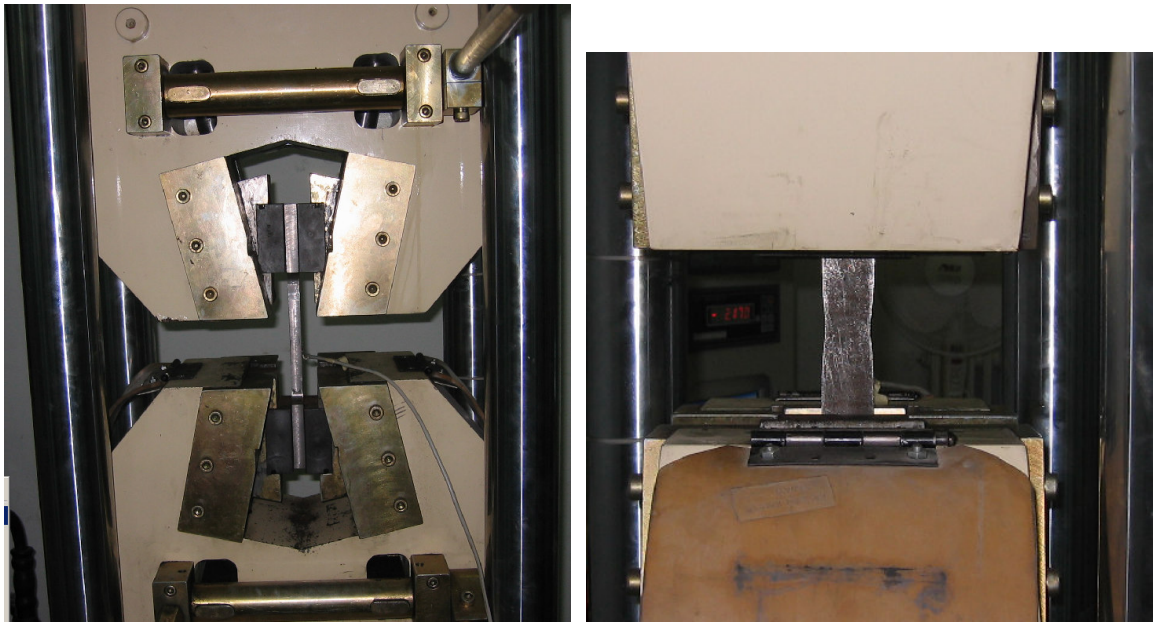

Figure C.33. Coupon tests

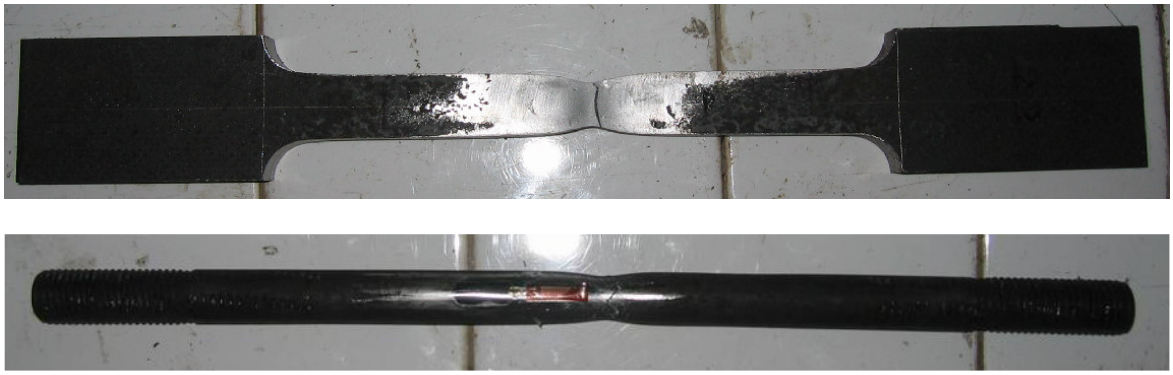

Figure C.34. Typical coupon samples after the coupon test

REFERENCES

1. Grundy, P., I. R. Thomas and I. D. Bennetts, "Beam-to-Column Moment Connections", *Journal of Structural Engineering*, ASCE, Vol.106, No. 1, pp. 313-330, 1980.

2. Packer, J. A., L. Bruno and P.C. Birkemoe, "Limit Analysis of Bolted RHS Flange Plate Joints", *Journal of Structural Engineering*, ASCE, Vol.115, No. 9, pp. 2226-2241, 1989.

3. Chiew, S. P., S. T. Lie and C. W. Dai, "Moment Resistance of Steel I-Beam to CFT Column Connections", *Journal of Structural Engineering*, ASCE, Vol.127, No. 10, pp. 1164-1172, 2001.

4. Schneider, S. P. and Y. M. Alostaz, "Experimental Behavior of Connections to Concrete-Filled Steel Tubes", *Journal of Constructional Steel Research*, Vol. 45, No. 3, pp. 321-352, 1998.

5. France, J. E., J. B. Davison and P. A. Kirby, "Strength and Rotational Response of Moment Connections to Tubular Columns Using Flowdrill Connectors", *Journal of Constructional Steel Research*, Vol. 50, pp. 1–14, 1999.

6. France, J. E., J. B. Davison and P. A. Kirby, "Strength and Rotational Stiffness of Simple Connections to Tubular Columns Using Flowdrill Connectors", *Journal of Constructional Steel Research*, Vol.50, pp. 15–34, 1999.

7. France, J. E., J. B. Davison and P. A. Kirby, "Moment-Capacity and Rotational Stiffness of Endplate Connections to Concrete-Filled Tubular Columns With Flowdrilled Connectors", *Journal of Constructional Steel Research*, Vol. 50, pp. 35–48, 1999.

8. Beutel, J., D. Thambiratnam and N. Perera, "Cyclic Behaviour of Concrete Filled Steel Tubular Column to Steel Beam Connections", *Engineering Structures*, Vol. 24, No. 1, pp. 29-38, January 2002.

9. Peng, S. W., *Seismic Resistant Connections for Concrete Filled Tube Column-to-WF Beam Moment Resisting Frames*, Ph.D. Thesis, Lehigh University, March 2001.

10. Ricles, J. M., S. W. Peng, and L.W. Lu, "Seismic Behavior of Composite Concrete Filled Steel Tube Column-Wide Flange Beam Moment Connections", *Journal of Structural Engineering*, ASCE, Vol. 130, No. 2, pp. 223-232, 2004.

11. Neves, L. C. and F. C. T. Gomes, "Semi-Rigid Behavior of Beam-to-Column Minor-Axis Joints", Proc., *IABSE Int. Colloquium on Semi-Rigid Structural Connections*, Istanbul, Turkey, pp. 207–216, 1996.

12. Gomes, F. C. T., J. P. Jaspart and R. Maquoi, "Behavior of Minor Axis Joints and 3-D Joints", *Proceedings of the 2nd State-of-the-Art Workshop on Semi-Rigid Behavior of Civil Engineering Structural Connections*, Prague, pp. 111–120, 1994.

13. Gomes, F. C. T., "Moment Capacity of Beam-to-Column Minor-Axis Joints", *Proceedings of the IABSE International Colloquium on Semi-Rigid Structural Connections*, Istanbul, Turkey, pp. 319–326, 1996.

14. Vandegans, D., "Use of Threaded Studs in Joints Between I-Beam and R.H.S Columns", *Proceedings of Cost C1 Workshop*, 1996.

15. Silva, L. A. P., L. F. N. Neves and F. C. T. Gomes, "Rotational Stiffness of Rectangular Hollow Sections Composite Joints", *Journal of Structural Engineering*, ASCE, Vol.129, No. 4, pp. 487-494, 2003.

16. Weynand, K. and J. P. Jaspart, "Application of the Component Method to Joints Between Hollow and Open Sections", *CIDECT Draft Final Report*: *5BM*, August 2002.

17. Jaspart, J. P., C. Pietrapertosa, K. Weynand, E. Busse and R. Klinkhammer, "Development of a Full Consistent Design Approach for Bolted and Welded Joints in Building Frames and Trusses Between Steel Members Made of Hollow and/or Open Sections - Application of the Component Method", *CIDECT Report: 5BP-4/04*, November 2005.

18. Shen J. and A. Astaneh-Asl, "Hysteretic Behavior of Bolted-Angle Connections", *Journal of Constructional Steel Research,* Vol. 51, pp. 201–218, 1999.

19. Shen J. and A. Astaneh-Asl, "Hysteresis Model of Bolted-Angle Connections", *Journal of Constructional Steel Research*, Vol. 54, pp. 317–343, 2000.

20. Lu L. H., *The Static Strength of I-Beam to Rectangular Hollow Section Column Connections*, Delft University Press, Delft, 1997.

21. ENV1993-1-1:1992, *Eurocode 3 Part 1.1. Revised Annex J Joints in Building Frames, Edited Approved Draft*, CEN/TC250/SC3, January 1997.

22. EN 1993-1-8:2005, *Eurocode 3: Design of Steel Structures – Part 1-8: Design of Joints*, CEN, Brussels, May 2005.

23. EN 10002-1:2001, *Metallic Materials – Tensile Testing – Part 1: Method of Test at Ambient Temperature*, *European Standard*, CEN, Brussels, July 2001.

24. ECCS – Technical Committee 1, *Recommended Testing Procedure for Assessing the Behaviour of Structural Steel Elements Under Cyclic Loads*, No.45, European Convention for Constructional Steelworks, Brussels, 1986.

25. Gerardy, J. C. and J. B. Schleich, *Technical Steel Research: Properties and Service Performance - Semi-Rigid Action in Steel Frame Structures*, Commission of the European Communities, Luxembourg, 1992.

26. Mazzolani F. M. and V. Piluso, *Theory and Design of Sesmic Resistant Steel Frames*, E&DN SPON, London, 1996.

27. Bijlaard F. S. K and C. M. Steenhuis, “Prediction of the influence of connection behaviour on the strength, deformations and stability of frames, by classification of connections”, *2nd International Workshop*, Pittsburgh, 1991.

28. EN 1993-1-1:2005, *Eurocode 3: Design of steel structures - Part 1-1: General rules and rules for buildings,* CEN, Brussels, May 2005.

29. FEMA-355D, *State of the Art Report on Connection Performance*, SAC Joint Venture on behalf of FEMA, September 2000.

REFERENCES NOT CITED

1. Calado L., G. D. Matteis and R. Landolfo, “Experimental Response of Top and Seat Angle Semi-Rigid Steel Frame Connections”, *Materials and Structures*, Vol. 33, pp. 499-510, October 2000.

2. Kurobane Y., J. A. Packer, J. Wardenier and N. Yeomans, *CIDECT Design Guide 9: Design Guide for Structural Hollow Section Column Connections*, Verlag TÜV Rheinland GmbH, Köln, 2004.

3. Rondal J., K. G. Würker, D. Dutta, J. Wardenier and N. Yeomans, *CIDECT Design Guide 2: Structural Stability of the Hollow Sections*, Verlag TÜV Rheinland GmbH, Köln, 1992.